SPECIAL ISSUE

TECHNICAL, SCIENTIFIC AND RESEARCH REPORTS

Vol. 4 (2012)

PREMIER Analysis of Campaign Data
ESA-ESTEC Contract 4000101374/NL/10/CT

Special Issue

PREMIER Analysis of Campaign Data
ESA-ESTEC Contract 4000101374/NL/10/CT

TECHNICAL, SCIENTIFIC AND RESEARCH REPORTS

VOL. 4 (2012)

Publisher: "Nello Carrara" Institute of Applied Physics (IFAC) - CNR, Florence
Editor: Daniela Mugnai

Topics - Physical Sciences:

- Electromagnetism and Microwaves,
- Atmosphere and Surface,
- Conservation and Diagnostic (Cultural Heritage),
- Laser
- Microoptics
- Remote Sensing (interaction and management of life environments)
- Biophotonics
- Sensors
- Solid State.

Publication Information: ISSN: **2035-5831**
Articles can be published both in Italian and in English. The publication is open access.

TSRR

IFAC-TSRR vol. 4 (2012) 79-239

PREMIER Analysis of Campaign Data
ESA-ESTEC Contract 4000101374/NL/10/CT

Ugo Cortesi [(1)], Samuele Del Bianco [(1)], Marco Gai [(1)],
Bianca Maria Dinelli [(2)], Elisa Castelli [(2)],
Daniel Gerber [(3)], Hermann Oelhaf [(4)], Wolfgang Woiwode [(4)]

([1]) Istituto Fisica Applicata "Nello Carrara" del CNR (IFAC-CNR)
([2]) Istituto di Scienze dell'Atmosfera e del Clima, ISAC-CNR
([3]) Rutherford and Appleton Laboratory, STFC-RAL
([4]) Karlsruhe Institute of Technology, KIT, IMK-AFS

 ISSN 2035-5831

1 Introduction

This document is the Final Report of the project "Premier Analysis of Campaign Data" (PACD) for the ESA-ESTEC Contract N. 4000101374/NL/10/CT aimed at processing Level 1 (L1) data acquired by the MARSCHALS instruemnt onboard the M-55 Geophysica high-altitude research aircraft during the Test Campaign in November 2009 at mid-latitude (TC9 campaign Oberpfaffenhofen, Germany, Lat. $48.1\,^{\circ}\mathrm{N}$, Lon. $11.3\,^{\circ}\mathrm{E}$) and during the scientific campaign in March 2010 in the Arctic region (PremierEx campaign, Kiruna, Sweden, Lat. $67.8\,^{\circ}\mathrm{N}$, Lon. $20.4\,^{\circ}\mathrm{E}$). The document describes the research activitites conducted in the period from the Kick-Off Meeting (12.06.2010) to the Final Meeting (14.06.2011) and the consolidated results obtained during Phase 1 and Phase 2 of the PACD project.

The activities carried out in the course of the project reporting period mostly focused on the following work-packages:

- Adaptation and upgrading of the code developed by IFAC and ISAC for the analysis of MARSCHALS measurements (WP-2000)
- Intercomparison of IFAC/ISAC and RAL foward models (WP-3000)
- Analysis of the data acquired by MARSCHALS during the TC9 campaign and the PremierEx campaign (WP-4000/4100)
- MARSCHALS data validation (WP-5000/5100)
- Assessment of Clouds (WP-6000/6100)
- Synergy of mm-wave and IR measurements (WP-7000/7100)

The main outcome and conclusions for the above mentioned activities are presented and discussed with emphasis on the analysis of the PremierEx campaign dataset due to the better performances achieved by the MARSCHALS instrument during this Scientific Flight compared to the Test Flight In section 2, a summary of the key modifications implemented in the pre-processor and retieval codes is reported. In section 5, preliminary results of the first retrieval analysis of the measurements obtained by MARSCHALS during the Test Flight of 04.11.2009 are shown and conclusions are derived on the performance of the retrieval of the target species: Temperature, H_2O, O_3, HNO_3, N_2O, CO.

2 New characterization data and code verification

MARSCHALS Level 2 (L2) data analysis is performed using the L2 software suite developed in the context of the previous study supported by ESA: "*The Scientific Analysis of Limb Sounding Observations of the Upper Troposphere*", Contract N. ESTEC/Contract 16530/02/NL/MM. The software suite is mainly composed by two modules:

1. **SAMM** (**S**upervising **A**nalyzer of **M**ARSCHALS **M**easurements)
   This module is a tool dedicated to perform a first selection of the MARSCHALS measurements, to convert the data contained in the L1 files in a format readable by the MARC code, and to generate a preliminary overview and diagnostic of the flight data.
2. **MARC** (**MA**RSCHALS **R**etrieval **C**ode)
   This module contains the core part of the code devoted to the retrieval of vertical profiles of atmospheric constituents, as well as instrumental scalar quantities to assess the quality of the measurements. The retrieval is performed by processing a set of measured (or simulated) spectral data.

More details about the MARC and SAMM modules can be found in the Level 2 ADD [16] and in the Level 2 User Manual [17].
In this section we recall some of the features of the pre-processor code (SAMM) useful for the subsequent discussion and we report the new functionalities of SAMM and MARC codes implemented for the handling and for the analysis of the data acquired during the PremierEx campaign. A more detailed description of the pre-processor and of the retrieval code can be found in the SCOUT-O3 analysis report [18].

The data extraction routines of SAMM were tested using the SCOUT-O3 flight campaign data. Both spectral and other data necessary for the L2 analysis were compared with data extracted by using an application provided by the L1 team, which is Level1b2CSV.exe.

2.1 The main features of the pre-processor

The main features of the pre-processor were developed during SCOUT O3 analysis, in order to allow the L1 data processing by using MARC retrieval module.

- *Rearrangement of the Lines Of Sight (LOS)*
  in the L1B data file, the LOSs are not monotonically sorted with decreasing (or increasing) pointing angle; the pre-processor rearranges the LOS in increasing order;
- *Rearrangement on the spectral data*
  in L1B data file the spectral data, as well as the spectral error and all related quantities are not sorted with increasing frequency; the pre-processor rearranges the spectral channels with frequencies in increasing order;
- *Rearrangement on the filter spectral response*
  Spectral response is provided for each filter as a function of Low Frequency; the pre-processor translates this data in the Band B, C, and D frequency using the local oscillator frequency;
- *Implementation of manual selection of the LOS*
  the user can exclude one or more LOS from the file of observations; this manual selection has been added to exclude LOS having large values of χ^2-test.
- *Computation of the average spectral error*
  For each LOS, the pre-processor computes an average (root mean square (rms)) value for the spectral error; the user can decide to use the original error or the averaged one in the retrieval.
- *Treatment of spectra containing unrealistic values*
  Some spectra in band B contain channels having unrealistic values (null or very large values) in spectral data and/or in spectral data errors; when the file of the observations to be analysed is produced, these channels can be replaced with values selected by the user. This feature of the pre-processor enables the exclusion of the unrealistic values from the analysis by introducing a large value in the spectral error. The channels marked as unrealistic are not taken into account when the average spectral error is computed.

2.2 Characterization of the Level 1B data

2.2.1 Overview of Level 1B data

The SAMM pre-processor produces a set of output files used to characterize the data acquired during the flight. Among these, the *flight overview* contains general data related to the measurement campaign.

Some results extracted from the flight overview in the case of the 04.11.2009 flight are reported in section 5.1.

Along with the flight overview, the pre-processor generates a *scan overview* file containing auxiliary data related to a specific selected scan: the geo-location of the instrument (altitude, latitude, longitude); the pointing angle; the geo-location of the refracted tangent point (altitude, latitude, longitude); the values of the spectral quantifiers computed by the pre-processor (continuum, noise and contrast levels).

2.2.2 Sweep selection criteria

For each measured scan, the pre-processor enables either an automatic selection or a manual selection of the sweeps which are going to be analysed.

The main automatic selection criteria are:

- *Altitude range selection*: only sweeps having tangent altitude included in a selected range are extracted;
- *Noise selection*: only sweeps having noise less than a noise threshold are extracted;
- *Contrast level selection*: only sweeps having a contrast level greater than a threshold value are extracted;
- *Tangent altitude behaviour*: if two consecutive scans have increasing pointing angles, but not decreasing tangent altitudes, the lowermost is automatically excluded.

The automatic selection of the sweeps can be manually modified by editing a LOG file automatically produced by SAMM. The file, along with the scan diagnostics, contains a flag that is automatically set to 1 if the sweep has been included in the data to be analysed, or to zero if the sweep has been discarded. Changing manually the flag the automatic selection is overwritten in a subsequent run of the SAMM code.

2.3 New features of the pre-processor

The format of MARSCHALS Level 1B data provided by the L1 team is basically unchanged from the SCOUT-O3 campaign, however some additional features are included in the pre-processor to better characterize the actual data.

2.3.1 Spectrum contrast level

This quantifier can be used to identify and/or filter the observations having a low contrast in the spectral lines.

In the SCOUT-O3 version of SAMM the contrast level was defined as the ratio between the mean spectral intensity in two frequency intervals of each band. In the new version of SAMM the contrast level related to a given spectrum is defined as the difference between two reference intensities: I_{peak} (located on a strong line of the spectrum) and I_{cont} (located in a continuum region).
Reference intensities are evaluated by averaging the spectral intensity over given spectral intervals, specific of each band, as described below:

Band B:
I_{peak} is evaluated as the mean value on the interval [301.6 - 302.0] GHz, for a total of three spectral points. This interval contains the strongest O_3 line in the band.
I_{cont} is evaluated as the mean value on the interval [295.6 - 296.4] GHz, for a total of five spectral points.

Band C:
I_{peak} is evaluated as the mean value on the interval [324.9 - 325.3] GHz, for a total of three spectral points. This interval contains the strongest H_2O line in the band.
I_{cont} is evaluated as the mean value on the interval [322.5 - 323.3] GHz, for a total of five spectral points.

Band D:
I_{peak} is evaluated as the mean value on the interval [343.0 - 343.4] GHz, for a total of three spectral points. This interval contains the strongest O_3 line in the band.
I_{cont} is evaluated as the mean value on the interval [347.6 - 348.4] GHz, for a total of five spectral points.

2.3.2 Averaged Brightness Temperature of each spectrum

This quantifier can be used to identify and/or filter the observations having anomalous behaviour due to either pointing problems or cloud contamination. The averaged Brightness Temperature (BT_{av}) quantifier is computed by averaging the spectral intensity over the whole spectral range of the band:

$$BT_{av} = \frac{\sqrt{\sum_{i=1}^{N} BT_i^2}}{N} \tag{1}$$

Where BT_i is the brightness Temperature of spectral channel i, N is the number of channels of the considered band. The BT_{av} quantifier is reported in the scan_log file.

2.3.3 New format for some auxiliary files

New reading routines have been developed in order to manage the new format of some auxiliary files (Instrumental Line Shape (ILS) and Field Of View (FOV)).

2.3.4 Mean spectrum and standard deviation

A new significant feature implemented in the pre-processor is the computation of the mean spectrum and of the standard deviation. The mean spectrum is computed by averaging all the observations acquired at the same nominal pointing angle.

Some examples of mean spectra in case of the 04.11.2009 flight are reported in figures 1, 2 and 3.

2.3.5 Observations dataset

By using the new developed feature, the pre-processor is able to create different configurations of the observation dataset resulting from different definitions of the observed spectrum and of the measurement error. The different

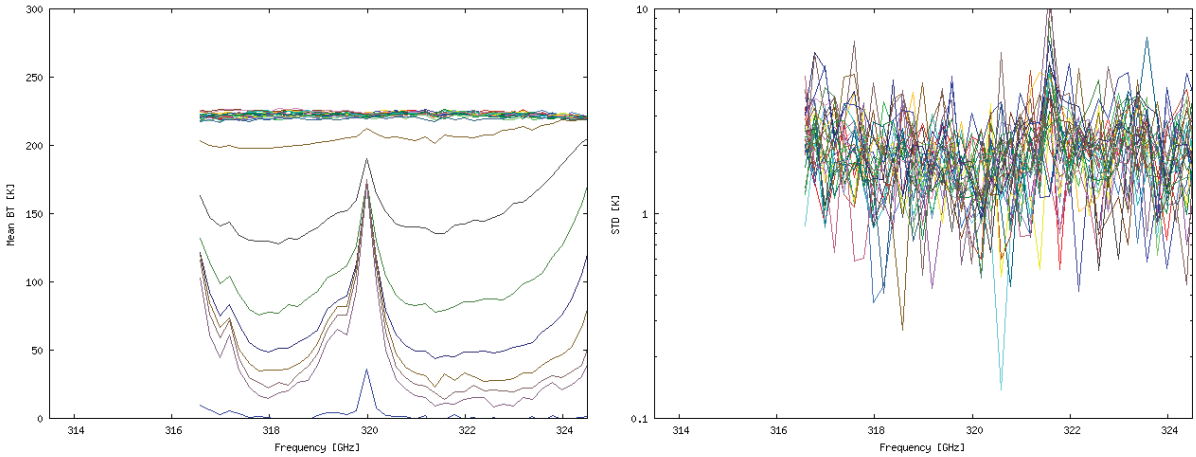

Fig. 1: Example of MARSCHALS mean spectra of 04.11.2009, band C, scan 30

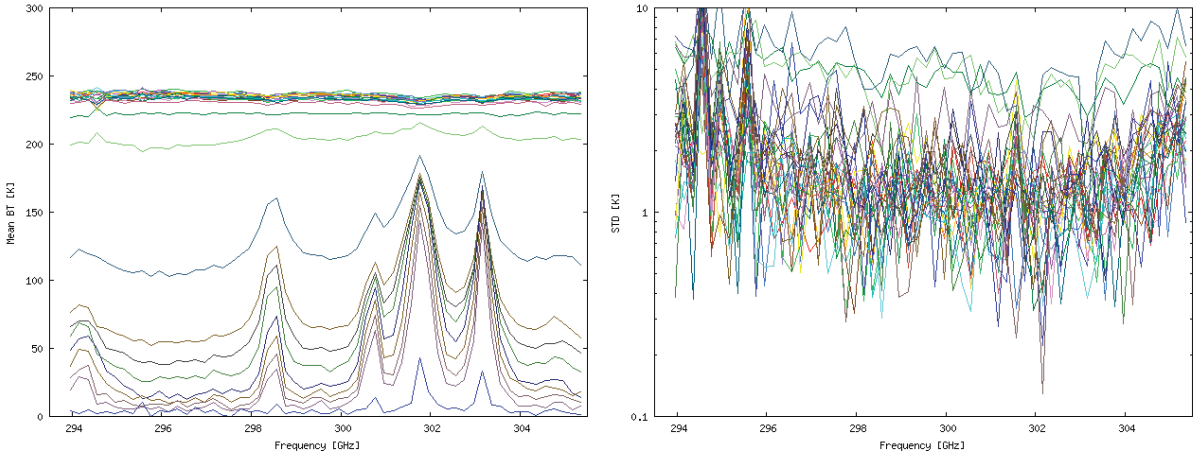

Fig. 2: Example of MARSCHALS mean spectra of 04.11.2009, band B, scan 31

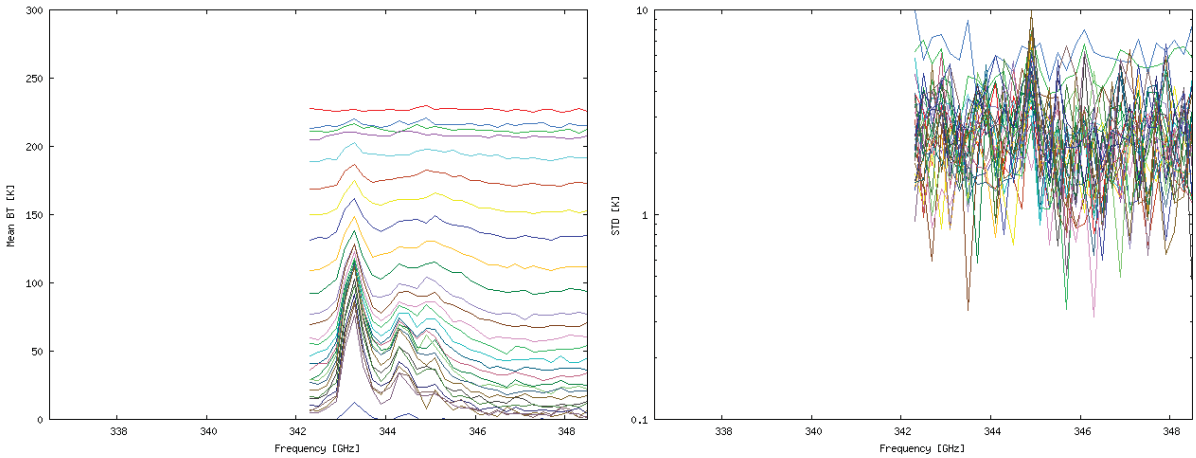

Fig. 3: Example of MARSCHALS mean spectra of 04.11.2009, band D, scan 32

configurations will be evaluated during the retrieval activity in order to find the best retrieval configuration.

Dataset configuration 1: single spectrum and measurement error
In this configuration the pre-processor creates, for each scan, a file containing all the atmospheric observations (matching the filtering criteria set by the user) and the measurement error.
In detail:

- Spectrum: single observation spectrum;
- Error: spectral error, including covariance, extracted from L1B file.

Dataset configuration 2: mean spectrum and standard deviation
In this configuration the pre-processor creates, for each scan, a file containing mean observations and standard deviation.
The observation is identified by the mean value of pointing angle, tangent altitude, instrument altitude.
In detail:

- Spectrum: mean spectrum computed on observations having the same nominal pointing angle;
- Standard deviation computed on observations having the same nominal pointing angle; no measurement covariance is taken into account (diagonal measurement VCM).

Note: data rejection
A data rejection criterion is applied in the computation: the observations along a line of sight having a tangent altitude that differs more than two standard deviation and more than 100 m from the mean tangent altitude are rejected from the statistics; a new mean and standard deviation are computed using the remaining elements.

Dataset configuration 3: single spectrum and standard deviation
the pre-processor creates, for each scan, a file containing all the atmospheric observations (matching the filtering criteria set by the user) with an associated error estimated using the standard deviation of the observed spectrum computed on the observations having the same nominal pointing angle.
In detail:

- Spectrum: single observation spectrum;
- Error associated to the spectrum: Standard deviation computed on the observations having the same nominal pointing angle; no measurement covariance is taken into account (diagonal measurement VCM).

Dataset configuration 4: single spectrum and rms noise
the pre-processor creates, for each scan, a file containing all the atmospheric observations (matching the filtering criteria set by the user) with an associated error estimated using the mean rms noise of the observed spectrum.
In detail:

- Spectrum: single observation spectrum;
- Error associated to the spectrum: rms noise computed using the spectral errors associated to the spectrum; no measurement covariance is taken into account (diagonal measurement VCM).

2.4 New features of the MARC code

The MARC code is basically unchanged from the code used for the SCOUT-O3 campaign data analysis, however some parameter has been changed to model the instrumental characterization and some additional features has been included. In particular, in the following we describe the implementation of the frequency shift retrieval and of the exportation of the input needed to the data fusion analysis.

2.4.1 Implementation of frequency shift retrieval

In order to reduce the systematic errors due to the instrumental characterization and to produce a feedback to the L1 team on the quality of the spectral calibration, the possibility to retrieve the frequency shift has been implemented in the MARC code. This parameter is a band dependent parameter so if we analyze a measurement performed on 3 bands, 3 different values of the frequency shift are provided by the code. This parameter is not

geometry dependent because we assume that the frequency shift is due to the instrumental characterization. The frequency shift parameter is a frequency offset introduced in the ILS. MARC compute the Jacobian preforming the convolution twice: the first one using the actual value of the frequency shift and the second one using the actual value plus the frequency step equal to the fine frequency grid used in the simulation (2.5 MHz). This retrieved parameter can be fitted using the logical flag added in the settings file. If it is retrieved by MARC the user has to provided in the settings file the a priori information in term of initial guess and a priori error, and the Marquardt parameter. If the frequency shift retrieval is enabled, MARC provides the frequency_shift.dat file with information on the frequency shift retrieval related on last iteration of the retrieval and on the initial guess used.

2.4.2 Frequency shift retrieval results on simulated spectra

Tests have been performed to evaluate the correctness of the procedure: a frequency shift has been introduced in the simulated observations and we have performed the retrieval in order to fit the actual value. This test has been repeated fitting the frequency shift alone and using the standard settings configuration related to MARSCHALS analysis and we obtained a good evaluation of the frequency shift in terms of accuracy and precision.In particular, using 1K as MARSCHALS measurement error, the accuracy is 1-2 MHz and a frequency shift of +20, -20, +20 MHz have been retrieved in band B, C, and D respectively.

2.4.3 Implementation of the exportation of the MSS input products

The Measurement Space Solution (MSS) is a new type of representation of the information retrieved about the vertical profile of an atmospheric constituent [3]. In this new representation the profile is not given, as in classical retrievals, by a sequence of values as a function of altitude, but as the combination of a set of functions each weighted with a measured amplitude. The set of functions are those that belong to the functional space in which the measurement is performed (the so called "measurement space"). The profile obtained in this new way does not directly provide, as classical retrievals do, a useful graphical representation, but has other important advantages that make it a tool for the full extraction of the information that the observations contain about the profile that is being retrieved. The MSS theory is briefly described on the IFAC web site: http://ga.ifac.cnr.it/products-and-facilities/mss-products.html.

MARC has been modified in order to export at the last retrieval iteration all the information to calculate the MSS. In particular MARC exports:

- 1) the vector $(S_y^{-1/2} * (y - F(x_0))$, where S_y in the total (random and systemic) VCM of the observation, y are the observations and $F(x_0)$ are the simulations at the last retrieval iteration;
- 2) the matrix $S_y^{-1/2} * K$, where K is the Jacobian matrix;
- 3) the vector x_0 that is the state vector at the last retrieval iteration.

A stand alone software has been implemented in order to compute the MSS related to MARSCHALS and MIPAS data and to preform the data fusion.

3 Intercomparison of MARC and RAL forward models

In this section, we report the results of the comparison of the forward models implemented in the MARC code by IFAC/ISAC and in the FM2D code by RAL. The radiative transfer code of MARC is illustrated in Sections 5 and 6 and in references therein. Details about the RAL forward model are provided in sub-section 3.1.

3.1 Description of the RAL forward model

RAL uses its in-house radiative transfer code called FM2D for all results presented on their behalf in this study. FM2D stands for 2-Dimensional Forward Model, indicating the capability of the code to be used in a 2-Dimensional tomographic retrieval scheme, but the scope of this study only requires 1-Dimensional calculations. FM2D is a mature, modular code which has been used in a number of past ESA studies, as well as for the data analysis and simulation of various remote sensing instruments. It has been originally developed for the MASTER 1^{st} Extension Study and an in depth description of the model can be found in the corresponding Final Report [8] and in the Final Report on the 1^{st} Extension [9]. FM2D had been compared to other radiative transfer models in the past, e.g. to the University of Oxford RFM (Reference Forward Model) [10] and University of Chalmers, Moliere5 [25] and

successful matches have been achieved in all cases.

In the following we give a short description of some of the control parameters, in order to outline the scope within which they can be modified to match the output of the MARC forward model code:

Gas Profiles: Vertical profiles of trace gases, Temperature and pressure can be freely chosen. If the profile spacing is coarser than the forward model grid, then profiles will be interpolated accordingly. If the input profiles span less than the full range of the forward model grid, then missing values will be extrapolated. It is worth pointing out at this point that grid interpolation is a possible error source between different forward models.

Line Shapes: The following spectral line shapes are supported by FM2D

- Lorenz
- VanVleck/Weisskopf
- Voigt
- Combined VVW/Voigt

Atmospheric Continua: The following continuum absorption can be switched on/off at will

- H_2O continuum
- N_2 continuum
- O_2 continuum

Continuum models: The following formulations of continuum absorption can be selected

- Liebe89 (in combination with the following line shapes: Voigt, VVW or both)
- Liebe93 (in combination with the following line shapes: Voigt, VVW or both)
- CKD (in combination with the following line shapes: Voigt)
- Any explicit profile of absorption coefficients at one (or two) given frequencies to be added to the line-by-line absorption. If absorption coeffients are defined at two frequencies then the additional absorption takes the form of a slope over the spectral band.

Atmospheric Scans: Can be defined in units of off-nadir angles, geometric (i.e. non-refracted) tangent height or true (i.e. refracted) tangent height.

Background Radiance: Can be either switched on or off, or set to a fixed value of 2.74 K. Default is switched on.

Surface Emissivity: Can be set to values from 0 (100% reflectance) to 1 (100% absorption).

Refraction: Can be switched on or off. If switched on the earth radius can be selected. T, p, and gas profiles will also have an impact of the calculated refraction.

Frequencies: Any frequency grid is possible, even arbitrarily spaced ones.

Output Parameters: The following output units are possible

- Radiance (Brightness Temperature)
- Total absorption coefficients at all atmospheric levels
- Path transmittance

Spectral Line Data: Any spectral line data file in HITRAN format can be used. For some continuum choices (e.g. Liebe) a separately defined H_2O line data file has to be used. (The latter can be manually overridden if needed).

Instrument Line Shape: The instrument line shape is defined in a FILTER_FILE, which contains the centre frequencies of each channel and for each channel the path to a corresponding (normalised) channel response file. We are using the filter functions as measured in the lab at RAL.

Antenna Pattern: The shape of the antenna pattern is given in a separate file. The range over which is defined has to be fully covered by the range of the pencil beams (see below) or a convolution error will result.

Pencil Beams: The angles at which the antenna pattern is to be evaluated in order to calculate the signal at a given bore sight.

Forward model grid: Any arbitrarily spaced altitude grid at which to compute the atmospheric radiance can be specified. The altitude grid has to fully cover the scan range or else an error will result. For limb sounding the forward model grid has to include the platform altitude.

3.2 Scope and strategy of the forward model intercomparison

The following statement in the SOW defines the threshold criteria for a successful intercomparison:

> "It shall be demonstrated that residual differences between both models do not lead to significant differences in retrieved products, i.e. the differences need to be negligible with respect to Level 2 accuracy requirements in the PREMIER MRD /MRD2009/."

During the first phase of the intercomparison, in the intermediate absence of retrieval simulations, we have to find a quality criterion based on our past experience which will allow us to judge if any two given modeled spectra are close enough to likely fulfill the SOW criterion outlined above. As a working hypothesis, we assume that simulated spectra including continuum absorption and the full instrument functions should usually agree to within 0.1 K with each other. Monochromatic spectra should agree to about 0.1 K. These numbers assume that all parameters of the two forward models are absolutely identical. In case of larger discrepancies in the underlining differences in the model code need to be identified.

The plan was to conduct the model comparison as follows. We will start with a comparison of monochromatic spectra (i.e. neither instrument line shape nor antenna convolution are accounted for) and an atmosphere without either refraction or continuum absorption. If the residual differences fall within our set threshold, then additional complexity is added to the scenario as follows:

1. Instrument Line Shape (ILS), aka filter functions or channeliser spectral response)
2. Continuum
3. Refraction
4. Field of View (FOV), aka antenna convolution

If at any point the discrepancies turn out to be larger than our set thresholds, then we would simplify the scenario in order to pinpoint the source of error (e.g. single spectral lines, single layer atmosphere, etc). In practice it turned out that the comparison was much more challenging and complicated than anticipated. As a result of this the features of the models had to be extended quite significantly (more details are given later in the text in the corresponding sections).

3.3 Definition of input parameters

The initial input parameters were defined mostly by RAL based on an existing setup to analyse PremierEx data. The atmospheric profiles were computed by interpolating ECMWF fields to tangent point locations and altitudes which correspond to the actual measurements taken by MARSCHALS along the flight track of the PremierEx flight. This implies that the returned profiles were only defined at the MARSCHALS scan angles, which are not exactly even spaced and which did not always reach down to Zero kilometers. While not initially perceived to be an issue, this was later discovered to cause significant interpolation errors. As a result the grid spacing had to be reduced, and consequently the profiles had been replaced by a set of RFM reference profiles which are fully specified from 0 km up to 120 km. The profiles we finally used are shown in Figure 4.

The definition of the instrument functions (ILS and FOV) were provided by RAL based on measurements of the instrument performance performed in the context of the UAMS instrument upgrade project (ESA project). The

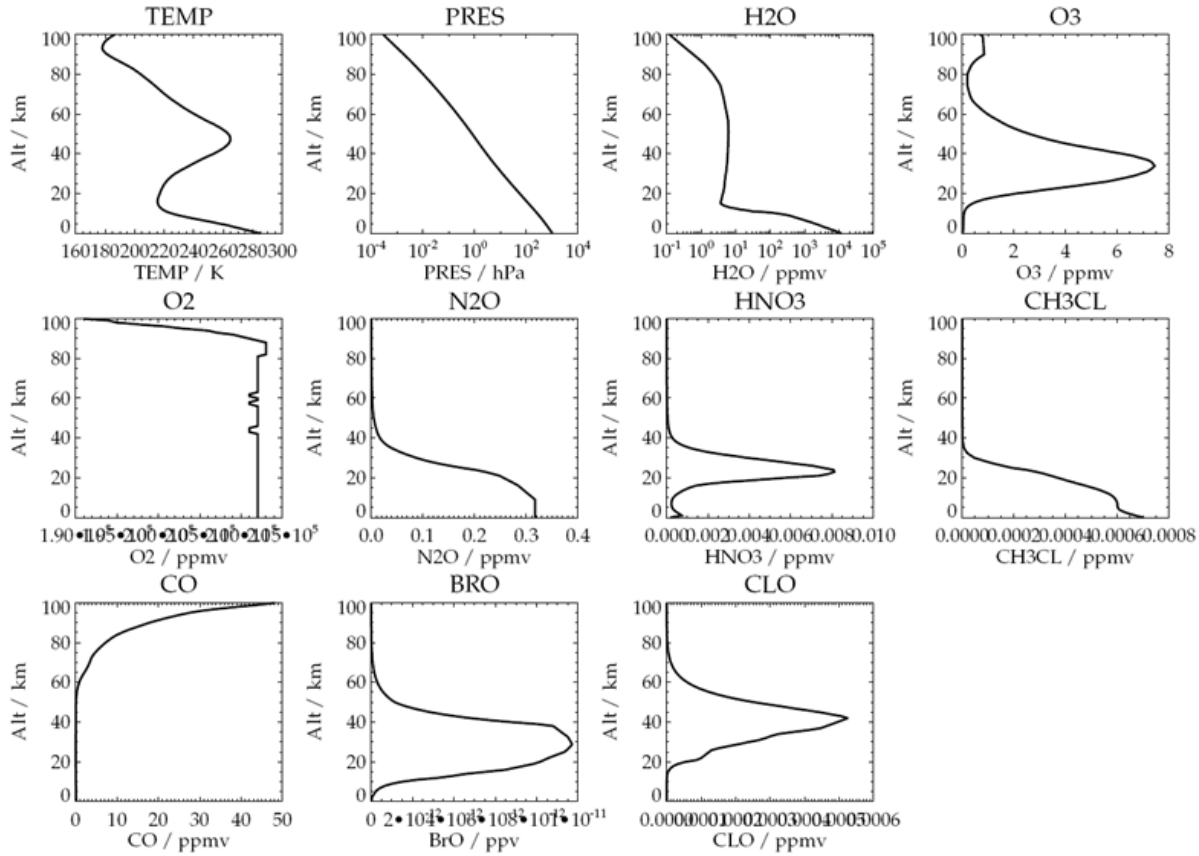

Fig. 4: Input profiles used for the FM intercomparison studies (Source: RFM reference profiles)

FM intercomparison is still based on the antenna patterns measured in 2005 after the Darwin campaign, because the newest results were still outstanding.
The following input parameters have been defined by the IFAC team, because they cannot be modified at will in the MARC code:

- Monochromatic frequency grid (2.5 MHz)
- Spectral line data file (from a study by Verdes et al. [26] converted to HITRAN format by IFAC)

3.4 Monochromatic calculations

In the following sections we present the results of the monochromatic simulations. We only present milestone findings to illustrate the process we have gone through and the conclusions we have drawn if they had a feed back on the process itself (i.e. where as a result of a simulation we had to make changes to the code or the setup).

3.5 Initial setup (full atmosphere)

Figure 5 shows the residual difference of RAL spectra minus IFAC spectra based on the initial input parameters and model configurations. This represents the state as it was presented at the first project meeting at Florence (PM1) in August 2010. Explicitly this means that the atmospheric profiles were the coarsely gridded, interpolated ECMWF profiles and the forward model grid was the initial grid of 1 km spacing in the troposphere, 5 km spacing in the stratosphere and 10 km spacing in the mesosphere.
There are some obvious problems with the spectra in Figure 5:

- A residual which looks like a frequency shift on the 325 GHz H_2O line
- Residuals shaped like delta functions, which indicate that the mesospheric contribution is misrepresented

- A continuum-like residual which seems to be strongest at 5 km - 6 km

As a conclusion, the following changes have been implemented:
The spacing of the forward model grid has been reduced. The minimal spacing of 1 km has been reduced to 200 m and the maximum spacing of 10 km has been reduced to 1 km. The reason for this was to mitigate discrepancies introduced by interpolation of atmospheric profiles when the radiative transfer equation is solved for a given pencil beam through the atmosphere. On top of that, the vertical resolution of the gas, Temperature and pressure profiles have been increased as well. They are now defined at the exactly the same altitudes as the forward model grid, further mitigating the need for interpolation.

The need to do this had a knock-on effect on the input profiles themselves. Because the interpolated ECMWF profiles were rather coarse only exist down to the lowest tangent point it was difficult to map them to the new forward model grid. Consequentially we decided to use the RFM reference profiles as a new basis for our intercomparison, as these are already defined at a rather high resolution from 0 km up to 120 km. To address the perceived frequency shift that line shape functions have been analysed and it was found that the MARC code used a frequency shift parameter in the calculation of the VVW line shape which was not present in FM2D. RAL have now implemented this frequency shift in FM2D which has resolved this issue.

Figure 6 shows the same residuals after the implementation of the fine forward model grid and input profiles, as well as the inclusion of the frequency shift parameter in the VVW line shape calculation in FM2D.

When we compare Figure 5 with Figure 6 we see that the frequency shift has disappeared, and that the mesospheric spikes are significantly reduced (from more than 14 K to about 4 K). With this respect the modifications have been a significant improvement. The flat, view angle dependant residual is persistent and is addressed in the next stage.

3.6 Single H_2O and O_3 lines

Our working assumption was that the flat, view angle dependent residual could be due to a misrepresentation of the spectral line shape (especially in the wing of the strong H_2O line). We have therefore decided to introduce scenarios where only a single spectral line is calculated. For this we have selected the strongest H_2O and O_3 lines at 325 GHz and 320 GHz respectively. In both cases we have performed simulations first using a simple Voigt line shape function, and then the (default) combined line shape function of Voigt and VanVleck-Weisskopf (where Doppler width becomes significant). This comparison will show if the observed discrepancies are introduced by a different implementation of the VVW line shape. The results of this comparison are shown in Figure 7. Top row depicts the residuals of the RAL ozone spectrum minus the IFAC ozone spectrum, and the bottom row shows the same picture for the H_2O line. In the left column Voigt line shape is used, the right column uses a combines Voigt/VVW line shape.

It is immediately obvious that both results are similar beyond distinction and that basic residuals of close to 1 K are already present in the simple case of a Voigt line shape. This leads us to conclude that the source of the discrepancies is to be found at the spectroscopy level, even before a spectral line shape is applied.

3.7 Single layer homogeneous atmosphere

In order to discover the persistent discrepancies, an even more basic scenario was devised. This test scenario consists of a single layer atmosphere at a constant Temperature of 250 Kelvin, a constant pressure of 100 hPa and as a single component contains water vapour at a mixing ratio of 10 ppmv. This setting (which obviously defies reality) is comparable to a gas cell measurement. The advantage of this setting is that all spectral parameters, which are Temperature or pressure dependent, only have to be calculated once, and are therefore easier to cross-compare. Figure 8 shows the residuals for this most basic of all scenarios, which at 0.14 Kelvin are still larger than we would expect.

We have consequently modified the code to output all the intermediate spectroscopic parameters, and have found a significant mismatch of 1-2 % in the Temperature- and pressure corrected line strength parameter. This parameter is calculated from the partition functions, which are different for the two codes. FM2D used the Liebe partition functions, whereas MARC uses a definition of partition functions which go together with the spectral database and the continuum model they are using.

The partition function currently used into the MARC code is the one described in [11]: for each molecule, the total internal partition functions are tabulated every 25 K from 60 to 3010 K and then are interpolated at the requested temperature by a 4-point Lagrange interpolation.

RAL have consequently modified FM2D to be able to use the MARC partition functions as a module. The result for the single layer atmosphere where FM2D is run with the MARC partition functions is shown in Figure 9. The residuals have been reduced by more than an order of magnitude. Extrapolating these findings on the initial

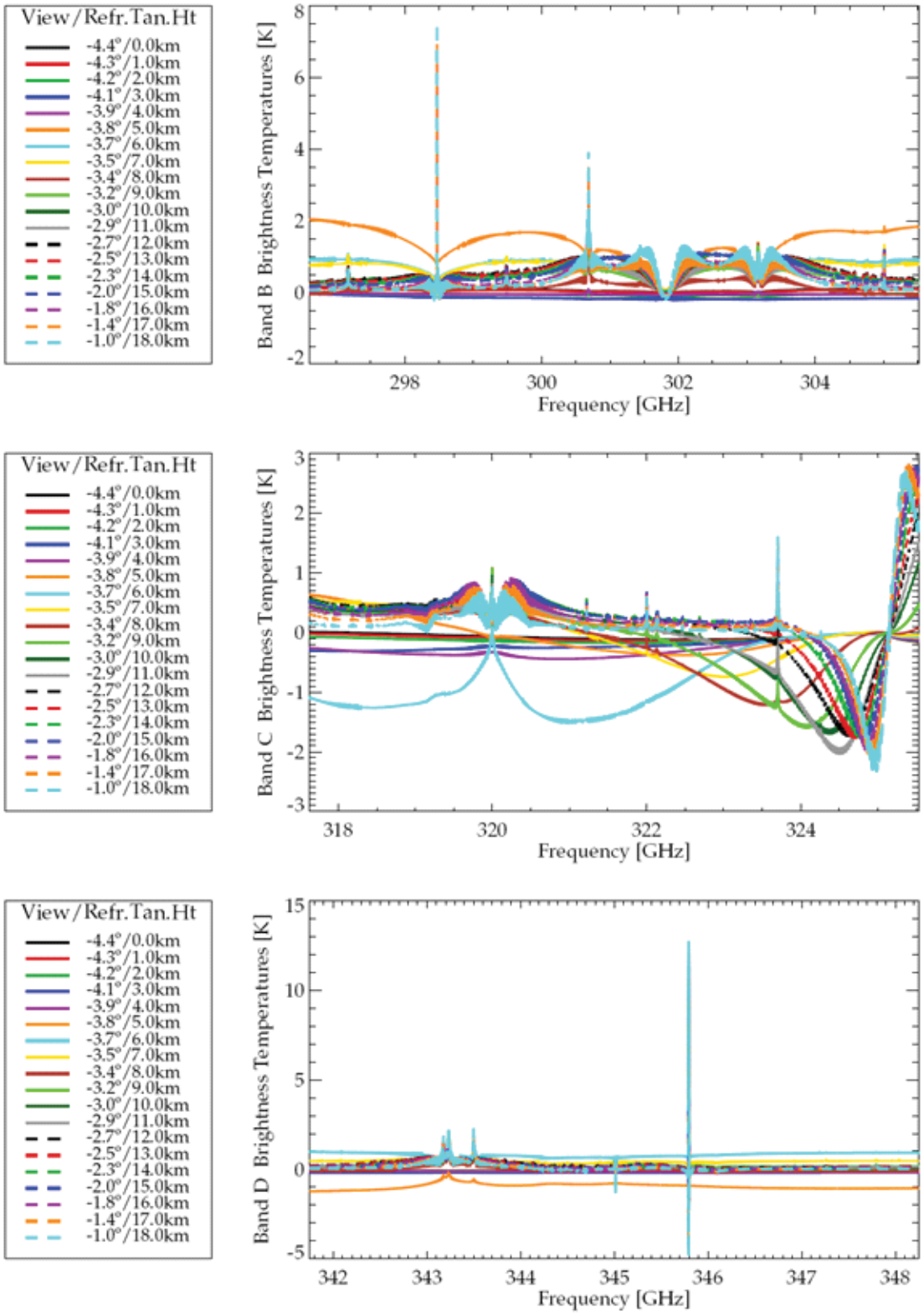

Fig. 5: Monochromatic simulations based on initial input parameters and model settings

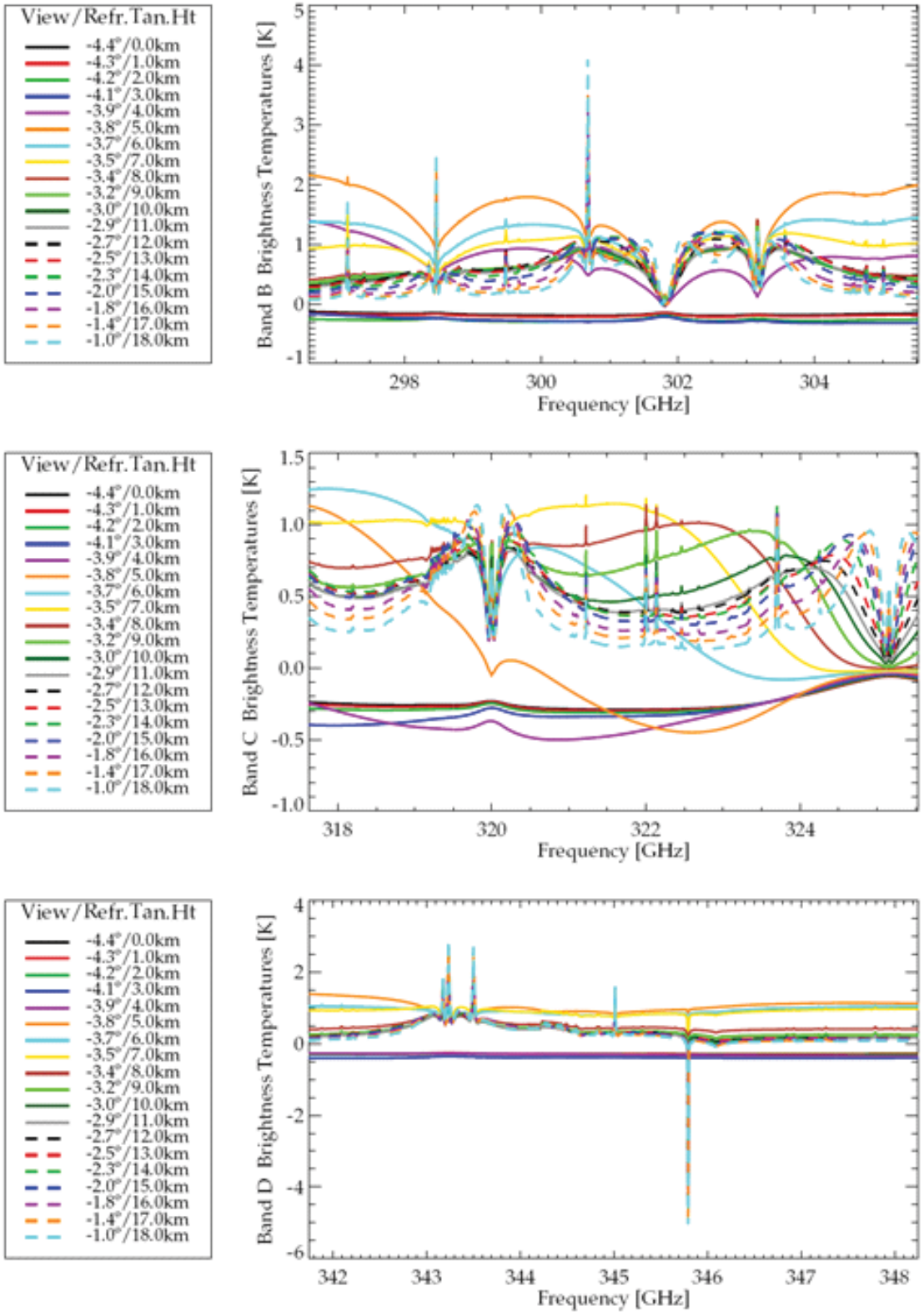

Fig. 6: Residuals from simulations with the new, very fine altitude grid and profiles

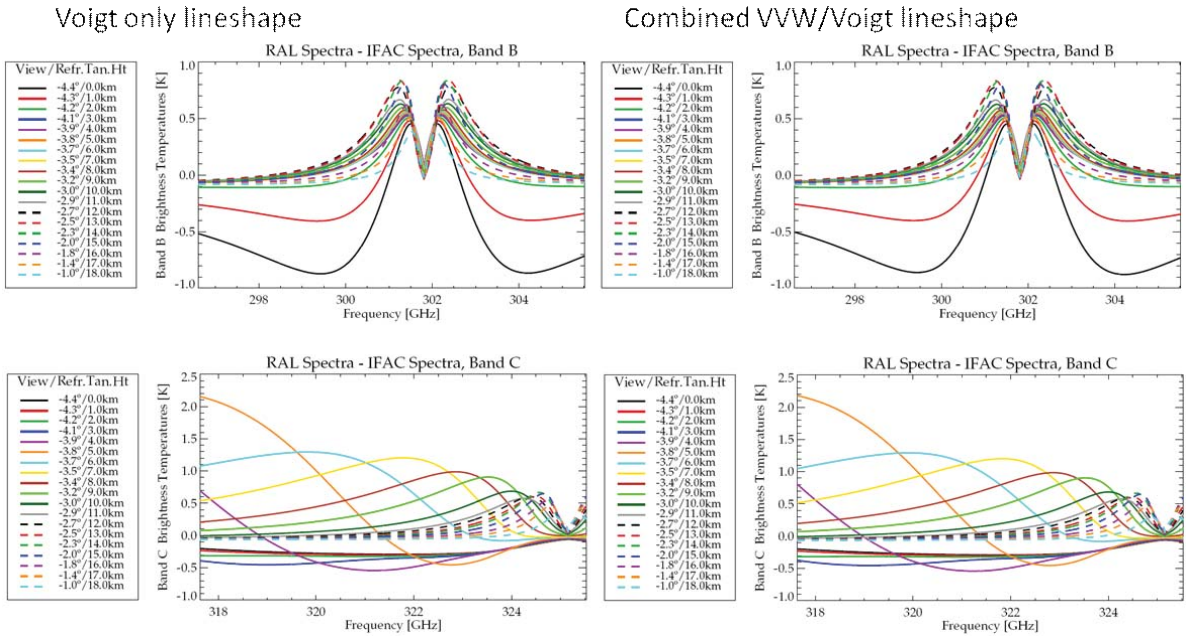

Fig. 7: Comparison of single line residuals for ozone (top row) and water vapour (bottom row). The differences are indistinguishable whether Voigt line shape is used (left column) or whether we use the combined Voigt/VVW line shape (right column)

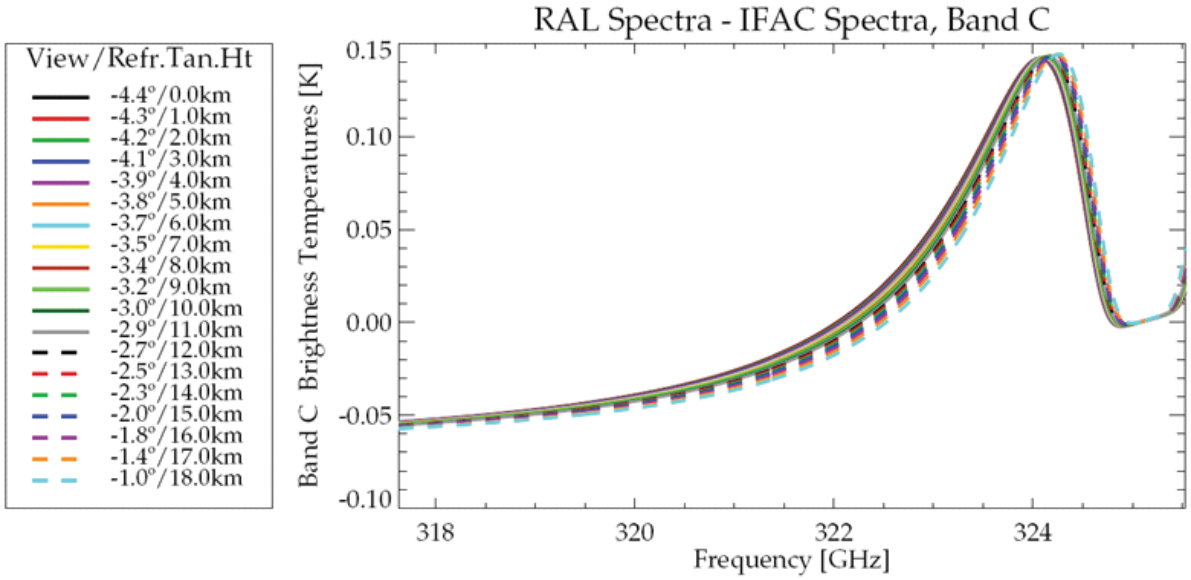

Fig. 8: Residuals for a single layer atmosphere of 250 K, 100 hPa and 10 ppmv H_2O

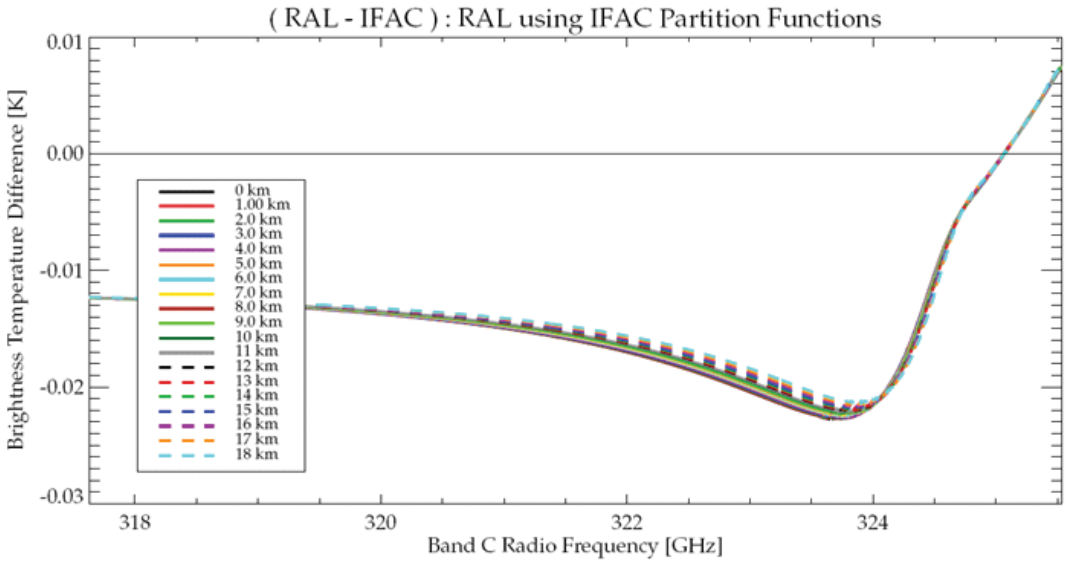

Fig. 9: Residuals for a single layer atmosphere after the FM2D code had been upgraded to use the MARC partition functions

results for the full atmosphere (Figure 5) indicates that the current discrepancies of roughly 2 K would be reduced to below 0.1 K, which is the acceptable threshold for monochromatic simulations.

3.8 Final monochromatic simulation

Applying the partition function upgrade in FM2D to monochromatic simulations of the full atmosphere yields the results shown in Figure 10. As expected, the residuals are within the 0.1 K threshold we have set ourselves as a target. The exceptions are some remaining spikes, but these will be flattened by the instrument line shape convolution discussed in the following section.

3.9 Instrument line shape

The instrument line shape convolution was first applied to the idealized case of the single layer atmosphere.

Figure 11 shows the residuals for the single layer atmosphere after the ILS convolution. The maximum error has increased from 0.02 K of the un-convoluted case (see Figure 12) to 0.04 K, which is still very low, and the average error is still below 0.02 K.

Figure 12 shows the comparison of the spectral radiances in all three MARSCHALS bands and for the full atmosphere once the ILS convolution has been applied. The residuals for a full atmospheric scan from 0 km to 18 km are generally within fractions of one tenth of a Kelvin, but the views around the tropopause layer- where the gradients in atmospheric constitution are largest and where potential ray tracing differences will have the largest impact differ by as much as 0.1 K, which is still comfortably within the threshold we are aiming at in this study.

3.10 Atmospheric continuum

There is no common model in both FM2D and MARC to simulate the spectrally flat emissions due to the atmospheric H_2O, O_2 and N_2 continua. FM2D supports the modeling of the atmospheric continuum emission either by use of the Liebe89, Liebe93 or CKD continuum model (see Section 3.1), or by explicitly specifying a column of absorption coefficients at each model grid level. MARC uses the continuum model formulation given in the ESA study by Verdes [26].

To get a first estimate of the expected impact the use of a different continuum model would have, RAL have performed a direct comparison of the three following continuum models: Liebe89, Liebe93 and the IFAC continuum model. In this study, the continuum absorption coefficients have been calculated in the 10 - 15 cm^{-1} interval (300 - 450 GHz) for a given atmospheric composition. The results of this comparison are shown in Figure 13.

The observation we have made is that the IFAC continuum model seems to follow the Liebe93 model in the way it evolves over altitude (exceeding Liebe89 at low altitudes but falling short of Liebe89 at high altitudes),

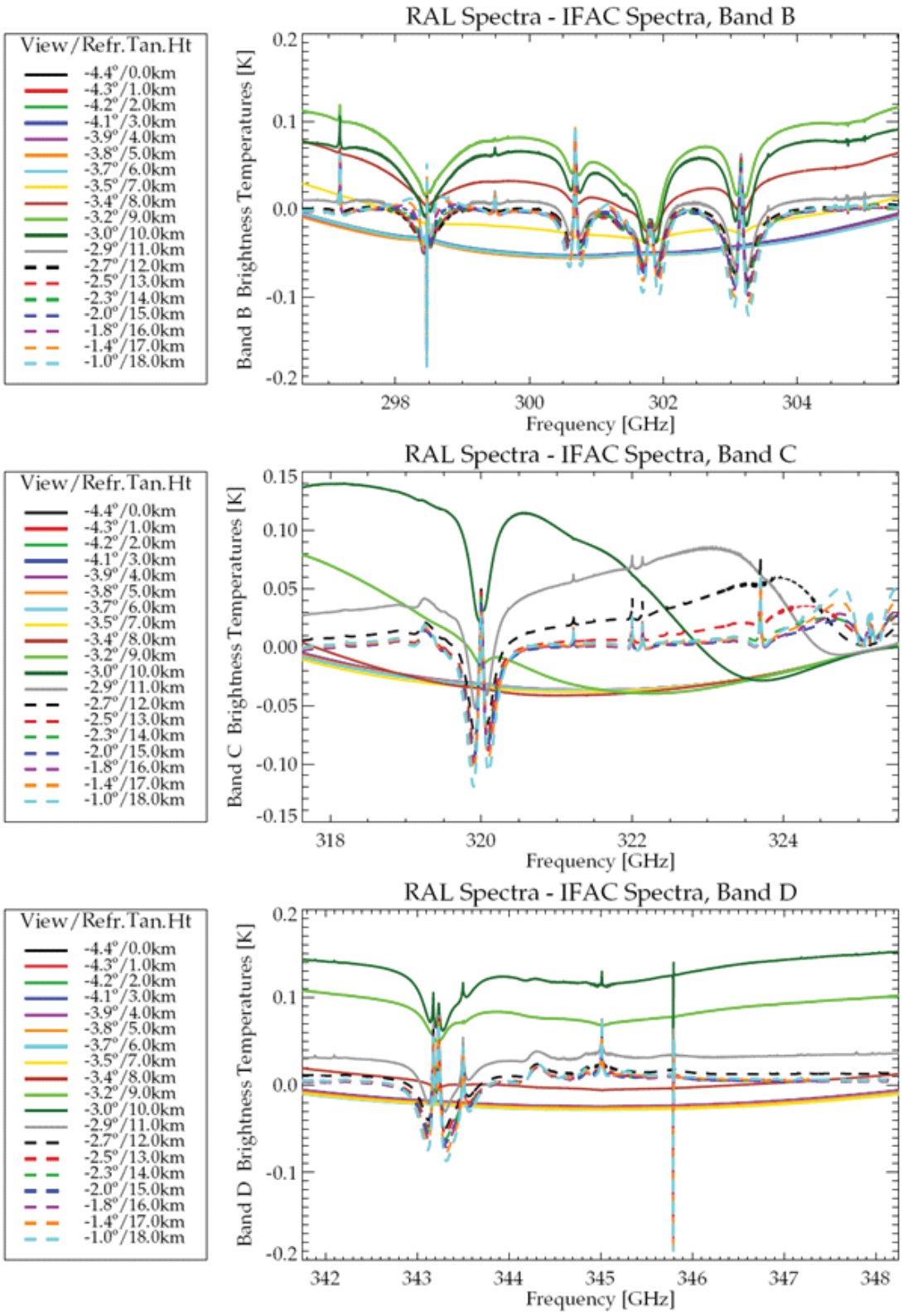

Fig. 10: Monochromatic simulation of the full atmosphere (FM2D is implementing the MARC partition function routine)

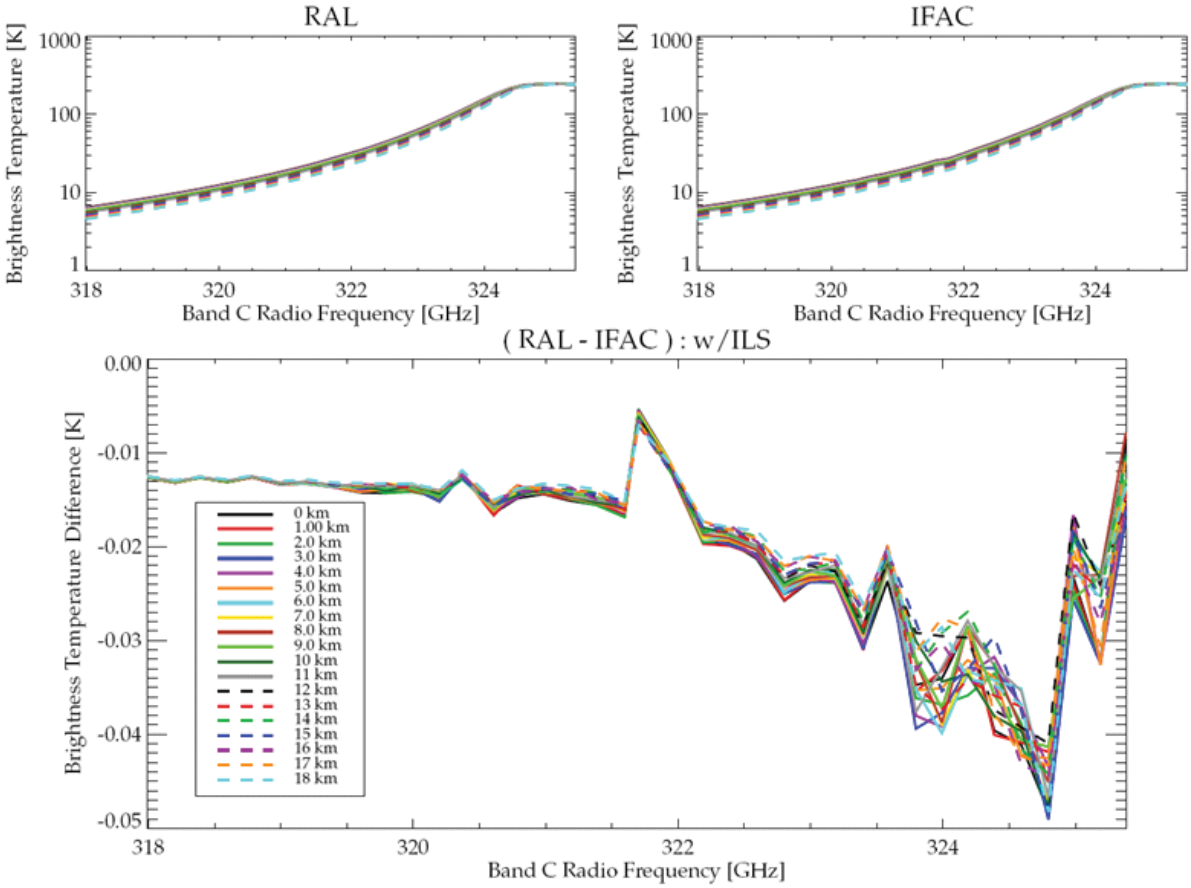

Fig. 11: Residuals for the single layer atmosphere scenario with the Instrument Line Shape (ILS) convolution applied

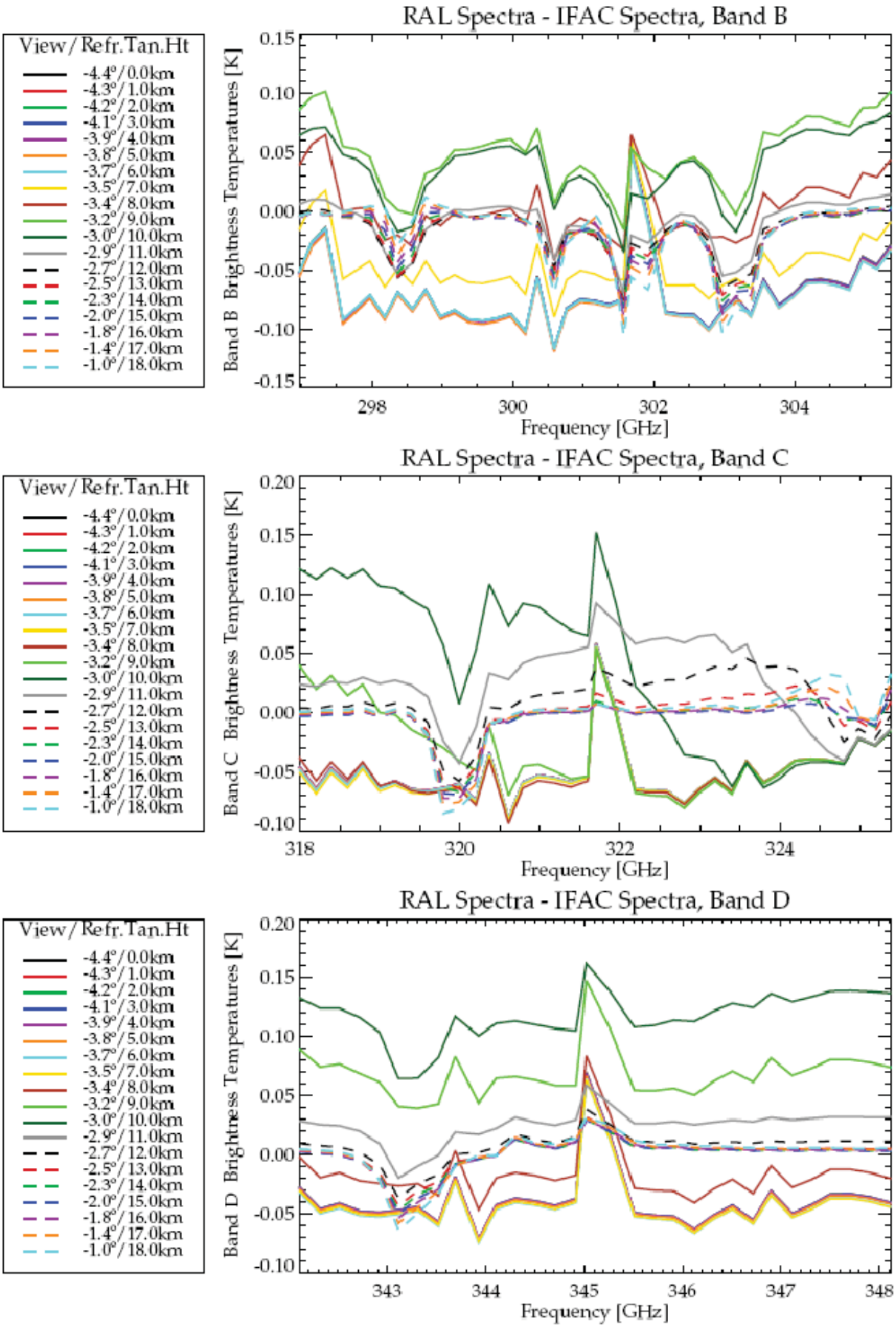

Fig. 12: Comparison of spectral radiances for all three bands after the spectral response (ILS) convolution

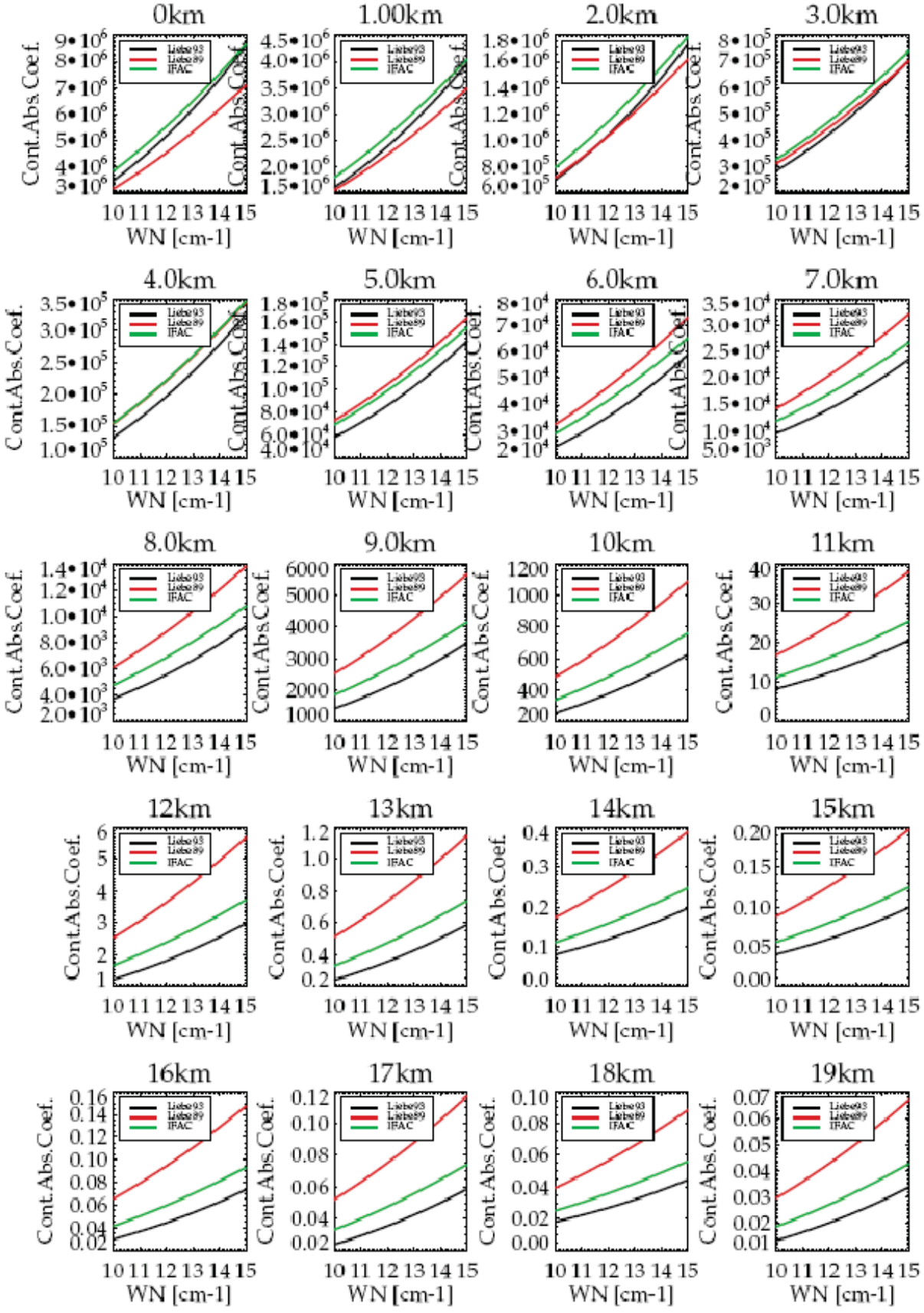

Fig. 13: Comparison of the IFAC continuum model with Liebe89 and Liebe93 at different altitudes

while at the same time returning consistently lower values in comparison than Liebe93. In any case, the 3 models are distinctive enough to conclude that not any one model can be used instead of the other one, so for the onset of the study RAL are using the IFAC continuum model formulation for their simulations.

Figure 14 shows the comparison of monochromatic spectral radiances for all three bands including the atmospheric continuum contribution. The observed discrepancies are generally well within the 0.05 K levels, with only the 10 km view reaching a max discrepancy of 0.08 K. Compared to the monochromatic case without continuum (shown in Figure 10) the discrepancies have actually been slightly reduced, which we believe could be due to the fact that the spectral features are attenuated by the continuum contribution (spectral lines are less steep) and that therefore errors linked to spectral line-shape or line-width have a reduced absolute impact.

Figure 15 shows the same comparison, but this time the spectral response functions (ILS convolution) are applied as well. The overall discrepancy is of the order of 0.05 K with individual maximum spikes to 0.1K. These numbers again are slightly more favorable than in the corresponding case without atmospheric continuum (Figure 12).

3.11 Atmospheric refraction

We have identified that the two models use slightly different formulas in order to compute the refraction of a beam of radiation due to the atmospheric density and water vapour profiles (dry and wet terms).

The refractivity profiles returned by the two formulas do differ, but to get an indication of the impact that different refraction formulas will have on the radiative transfer a direct comparison of refracted tangent altitudes is shown in Figure 16. Figure 17 shows the impact on the refraction formula on the spectral radiance, and again the differences are marginal and therefore insignificant for the outcome of this study. Therefore for the remainder of this study each forward model code will be run using its native refraction code. The conclusion from this comparison is that the impact of the selection of refractivity formula on actual ray tracing (e.g. tangent altitudes) is insignificant.

Figure 18 shows the residual spectral radiances in all three MARSCHALS bands when refraction is taken into account (in addition to the spectral response convolution and the atmospheric continuum contribution). The differences between the two models are now generally in the range of $\pm$ 0.1 K, with the (exceptional) maximal difference of 0.3 K for the least well behaved view at nominal 12 km (refracted 11.6 km). Even this maximal discrepancy is still well within the worst case threshold of 1 K defined at the start of the study, and average values are in good accordance with a stricter threshold of 0.1 K, which is already significantly below the noise level of the radiometer.

3.12 Field Of View convolution

The FOV used in the study are shown in Figure 19. The FOV, which have been normalised to unity for the sake of the convolution, are the same ones as used for the analysis of the Darwin measurement campaign. This is because when the input parameters had to be defined at the outset of the study new measurements of the antenna had not yet been available. Also shown in Figure 19 are the angles of the 13 pencil beams at which the antenna response is sampled for the convolution.

Figure 20 shows the differences in spectral radiance between the RAL forward model FM2D and the IFAC forward model MARC for all three spectral bands. These simulations depict the full set of instrumental and atmospheric parameter, i.e. spectral response functions (ILS), antenna convolution (FOV), atmospheric continuum and refraction. We show the results for an un-refracted tangent view at 10 km sampled by 13 pencil beams as shown in Figure 19. The 20 km view was chosen because in previous simulations this is where the largest discrepancies had been observed. Other views will be better behaved than this one, so the numbers we get for the 10 km view are a worst case scenario.

Figure 20 shows generally flat residuals of the order of 0.02 K - 0.03 K, depending on spectral band, with a singular spike of 0.05 K - 0.1 K in amplitude at the frequency of the IF notch filter channel. We have established the origin of the spike in the section on ILS convolution, illustrated in Figure 10. But even this spike is within the most stringent threshold value of 0.1 K, so there is no need for further actions.

3.13 Conclusions and lessons learned

Table 1 shows an overview of the differences δT between the two forward model spectra at various milestones of the FM comparison study. For each spectral band individually, the overall residual is listed in the first column (Avg). In scenarios where we observe differences that are significantly larger than the average value these outliers are listed in the second column (Max). This is e.g. the case where spectra match to within a uniform level at most

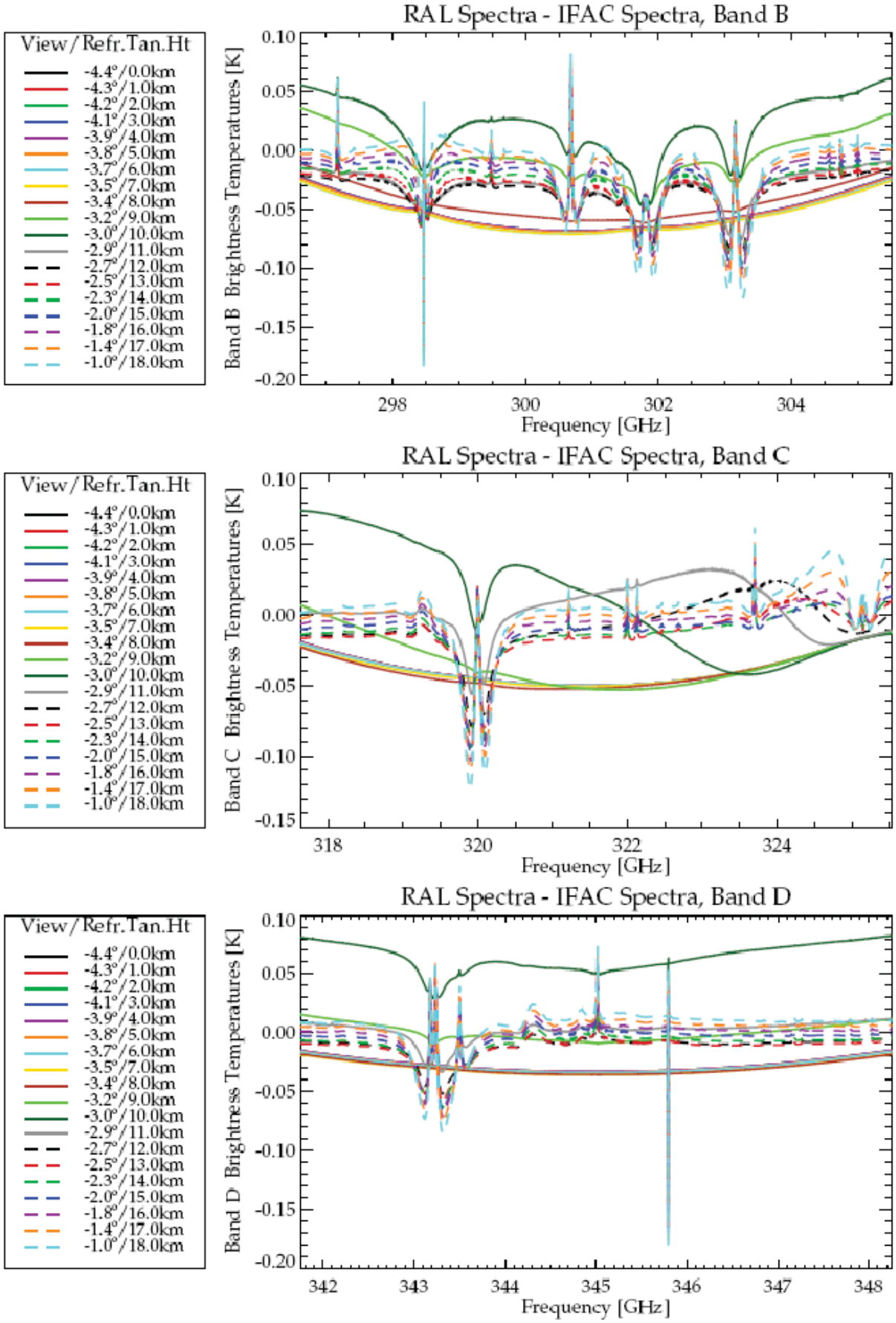

Fig. 14: Comparison of monochromatic spectral radiances where FM2D uses the IFAC partition-function and continuum-emission routines

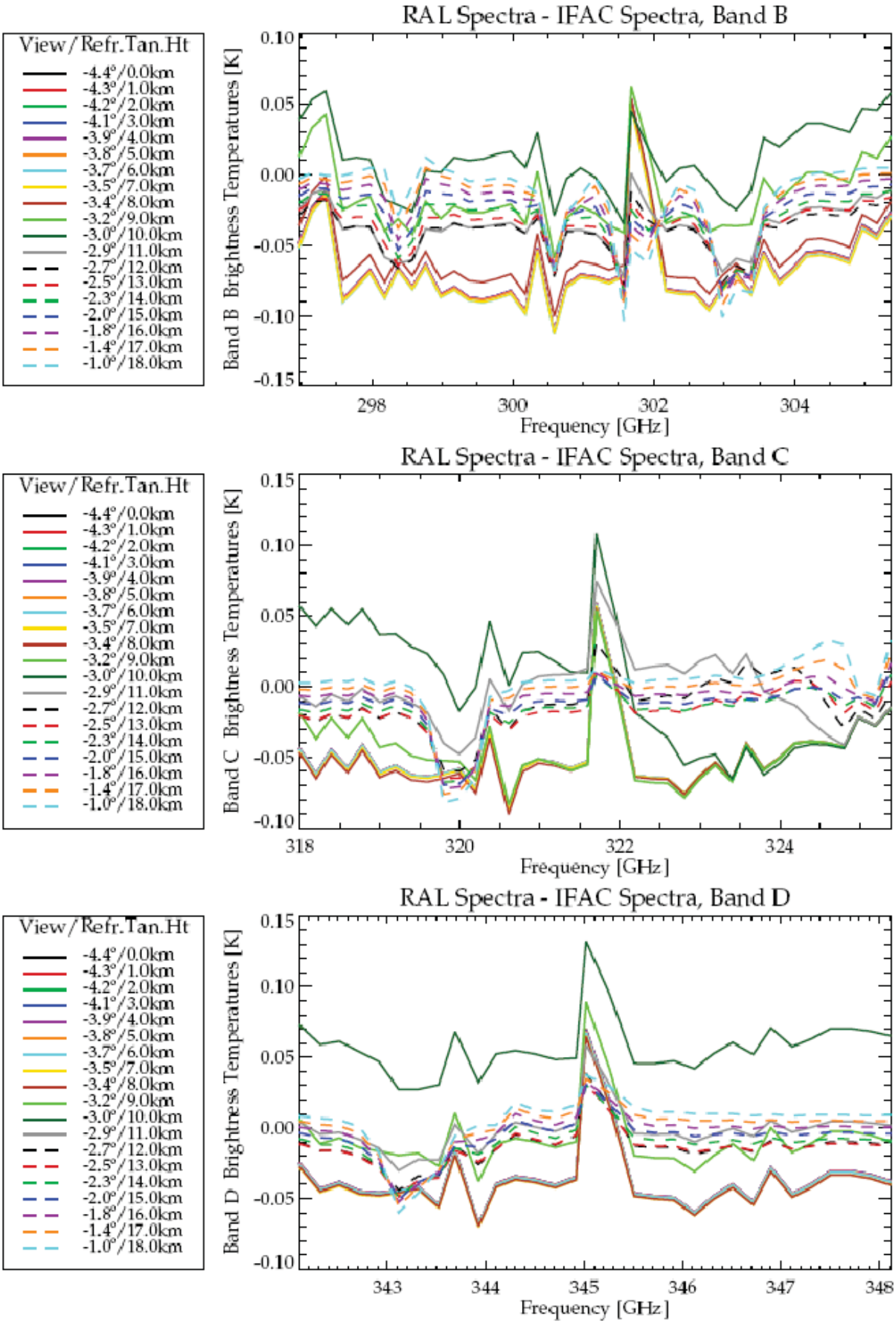

Fig. 15: Comparison of spectral radiances after the spectral response convolution (ILS), where FM2D uses the IFAC partition-function and continuum-emission routines

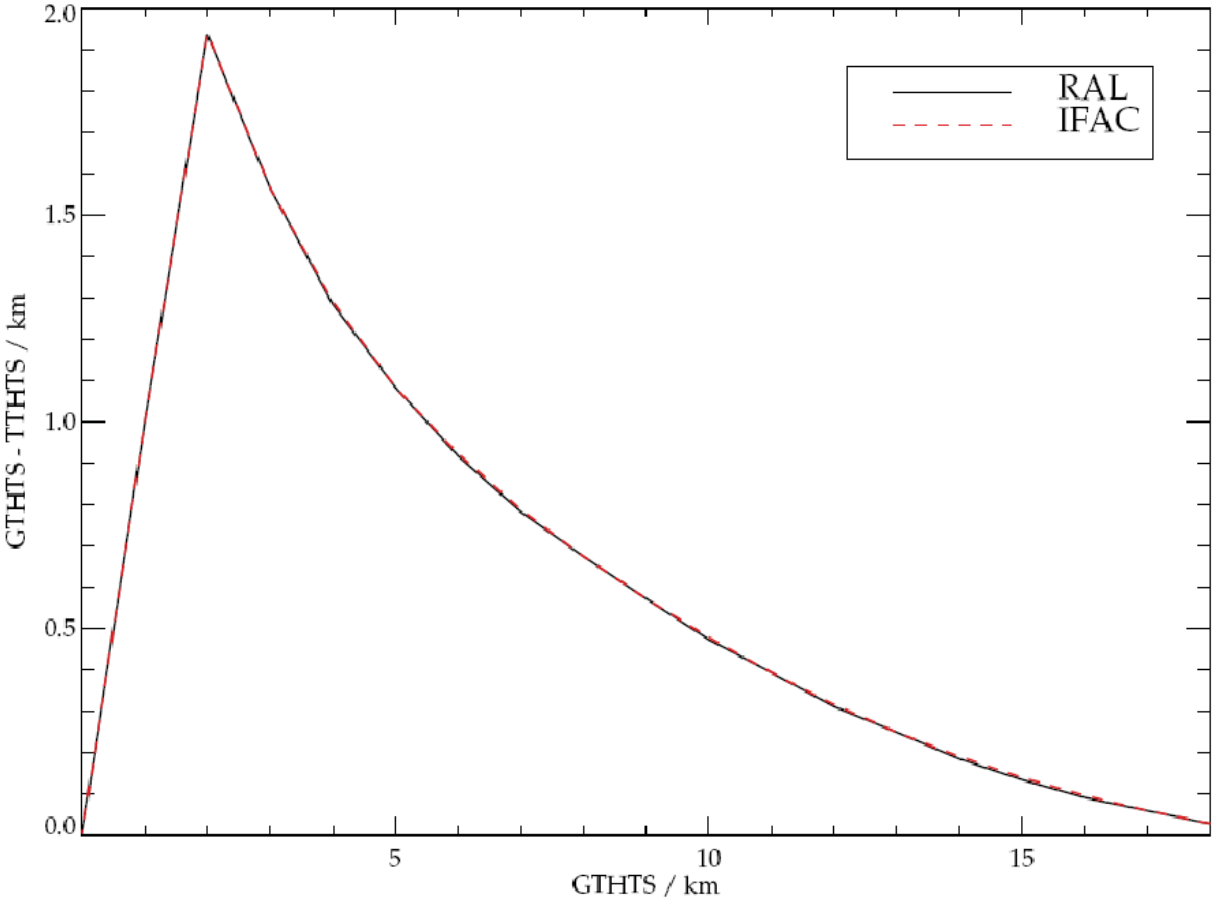

Fig. 16: Difference between refracted and non-refracted tangent altitudes for the two different formulations of refraction by RAL and IFAC (for altitudes below 2 km the refracted beams intersect with the earth surface, in which case an altitude of Zero is defined). The difference between the two formulae is negligible

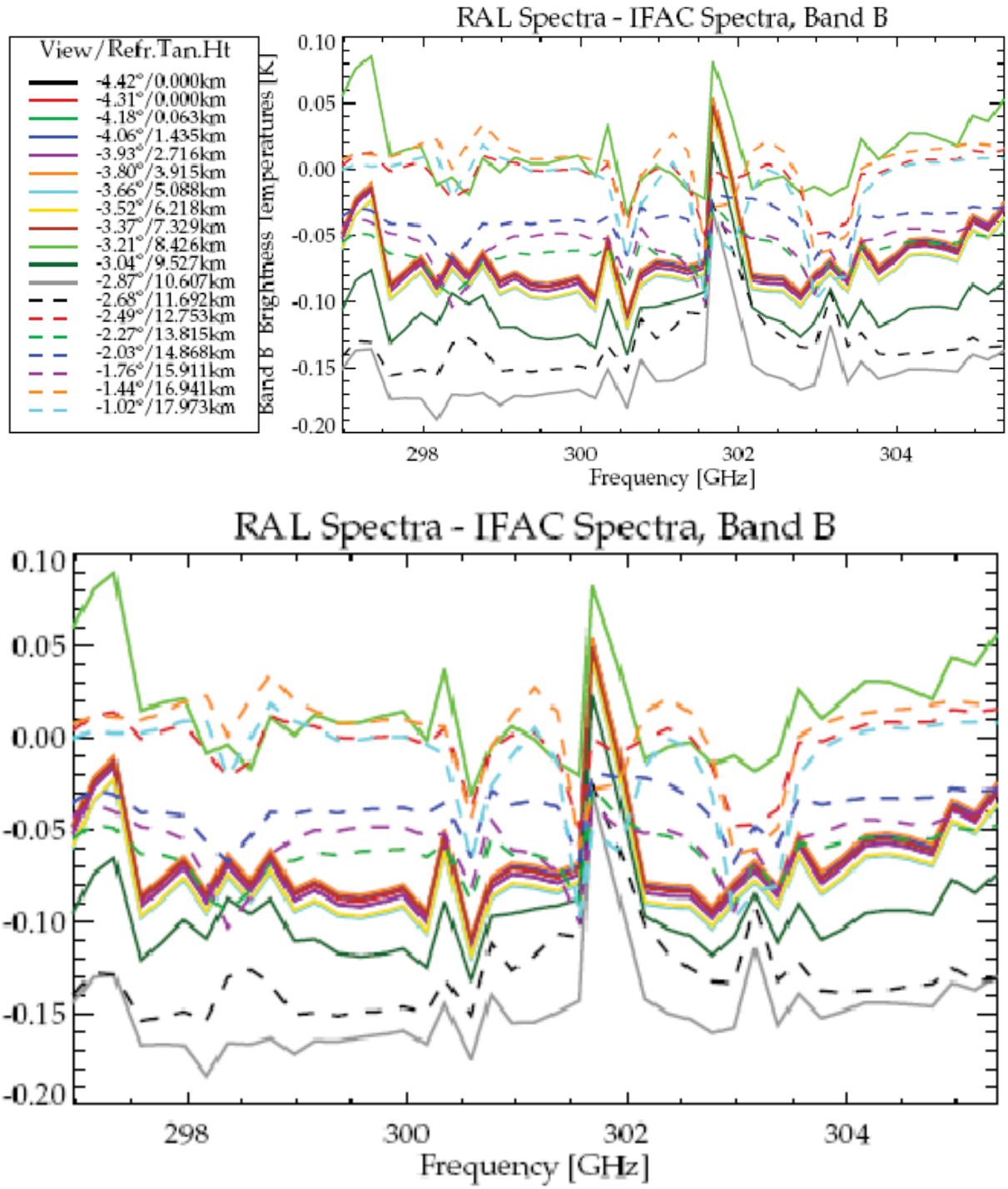

Fig. 17: Comparison of refracted spectra using the RAL refraction code (top panel) and the IFAC refraction code (bottom panel) for Band B. The differences are at levels insignificant to the study

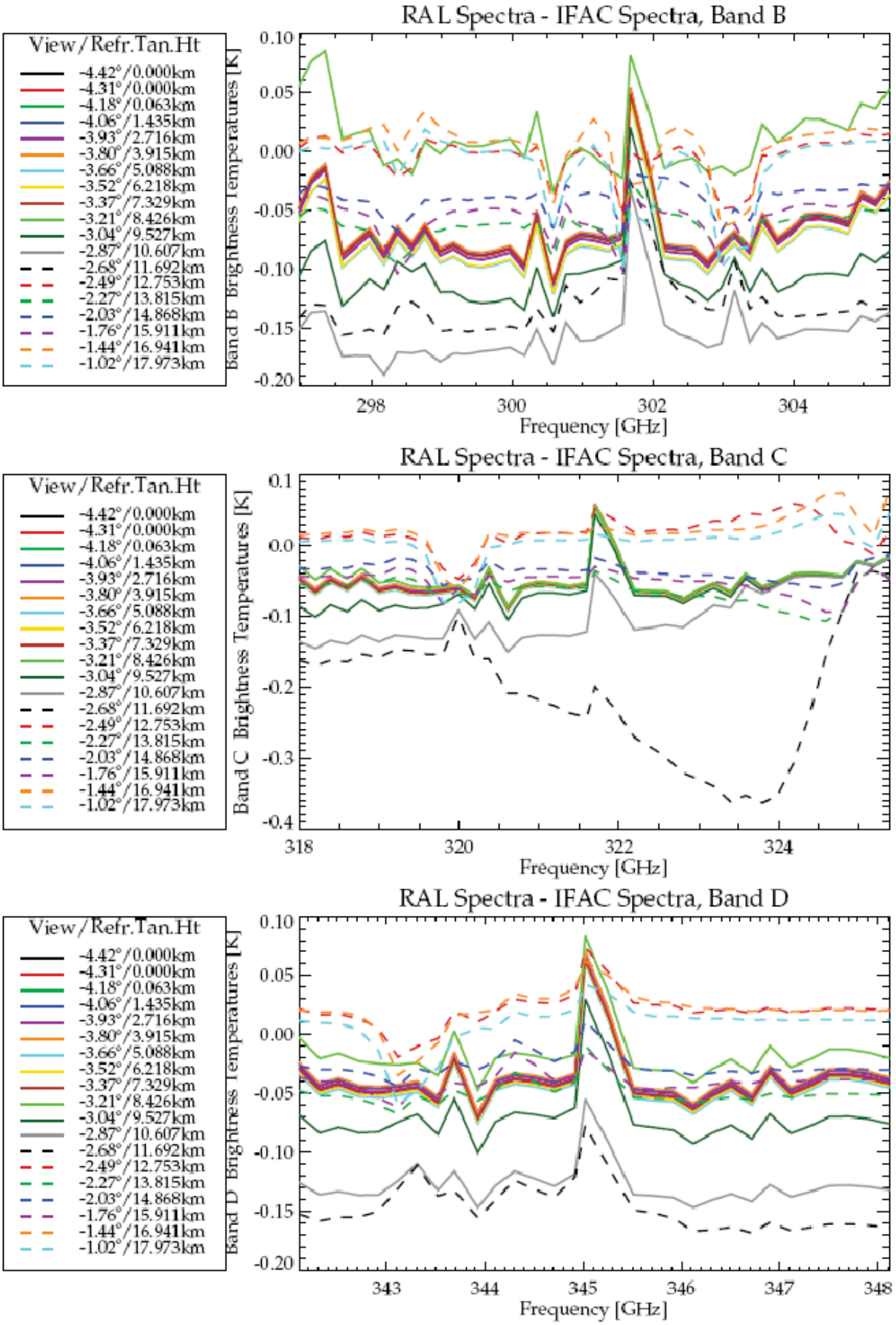

Fig. 18: Comparison of RAL and IFAC spectral radiances including refraction (in addition to ILS convolution and atmospheric continuum contribution

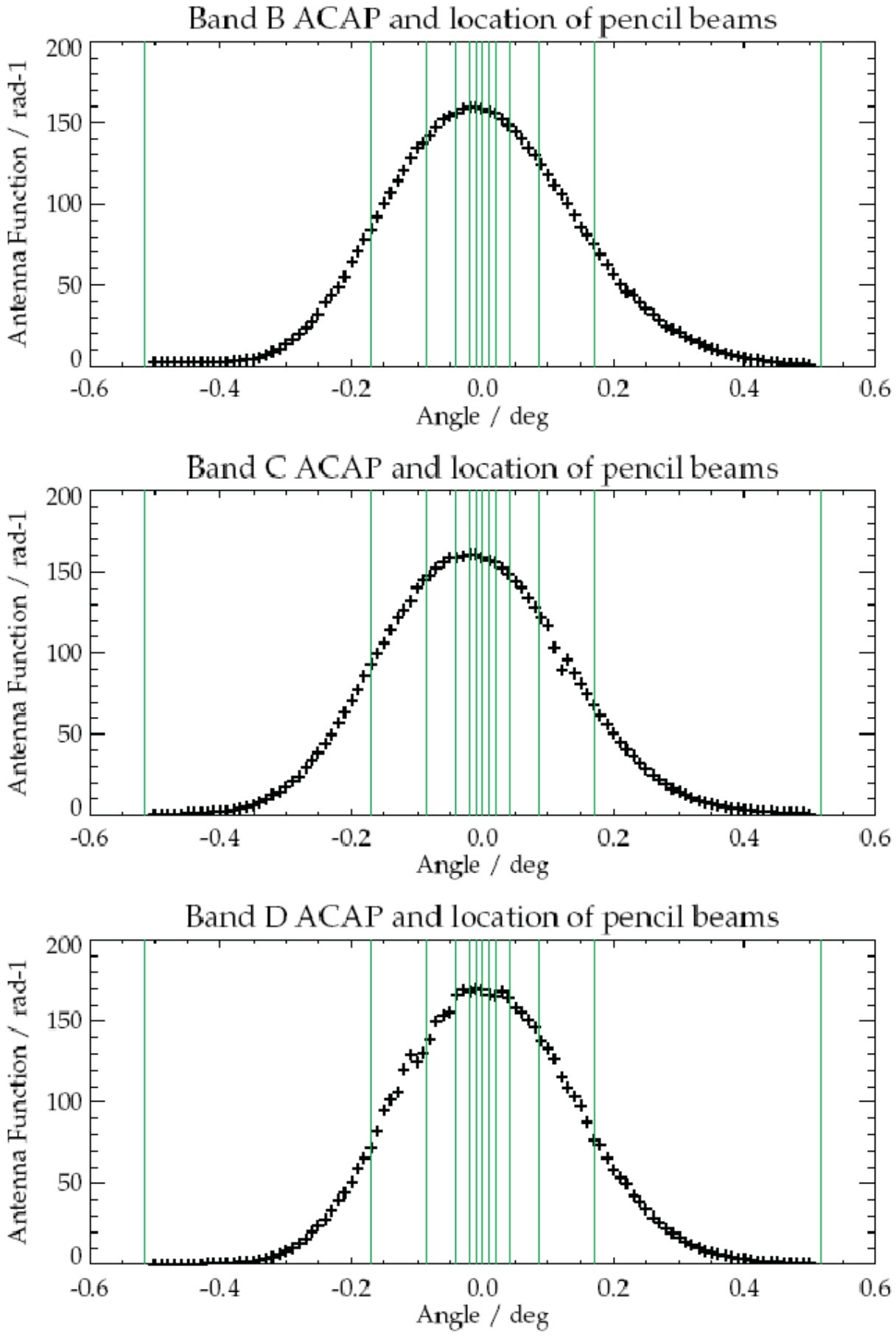

Fig. 19: FOV used in this study, together with the location of pencil beam angles used for the field of view (FOV) convolution

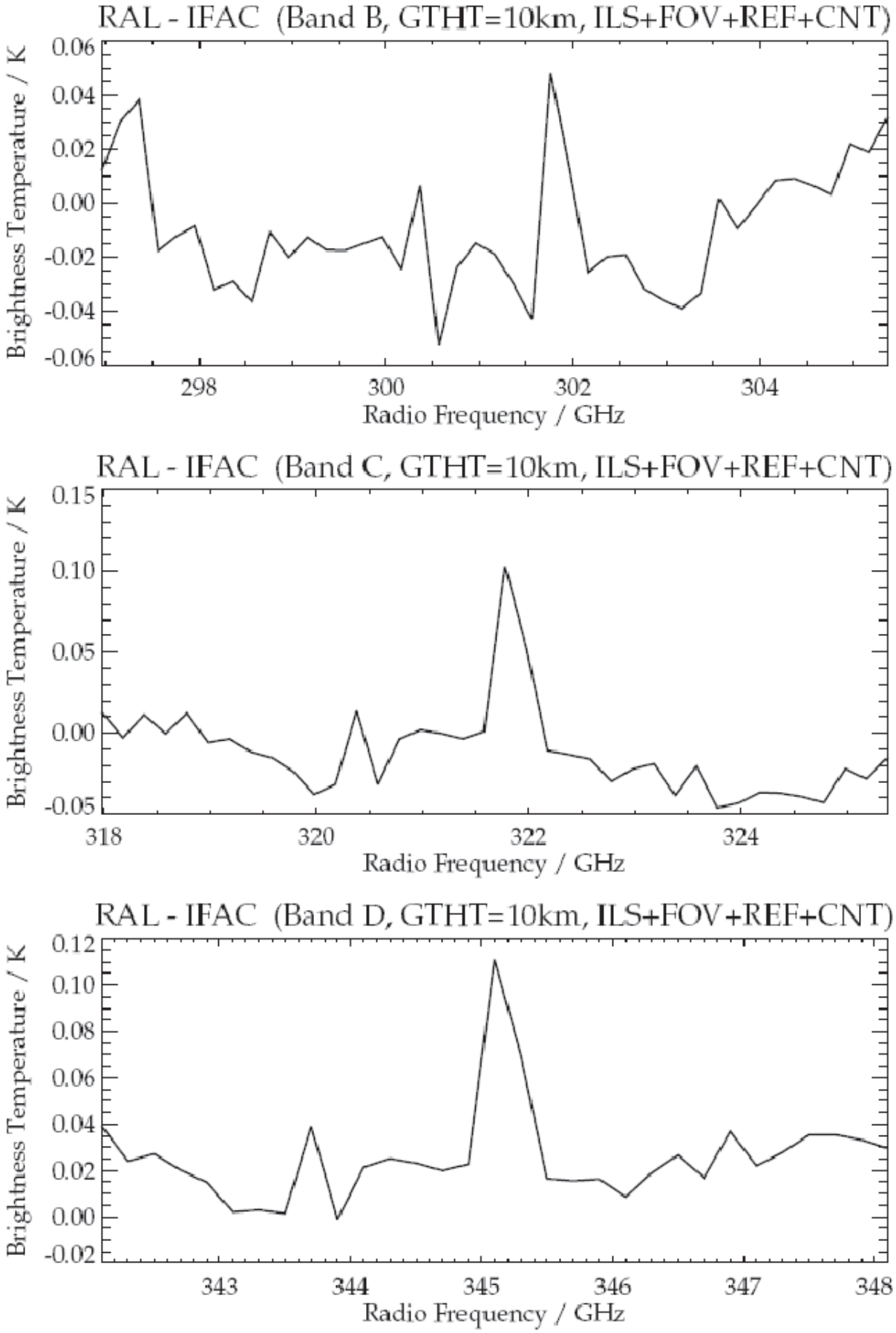

Fig. 20: Final comparison of radiance differences between FM2D and MARC for the most divergent 10 km geometrical tangent view (all instrument and atmospheric parameters accounted for)

frequencies bar some delta spikes from mesospheric layers. In this example the average number would indicate the broadband consensus, whereas the maximum number would indicate the discrepancy at the peak level. Similarly, if all but 1-2 views within a full atmospheric scan show comparable differences, then the average number will indicate the residual for a typical view, whereas the maximum number will give the residual of the atypical view.

Once the discrepancies at the spectroscopic level had been sorted out, the match between the two different forward models became satisfactory even to within the strictest of thresholds of 0.1 Kelvin! That match could be upheld even by adding the various instrument effects, like the ILS function, the FOV convolution, as well as atmospheric effects like beam refraction and continuum emission/absorption. Not shown in the table below are some of the intermediate results from the numerous iterations at every step which were sometimes necessary to iron out computational issues.

Tab. 1: Summary of the differences in spectral radiance δT at the individual steps of the FM comparison study

Band	B	B	C	C	D	D
Experiment	Avg (K)	Max (K)	Avg (K)	Max (K)	Avg (K)	Max (K)
Initial monochromatic simulation	1.5	7	1	3	2	12
+ Pressure frequency shift	1.5	4	1	1.3	1.5	4
Finer altitude grid in Mesosphere	1.2	2	0.7	1.2	0.6	1.4
Finer altitude grid in UTLS	0.3	0.6	0.3	0.4	0.2	0.4
Partition functions	0.08	0.11	0.06	0.15	0.07	0.15
+ Instrument line shape	0.08	0.1	0.06	0.15	0.07	0.15
+ Atmospheric continuum	0.08	0.08	0.08	0.1	0.06	0.13
+ Atmospheric refraction	0.15	0.15	0.1	0.3	0.08	0.16
+ Field Of View convolution	0.02	0.05	0.03	0.1	0.02	0.11

4 Delivered Level 1B data and auxiliary information

Two successfull flights have been performed: one on November 9, 2009 and one on March 10 2010. The first flight was performed during the Test Campaign in November 2009 at mid-latitude (TC9 campaign Oberpfaffenhofen, Germany, Lat. $48.1\,^{\circ}$N, Lon. $11.3\,^{\circ}$E) and will be referred to as the Test Flight. The second flight was performed during the scientific campaign in March 2010 in the Arctic region (PremierEx campaign, Kiruna Sweden, Lat. $67.8\,^{\circ}$N, Lon. $20.4\,^{\circ}$E) and will be called the Scientific Flight.

The measurements strategy adopted by MARSCHALS during the Test and Scientific Flights was the same used for the SCOUT-O3 campaign, that is the scans are made of more than 200 spectra on a single band with the commanded pointing of several sweeps at constant viewing angle and the viewing angle varied at 1 km steps in tangent altitude. The number of sweeps acquired at the same commanded pointing were intended to compensate for the S/N ratio of the real measurements different from the required value of 1 K. During the flight the pointing was not completely actively corrected for the aircraft roll so that not always the observations with the same commanded pointing angle were measured at the same tangent altitude. This makes the intended avergaing procedure impossible and therefore in the analysis each line of sight has to be considered independently. For each flight RAL delivered several versions of the level 1B data, each containing improvements of the data itself or of the auxiliary files.

The level 1b datasets delivered by RAL for the Test Flight are reported in table 2. The first three files were delivered at the beginning of the project and were used for a preliminary anaysis of the Test Flight, reported in section 5, together with the ILS and FOV definition coming from the previous analysis of MARSCHALS data acquired during the SCOUT-O3 Campaign.

At a later stage a new set of data was delivered along with a new noise, FOV and ILS characterization. This final delivery was the one used for the final analysis of the Test Flight.

Also for the Scientific Flight, two different datasets have been delivered by RAL and used for the analysis. In the preliminary dataset, as for the Test Flight, the calibrated spectra and all the related instrumental data have been included by RAL in a single file, from where we have extracted the data and converted them into a format suitable to the code (MARC) used for the retrievals. Again ILS and FOV were the same of the SCOUT-O3 flight. The file delivered by RAL is reported in the first row of Table 3.

On July 2010, RAL provided the new ILS characterization and the new band definitions. The new band definitions are reported in Table 4 and in Figure 21 along with the data used in the SCOUT-O3 analysis. Both the

Tab. 2: List of Test Flight Level 1B data files.

Data File	pointing Correction
mar_20091104_200911261033_00111b_RollAngleCorrectedWith02sFilter.dat	dt02
mar_20091104_200911261033_00111b_RollAngleCorrectedWith10sFilter.dat	dt10
mar_20091104_200911261033_00111b_RollAngleCorrectedWith60sFilter.dat	dt60
mar_20091104_201104080952_00111b.dat	dt02
mar_20091104_201104080954_00111b.dat	dt05
mar_20091104_201104080955_00111b.dat	dt10
mar_20091104_201104080956_00111b.dat	dt20
mar_20091104_201104080958_00111b.dat	dt40
mar_20091104_201104080959_00111b.dat	dt60

Tab. 3: List of the Scientific Flight Level 1B data files.

Data File	pointing Correction
mar_20100310_201003111300_00111b_dt10.dat	dt10
mar_20100310_201010291227_00111b.dat	dt02
mar_20100310_201010291228_00111b.dat	dt02
mar_20100310_201010291230_00111b.dat	dt02
mar_20100310_201010291232_00111b.dat	dt05
mar_20100310_201010291234_00111b.dat	dt10
mar_20100310_201010291235_00111b.dat	dt20
mar_20100310_201010291237_00111b.dat	dt40
mar_20100310_201010291239_00111b.dat	dt60

number of channels and the spectral range covered by the bands have changed in the new characterization. The impact of these changes on the retrieval is described in section 6.3.2.

In October 2010 RAL delivered the final dataset containing different Level 1B files with a new noise characterization. Each file was produced correcting the pointing with a filter of different time width (dt). The list of delivered files is given in Table 3. An example of the new noise characterization with respect to the one provided in the preliminary data set is shown in Figure 22, where the noise level read from the two versions of the Level 1B data is plotted for one scan for each band (scan 10 in band B, scan 12 in band C and scan 11 in band D). A more general overview of the changes in the noise level introduced by the new noise characterization is given in Figure 23, where both the new and the old characterization for the scans from 6 to 53 are reported. As can be noticed from the figure the unrealistic, very low values of the noise level in band C completely disappear. Furthermore the maximum value of the noise level is lower than the old one in all bands. The impact of the new noise characterization on the retrieval is discussed in section 6.3.3.

Respect to the preliminary dataset also a new FOV characterization has been provided in the final release. The new FOV characterization for each band is plotted in red in Fig. 24 together with the old one (red). The impact of the new FOV characterization on the data analysis is discussed in section 6.3.4. The final delivery of the Level 1B file dataset together with new FOV, ILS and band definitions have been used for the final analysis of the Scientific Flight.

Tab. 4: Band definition for SCOUT-O3 and PremierEx

	SCOUT-O3		PremierEx	
Band	initial frequency GHz	n. of points	initial freq. GHz	n. of points
B	294.16	58	296.76	44
C	316.58	45	317.78	39
D	342.30	33	341.90	32

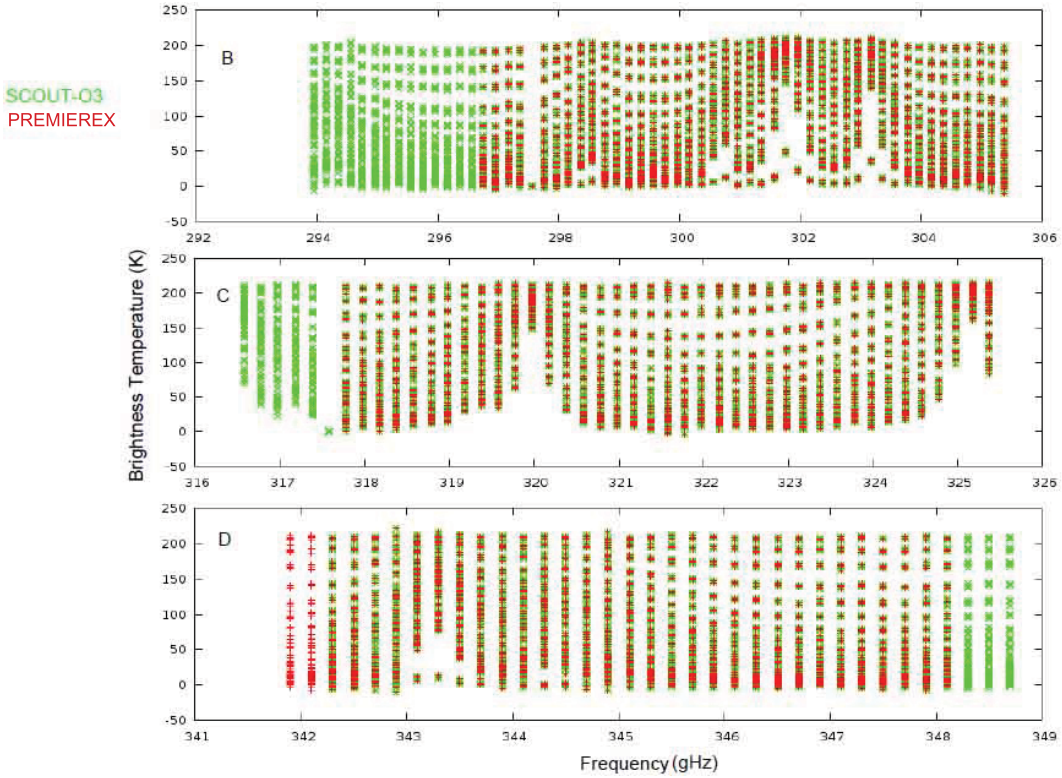

Fig. 21: Bands spectral ranges in SCOUT-O3 (green) and PremierEx (red) dataset.

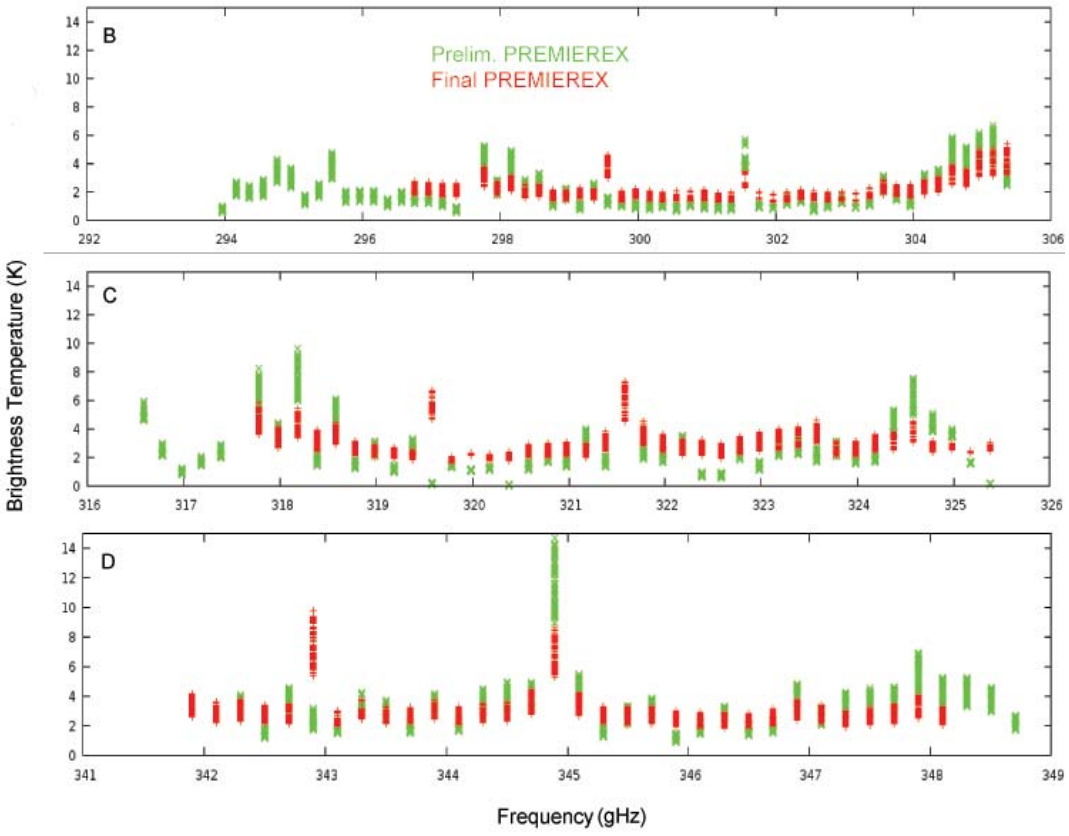

Fig. 22: Noise level as read from the dt10 Level 1B file for scan 10, 11 and 12 of the old characterization delivery (green) and of the new one (red).

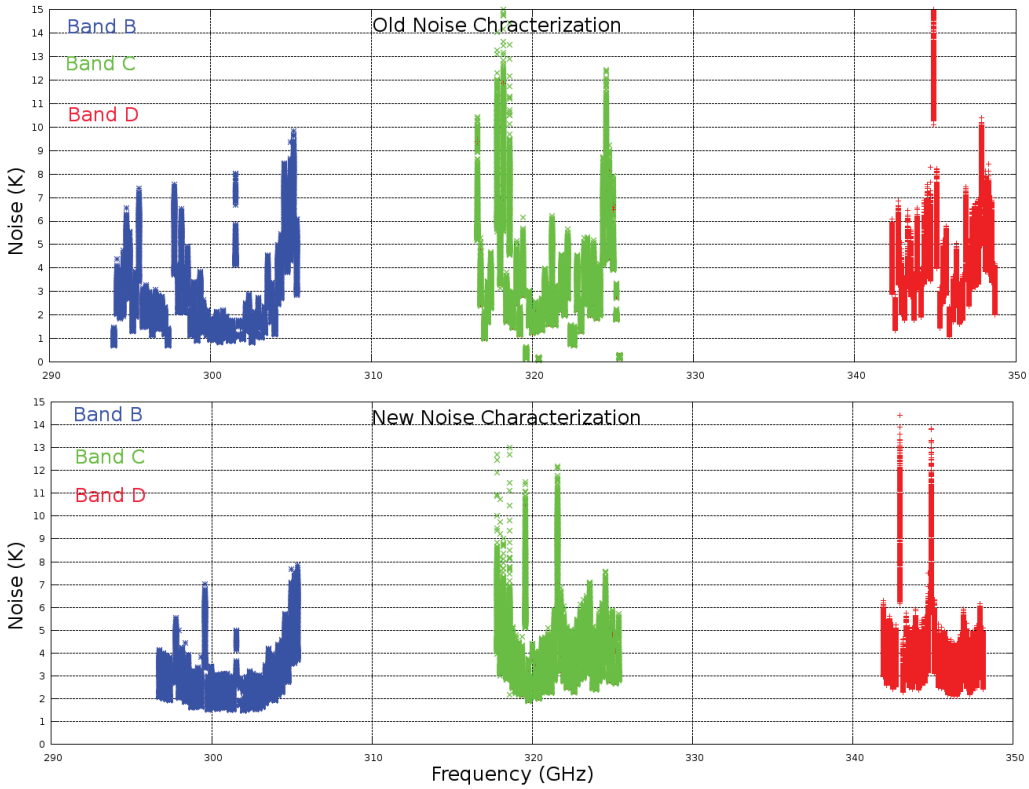

Fig. 23: Noise level values as read from Level 1B files for each band and spectra belonging to scan from 6 to 53 for the old (upper panel) and the new (lower panel) noise characterization dataset.

5 Analysis of MARSCHALS Test Flight measurements

In this section, we report the results of the analysis carried out on MARSCHALS Level 1B data acquired during the Test Flight on 04.11.2009 the delivery of the final Level 1B data for the Test Flight was performed long after the delivery of the consolidated dataset of the Scientific Flight. Therefore all the retrieval optimizations have been done for the Scientific Flight and the results have then been applied to the Test Flight. So it would have been more realistic to report the analysis of the Scientific Flight before the analysis of the Test Flight. However, in this report we wanted to respect the cronological order of the measurements. Therefore in this section we will extensively refer to work described in the subsequent sections.

The Level 1B files delivered by RAL for the preliminary and final analysis of the measurements acquired during the Test Flight are listed in Table 2. For both deliveries, there are different versions of the Level 1 data, each obtained with the pointing information corrected using different time width of the high/low pass filters. All the reported tests were performed on the Level 1 data file corrected with the 10 sec filter width. The noise level used in the analysis was directly read from the Level 1B data. The reported analysis was performed after the Scientific Flight data analysis, therefore the optimization of the retrieval configuration was not repeated. A thorough description of the retrieval choices used in this analysis can therefore be found in section 6.3.

5.1 Geophysical Scenario

5.1.1 Flight overview

The flight track of MARSCHALS Test Flight is shown in Figure 25, while figure 26 reports the altitude of the M-55 aircraft during the flight plotted versus the flight time (UTC).

As can be seen in Fig. 25 the M-55 made a lot of turns during the flight, with the result that MARSCHALS scans sampled the atmosphere in many directions. This is highlighted in the three panels of Fig. 27, that show the position of the tangent points of the scans of band B (top panel), C (central panel) and D (bottom panel) during the flight. In the three panels of Fig. 28 we report the tangent altitudes of the observations of bands B (top panel), C (central panel), and D (bottom panel). The plots show that there is an uneven altitude coverage during the flight and that for some of the scans, such as scan 13, 14 and 31, the altitude distribution of the tangent points covers a reduced range.

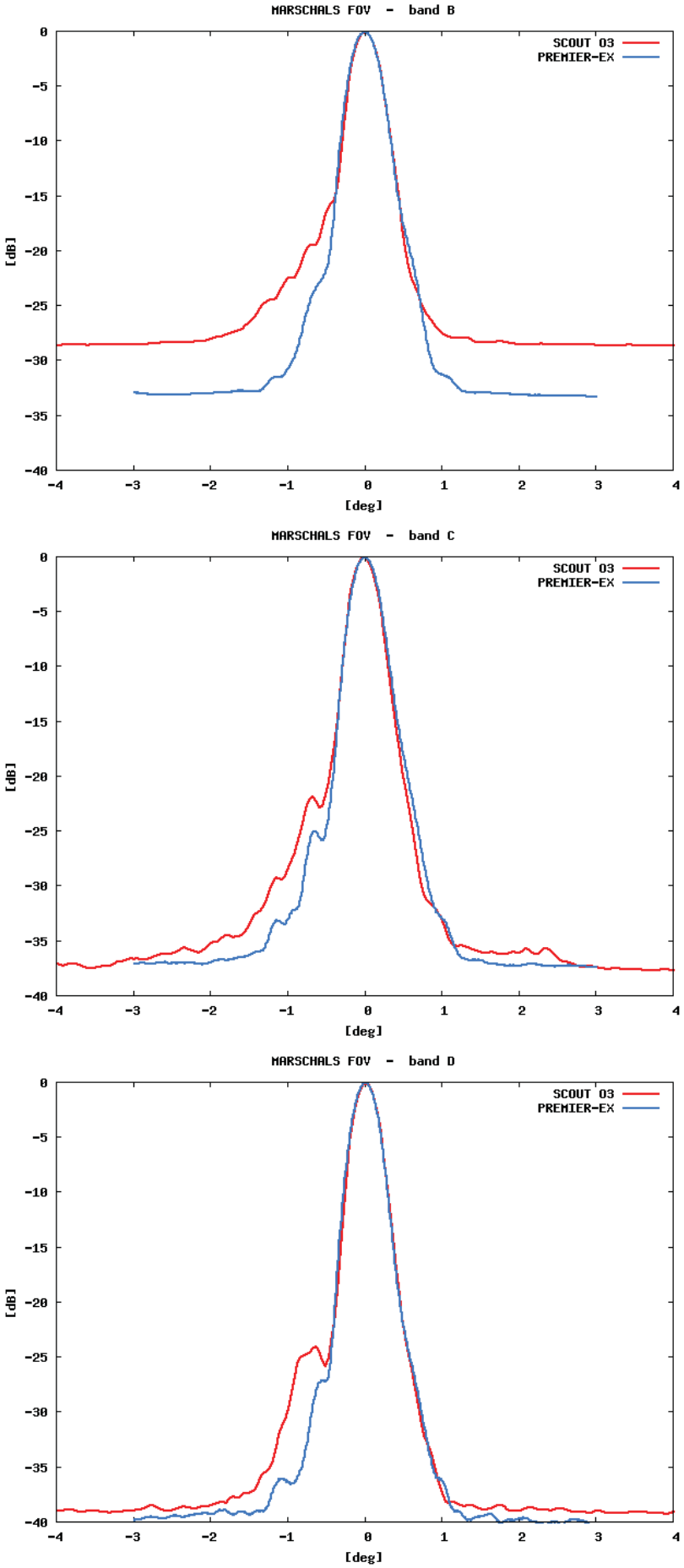

Fig. 24: FOV for each MARSCHALS band in the SCOUT-O3 (red) and PremierEx (blue) dataset.

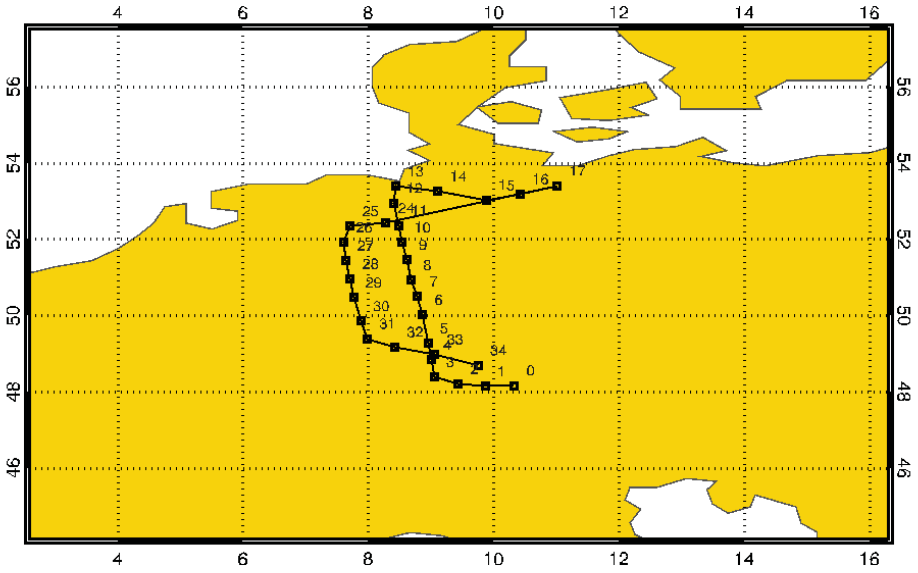

Fig. 25: The TC9 flight track plotted versus latitude and longitude. The black dots show the average position of each scan.

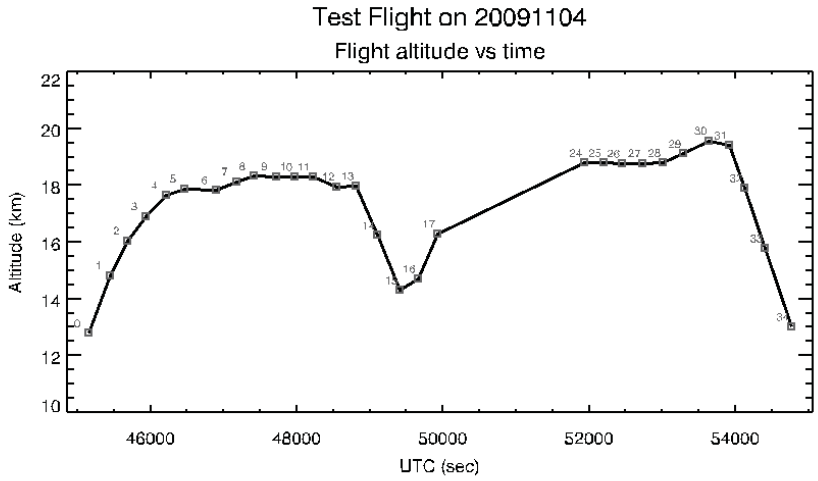

Fig. 26: The flight altitude and the analysed scans position plotted versus the Universal Time Coordinate (UTC)

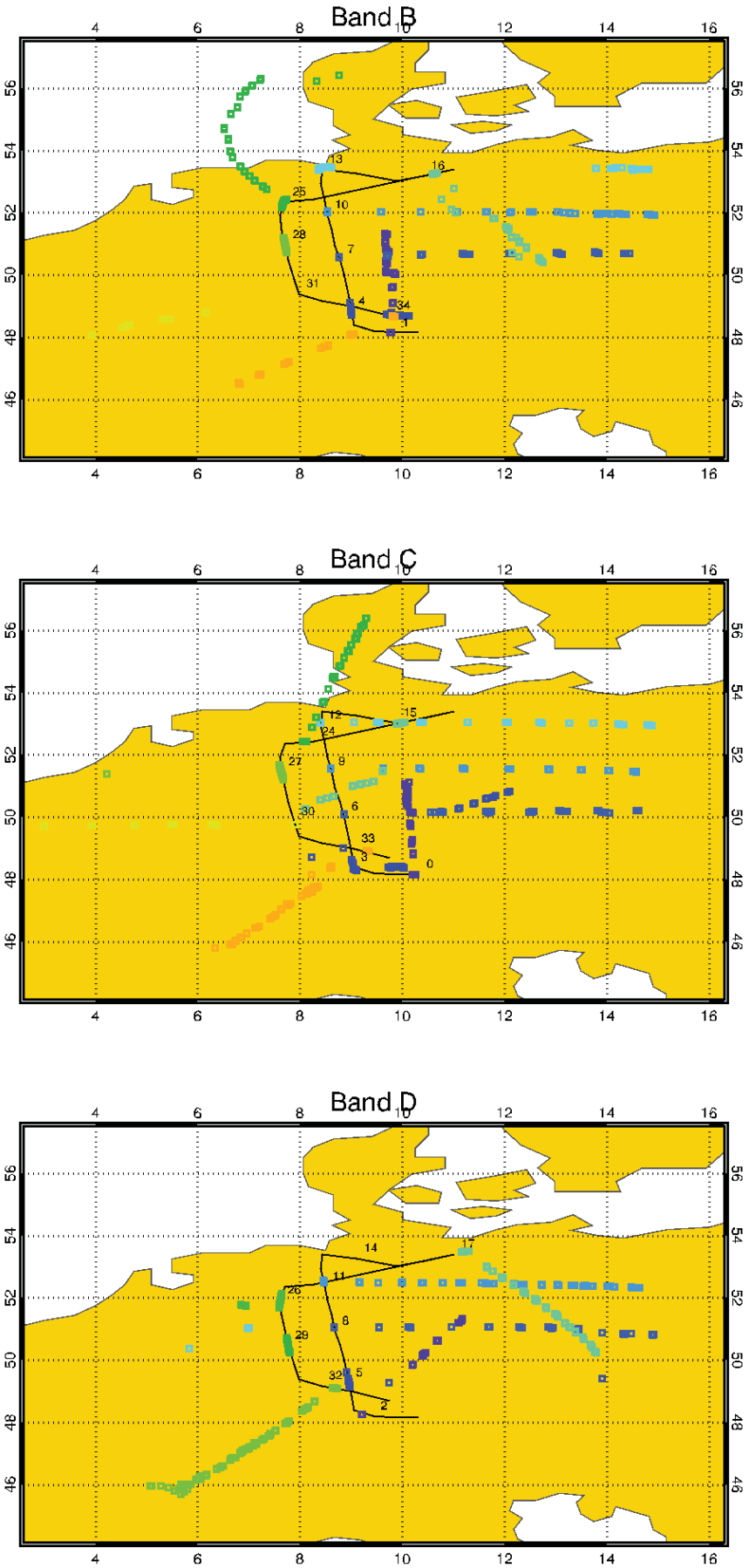

Fig. 27: The flight track with the geolocation of Band B (top) Band C (middle) and Band D (bottom) tangent points plotted versus latitude and longitude

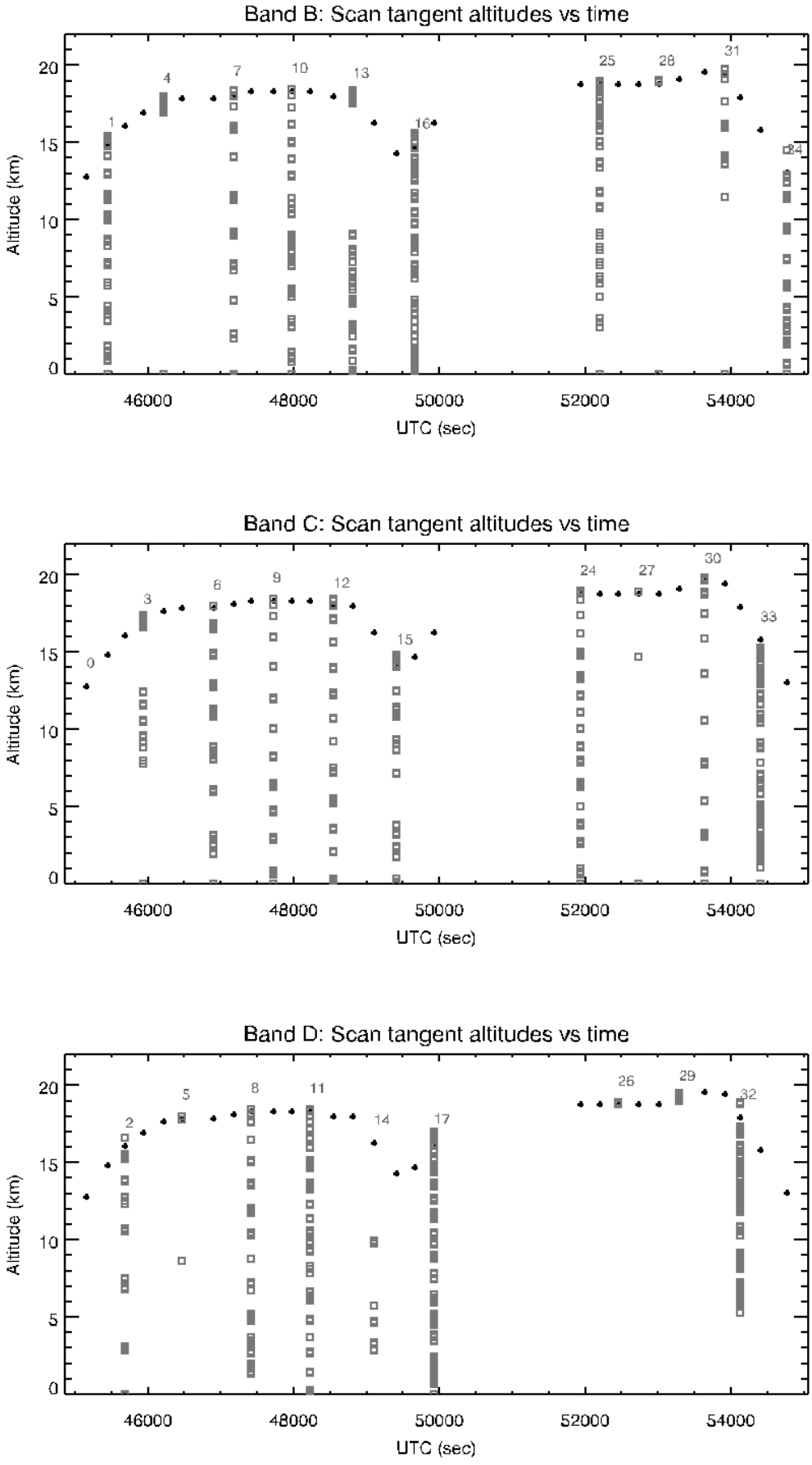

Fig. 28: The flight altitude and the analysed scans tangent altitudes position plotted versus the UTC. Top panel: band B, central panel: band C, bottom panel: band D.

Fig. 26 shows that there are two parts of the flight (from scan 4 to 13 and from scan 24 to 31) where the aircraft altitude was nearly constant, a requirement for having the MARC code working at its best. While from scan 24 to 31 the aircraft made a lot of turns, the part from scan 4 to 13 corresponds also to the part of the flight were the flight track followed a straight line. We therefore expect to have the best data for the analysis from scan 4 to 13. However the preliminary analysis has been performed on all the available scans.

5.1.2 Initial Guess Atmosphere

A preliminary step for the analysis of MARSCHALS observations is the definition of the status of the atmosphere that is used also as a priori information for the retrieved targets. Therefore the initial status of the atmosphere has to be as close as possible to the true status of the atmosphere, in order to minimize the impact of interfering species whose VMRs are not a retrieval target and to have a good a priori estimate of the profiles that are the retrieval targets. As a starting point we have used the IG2 database [19](developed by J. Remedios for the analysis of MIPAS/ENVISAT spectra) for a mid-latitude atmosphere. The IG2 database contains one average profile valid over a wide latitude band, along with the 1-sigma variability of that latitude band. The IG2 profiles were used for the target species N_2O, HNO_3 and CO and for all the interfering species. Temperature, pressure, water and ozone can be extracted from the ECMWF (European Center for Medium range Weather Forecasting) database, on a personalized latitude and longitude grid. So for the ECMWF species listed above we have used a profile personalized for each analysed scan.

5.1.3 Initial Guess Atmosphere: ECMWF data

ECMWF data were extracted from the MARS Archive (Meteorological Archival and Retrieval System). In this database data for Temperature (K), Specific Humidity (Q) (kg/kg) and Ozone Mass Mixing Ratio (MMR) (kg/kg) can be retrieved on a chosen latitude-longitude grid and on model levels. The MARS archive contains datasets reported over different numbers of model levels: 16, 19, 31, 40, 50, 60, 62, 91 each relative to different pressure ranges. Data for the geopotential (m^2/s^2) and for the pressure (hPa) at the surface can also be extracted on the same latitude-longitude grid.

The value of the pressure at each model level can be calculated through a given formula using the value of the pressure at the surface [1]. The data of the MARS archive are available at four different times for each day: at 00:00, 06:00, 12:00 and 18:00 (UTC).

Since the atmospheric status used in the MARC code has to be reported on an altitude grid, it is necessary to convert the pressure-dependent profiles into altitude-dependent ones. This conversion can be operated using the geopotential altitude at surface and the hydrostatic equilibrium through the use of pressure and Temperature profiles. In our study we decided to use the 91 model levels data to obtain vertical profiles of Temperature, pressure, O_3 and H_2O on a high resolution vertical grid that extends up to 70-78 km.

5.1.4 Initial Guess Atmosphere: Scan dependent ECMWF profiles

As we have mentioned before, the ECMWF data are available on a chosen latitude and longitude grid. For the 04.11.2009 flight the used latitude-longitude grid was:

- Latitude grid from 45 deg to 56 deg with a step of 1.125 deg
- Longitude grid from 0 deg to 16 deg with a step of 1.125 deg

According to the fact that the flight was performed approximately from 12:00 to 14:00 UTC, we retrieved the ECMWF datasets for 12:00 UTC and 18:00 UTC of 4 November 2009. The ECMWF profiles were interpolated in latitude, longitude and time in order to obtain the profiles at the time and at the average geo-locations of MARSCHALS scans. This process was applied to Temperature, pressure, Q and O_3 MMR altitude profiles.

In order to obtain H_2O and O_3 VMR profiles the data for Q and Ozone MMR needed to be converted. For the conversion of Q into H_2O VMR we have used the same expression reported in Equation 5-1 of [2], while for the conversion of O_3 MMR into O_3 VMR we have used the expression reported in Equation 5-2 of the same technical note. The result of this procedure are altitude profiles from 0.5 to about 77 km for Temperature, pressure, O_3 and H_2O VMR at the time and geo-location of the analysed scans. The profiles have been estrapolated up to 100 km using the same strategy adopted in the SCOUT-O3 analysis, that is using the shape of the IG2 profiles.

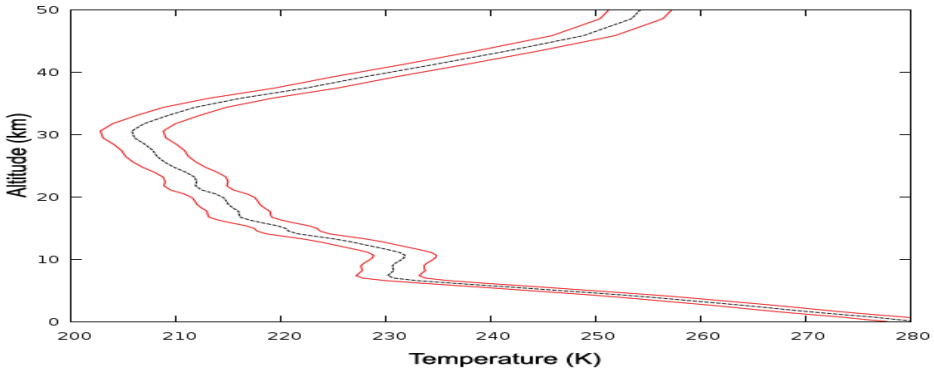

Fig. 29: Temperature initial guess profile for scan 24 +/- corresponding 3 K error.

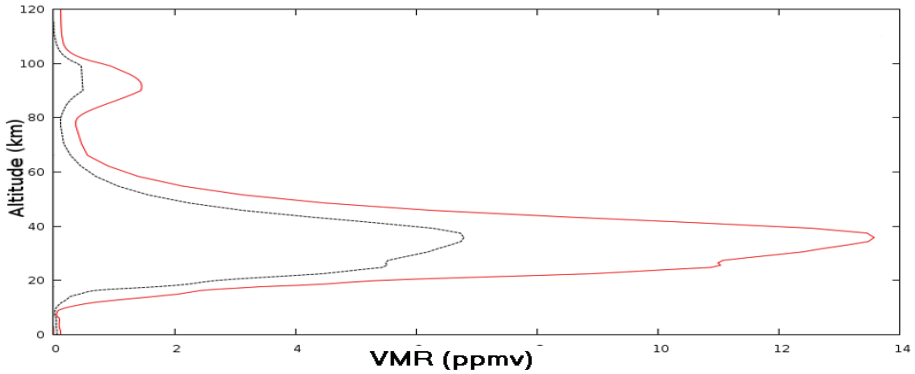

Fig. 30: O_3 initial guess profile for scan 24 +/- corresponding a priori error.

5.1.5 Initial Guess Atmosphere: a priori errors

Since in the MARC code we use Optimal Estimation to retrieve the atmospheric data, we need to define the error associated to the initial guess profiles that, in our analysis, are also used as a priori information. This error is very important because it defines the strength of the constraint imposed during the retrieval procedure. Moreover it is also used to characterize the quality of the retrieved data, through the use of the individual information gain quantifier. The error used in the preliminary analysis of the Test Flight was the 1 sigma variability obtained from the IG2 files for all the target species but for Temperature where a 3 K constant error was used (Fig. 29) and for water vapour, where the error is 100 percent from 77 km to 13.5 km and the 1 sigma variability below. For the final analysis, whose results are reported in the following subsections, the a priori errors were set following the procedure adopted for the analysis of the Scientific Flight where for water vapour and ozone the 1-sigma variability was substituted by the 100 % of the a priori profile when its value was lower (see in Fig. 30 an example for ozone) and for the other targets we have set the a priori error threshold to 50 %.

5.2 Retrieval results

5.2.1 Analysed dataset

Since for the Test Flight of 4 November 2009 all MARSCHALS bands were operating, we have performed the analysis on the spectra of all bands. This was the very first time that the MARC code was used on the data of Band D, while MARC was already used (SCOUT-O3 campaign) on the data of Band B, even if the measurements had problems, and on the data of Band C with satisfactory results [6] [18]. The preliminary analysis of the Test Flight data has been performed on all the scans present in the Level 1B file, without any screening, even if, as already said in section 5.1, we can expect the best performances for the scans from 4 to 13.

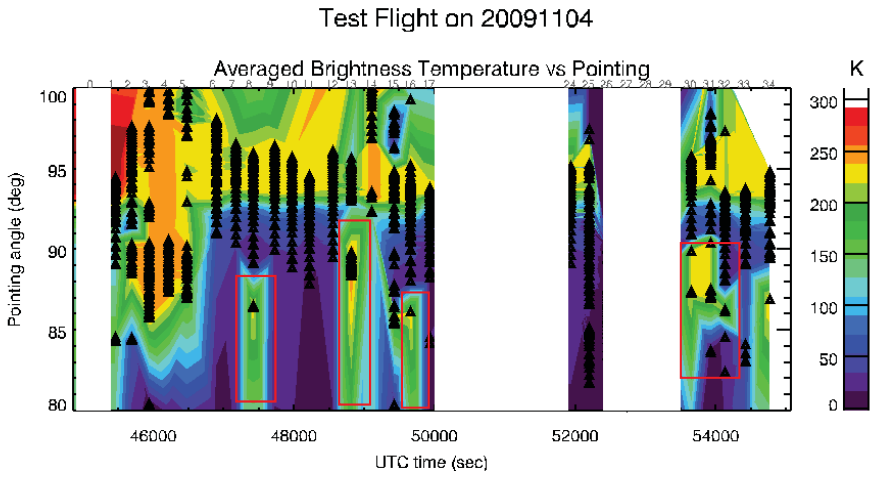

Fig. 31: BT_{av} quantifier plotted versus the zenithal pointing angle and the acquisition time.

5.2.2 Retrieval Features

Since the spectra of MARSCHALS bands could only be separately analysed, we could not perform the simultaneous retrieval of all the targets reported in [24].

So for each band the retrieval targets (as identified in [24]) were:

- Band B: the altitude distributions of T, H_2O, O_3, HNO_3 , N_2O and external continuum (Multi Target Retrieval).
- Band C: the altitude distributions of T, H_2O, O_3, HNO_3 and external continuum (Multi Target Retrieval).
- Band D: the altitude distributions of T, H_2O, O_3, HNO_3, CO and external continuum (Multi Target Retrieval).
- Scalar values of pointing bias, offset and gain for all bands

Common retrieval options for all the analysed scans (as used in the SCOUT-O3 analysis):

- Same vertical retrieval grid (target dependent)
- Use of the Optimal Estimation + Marquardt
- No hydrostatic equilibrium (anomalous T values could cause the reconstruction of a wrong pressure profile)
- Retrieval stops after 7 Gauss-Newton iterations

5.2.3 Preliminary analysis

The first test retrieval was performed on the measurements extracted from the L1 file without any filtering of the data apart from the removal of sweeps automatically performed with SAMM following the criteria listed in section 2.2.2 above. This first test highlighted the presence in the measurements of sweeps where the pointing reported in the level 1 file was not correctly evaluated. This was confirmed by the exam of the BT_{av} quantifier computed by SAMM for each sweep (see Sect. 2.3.2. In figure 31 the value of the BT_{av} quantifier is plotted versus the zenithal pointing angle and the acquisition time. The zenithal pointing angle is the pointing angle value referred to the zenith of the instrument geolocation, therefore when its value is lower than 90 the instrument is pointing above the flight altitude, while when its value is greater than 90 the instrument is looking deeper and deeper in the atmosphere. Therefore we expect that the value of the BT_{av} gets higher and higher with increasing values of the zenithal pointing angle. In figure 31 blue is associated with low BT_{av} values and red with high BT_{av} values. We can see that in the areas highlighted by the red boxes the BT_{av} shows anomalous behaviour, confirming the presence of some problem in the calibration of the pointing.

Since as for SCOUT-O3 measurements we had a redundancy of sweeps for each considered scan, we could safely remove the most problematic spectra from the analysis. Therefore we manually excluded the most problematic spectra from the analysis.

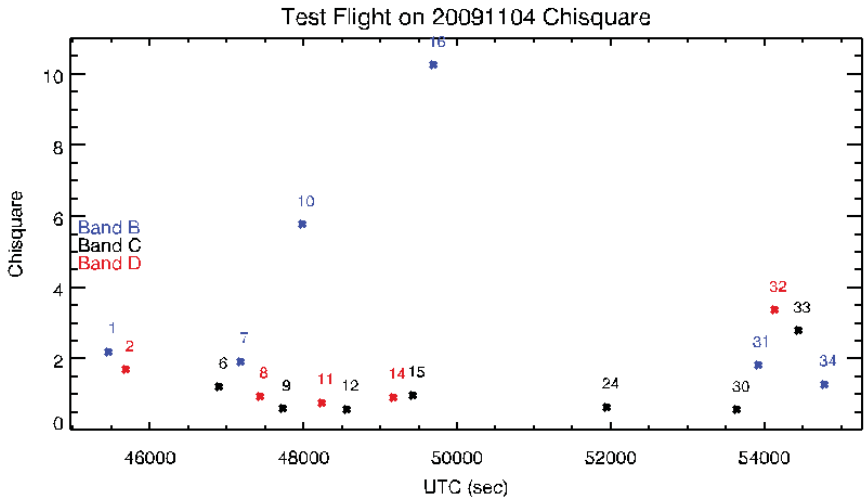

Fig. 32: final χ-test of the analysis of all bands

The new set of data was analysed using the strategy reported in Sect. 5.2.2, adopting all the optimizations found in the Scientific Flight analysis described in section 6. However, since the Test Flight was performed in a different location and season than the Scientific Flight, we performed some tests to tune the lowest tangent altitude of the observations used for the analysis: we saw that removing all measurements below 5 km gives good results in terms of χ-test , trace and information content value. Since for the Scientific Flight the CO retrieval was not giving very useful results, due to the low CO VMR in the sampled region, further tests were performed to tune CO retrieval strategy. We tested the use of the top of the atmosphere at 65 and 90 km, and found that the 65 km value produced a little improvement in terms of trace and information gain. We also varied the CO initial guess profile using a constant altitude profile with very low values (near 0). The retrieved CO profile was almost equal to the one retrieved using the IG2 profile as initial guess, thus evidencig very low influence of the inital guess on the retrieved profiles. The best vertical retrieval grids for the Test Flight data analysis were found to be the same used for the SCOUT-O3 data analysis.

The final results of the retrieval are summarized in figure 32, where the final values of the χ-test are plotted with respect to the acquisition time of the scans, while in Fig. 33 the quantifiers of the retrievals are reported.

As can be seen in Fig. 32, the χ-test value of the flight is on average close to 1 in the first part of the flight while it increases to a value of 2-3 in the second part, where however the M-55 was landing. High χ-test values were present for scans 3, 4, 5, 13, 16, 17 and 25. Those scans were performed during anomalous movements of the aircraft (i.e. ascent, dive, turns) where the commanded pointing and the achieved pointing can be very different, and their anomalous behaviour was expected. A separate exam was needed for scan 10, that is one of the scans recorded in the best part of the flight, that showed a final χ-test value greater than 5. A thorough investigation highlighted a residual anomaly in the pointing correction for some of the spectra of the scan. While the pointing changes monotonically, the measured spectral intensity remains stable. Therefore the retrieval procedure tries to compensate for the anomalous behaviour of the spectra, but the result is a discontinous residual well above the measurement noise, generating the high χ-test value. As can be seen in Fig. 33, the trace of the AK matrix and the information content of the retrieval is fairly constant through the flight apart for scans 2, 14, 31, and 34 where a lower than average information content and AK trace values are present. This is due to the smaller number of sweeps that can be used in the retrieval.

In Figures from 34 to 37 the results of the retrieved scalar quantities for all bands are reported. If the retrieved values of the offset and gain stay constant throughout the whole flight, this is an indication of a consistent calibration of the three measured bands. In figures 34 and 35 we see that for the part of the flight from scan 6 to scan 12 those quantities are fairly constant. The same applies to the data retrieved for Band C scans, while for the rest of the analised scans the results are a little bit more scattered. In particular we get a low gain value for the Band B scans 1, 2, 7, 25 and 34. While for scans 1,2 and 17 and 34 we may expect to have some problems, since they have been acquired during ascent and descent part of the flight, and scan 25 has been acquired during a turn of the aircraft, the anomalous value of scan 7 is more difficult to explain only on the basis of the measurement scenario.

The values obtained for the pointing bias reflects the behaviour found for the other scalar quantities, that is that in the first part of the flight (scans 6-12) we found constant values, while results are a little more scattered for the other parts of the flight. In figure 37 the retrieved frequency shift values for each band are reported. Band B

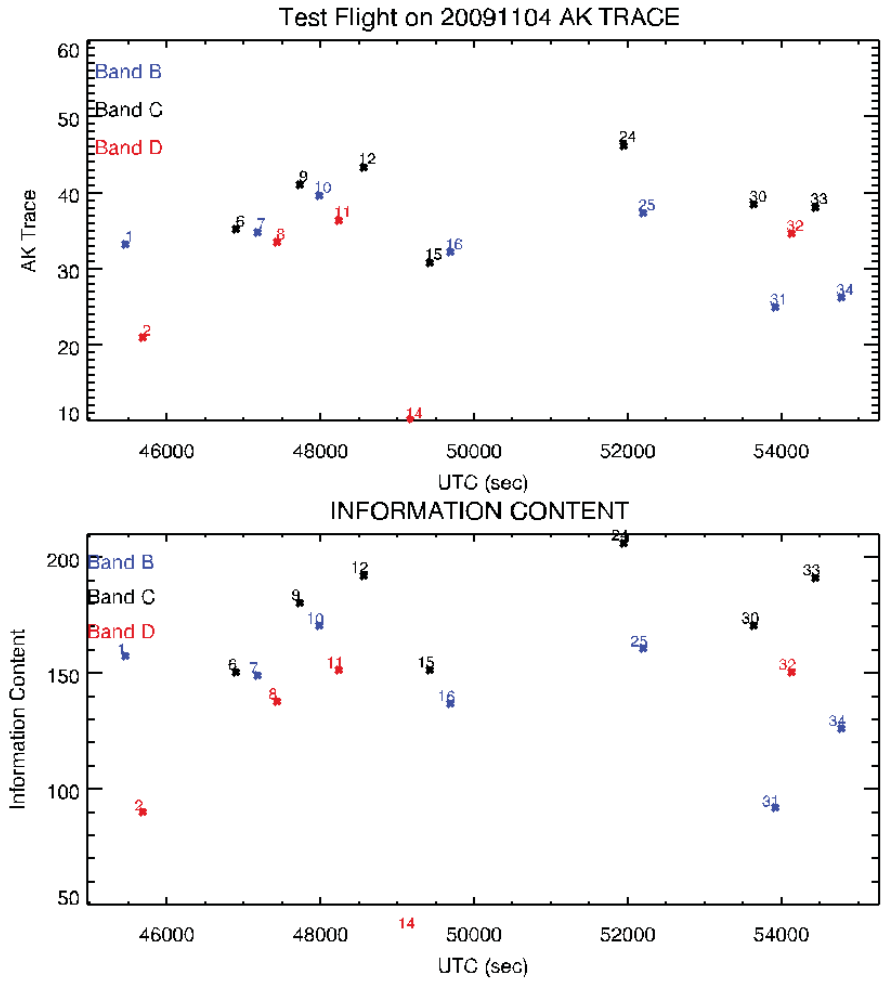

Fig. 33: final trace of the AK matrix and information content for the analysis of all bands

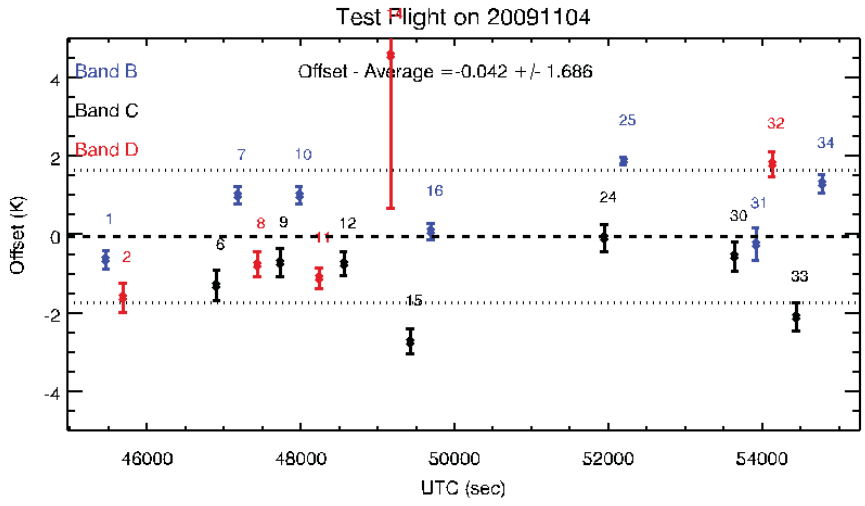

Fig. 34: final offset of the analysis of all bands

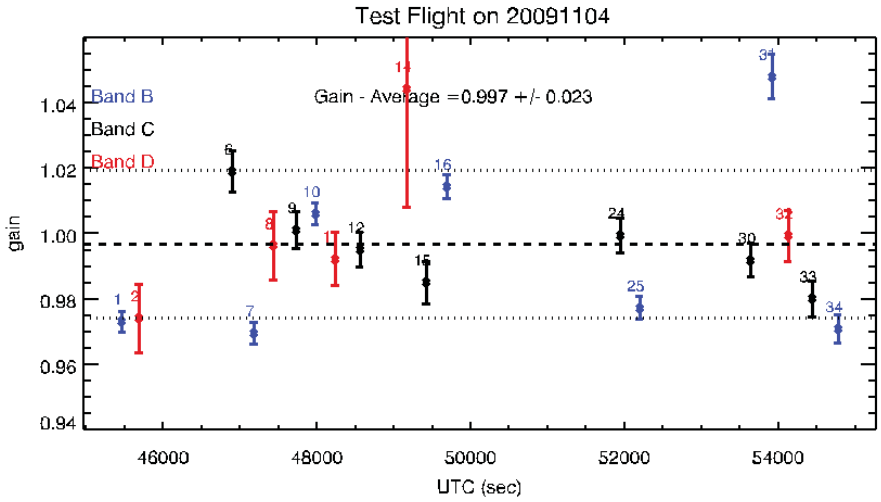

Fig. 35: final gain of the analysis of all bands

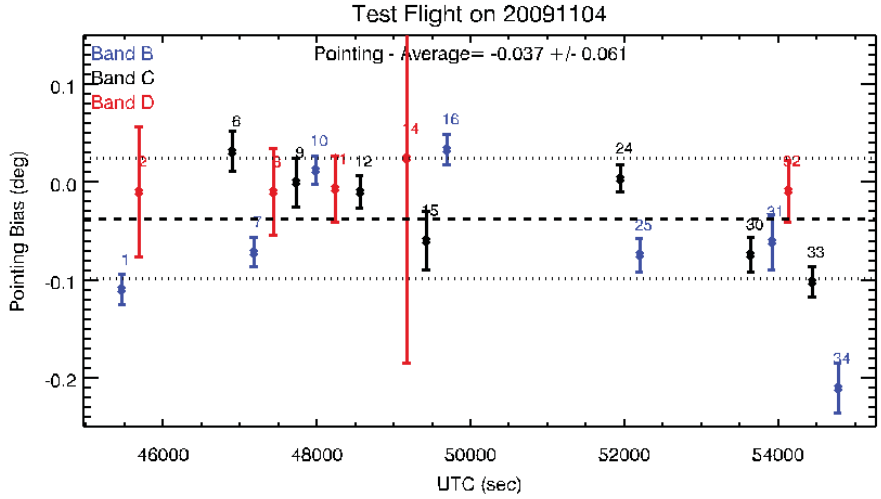

Fig. 36: final pointing bias retrieved in the analysis of all bands

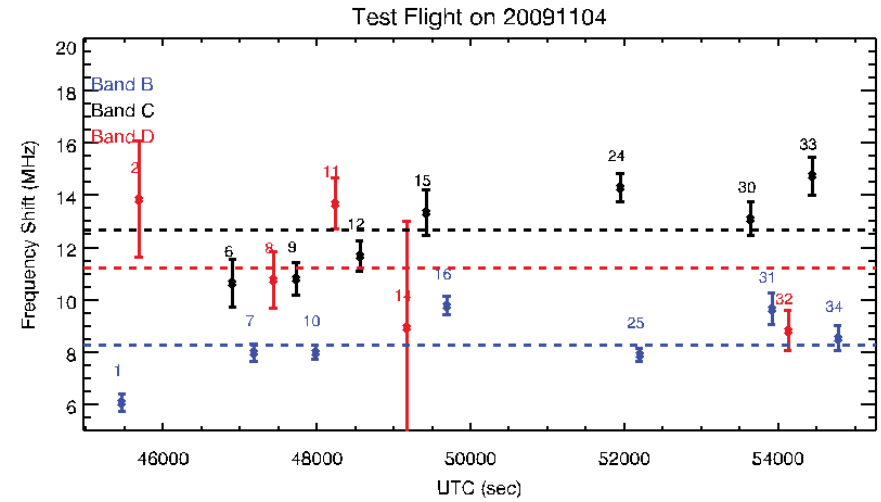

Fig. 37: final frequency shift retrieved in the analysis of all bands

frequency shifts are constantly assuming a lower value with respect to the other bands for the whole flight, with a mean value of about 8.5 MHz. Band C values are increasing with time, with a mean value of 12.5 MH. Band D retrieved values are between 11-14 MHz in the first part of the flight, then from scan 14 to scan 34 the values are lower getting closer to the Band B values. In all cases the retrieved frequency shift is well below the instrument spectral resolution that is about 200 MHz. All the retrieved scalar quantities of scan 14 have a very large error. This is due to the very low number of sweeps available for the retrieval (see figure 28).

An overview of the results of the analysis of the vertical distributed targets for the whole flight is reported in Figures from 38 to 42. As for the Scientific Flight, the Temperature retrieval works properly only for the scans of Band C. In particular, the Temperature retrieved from Band B measurements is unstable at low altitudes, while the one obtained from Band D measurements is dominated by the a priori profile. The same problem is present for the water retrieval: the maps of the biased errors and of the individual information content of figure 39 show that we have a good performance only for the Band C scans, while for Band B and D measurements the single profiles are very unstable and show very large errors.

For ozone we obtain good results in the first part of the flight, from scan 6 to scan 12, while in the second part of the flight some oscillations occurs at scan 31. For HNO_3 the reduced spectral range of band B produced low information content as discussed for the Scientific Flight data analysis (see Fig. 41). However, for band C and D retrievals we obtain a much better result than for the SCOUT-O3 flight: the information content of the measurements is good (values close to 2) and stable for the whole flight (see bottom panel of Fig. 41).

The retrieved external continuum shown in Fig. 42 is a merging of the values obtained for the external continuum of the three bands. The map in the figure shows that the cloud coverage seen during the flight did not produce opacity apart from scans 6, 10, 16 and 33. However, clouds do not seem to produce opacity that cannot be reproduced by just a continuum level, even if a high value of the χ-test is found for scan 16, possibly due to a descent of the aircraft.

5.3 Final Analysis

From the results reported in Sect. 5.2.3 we conclude that the best part of the Test Flight was the one from scan 6 to 12, and from scan 30 to 34, and for those scans we have tried to tune the retrieval strategy performing sequential retrievals.

We recall here that a sequential retrieval is performed analysing an individual scan, using the results of the analysis of the previous scan (profiles and VCM) as a priori information for the already retrieved targets. This should be equivalent to perform a multiple band retrieval.

Using the retrieval strategy adopted for the Scientific Flight data analysis, (see section 6.4) we performed the sequential retrieval starting the sequence from a band C scan, then a band B scan and then a band D scan (that is the temporal sequence used in the measurements), retrieving Temperature from band C only and using it in the subsequent scans B and D retrievals. Water vapour was retrieved in band C and the resulting profile was used as initial guess for band B and D retrievals. However, the Water Vapour profiles obtained in band B and D retrievals could not be used as a final product since the water vapour retrieval in these bands was performed only to account for the far wings of the water lines affecting the analysed spectral regions. We made an attempt to perform a recursive retrieval including Temperature in the targets, using the Temperature profile obtained for band C as initial guess for the band B analysis and the results of band B as initial guess for band D retrieval. The anomalous and oscillating profile produced by the band B retrieval affects the quality of the final Temperature profiles, therefore we did not adopt this strategy.

The results obtained with the strategy described above are shown in figures 43 to 55 for the best part of the flight (from scan 6 to 12) and for the final part of the flight (from scan 30 to 34) only. The obtained chisquare are similar to the ones obtained in the single band retrievals. As expected, the trace and information content obtained using the sequential fit strategy for band B and D are lower than the ones obtained during the single band analysis due to the smaller number of retrieved parameters. The retrieved scalar quantities are similar to the ones prevoiusly obtained. We note only a variation in the final χ-test and pointing and gain values obtained for scan 7. In particular the pointing value retrieved for scan 7 is about -0.16 deg lower then the value retrieved for the other scans from 6 to 12. Temperature and H_2O profiles retrieved from band C seem to produce good results while O_3 and HNO_3 retrievals produce results similar to the single bands retrievals. CO retrievals preformed for scans 8, 11 and 32 gives good results. Some oscillations are present in the N_2O retrieved from scan 7 and the information content for this target is higher in the first part of the flight. The retrieved external continuum, obtained from all the three MARSCHALS bands, is very similar to the one obtained in the case of the single band retrieval.

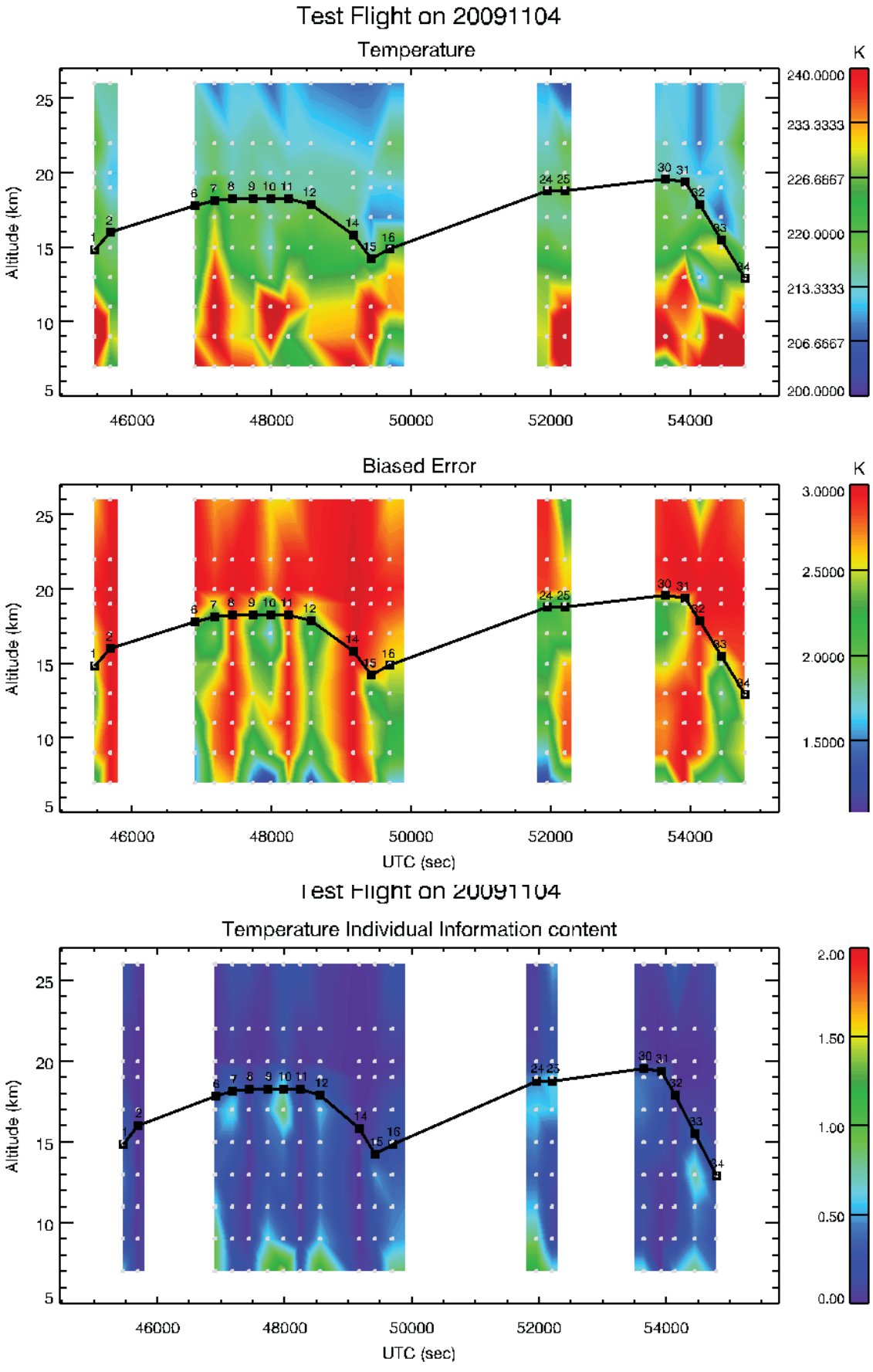

Fig. 38: Map of the Temperature versus altitude and acquisition time

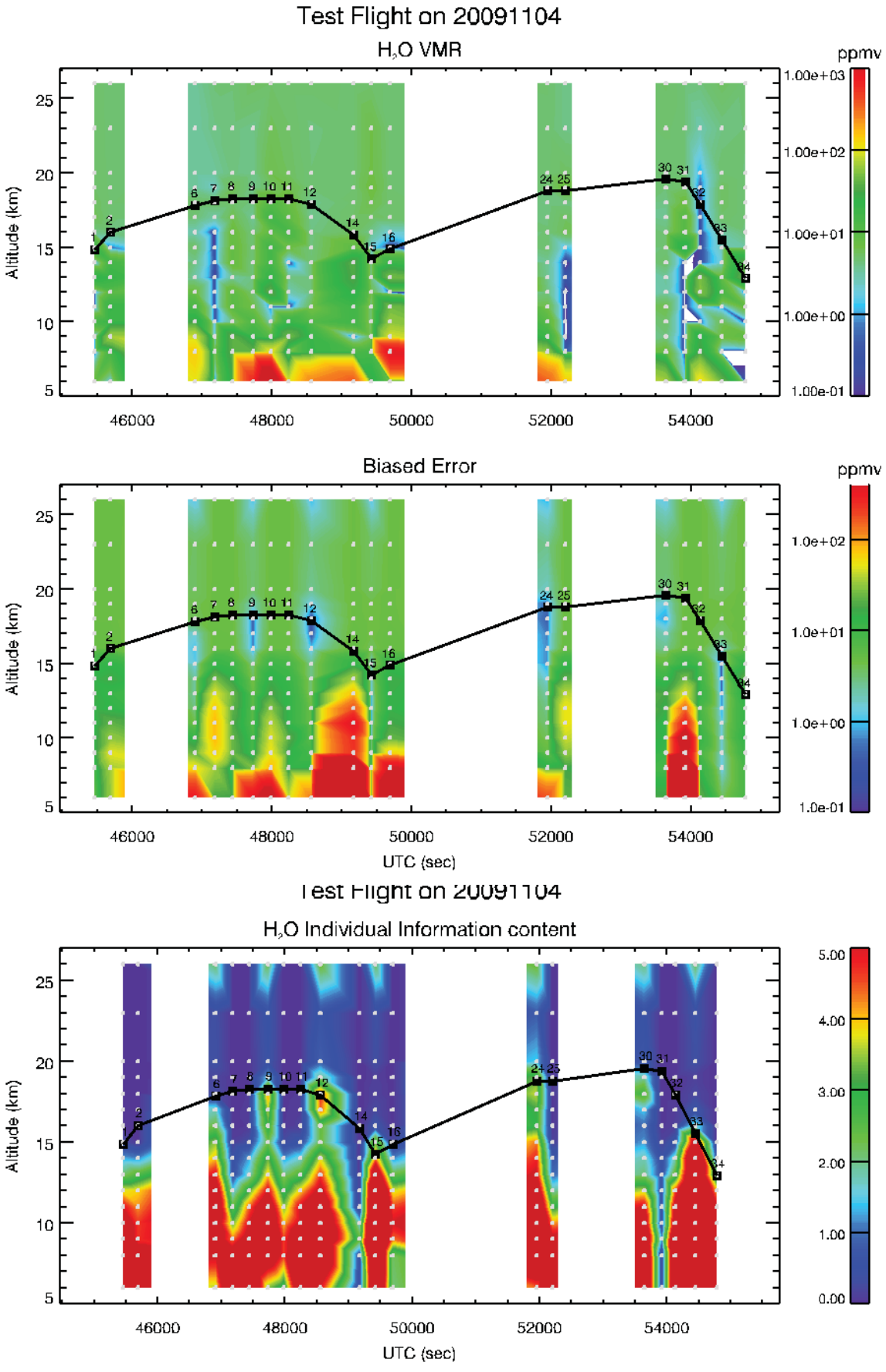

Fig. 39: Map of the H_2O versus altitude and acquisition time

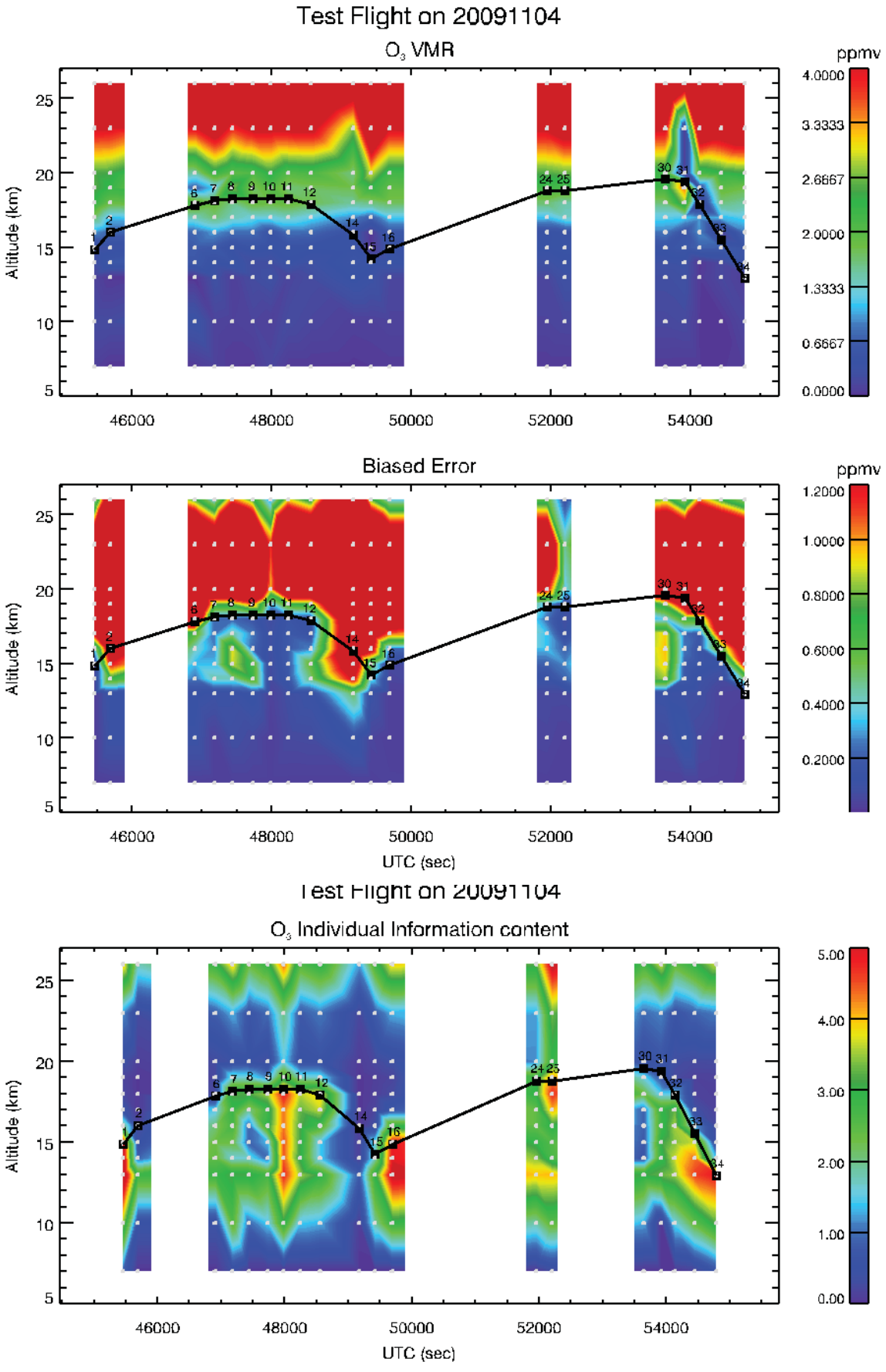

Fig. 40: Map of the O_3 versus altitude and acquisition time

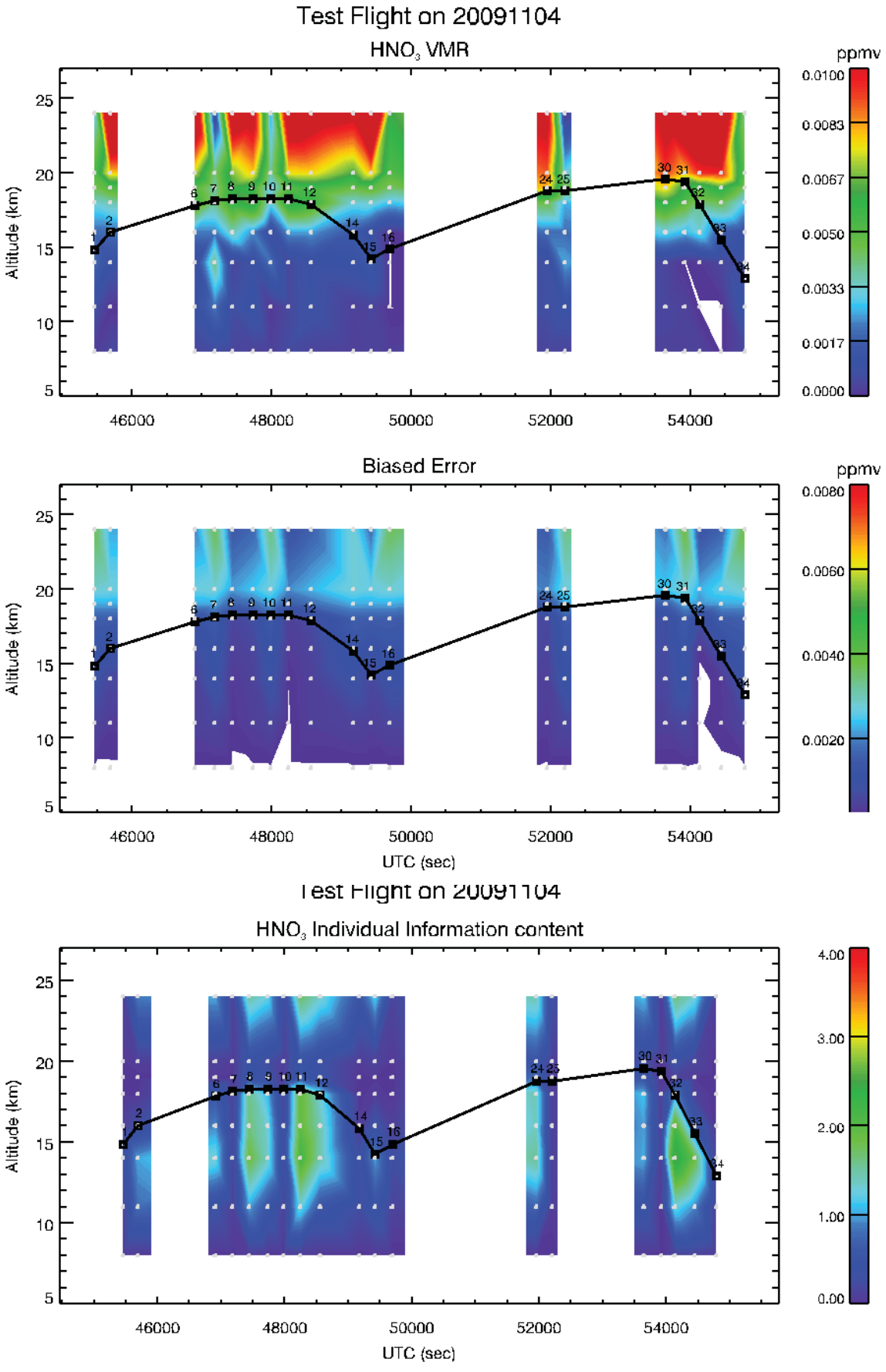

Fig. 41: Map of the HNO_3 versus altitude and acquisition time

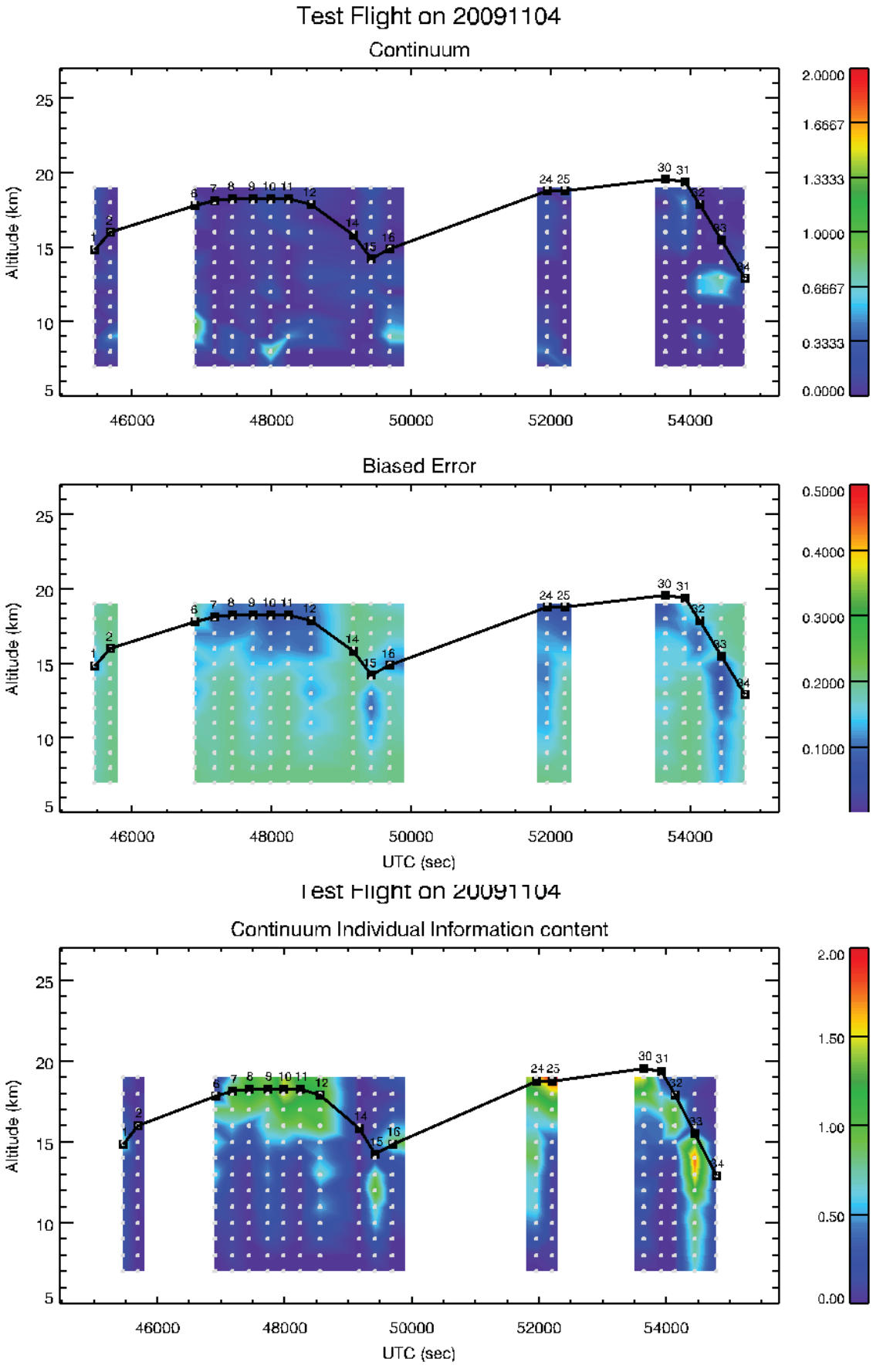

Fig. 42: Map of the external continuum versus altitude and acquisition time

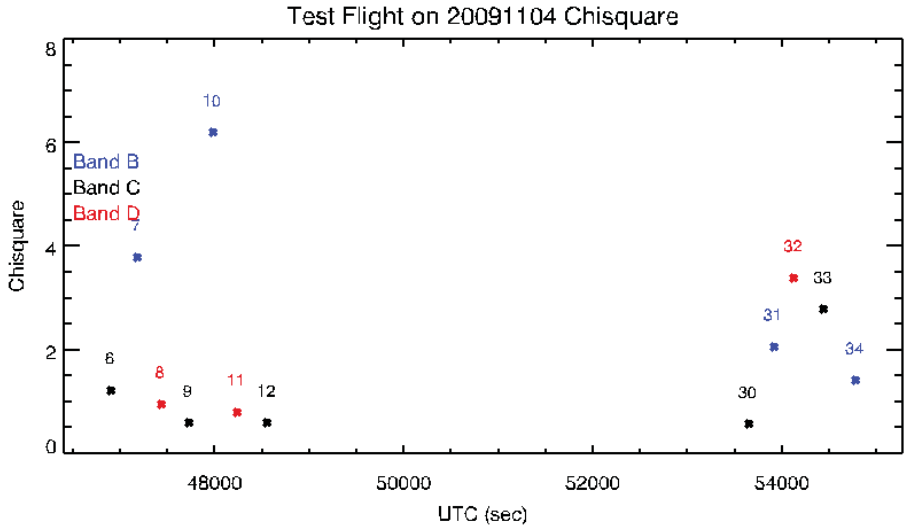

Fig. 43: final χ-test of the analysis of all bands using sequential fit.

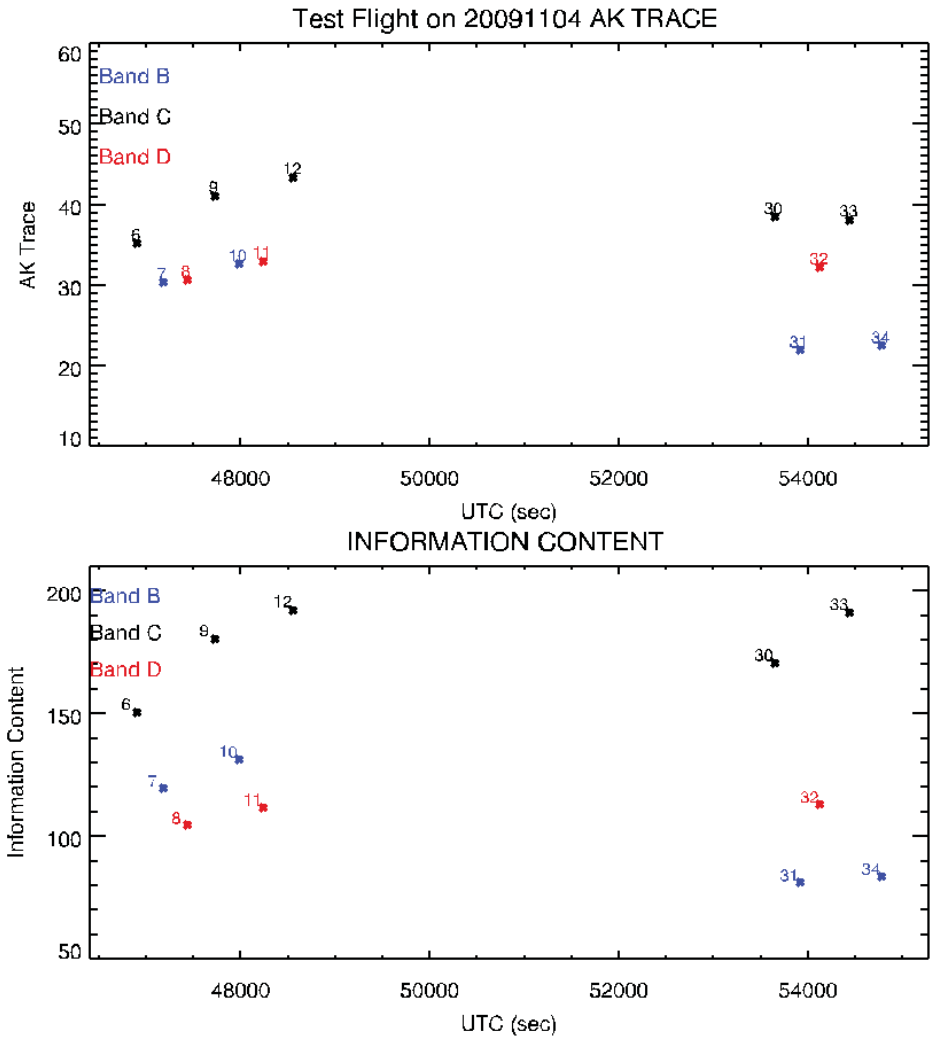

Fig. 44: final trace of the AK matrix and information content for the analysis of all bands (sequential fit).

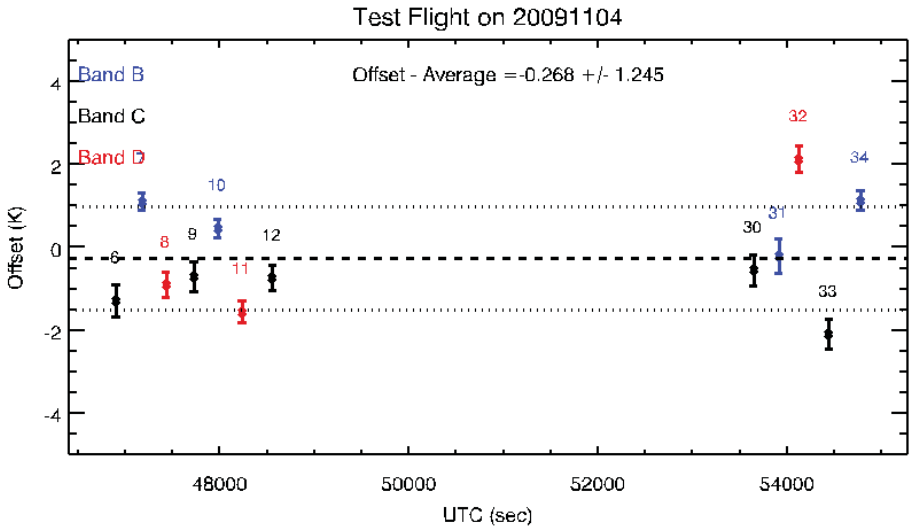

Fig. 45: final offset of the analysis of all bands (sequential fit).

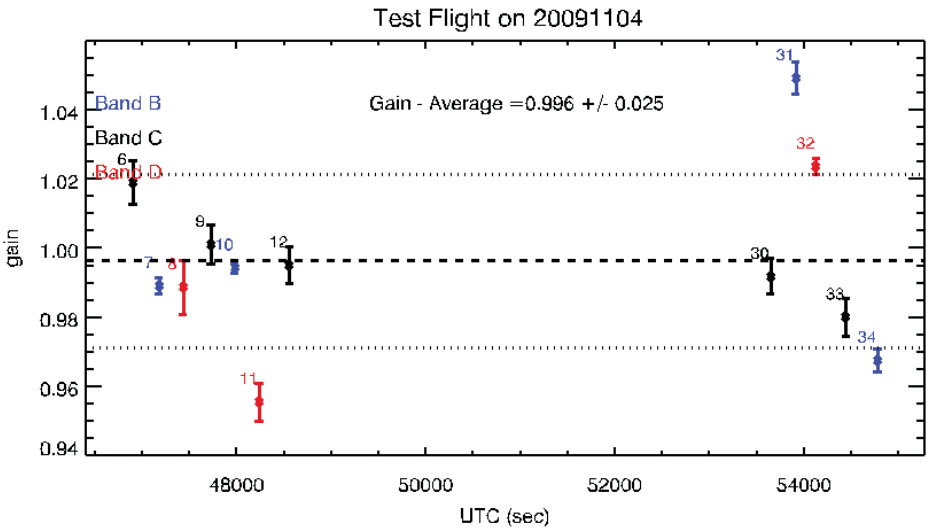

Fig. 46: final gain of the analysis of all bands (sequential fit).

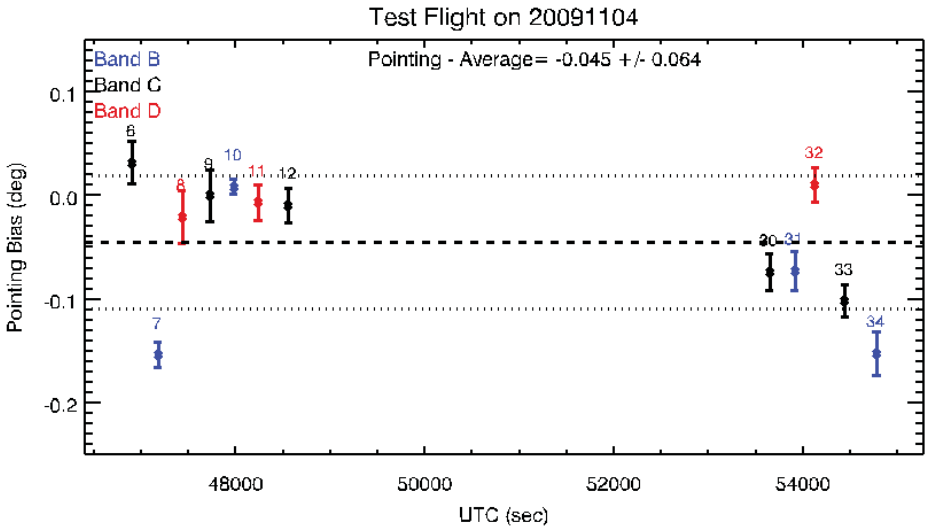

Fig. 47: final pointing bias retrieved in the analysis of all bands (sequential fit).

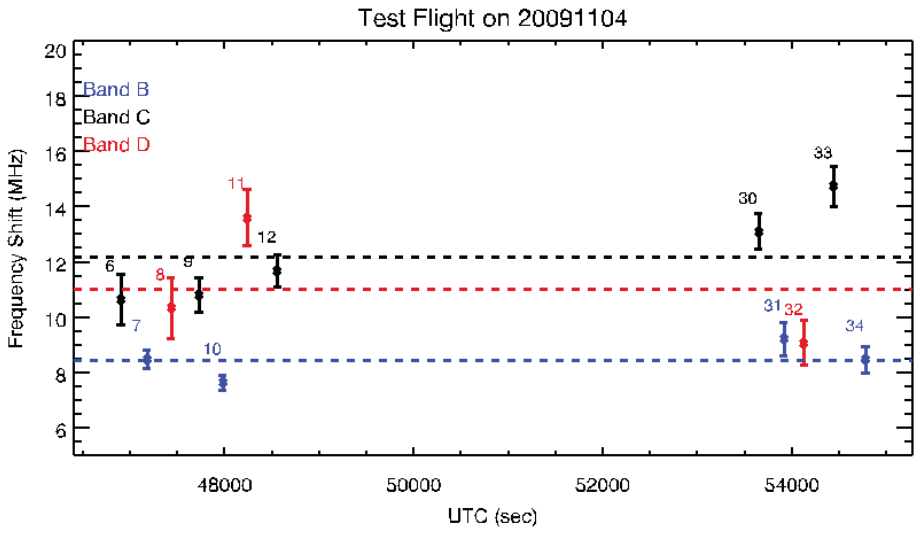

Fig. 48: final frequency shift retrieved in the analysis of all bands (sequential fit).

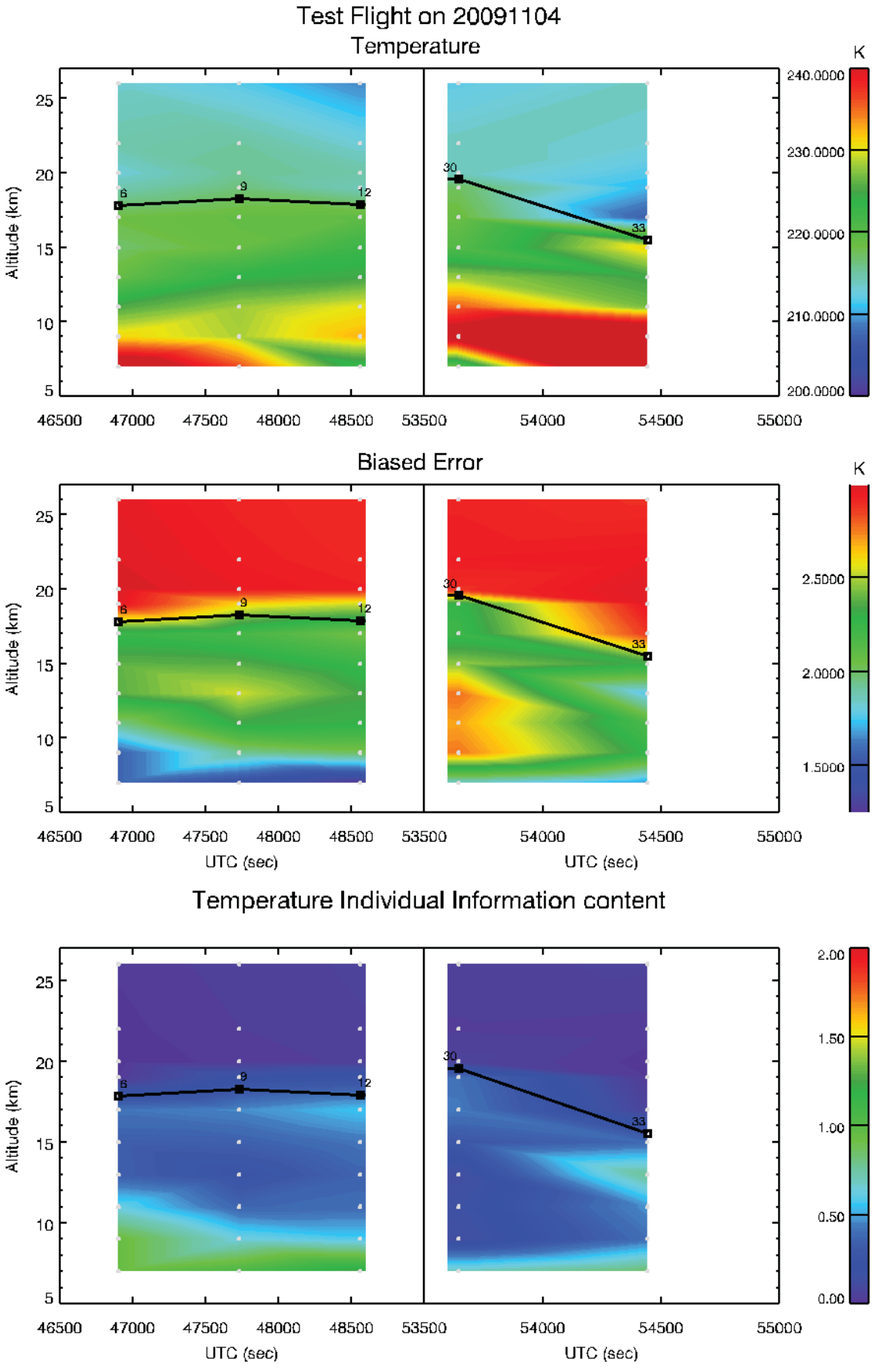

Fig. 49: Map of the Temperature versus altitude and acquisition time (sequential fit).

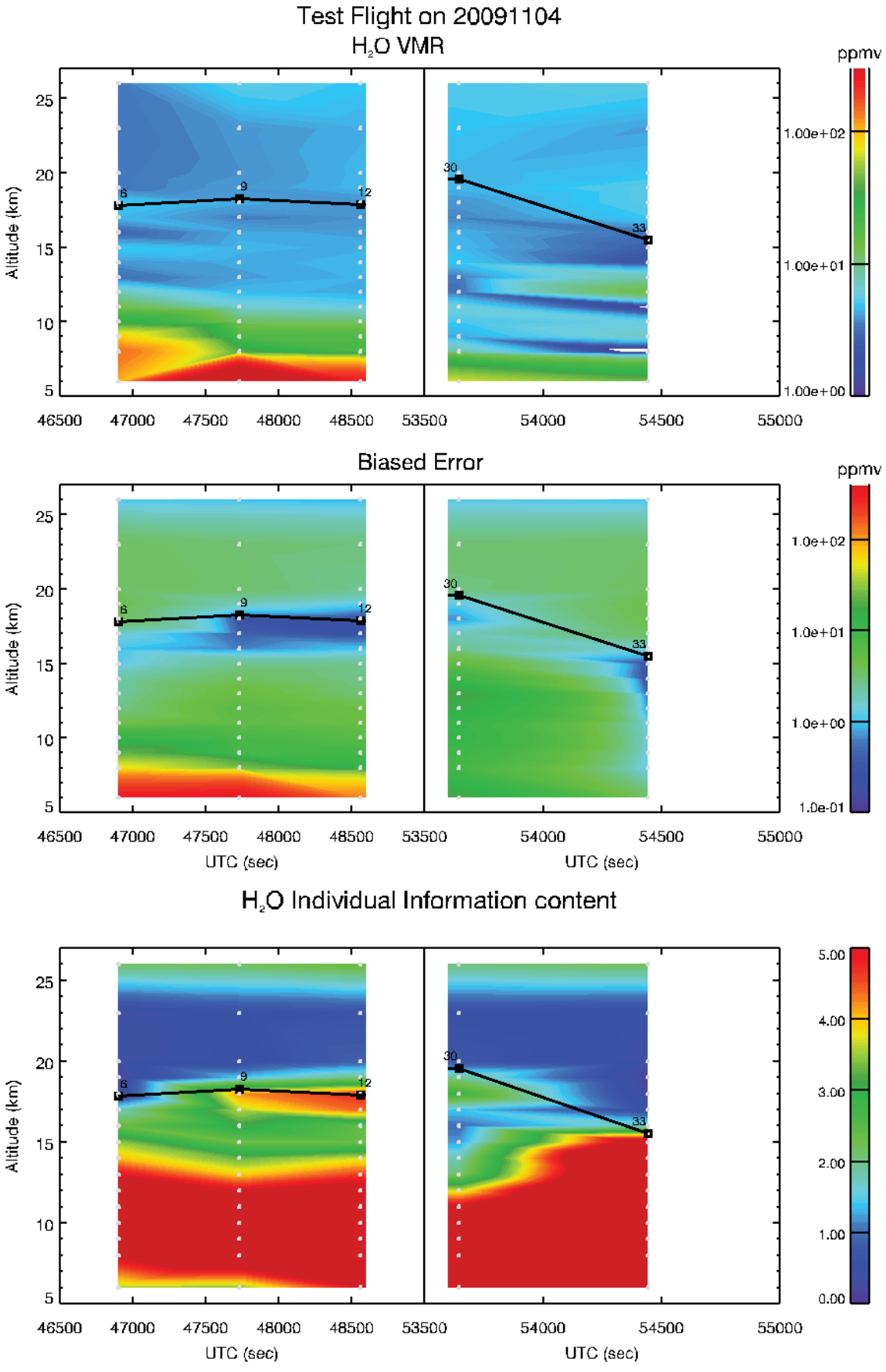

Fig. 50: Map of the H_2O versus altitude and acquisition time (sequential fit).

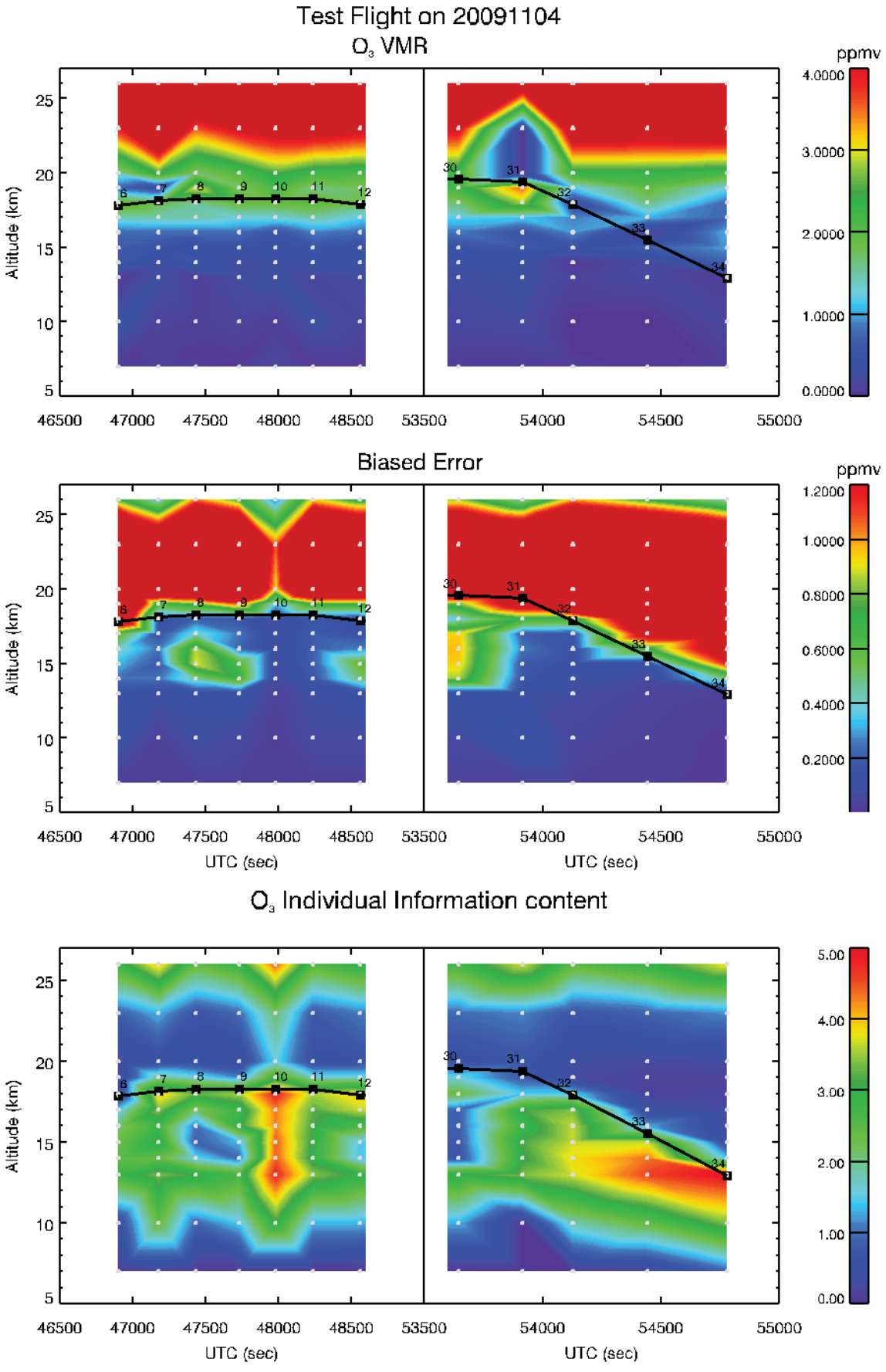

Fig. 51: Map of the O_3 versus altitude and acquisition time (sequential fit).

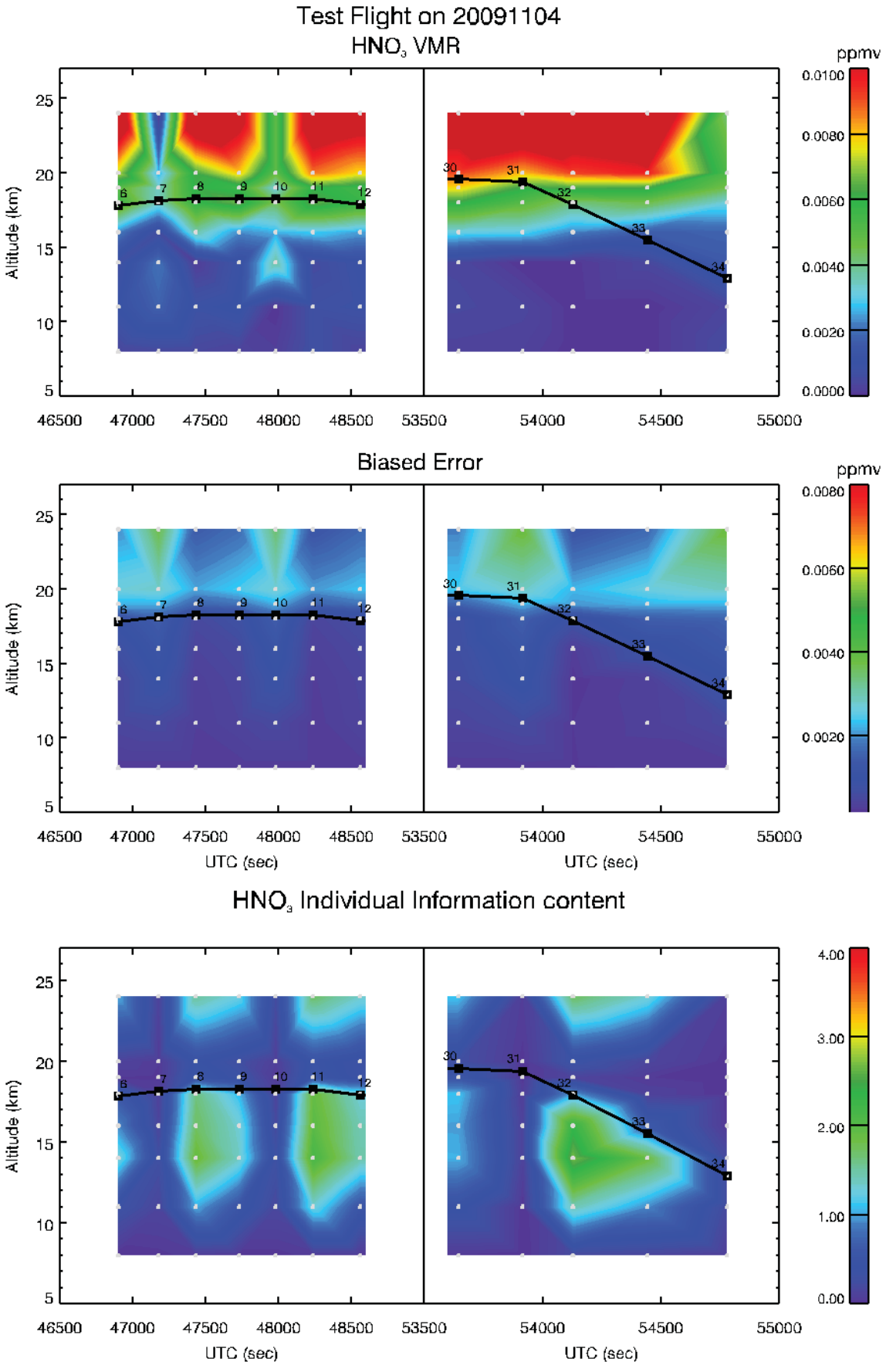

Fig. 52: Map of the HNO_3 versus altitude and acquisition time (sequential fit).

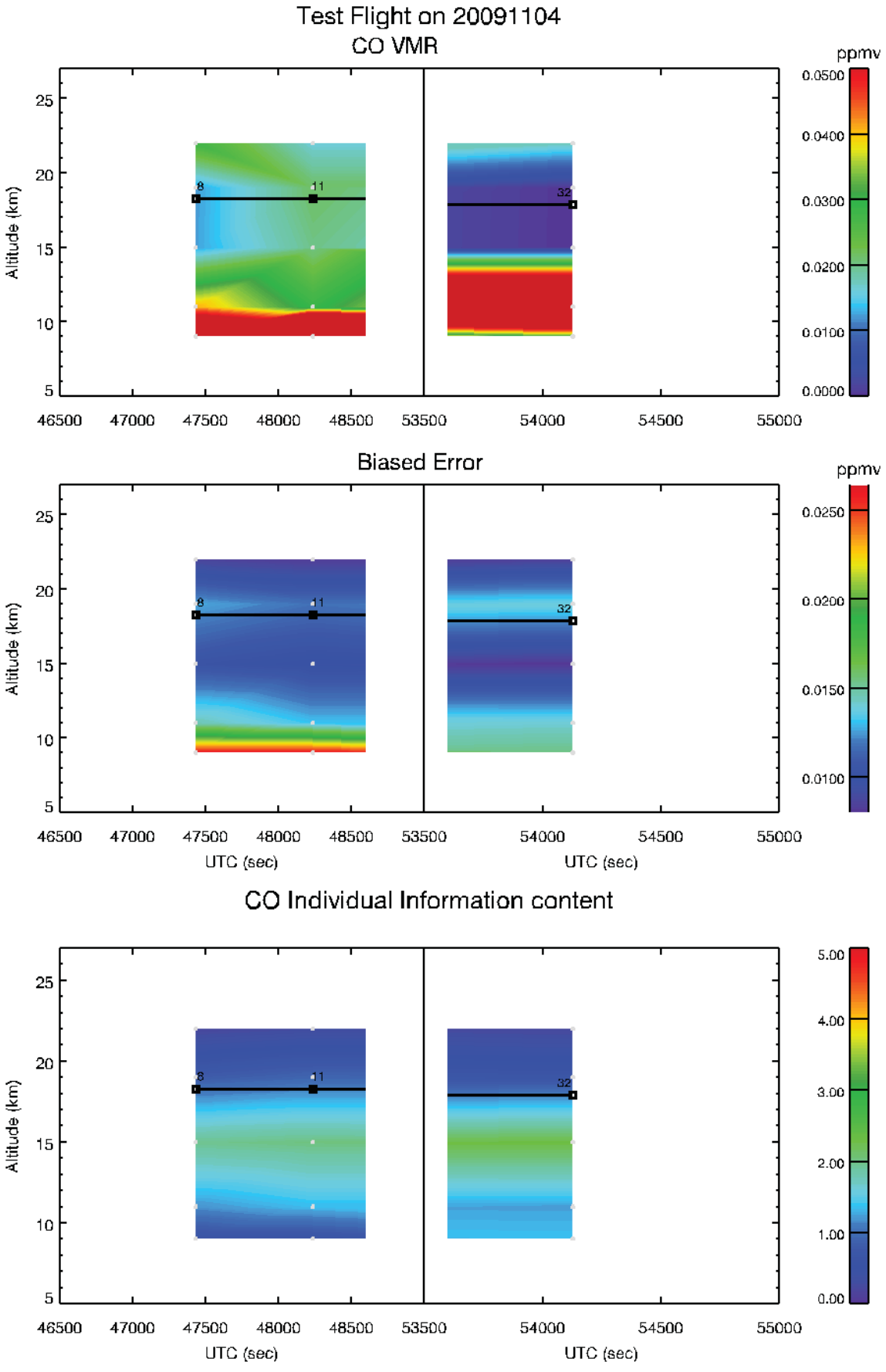

Fig. 53: Map of the CO versus altitude and acquisition time (sequential fit).

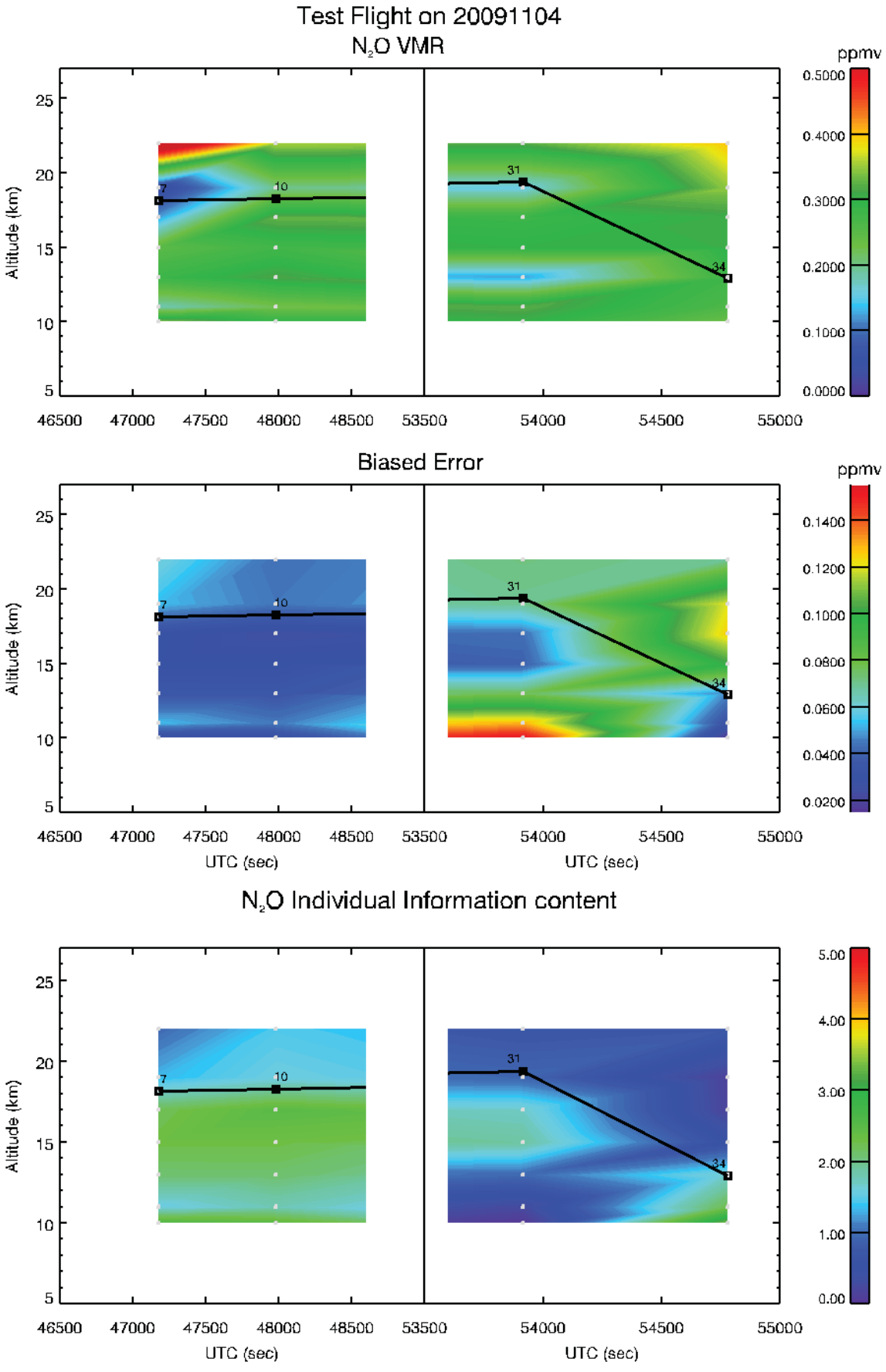

Fig. 54: Map of the N_2O versus altitude and acquisition time (sequential fit).

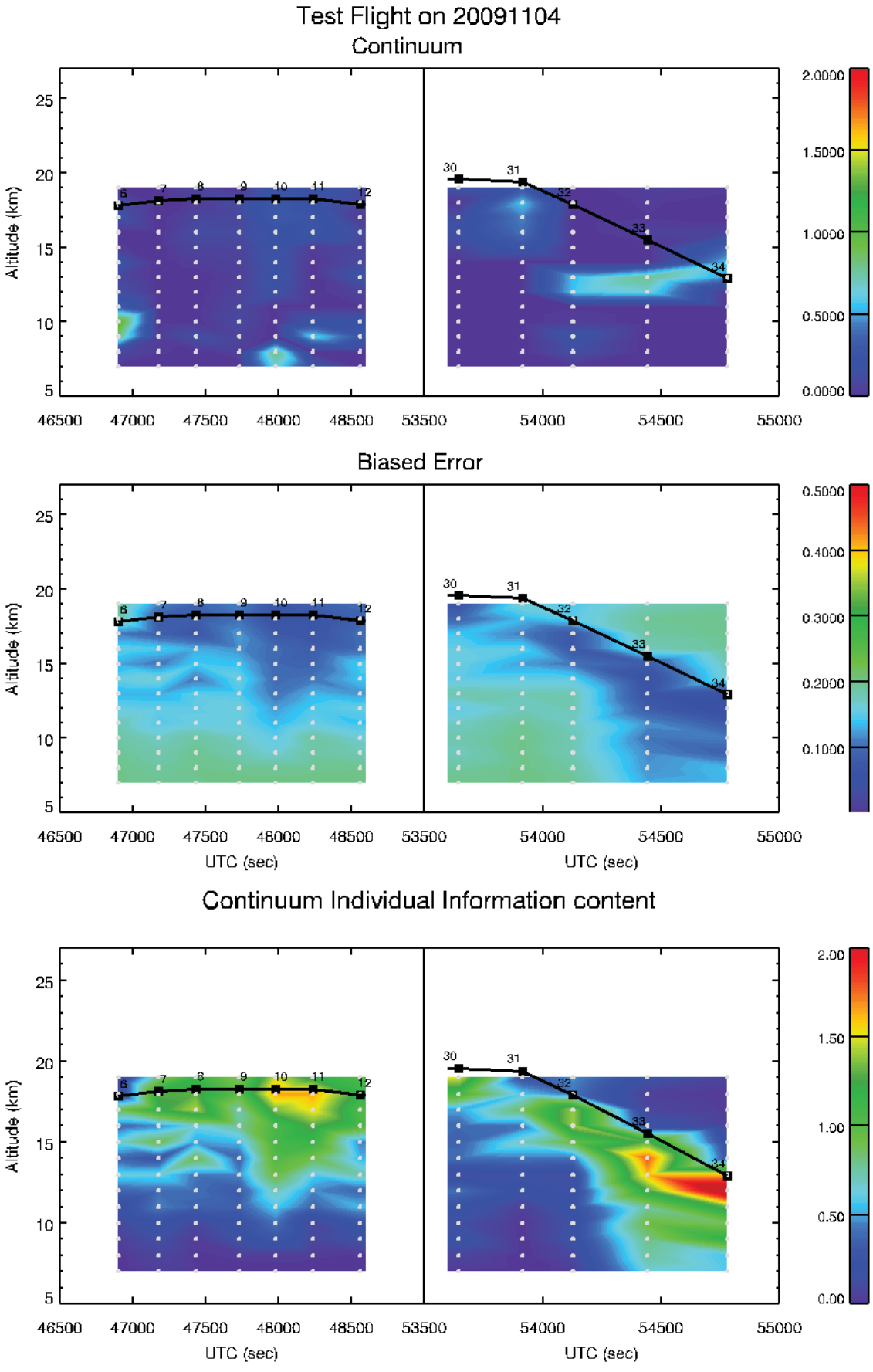

Fig. 55: Map of the external continuum versus altitude and acquisition time (sequential fit).

5.4 Recursive retrievals for O_3 and HNO_3

Following the strategy tested in the Scientific Flight analysis, and reported in section 6.5, we tried to perform a recursive retrievals for O_3 and HNO_3. This test was performed from scan 6 to 12 and from scan 30 to 34. The obtained results for O_3 and HNO_3 are shown in figures 56 and 57. As can be noticed comparing these figures with figures 51 and 52 we see the improvement obtained with the recursive strategy for the HNO_3 retrievals. In the case of O_3 some improvements was found for scan 8 while in the final part of the flight some oscillations are still present.

The Temperature and VMRs profiles retrieved with the sequential retrieval strategy, that provide good results also for the Tests flight analysis, were used for the validation exercise reported in section 9.

6 Analysis of MARSCHALS Scientific Flight measurements

In this section, we report the results of the analysis carried out on the MARSCHALS L1 data acquired during the Scientific Flight on 10.03.2010.

The main objectives of the analysis are:

- Optimize the retrieval strategy for MARSCHALS measurements
- Analyse the data to obtain the UTLS composition during the flight

6.1 Geophysical Scenario

6.1.1 Flight overview

The flight track of MARSCHALS PremierEx flight is shown in the top panel of Figure 58 while the bottom panel reports the altitude of the M-55 during the flight plotted with respect to the flight time (UTC).

As we can see in Fig. 58 the M-55 followed a triangular flight pattern, with the result that MARSCHALS scans sampled the atmosphere from latitudes 72 N to 74 N in the first part of the flight and from 70 N to 66 N during the second part, as highlighted in the three panels of Figure 59 that show the position of the tangent points of the scans of band B, C and D respectively during the flight. The bottom panel of Figure 58 shows that there are two parts of the flight (from scans 6 to 31 and from scans 35 to 53) where the aircraft altitude was nearly constant, a requirement for having the MARC code working at its best. However, looking at the three panels of figures 59 and 60 we see that scans 13, 34, and 40 of Band B, scans 2, 5, 32 and 35 of Band D and possibly also scan 33 of Band C, may not be good for the analysis because of the reduced altitude coverage and or because acquired during changes of direction of the aicraft. The three panels of figure 60 also show that there is an uneven altitude coverage of the three bands during the flight. This will affect the quality of the retrieval products, because of the different vertical distribution of the information content of each scan.

6.1.2 Initial Guess Atmosphere

The strategy used to define the initial atmospheric status for the analysis of the Scientific Flight was the same used for the Test Flight and it has been thoroughly described in section 5.1.2. The profile extracted from the IG2 database [19] were the ones relative to a polar winter atmosphere. ECMWF data were again obtained on a personalized latitude and longitude grid that for the flight of the 10^{th} March 2010 was:

- Latitude grid from 66 deg to 73 deg with a step of 1.125 deg
- Longitude grid from -2 deg to 23 deg with a step of 1.125 deg

Since the flight was performed approximately from the hours 08 to 10 UTC, we retrieved the ECMWF at two times: 06:00 UTC and 12:00 UTC. As described in sec 5.1.4 the ECMWF data have been interpolated to the average latitude, longitude and time of each measured scan. The profiles have been extrapolated up to 100 km using the same strategy adopted in the SCOUT-O3 analysis, that is using the shape of the IG2 profiles.

6.1.3 Initial Guess Atmosphere: a priori errors

The a priori error used in the analysis of the Scientific Flight for Temperature is a 3 K constant error, the same used for the Test Flight analysis and in line with the available information on ECMWF Temperature accuracy. For the other targets two different sets of a priori errors were used. As for the Test Flight (see Sect. 5.1.5), for the

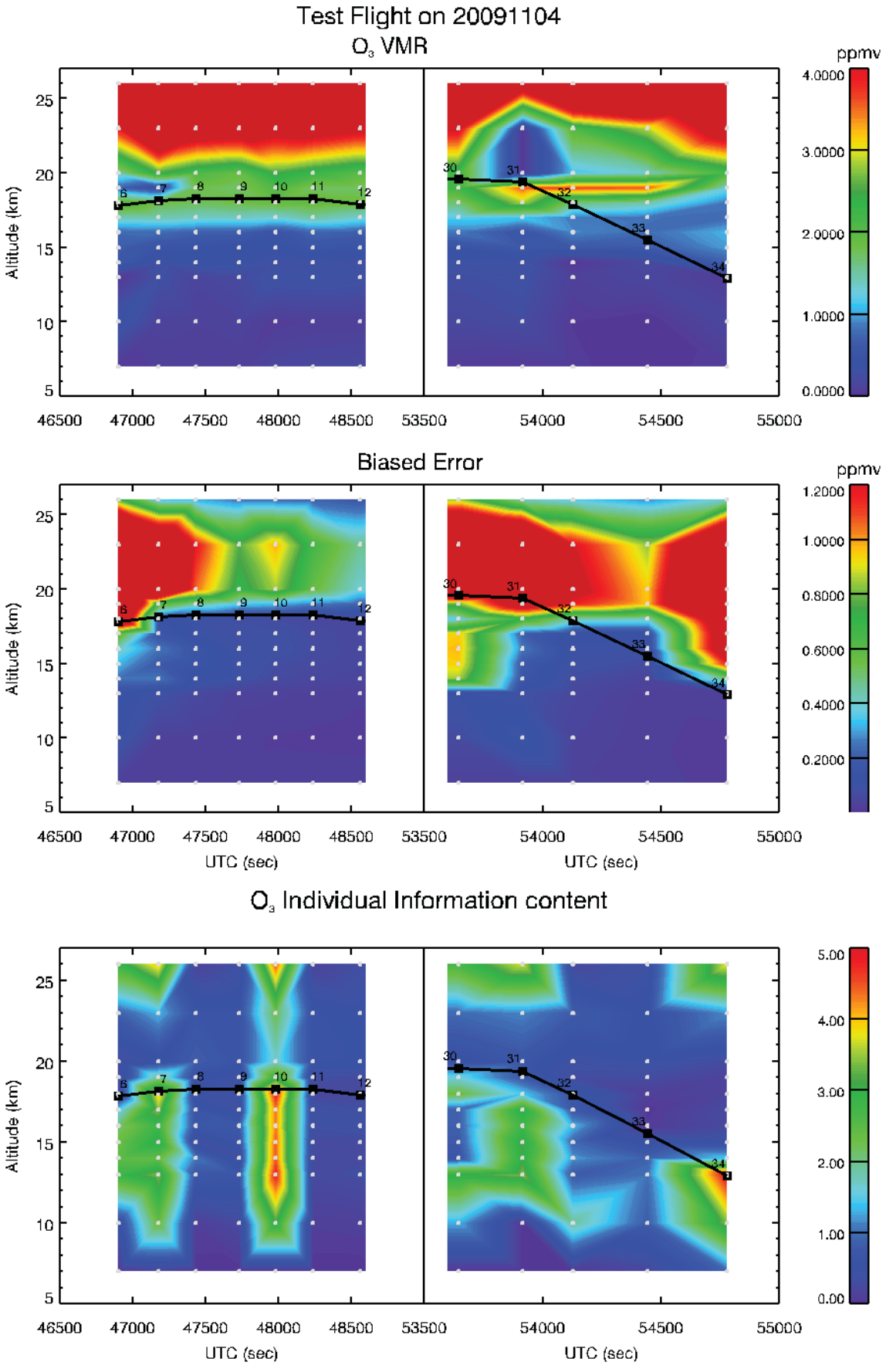

Fig. 56: Map of the O_3 versus altitude and acquisition time using recursive retrievals.

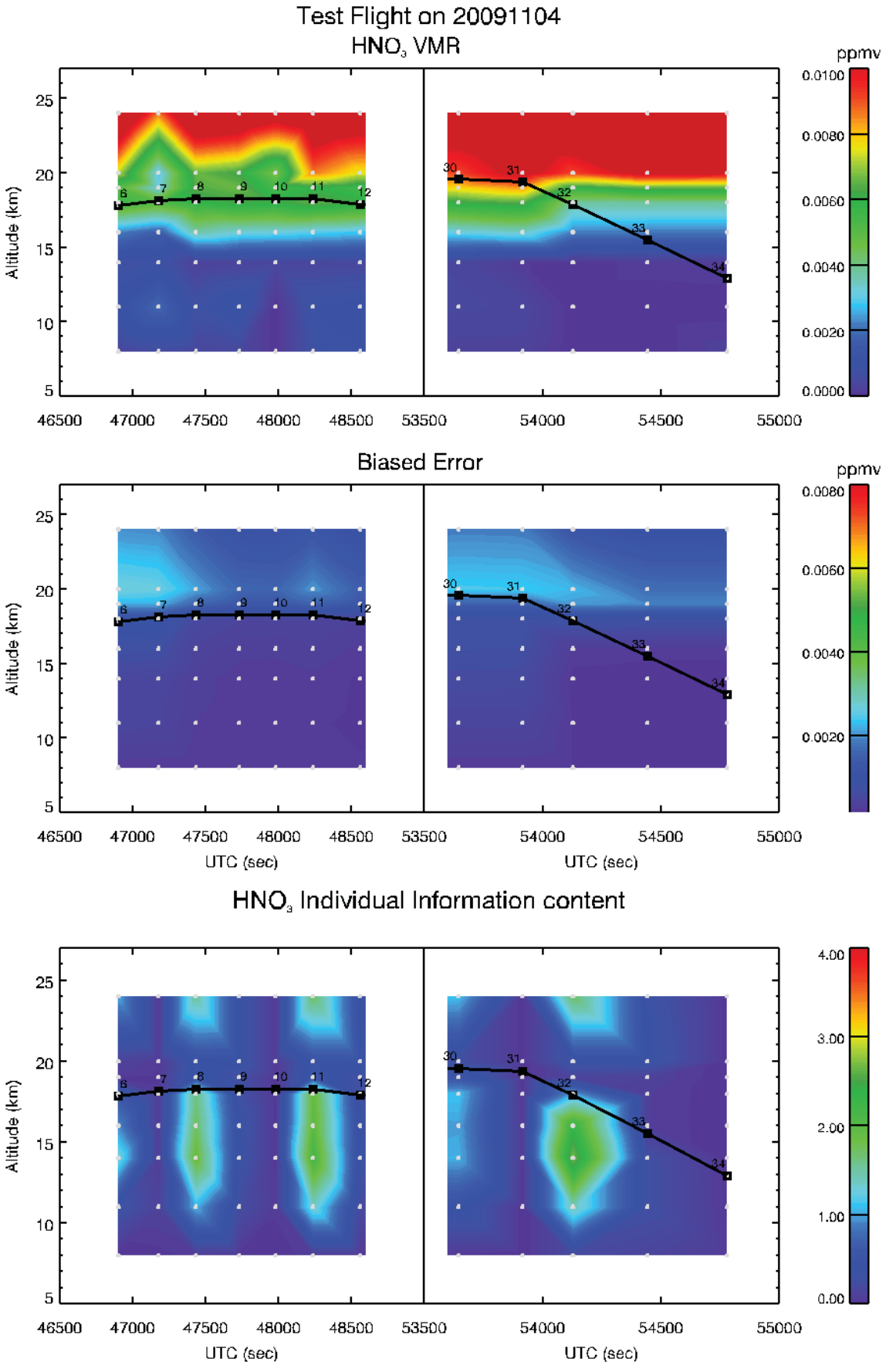

Fig. 57: Map of the HNO_3 versus altitude and acquisition time using recursive retrievals.

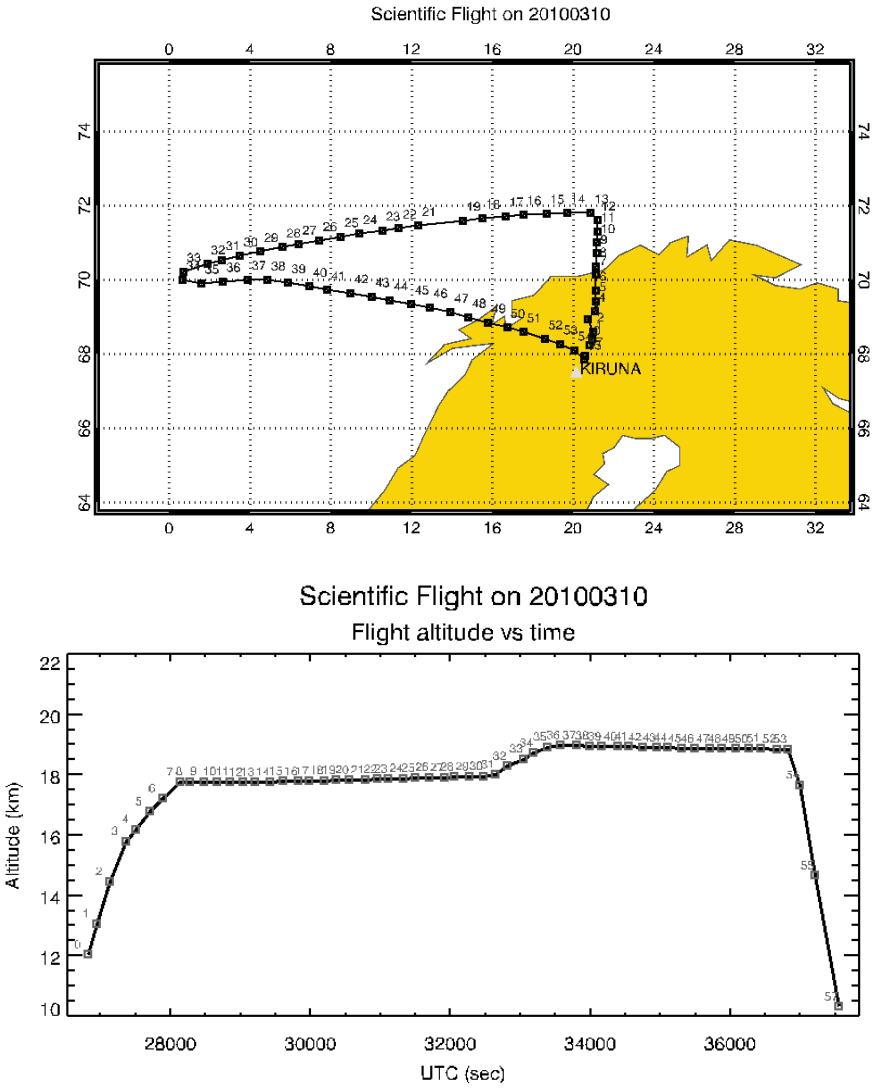

Fig. 58: top panel: the flight track plotted versus latitude and longitude. The black dots show the average position of each scan. Bottom panel: flight altitude and scan position plotted versus the acquisition time (UTC).

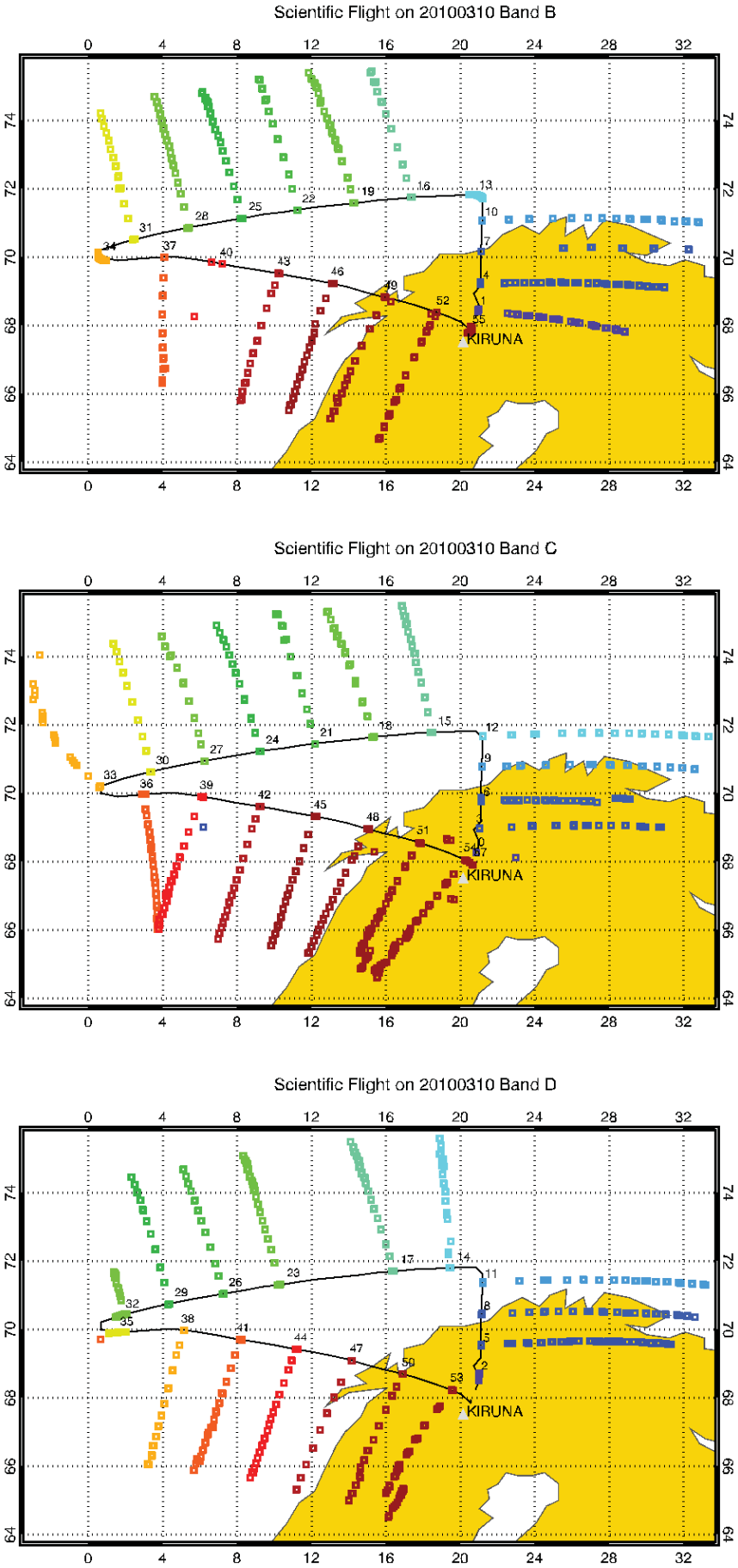

Fig. 59: The flight track with the geolocation of the tangent points of band B, C and D plotted versus latitude and longitude.

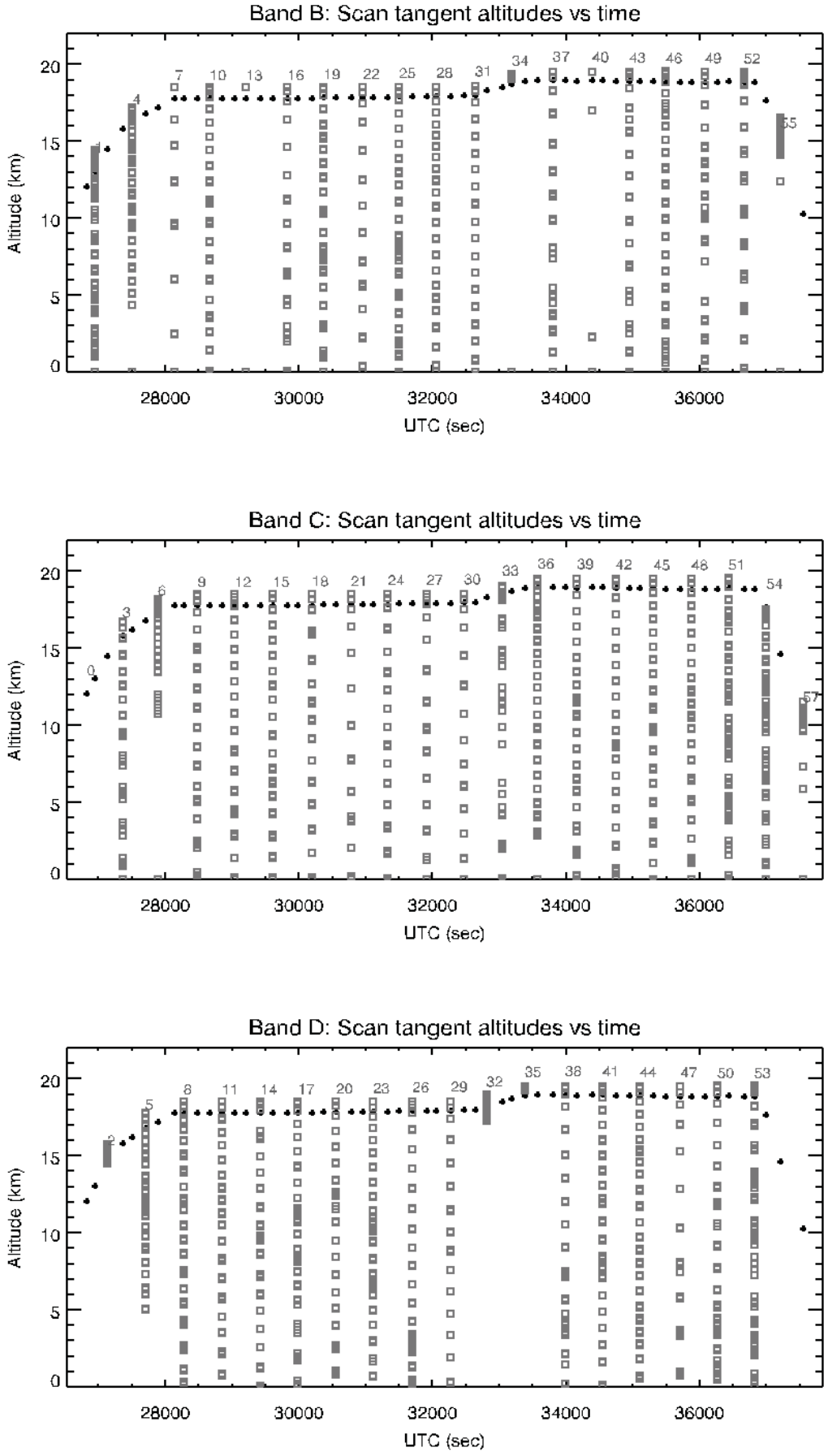

Fig. 60: The flight altitude and the analysed scans tangent altitudes position plotted versus time (UTC). Top panel: band B, central panel: band C, bottom panel: band D.

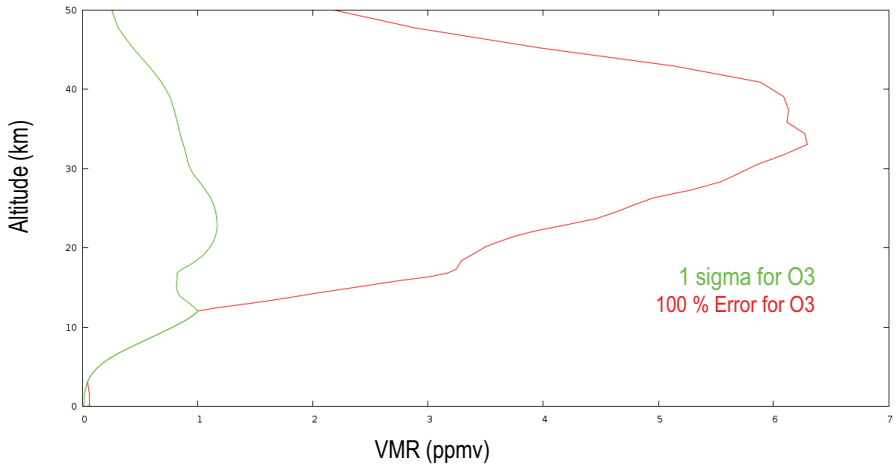

Fig. 61: O_3 error profiles for scan 24 using 1 sigma (green) or 100 % error (red).

preliminary analyses the 1 sigma variability estimated by Remedios [19] was used as a priori error. Since this value was sometimes too low, posing a too strong constraint on the retrievals, a different approach was used for the definition of the a priori errors for the final analysis. For water vapour and ozone the 1-sigma variability was substituted by the 100 % of the a priori profile when its value was lower than 100 % (as an example see Fig.61 for ozone).

A first retrieval test was performed using the same strategy for the other targets. Since for those targets the test produced profiles with large oscillations in the altitude ranges where the information content was low, we have set the a priori error threshold to 50 % . This strategy produced better results with a reduction of the oscillations in the altitude range with low information content and similar results in the altitude range with high information content.

6.2 Retrieval results

6.2.1 Analyzed dataset

Since for this flight all MARSCHALS bands were working, we have performed the analysis on the spectra of all bands. A preliminary analysis has been performed on all the scans present in the Level 1B files, without any screening, even if, as already said in section 6.1.1 and as can be seen in Fig. 60, we can expect the best performances for the scans from 6 to 31 and from 35 to 53. The reported analysis was performed using the different Level 1B datasets reported in Section 4. In general for the analysis we have used data obtained with the calibration method dt10.

6.2.2 Preliminary analysis

The preliminary analysis was performed using the same strategy of the Test Flight reported in section 5.2.2 A thorough description of the preliminary phase of the analysis of the Scientific Flight is out of the scope of this report, here we briefly recall the major issues. As for the Test Flight (see Section 5.2.3) a first test was performed using all the data contained into the preliminary Level 1B file listed in the first row of Table 3. This test highlighted that the delivered Level 1B data had some residual problem in the pointing calibration. However there were fewer problematic spectra than in the Test Flight. The removal from the analysis of the problematic spectra, that were mainly pointing above the flight altitude, reduced the values of the final χ-test and improved the quality of the retrieval products.

The cleaned set of data was analysed using the strategy reported in Sect. 5.2.2. The vertical retrieval grids (constant through the whole flight, but target dependent) used for this analysis were the same of the Test Flight and of the SCOUT-O3 analysis, and in the retrieval we used observations with tangent altitudes higher than 5 km. As already shown for the analysis of the Test Flight, also for the Scientific Flight the Temperature retrieval worked properly only for the scans of Band C. In particular, the retrieved Temperature obtained from Band B measurements was on average always too low around the flight altitude, while the one obtained from Band D was dominated by the a priori profile.

Some problems are also present for the Water Vapour retrieval: we have a good performance only for Band C scans, while for Band B and D the obtained profiles are very unstable and with very large error bars.

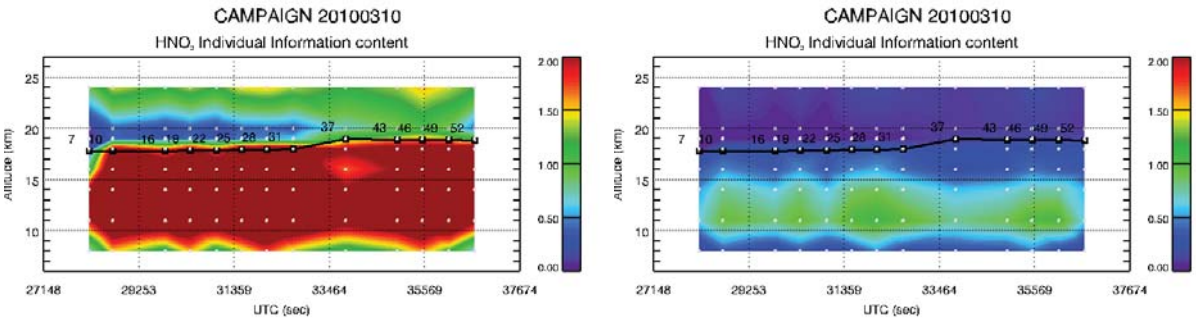

Fig. 62: HNO_3 information content values for Band B using SCOUT-O3 and PremierEx Band B definitions.

From the results obtained in the preliminary analysis we conclude that, as for the Test Flight, Temperature and Water Vapour can be safely retrieved only from the scans of Band C. Therefore further tests are needed to optimize the retrieval strategy in order to extract the best information from the Scientific Flight measurements.

6.3 Tuning the retrieval strategy

6.3.1 Sequential fit

Since the Temperature and water retrievals give satisfactory results only for the Band C analysis, as performed for the Test Flight we have investigated possible different sequential retrieval strategy:

- Sequential fit of T, H_2O, O_3, HNO_3, starting from a band C scan, and single retrieval of the single band targets (N_2O, CO)
- T retrieved in band C used for the following band B and D scans, single retrievals of H_2O, O_3, HNO_3, N_2O, CO
- T and H_2O retrieved in band C used for the following band B and D scans, single retrievals of O_3, HNO_3, N_2O, CO

As for the Test Flight the first strategy produced a final Temperature profile that showed anomalous values at flight altitudes, since the biased errors on Temperature in the band C + D retrievals were not very different from the a priori errors, so that they were not a stronger constraint for the Temperature retrieval of band B. The second strategy gave very good results. An attempt to fix the H_2O profile to the values of band C did not produce any improvement. The identified retrieval strategy for the final analysis was to use the water profile retrieved in band C as a priori for the subsequent scans, but to let the H_2O profile flow to account for the effects of the far wings of the water lines that may not be correctly reproduced using the band C retrieved values. Therefore the final retrieval strategy was:

- Band C Retrieval of scan N : T, H_2O, O_3, HNO_3, Pointing, gain, Offset, Continuum
- Band B Retrieval of scan N+1: H_2O, O_3, HNO_3, N_2O, Pointing, gain, Offset, Continuum (T from Band C scan N, a priori H_2O from band C)
- Band D Retrieval of scan N+2: H_2O, O_3, HNO_3, CO, Pointing, gain, Offset, Continuum (T from Band C scan N, a priori H_2O from band C)

where N is the scan number of band C.

6.3.2 Impact of new band definition

The analysis of the Test Flight was performed using the SCOUT-O3 bands definition (that is using the Preliminary1 configuration, see Section 4). The new band definitions changed the frequency boundary of each Band, so it could have an impact on the retrieval products. therefore we have performed a comparison of the results of the analysis of the Scientific Flight using the old and new band definitions.

No relevant differences were found for the analysis of Band C and Band D while the retrieval of HNO_3 in band B shows that the new band definition has caused a decrease of the information content for that molecule (see the two panels of Fig. 62). As already seen in section 4, the PremierEx band B definition covers a smaller spectral

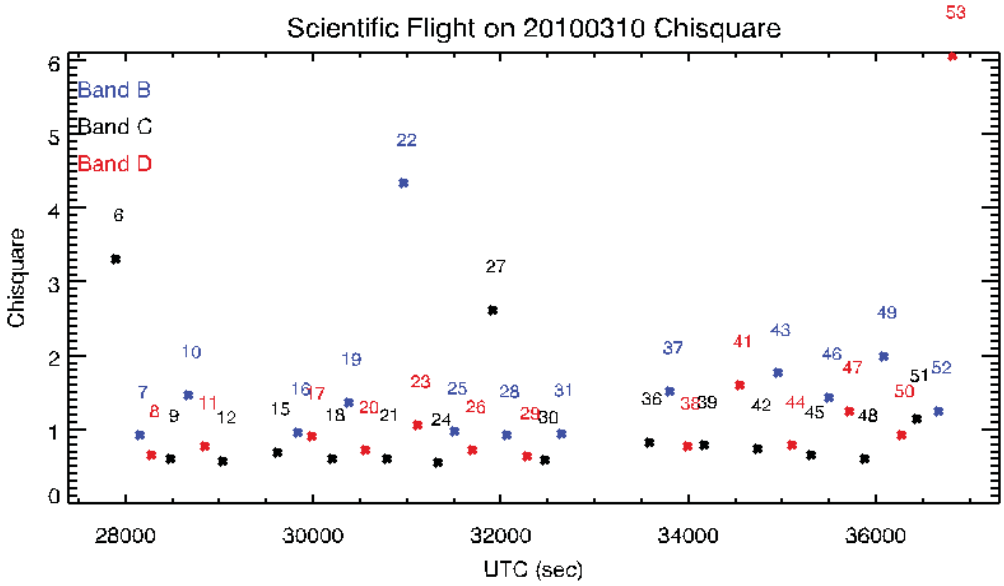

Fig. 63: χ-test values obtained in the final analysis with the new noise characterization, plotted for each scan (blue = band B, black = band C, red = band D) as a function of the acquisition time.

range than the SCOUT-O3 definition; in particular the the HNO_3 lines at the beginning of the band ($\tilde{2}$94 GHz) are completely discarded. This causes the reduction of the information content for the HNO_3 retrieval shown in Fig. 62.

6.3.3 New noise characterization

The difference between the new and the old noise characterizations has already been discussed in section 4 and is shown in Figures 22 and 23. Since the new noise has been thoroughly checked by the RAL team in the final analysis we have substituted the average L1 noise with the channel dependent noise directly read from the level 1 file.

The resulting χ-test values for the whole flight plotted as a function of the scan acquisition time are shown in Fig. 63. In the figure, the χ-test values are reported in different colours for each band C = black, B = blue and D = red). The χ-test values for the three bands are very similar, even if for band B we have on average higher χ-test values. Sometimes the χ-test assumes values below 1, expecially for band C and D scans, suggesting that the noise values reported in the level 1 file are on average overestimated.

6.3.4 Impact of new FOV characterization

The new FOV data extend for a wider angular interval than the old SCOUT-O3 FOV (see Fig. 24 where the SCOUT-O3 FOV is represented by the green line and the new FOV data are represented in red). However, in the region where the instrument angular response in higher, both FOV functions are very similar. In the preliminary analysis, the width of the maximum extension used for the FOV convolution was set at 1.6 deg. Due to the new FOV definitions that show some lobes also at angular distance from the FOV center greater than 0.8 deg, as shown in Fig. 24, we extended the width of the maximum extension used for the FOV convolution to 2.8 deg.

A comparison of the analysis performed with the new and old FOV functions shows negligible differences between the retrieved profiles, while a very small decrease can be noted for the degrees of freedom and for the information load possibly due to the weak altitude correlations introduced by the wider FOV extension.

6.3.5 Assessment of the impact of the width of the filter used for the correction of the pointing

The final set of data, delivered by RAL on October 2010, contains different versions of Level 1B files with the pointing information corrected using high/low pass filters of different time width (labelled as dt02, dt05, dt10, dt20, dt40, dt60 with the numbers representing the filter width in seconds).

Some test have been performed to evaluate the impact of the use of different filter width on the retrieval results. In general the use of different filter widths did not produce relevant differences even if the filter widths of 2 and

5 sec produce slightly worse results in terms of retrieved pointing corrections and χ-test . All the other retrieval quantifiers show very similar values with some filter width performing better on some scans and other filter width performing better on other scans. Also the mean retrieved pointing biases are very similar: -0.014 $\pm$ 0.039 deg for dt10, -0.013 $\pm$ 0.041 deg for dt20 and -0.012 $\pm$ 0.036 deg for dt40. Since none of the filter widths shows evidence of better performances with respect to the others we decided to stay with the Level 1 data obtained with the 10 seconds filter width for the final analysis.

6.3.6 Tuning of the retrieval grid

The vertical retrieval grids used for the Tests Flight were optimised during the theoretical retrieval study [24] and performed well for the banc C analysis of the SCOUT-O3 flight. Since the SCOUT-O3 flight was performed at tropical latitudes while the PremierEx flight is at polar latitudes, we have evaluated the possibility of both extending the vertical grid at lower altitudes and to change the vertical spacing of the target dependent retrieval grids.

As a starting point, we have used all the available observations down to the Earth in order to exploit all the available informations at low altitudes and we have proceeded to optimize the vertical retrieval grid of each target. Different vertical retrieval grids were tested, expecially for HNO_3 and CO. The adopted grids, chosen with the purpose of minimizing the oscillations and maximize the information gain, on both the first and the second part of the flight, are reported below:

- T: 24, 20, 18, 17, 15, 13, 11, 9, 7, 5
- H_2O: 24, 21, 18, 17, 16, 15, 14, 13, 12, 11, 10, 9, 8, 7, 6, 4
- O_3: 24, 21, 18, 17, 16, 15, 14, 13, 12, 11, 8, 5
- HNO_3: 23, 20, 17, 16, 14, 12, 9, 6
- N_2O: 20, 16, 14, 12, 10, 8
- CO: 21, 17, 13, 7
- External Continuum: 18, 17, 16, 15, 14, 13, 12, 11, 10, 9, 8, 7, 6

Since the lowest altitude in the optimized vertical retrieval grids is 4 km, we have tested the impact of removing observations with tangent altitude lower than 4 km from the analysed dataset. Removing the observations below an altitude of 2 km produces values of the trace and the information content that are usually lower, expecially in the first part of the flight, where the observations are located at higher latitudes. Therefore we have chosen to use all observations down to 0 km.

Finally, because the CO VMR reaches the maximum value in the higher part of the atmosphere (above 50 km), we repeated the analysis using 90 km and 65 km instead of 50 km as top of the atmosphere. This does not affect the retrievals of the other targets but produces an enhancement in the trace and information contents of band D. For this reason the top of the atmosphere has been extended at 65 km for all the bands.

6.3.7 Frequency shift retrieval

Since test retrievals on simulated spectra have demostrated that the retrieval of the frequency shift is possible, we tested its impact on the retrieval of PremierEx data. We recall here that, as already said in Section 2.4.1 we retrieve a frequency shift value for each band and therefore we will have a single value for each scan. The initial guess value for the frequency shift was set at 0.0 MHz for each band and its a priori error was set at the very high value of 1000 MHz.

In Figure 64, the values of the frequency shift (in MHz) together with the associated biased errors, and the average band value, are plotted with different colour for each band (blue for Band B, black for Band C, red for Band D) and the mean value is represented by a dashed line of the same colour. The retrieved frequency shift is similar for the three bands, with no significant variations during the flight, with the one of band C on average slightly higher than the band D one that in turn is higher than the band B one. The averaged values of the three bands frequency shift is reported in table 5. The retrieved shift is always much smaller than MARSCHALS frequency resolution ($\sim$ 200 MHz). The errors associated to the retrieved frequency shift are of the order of 1 MHz, showing the high accuracy of the retrieved values.

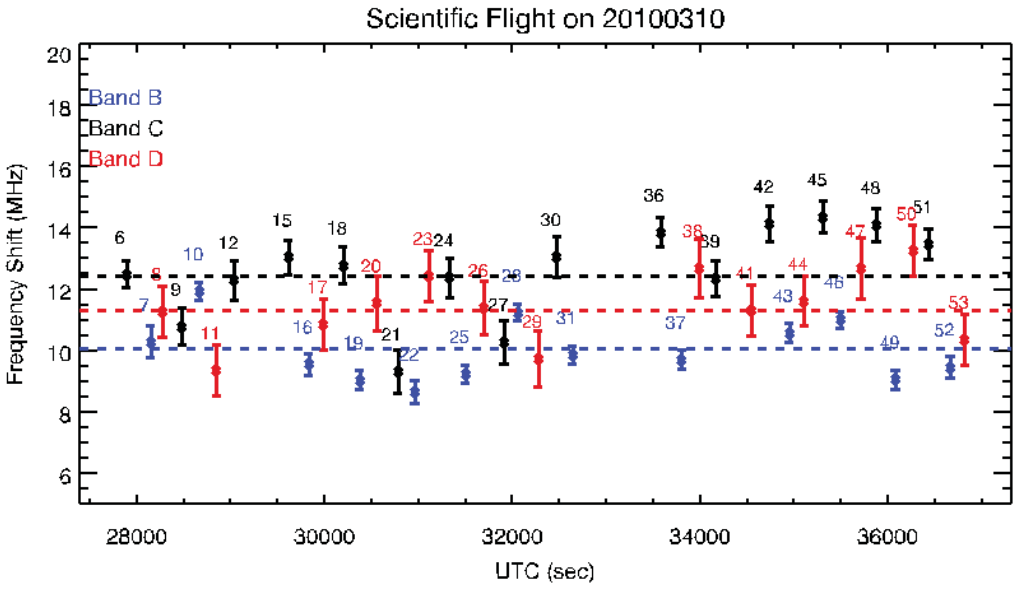

Fig. 64: Frequency shift retrieval for the PremierEx flight.

Tab. 5: Retrieved average values of frequency shift

Band	Frequency shift MHz	Biased Error MHz
Band B	10.06	0.97
Band C	12.43	1.43
Band D	11.31	1.81

6.4 Final analysis

All the tests performed in the previous sections have helped in identifying the best strategy to analyse MARSCHALS data during the PremierEx campaign in Kiruna.

The final analysis was then obtained using the following strategy:

- Noise level from new Level 1B files
- Use of the new FOV definition
- Use of the new ILS and band definitions
- Use of level 1 data obtained with a 10 sec. filter width for pointing correction
- Removal of problematic scans from the analysis
- Use of the optimized vertical retrieval grids
- Top of the atmosphere at about 65 km
- Use of observations with tangent altitudes down to 0 km
- Temperature retrieval for Band C only.
- Water VMR retrieval of Band C used as a priori for the other bands.
- Frequency shift retrieval

The results of the final analysis are summarized in Figures from 63 to 79. The information content of the Temperature retrieval is low for the whole altitude range with minimum values above the flight altitude and with values beetween 1 and 1.5 at altitudes below 11 km. We measure the tropopause at altitudes around 10 km, with a lower Temperature in the last part of the flight. The retrieved H_2O values, shown in figure 68 for band C only,

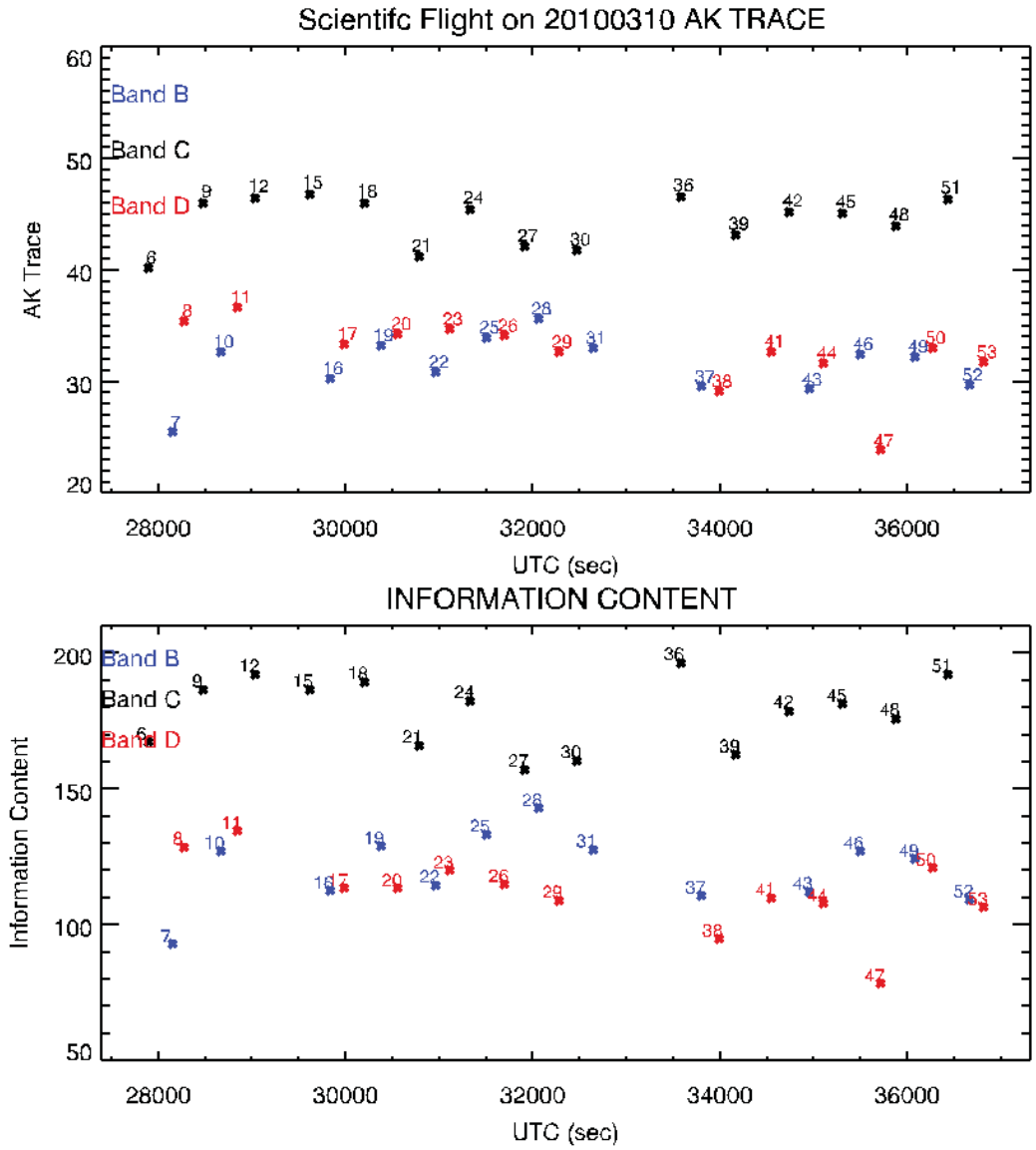

Fig. 65: Final analysis retrieval quantifiers (blue = band B, black = band C, red = band D)

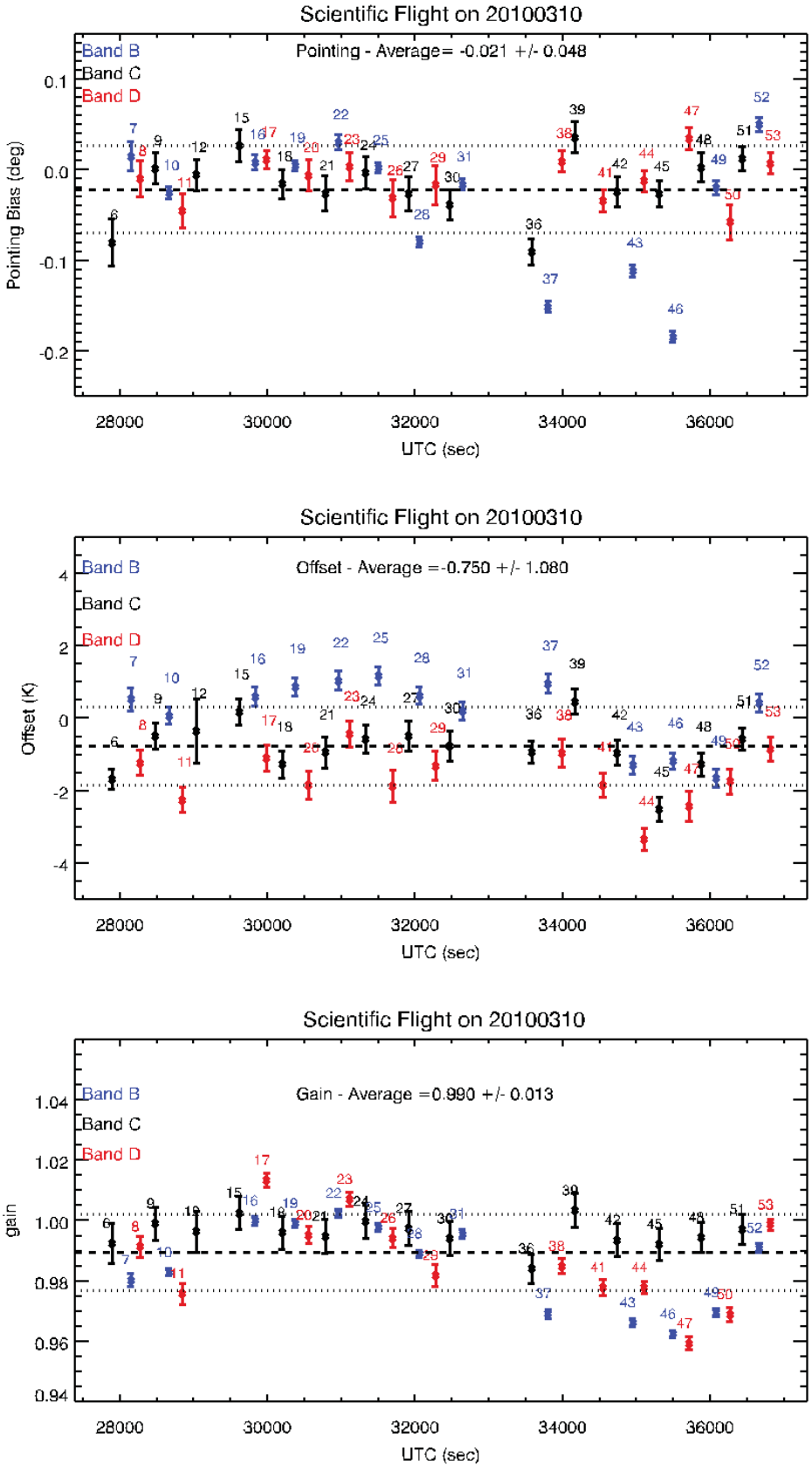

Fig. 66: Final analysis: retrieved pointing, offset and gain for each band (blue = band B, black = band C, red = band D)

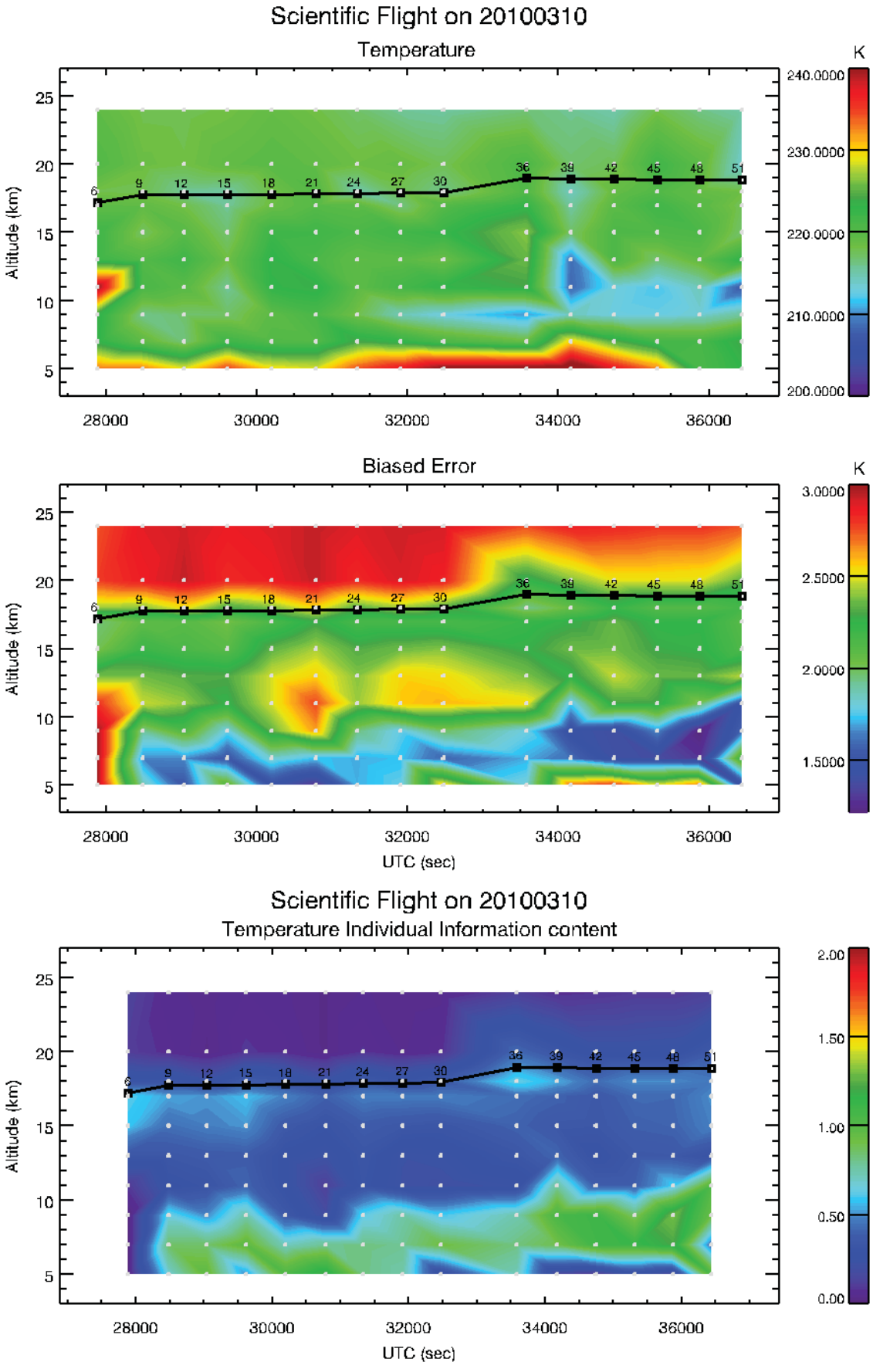

Fig. 67: Temperature from band C retrievals , biased error and information content.

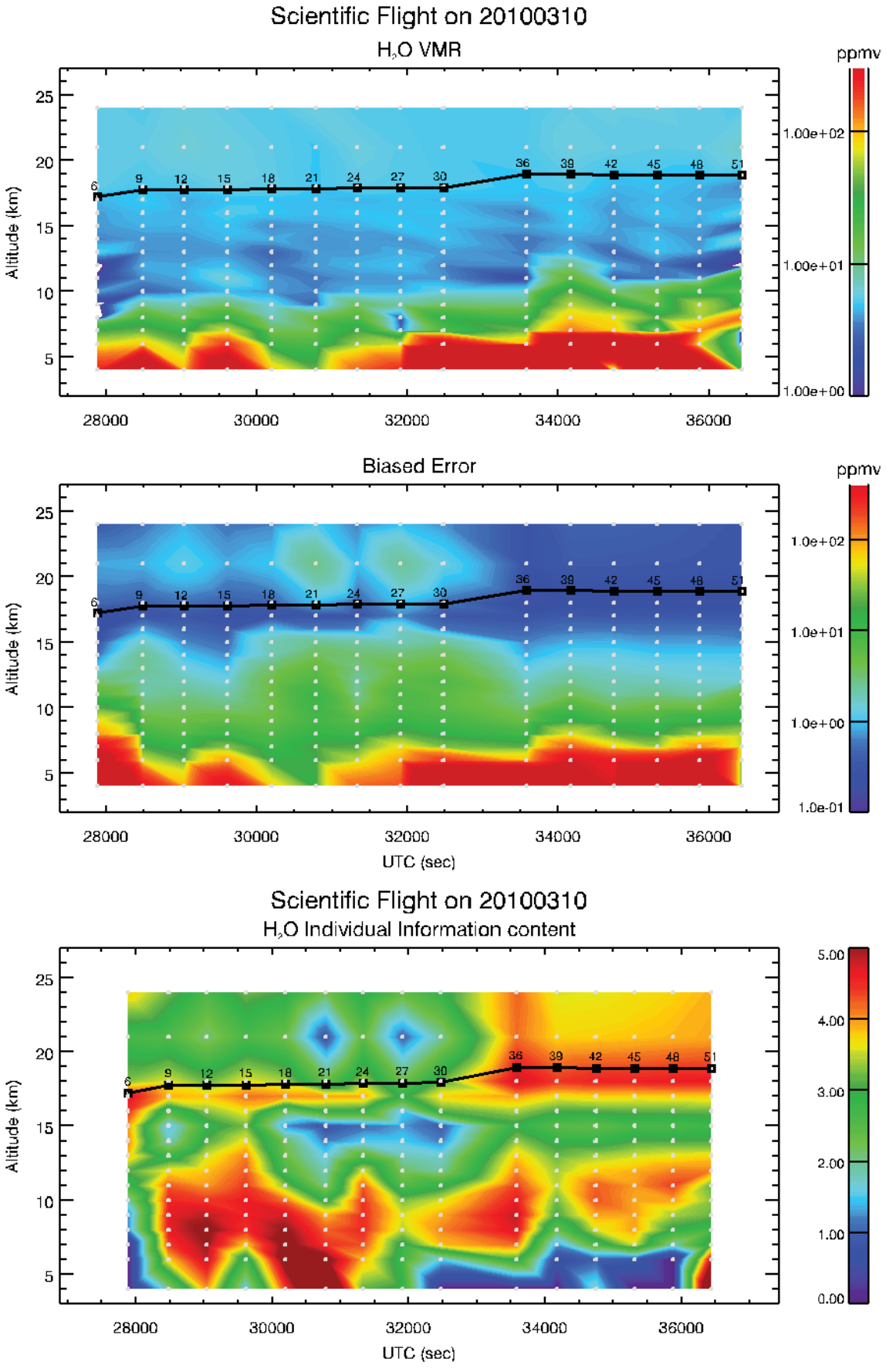

Fig. 68: H_2O retrieved from band C, biased error and information content.

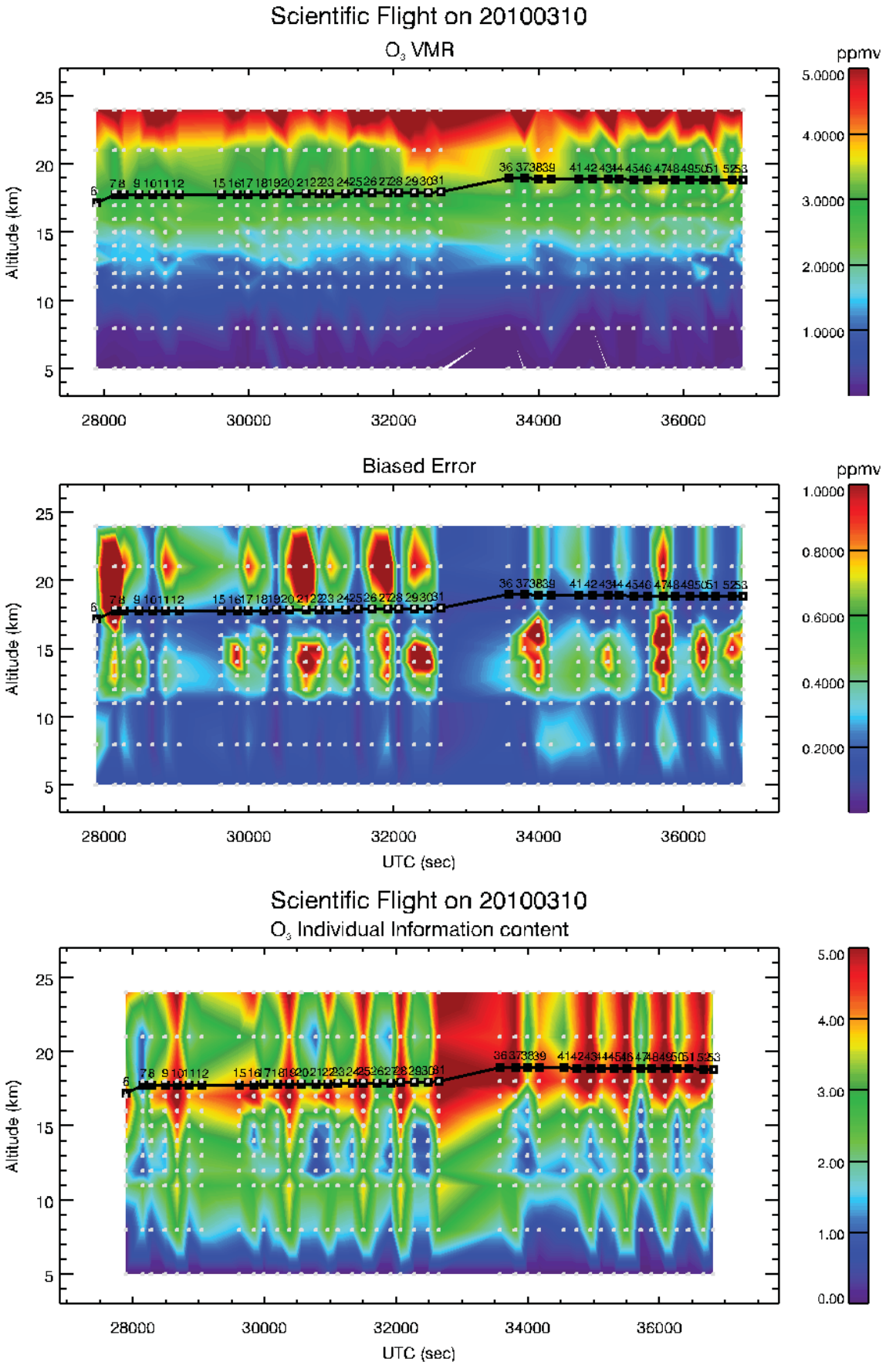

Fig. 69: O_3 retrieved using all the scans, biased error and information content.

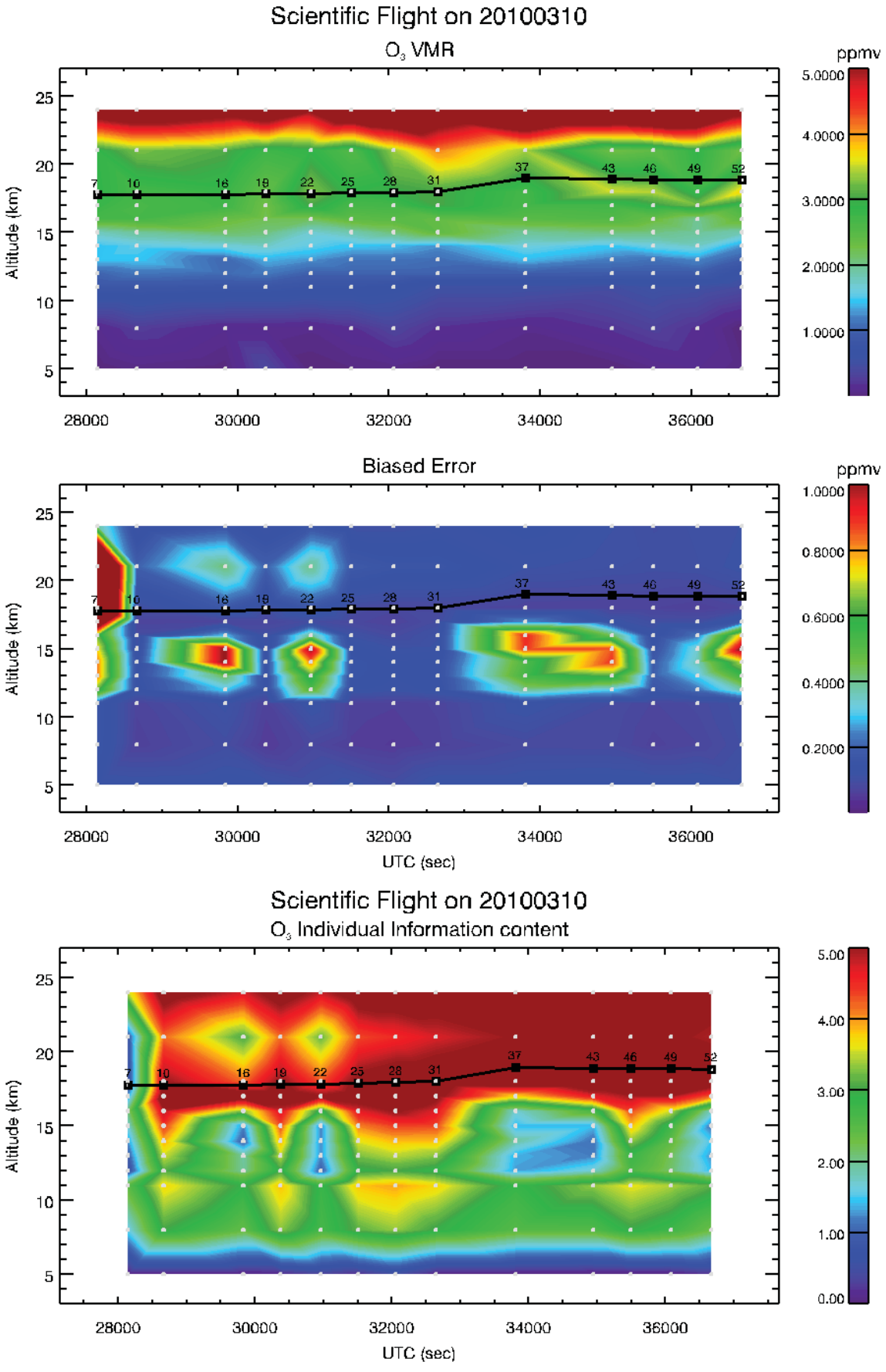

Fig. 70: O_3 retrievals from band B, biased error and information content.

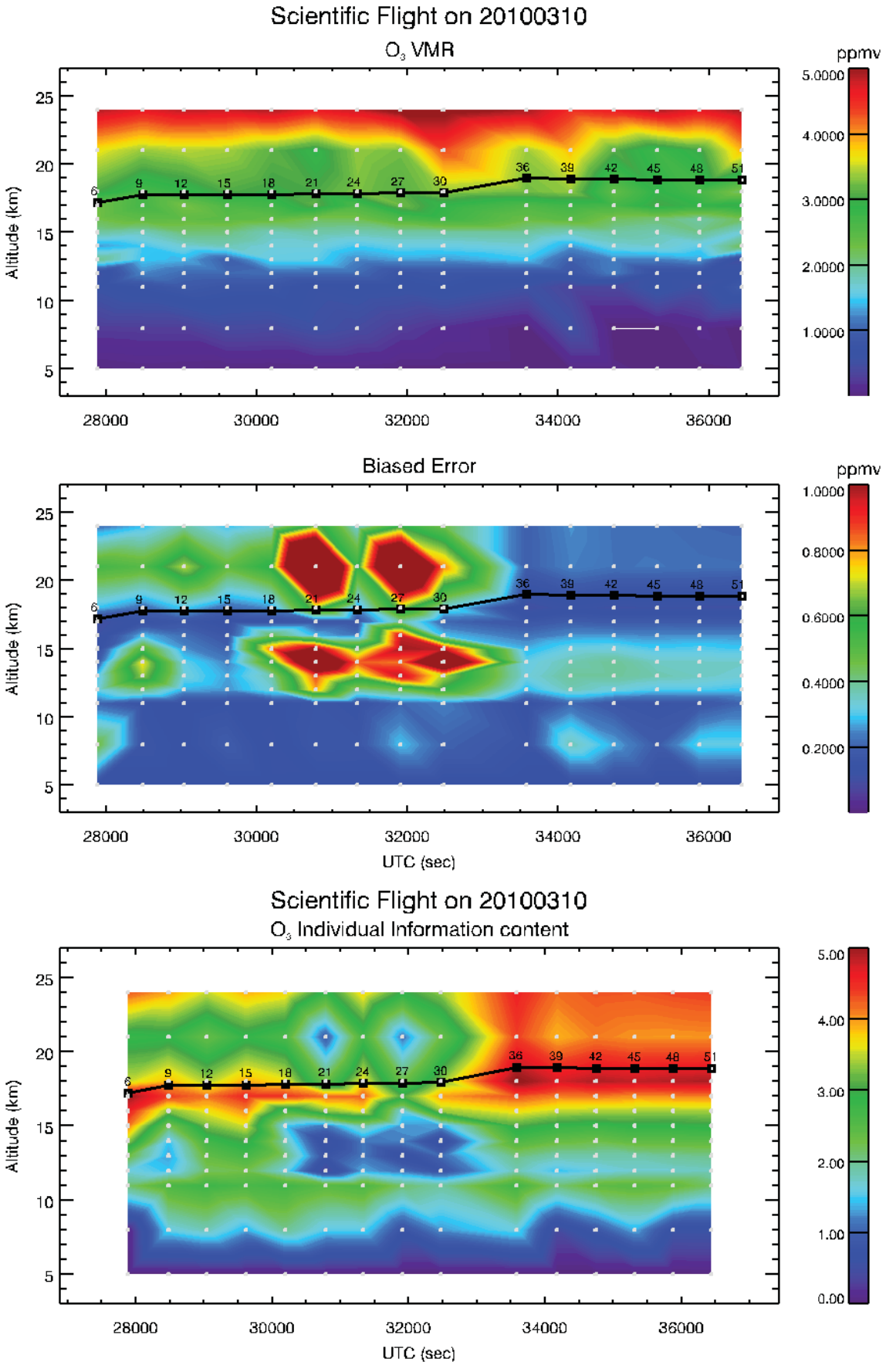

Fig. 71: O_3 retrievals from band C, biased error and information content.

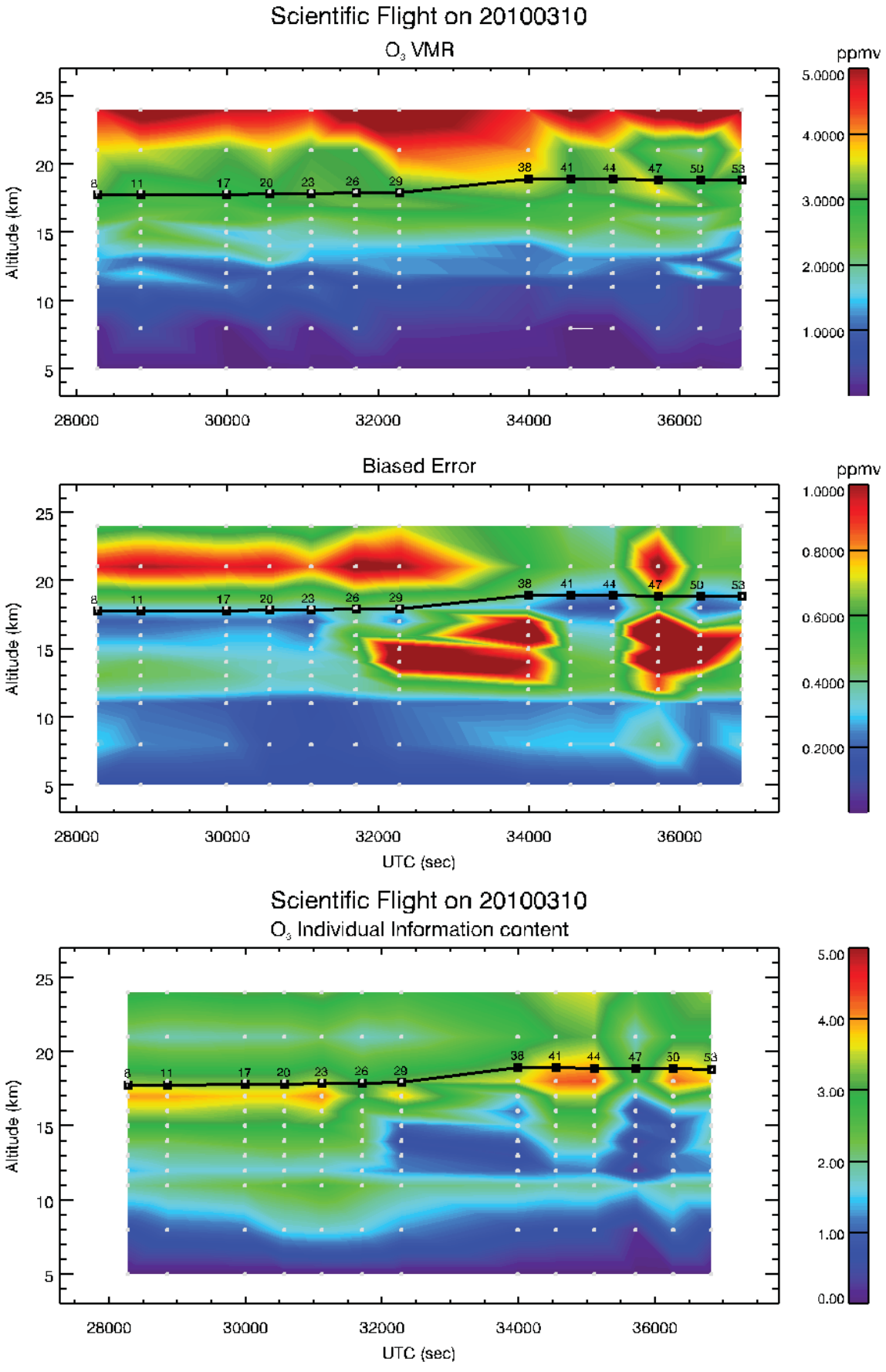

Fig. 72: O_3 retrievals from band D, biased error and information content.

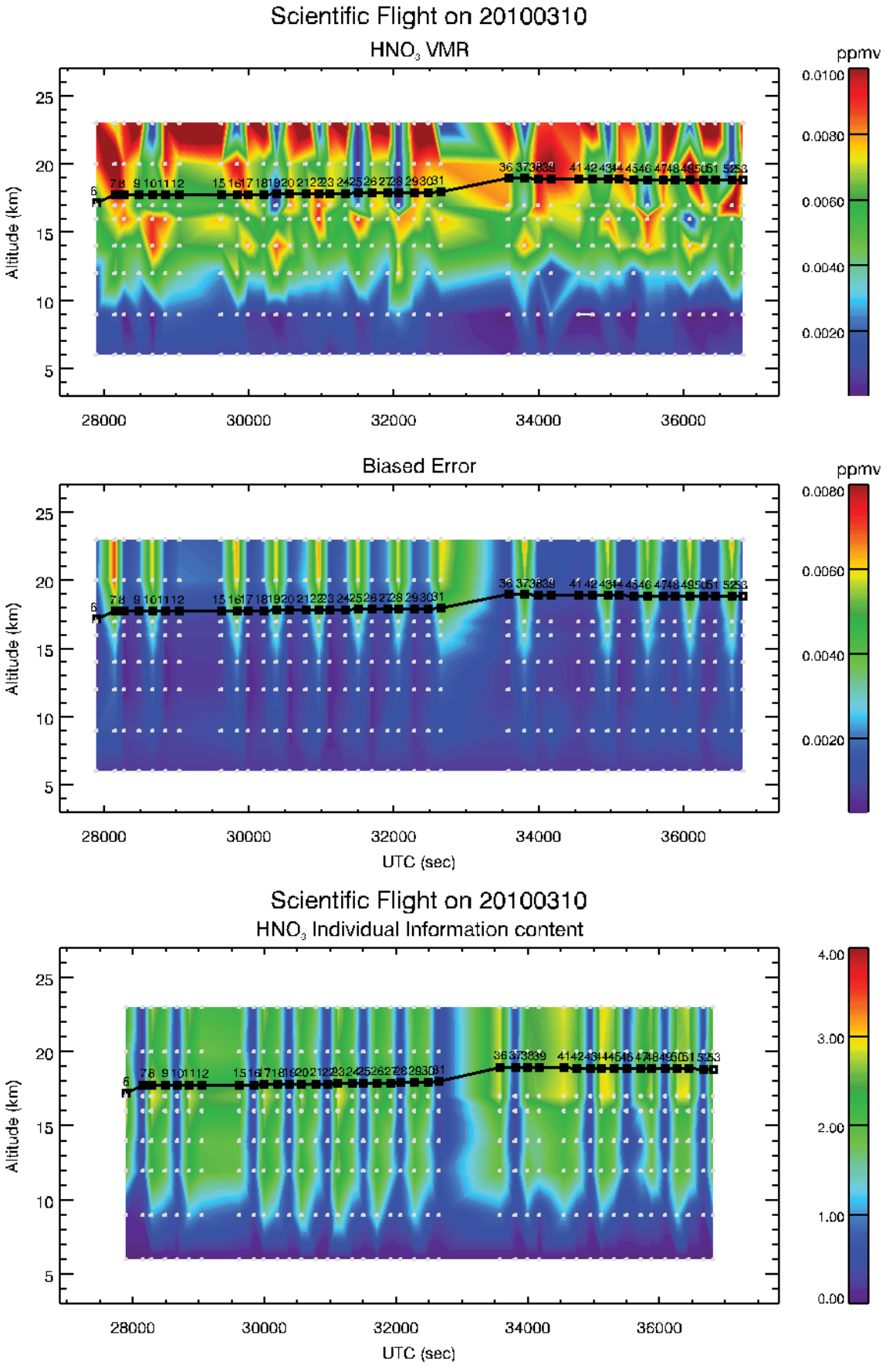

Fig. 73: HNO_3 retrieved using all scans, biased error and information content.

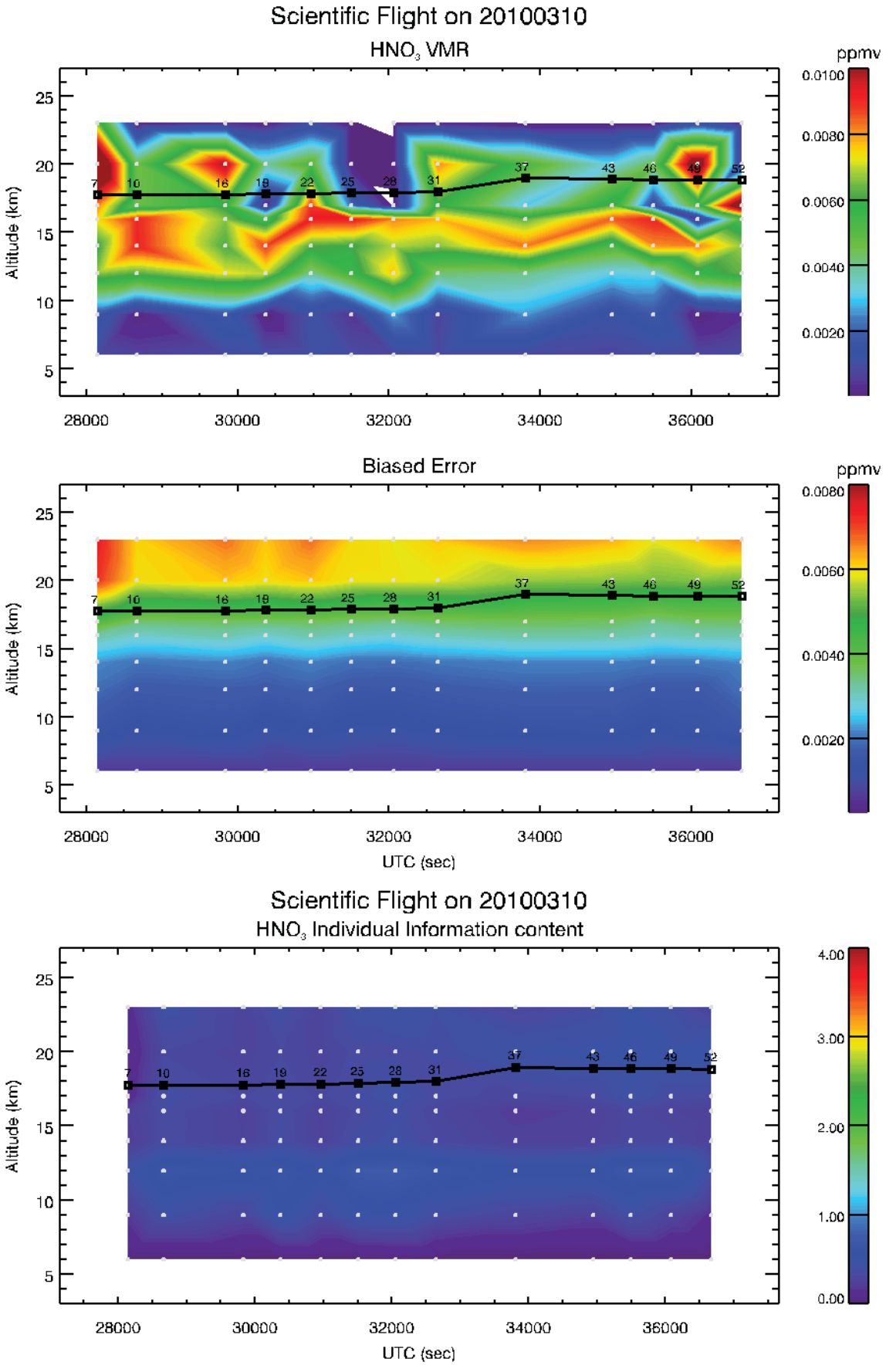

Fig. 74: HNO_3 retrievals from band B, biased error and information content.

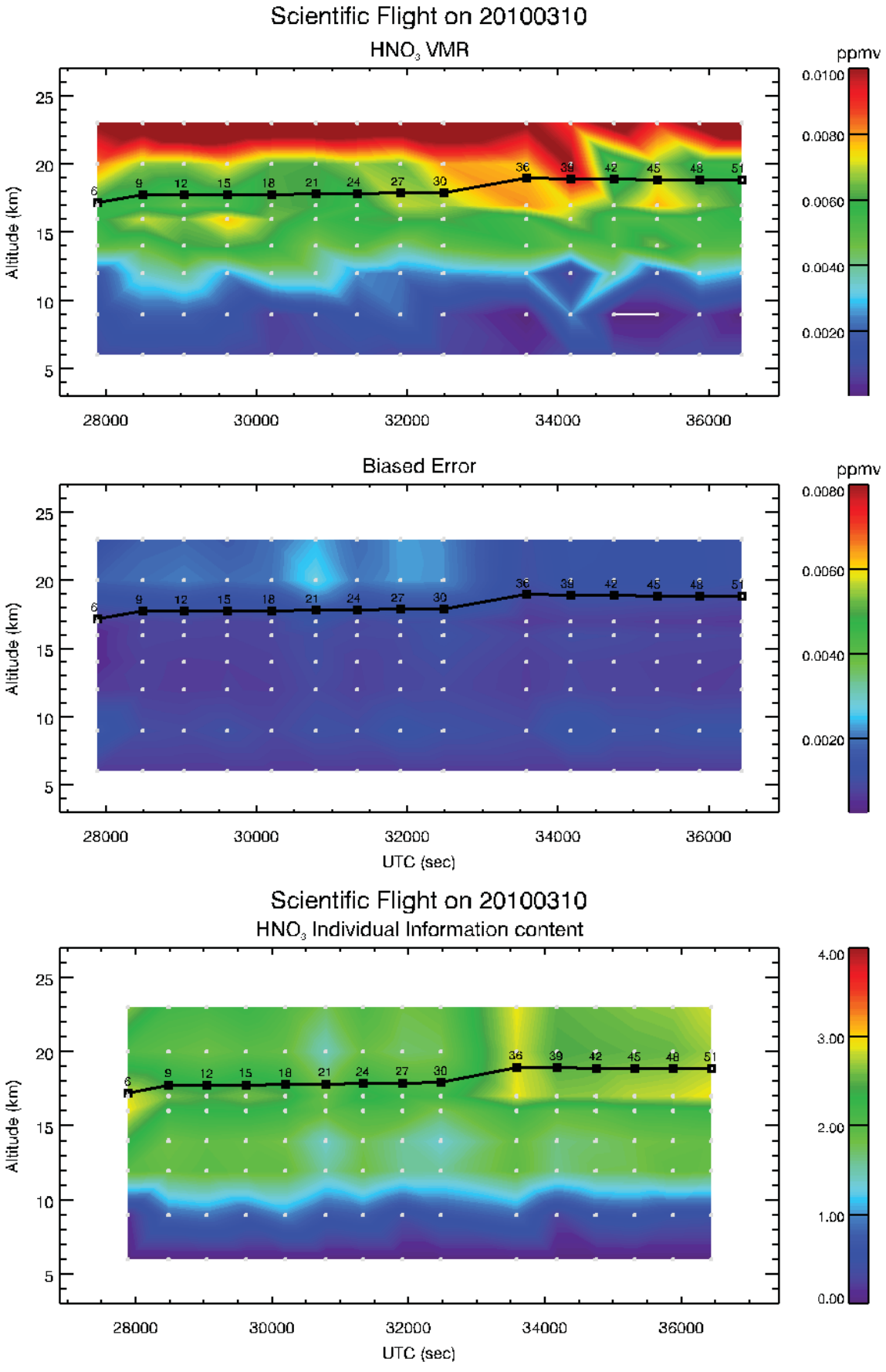

Fig. 75: HNO_3 retrievals from band C, biased error and information content.

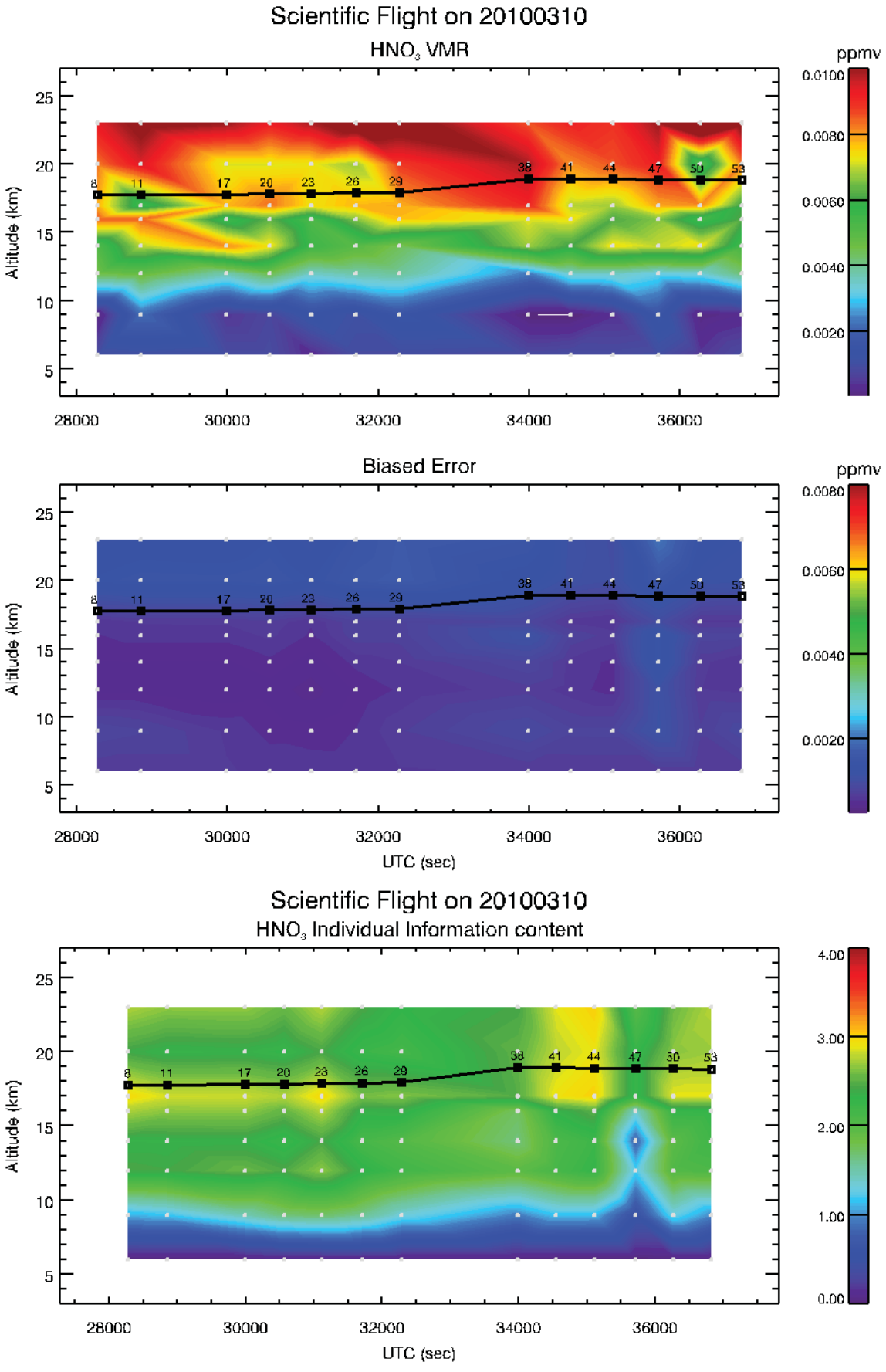

Fig. 76: HNO_3 retrievals from band D, biased error and information content.

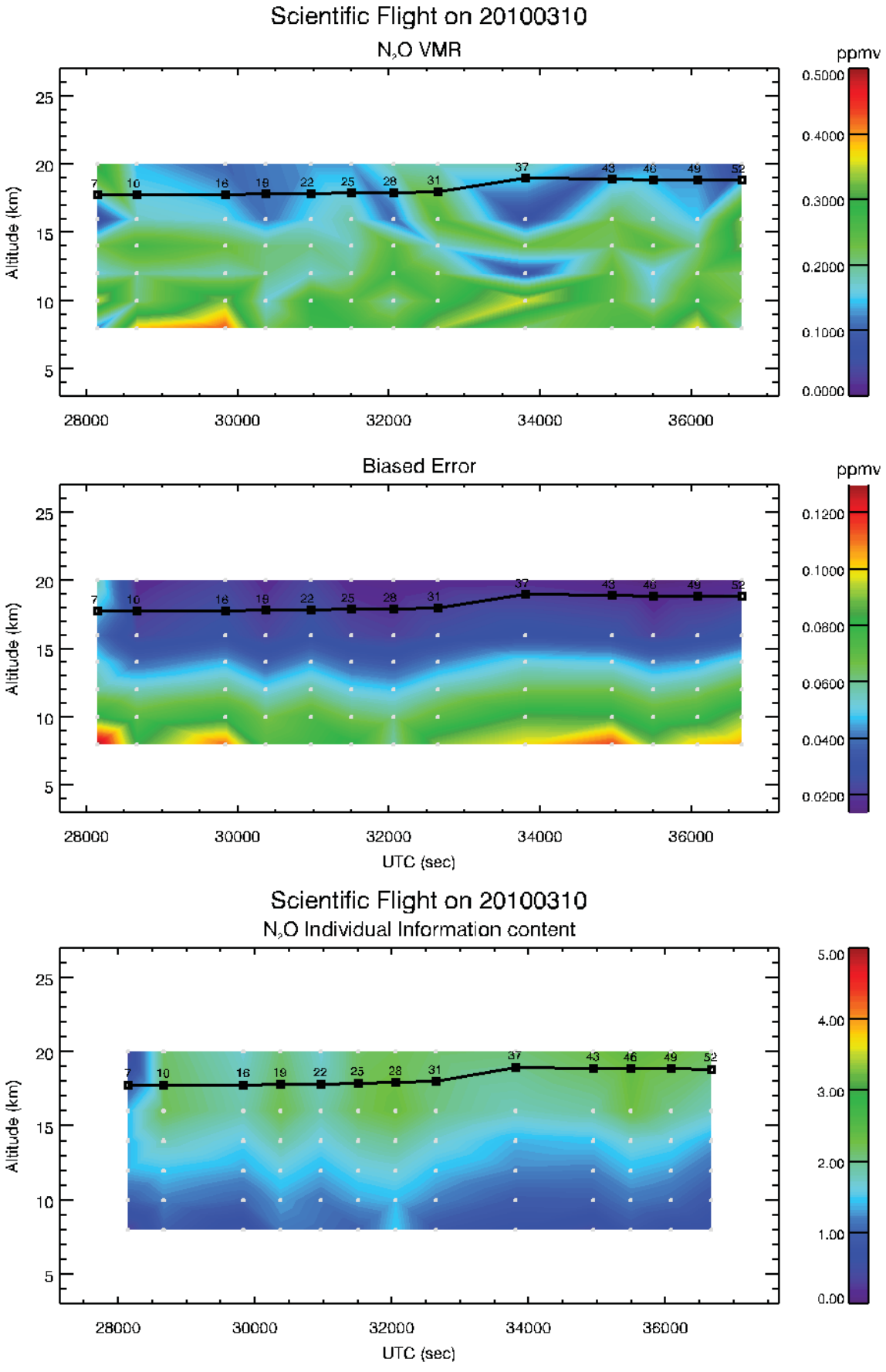

Fig. 77: N_2O retrievals (band B), biased error and information content.

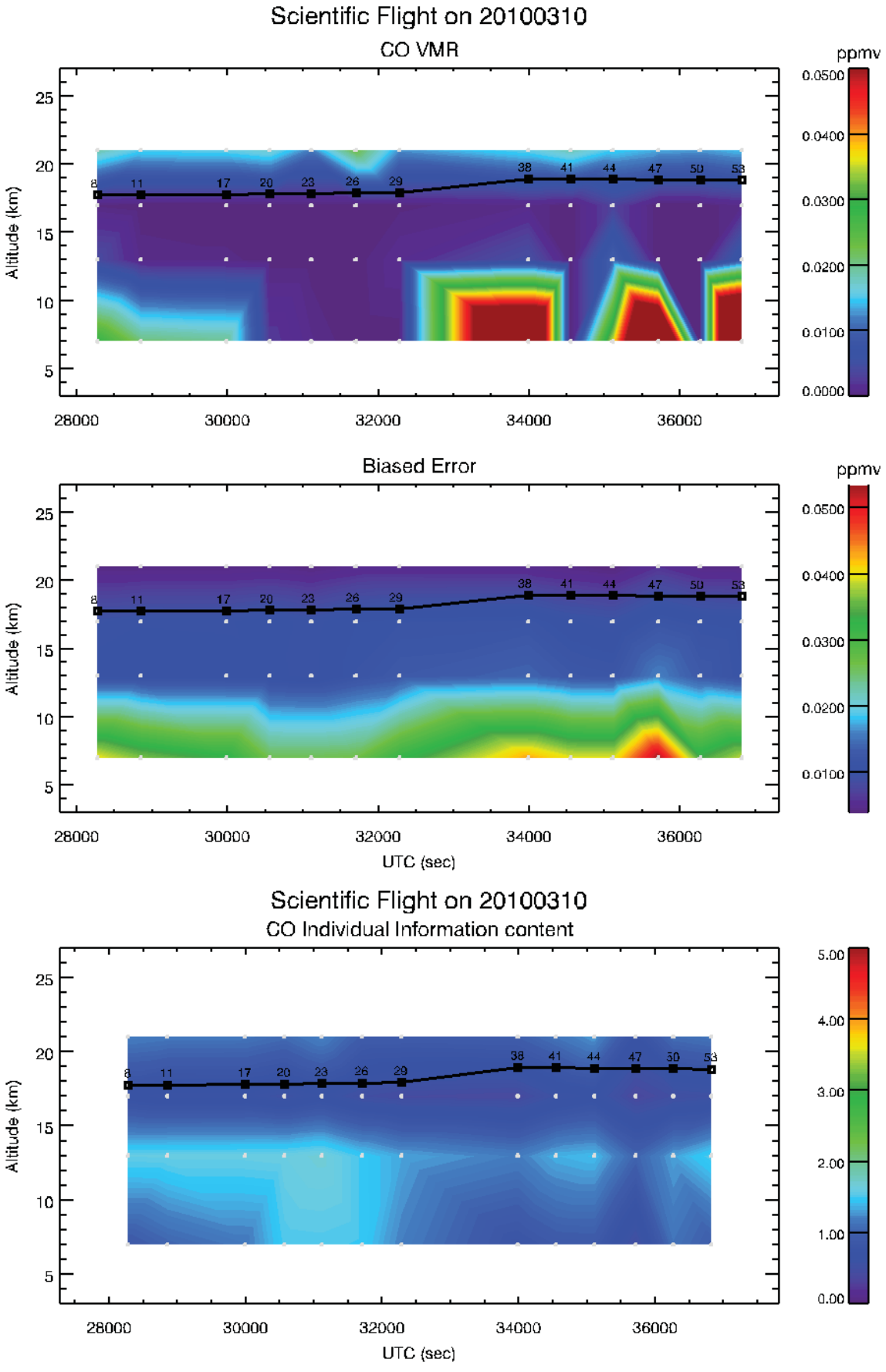

Fig. 78: CO retrievals (band D), biased error and information content.

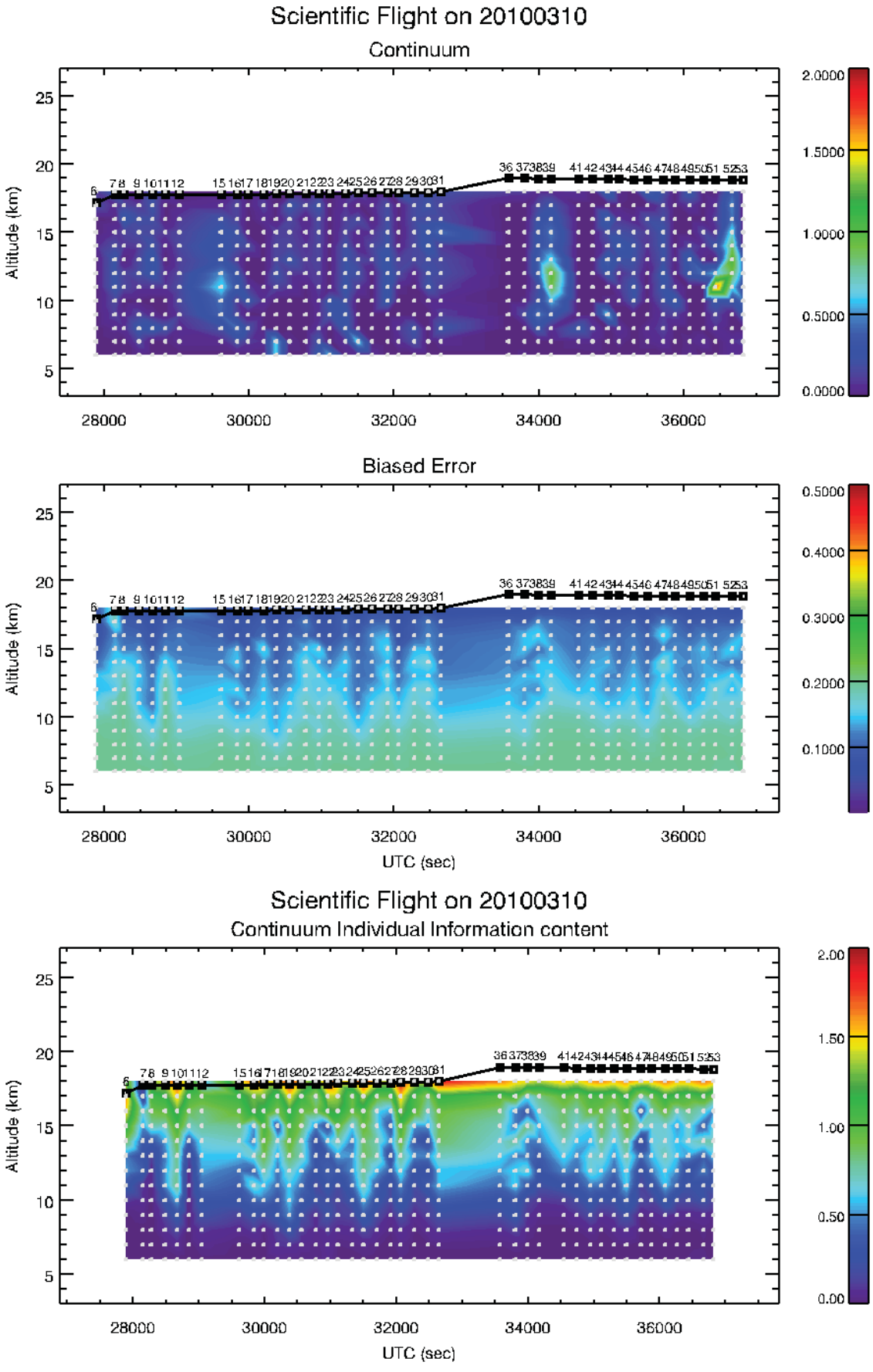

Fig. 79: External continuum retrieved using all bands, biased error and information content.

shows an uneven distribution, with higher values at low altitudes in the last part of the flight. The information load map in Figure 68 highlights that the information content in MARSCHALS measurements is not evenly distributed, with a lower value at 15 km. The increase in information content above flight altitude in the second half of the flight (see Figures 68 and 69) and the distribution of the information content in the vertical dimension are due to the uneven coverage of the measurements respect to altitude during the flight (see Figure 60) respect to the use of constant retrieval grids for all the flight. As can be noticed from the central panel of Figure 60, for example, the vertical coverage of measurements for scans 21, 27 and 30 (in Band C) in the altitude range below 18 km is reduced respect to other scans in the same band, while the retrieval grid used for retrievals in figures 68 and 69 are the same for all the band C scans. This produce a lower value of the information content below fight altitude for scans 21, 27 and 30 as can be seen from Figure 68, and also Figure 75. O_3 retrieval produces good results in all bands, even if the information content is higher above flight altitude in the measurements of band B. The information content for HNO_3 is very good in band C and D, while, as already discussed in section 6.3.2, it is very low in band B. N_2O retrieved values still show strong oscillations, despite the fact that the information content is acceptable down to 13 km. CO retrieved values show higher values in the last part of the flight at low altitudes; however for that region the information content is lower and therefore the retrieved data are mainly representing the a priori profiles. The external continuum mapped in Figure 79 shows that we may have some cloud influence for scans 15 (very low influence), 39, 51 and 52. However, looking at the final χ-test values obtained for those scans, we can conclude that the cloud contribution can be satisfactorily represented through the fit of an external continuum.

6.5 Recursive retrievals for O_3 and HNO_3

The results obtained in the final analysis show that for almost all targets the information content is different in each band. In particular, for targets whose spectral features are present in all bands, the accuracy of the retrieved VMR will benefit from the possibility to perform a simultaneous measurement, and therefore analysis, of the three bands. MARC can in principle handle a multiband retrieval, with the limitation of having the three bands acquired with the same observation geometry (same pointing angle and flight altitude). Since MARSCHALS measurement strategy is different, we have devised a retrieval strategy that can simulate the multi-band approach. Exploiting the possibility of MARC to perform recursive retrievals, using at each step the retrieved VMRs and the VCM of the previous step as a priori information, we have run the final analysis with the following approach: As in the final analysis band C is used to retrieve Temperature and H_2O, then we have retrieved O_3 and HNO_3 in this way: the retrieval of O_3 uses the ECMWF a priori only for the scans of band B, while the analysis of band D and C uses as a priori the results of the analysis of the previous scan. the retrieval of HNO_3 uses the ECMWF a priori only for the scans of band D, while the analysis of band C and B uses as a priori the results of the analysis of the previous scan. The final results for O_3 is shown in figure 80, where the top two panels show the map obtained using just the band C profiles and in the bottom two panels the results for the full flight. Comparing these maps with the figures 69 and 71 we see the improvement obtained with this strategy for O_3 retrieved in band C and for the whole flight. The same conclusion can be reached for HNO_3: the results shown in Fig. 81 compared with the figures 73 and 74 show the improvements achieved with the new strategy.

7 Conclusions of MARSCHALS Test Flight and Scientific Flight data analysis

From the results obtained in the analysis of the Test Flight and of the Scientific Flight we conclude that Temperature and Water Vapour can only be successfully retrieved from the Band C scans, while O_3 and HNO_3can be retrieved from all bands.

The flight pattern used in the Test Flight made it possible to perform a satisfactory analysis only in the first part of the flight, that is from scan 6 to 12, and for few sparse scans in the rest of the flight. Due to the measurement strategy, we only had 6 contiguous scans that could be used to test recursive retrievals, therefore the recursive retrieval strategy could only be thoroughly tested in the Scientific Flight analysis. The preliminary analysis of the Test Flight highlighted that the Level 1 data delivered by RAL had some residual problem in the pointing calibration.

The data delivered for the Scientific Flight had solved part of the shortcomings identified in the Test Flight analysis: the pointing problems almost disappeared and the noise characterization has definitely improved, even if the results of the analysis suggest an overestimation of the noise reported in the level 1B liles. The better flight pattern of the Scientific Flight enabled a thorough testing of all MARC features and a fine tuning of the best

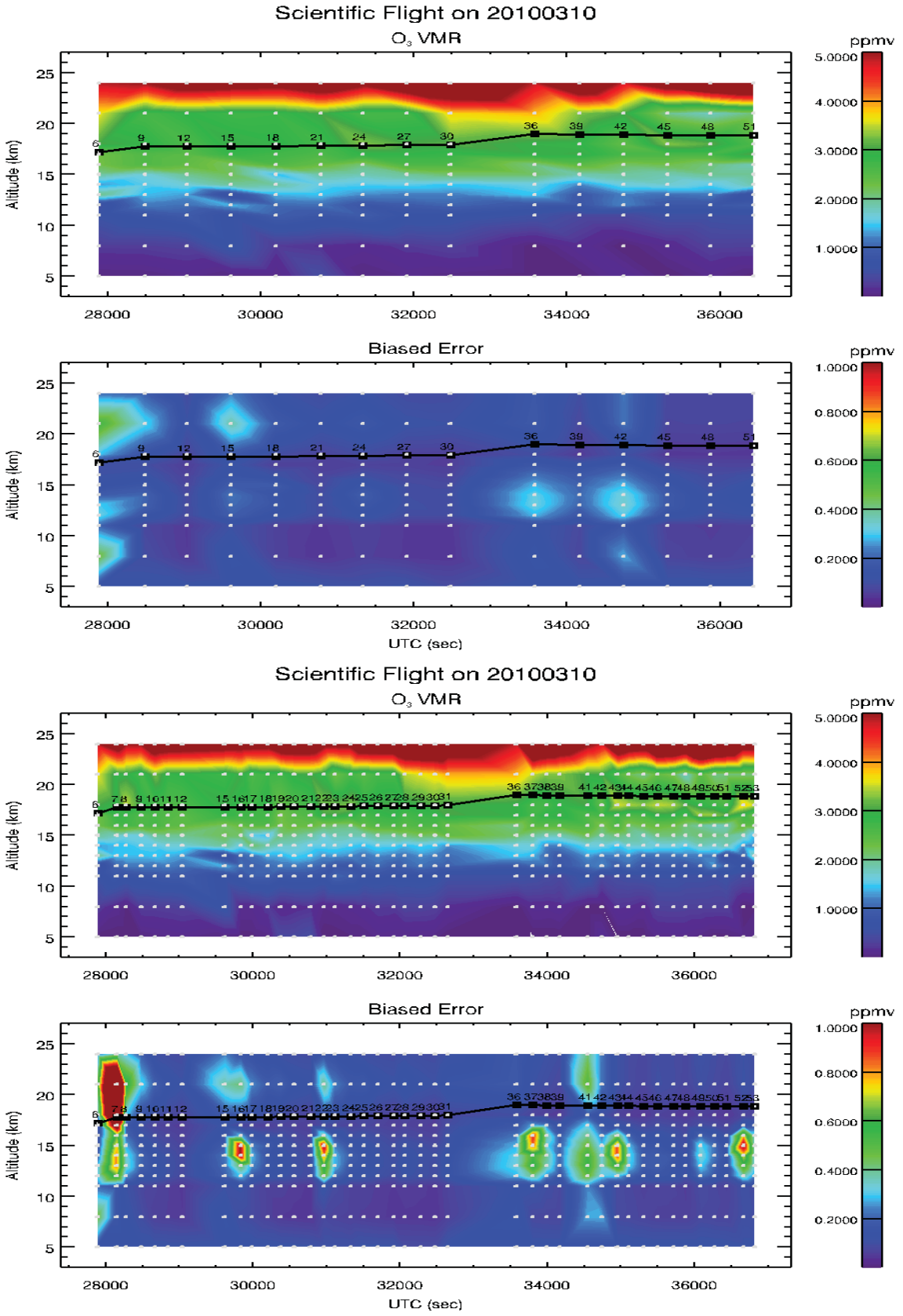

Fig. 80: O_3 obtained with the recursive retrievals strategy: top two panels show the results obatined for band C; bottom panels show the results obtained for the whole flight.

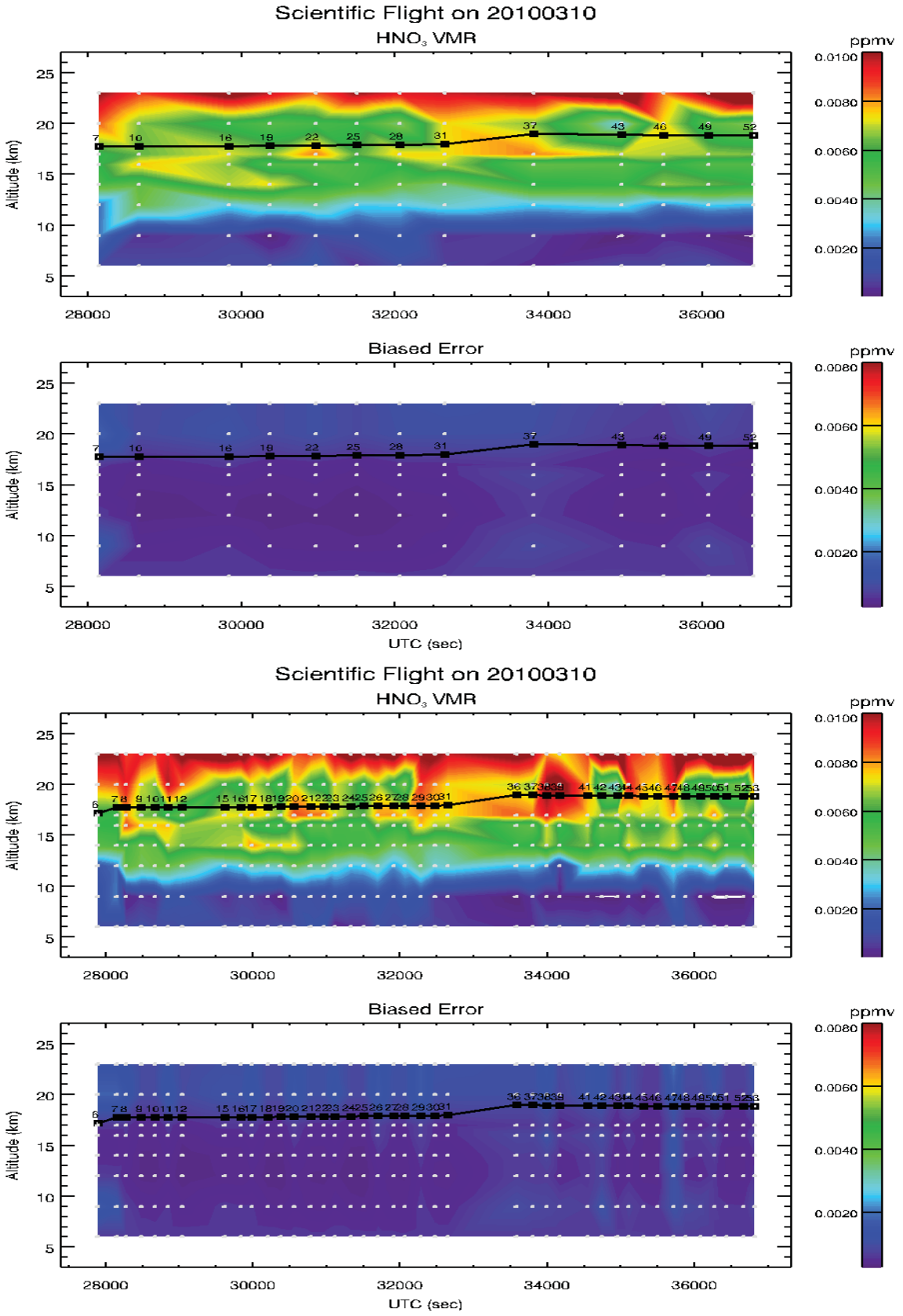

Fig. 81: HNO_3 obtained with the recursive retrievals strategy: top two panels show the results obatined for band B; bottom panels show the results obtained for the whole flight.

retrieval strategy for MARSCHALS measurements acquired in the present configuration. Main conclusion from the analysis exercise are:

- Temperature can be retrieved only from band C scans
- H_2O can be retrieved only from band C scans, but has to be included in the targets of the other bands to avoid retrieval instabilities
- O_3 can be retrieved from all the three bands; however the best strategy is to perform recursive retrievals starting from a band B scan (where the information content is higher)
- HNO_3 can be retrieved satisfactorily from band C and D scans; however using the recursive retrieval strategy we can extract the low information contained in the scans of band B. Our suggestion is to improve the receivers of band B so that to include the region around 294 GHz to get very good HNO_3 data for the whole flight.
- N_2O can be retrieved from band B measurements only, and its retrieval is problematic
- CO can be retrieved on 4 altitudes from band D data, but the information content during this flight was very small.

Those optimizations, applied to the Test Flight, gave similar results, but for CO . In fact during this flight the information content for CO was higher. However, since in the payload of the PREMIER satellite CO can only be measured by the sub-mm instrument in the spectral region covered by Band D, we have performed simulated retrievals to test the capability of the sub-mm instrument onboard airborne and spaceborne platform to detect CO.

8 Simulated retrievals of CO from aircraft and satellite measurements

Since the results of the CO retrieval during both the Test and the Scientific Flights were not very good, suggesting that MARSCHALS in the current configuration is not able to detect CO at the UTLS concentrations, we have performed some further test using simulated retrievals. The observations have been simulated assuming an instrument onboard a stratospheric aircraft or onboard a satellite, using both MARSCHALS spectral resolution and noise characterizations and the spectral resolution and noise of a future instrument measuring the UTLS region onboard the PREMIER mission. In total we have performed 4 simulations for 4 different instrumental configurations. The configurations are reported in table 6

Tab. 6: Instrumental configurations for CO retrieval simulations.

Mode	spectral resolution MHz	Noise K	ILS
S1	200	2	Band D ILS
S2	20	2	20 MHz Boxcar
S3	200	0.5	Band D ILS
S4	20	0.5	20 MHz Boxcar

For the aircraft instrument the flight altitude was set at 20 km and the vertical sampling was from 0 to 20 km in altitude at 1 km step plus two uplooking geometries. For the satellite instrument the vertical sampling was the one found on the PREMIER documents, that is 1.5 km steps from 2 to 14 km and 2 km steps from 14 to 26 km. The FOV function for the aircraft instrument was the one delivered for the PremierEx flights, while for the satellite instrument was set to have a Full Width at Half Maximum of abot 2 km at tangent point. The retrieval grid was the same for both instruments, that is from 4 to 26 km at 2 km steps. Four different atmospheres were tested, using the profiles of the IG2 database: Equatorial, Mid-latitude, Polar Summer and Polar Winter. The synthetic spectra were simulated using the standard atmosphere, while the retrievals used as initial guess for CO the standard profile plus its 1 sigma variability, with the a priori errors set to 100 %.

The results of the simulated retrievals are reported in Fig. 82 to Fig. 89 for a mid-latitude atmosphere. Each figure reports four panels, one for each instrument configurations. Figures 82 (satellite) and 83 (aircraft) show the reference profile used for the simulated spectra (green line), the retrieved profile (blue line) with the retrieval error bars (black lines) and the initial guess/a priori profile (red solid line) and the a-priori profile +/- the a-priori errors (red dashed lines). Figures 84 and 85 report the value of the retrieval error in ppmV (red lines) and the difference between the retrieved and the reference profile (green line). Figures 86 and 87 report the Averaging Kernels for the

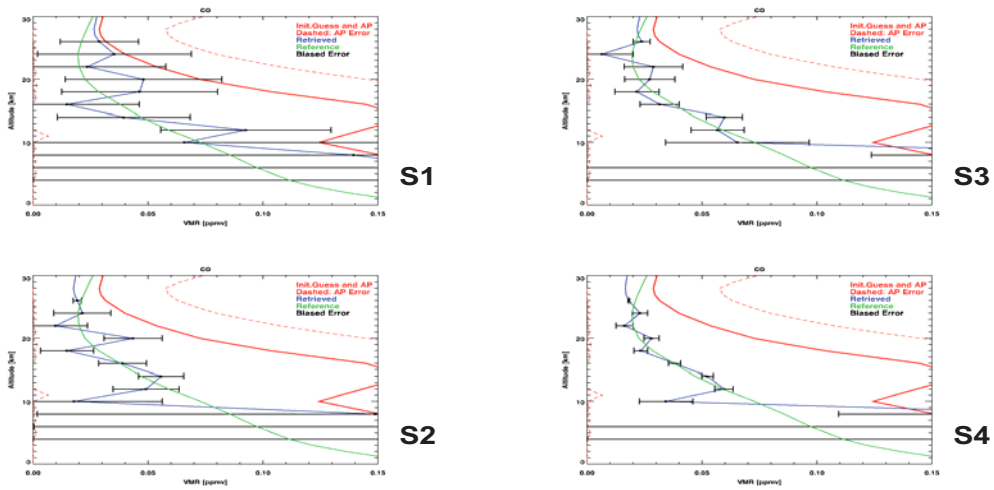

Fig. 82: CO profiles for the 4 satellite instrument configurations: red solid line shows the initial guess (a-priori) profiles, red dashed line shows the limits of the a-priori error, green solid line is the reference profile, blue solid line is the retrieved profiles, black lines represent the retrieval error.

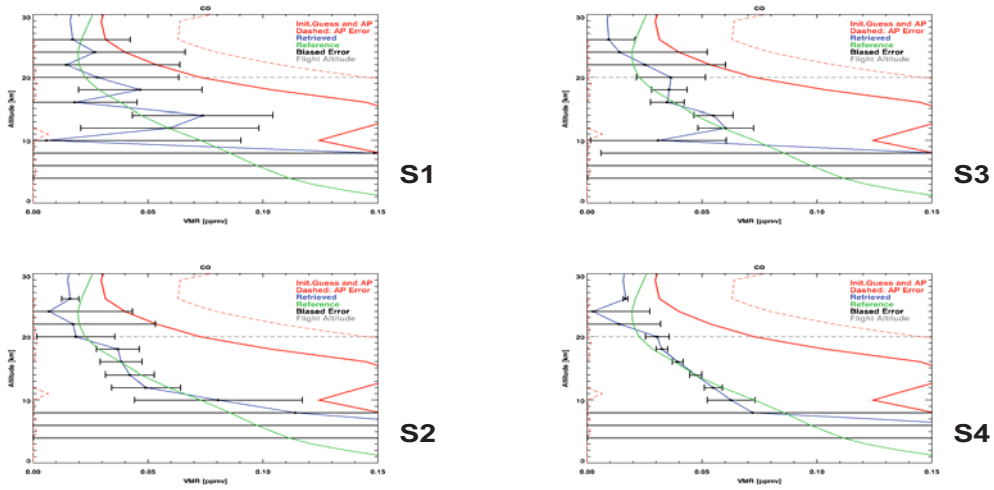

Fig. 83: CO profiles for the 4 aircraft instrument configurations: red solid line shows the initial guess (a-priori) profiles, red dashed line shows the limits of the a-priori error, green solid line is the reference profile, blue solid line is the retrieved profiles, black lines represent the retrieval error. In grey the flight altitude is marked.

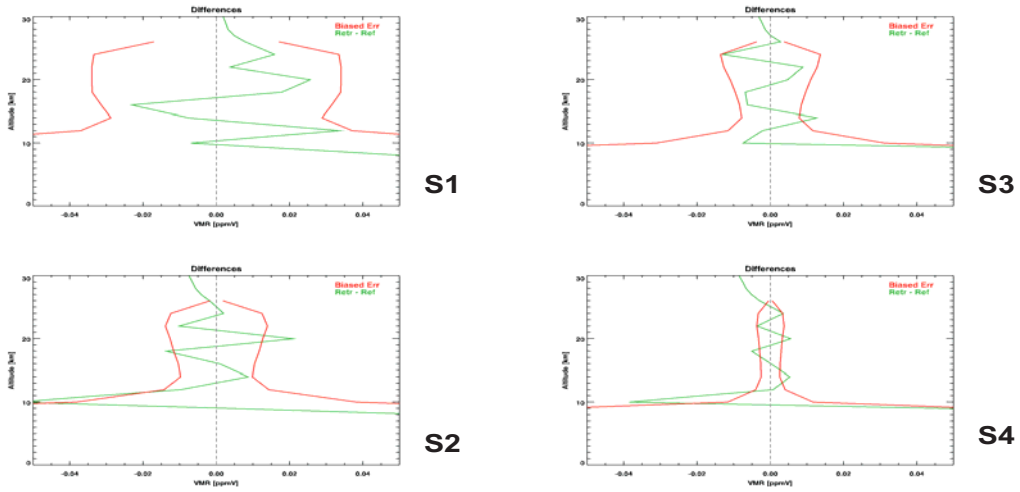

Fig. 84: CO differences for the 4 satellite instrument configurations: red solid lines show the limits of the retrieval error, green solid line is the retrieved minus reference profile.

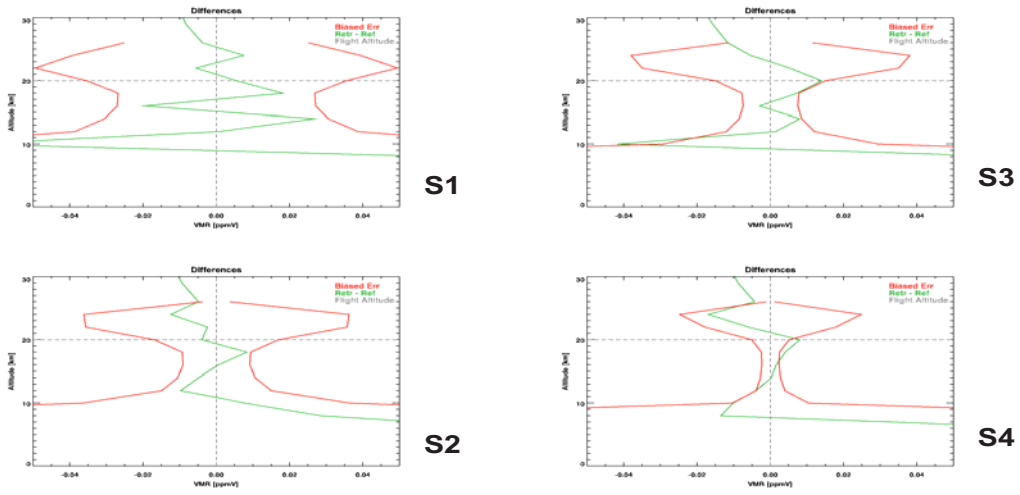

Fig. 85: CO differences for the 4 aircraft instrument configurations: red solid lines show the limits of the retrieval error, green solid line is the retrieved minus reference profile, in grey the flight altitude is marked.

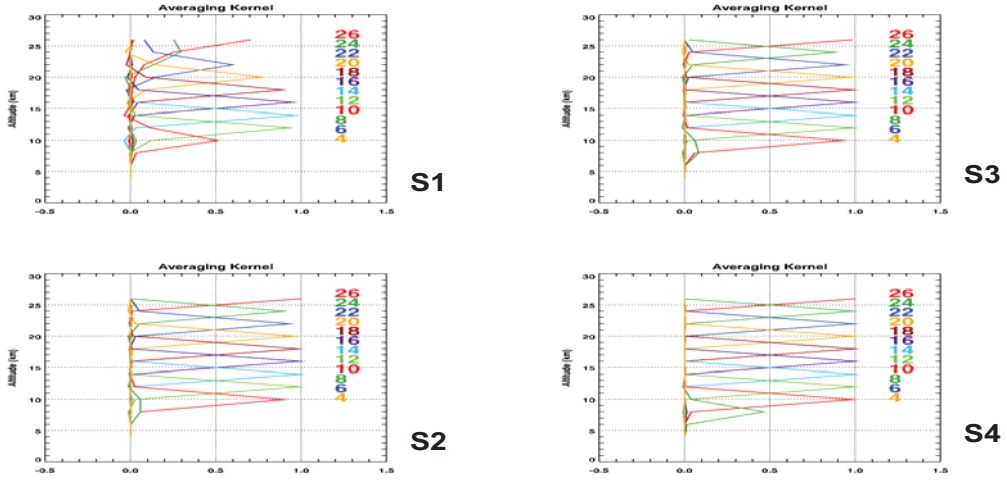

Fig. 86: CO Averaging Kernels for the 4 satellite instrument configurations: different colors represent retrieved values at different altitudes.

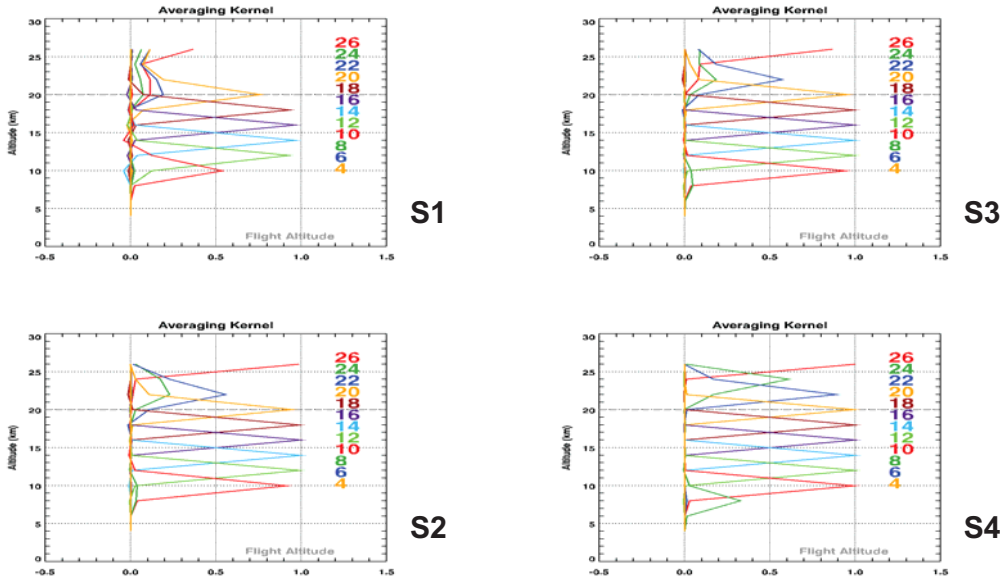

Fig. 87: CO Averaging Kernels for the 4 aircraft instrument configurations: different colors represent retrieved values at different altitudes.

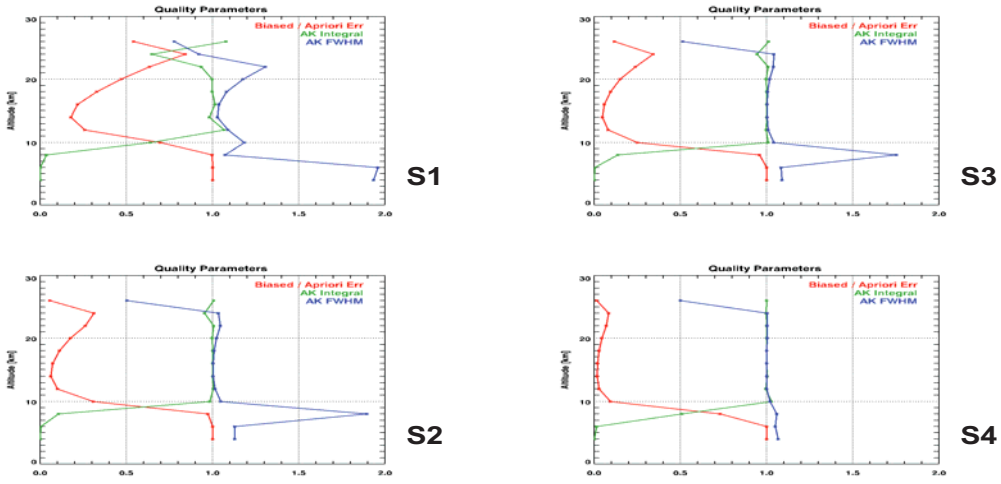

Fig. 88: CO retrieval quantifiers for the 4 satellite instrument configurations: the red lie is the ratio between the biased and the a priori errors, the green line represents the Averaging Kernel integral and the blue line represents the FWHM of the Averaging Kernels measured in units of altitude difference between adjacent retrievd altitudes.

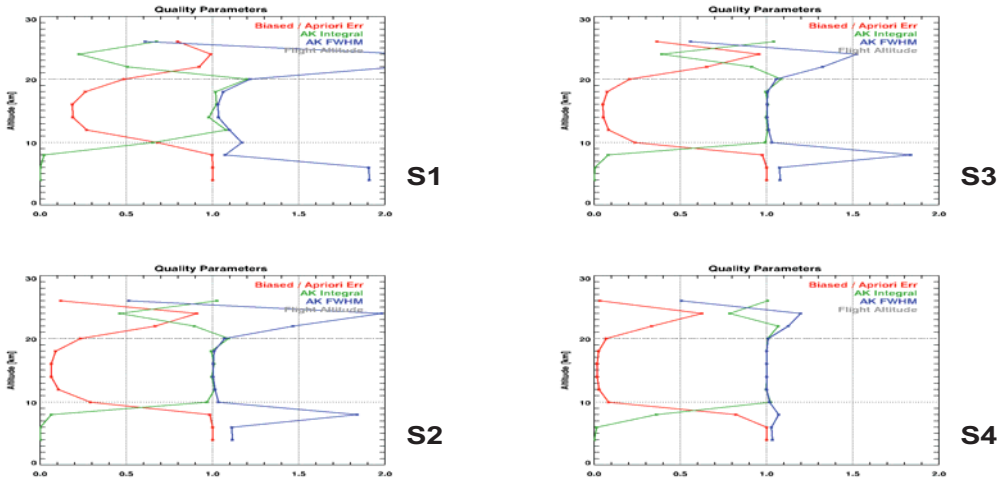

Fig. 89: CO retrieval quantifiers for the 4 aircraft instrument configurations: the red lie is the ratio between the biased and the a priori errors, the green line represents the Averaging Kernel integral and the blue line represents the FWHM of the Averaging Kernels measured in units of altitude difference between adjacent retrievd altitudes. In grey the flight altitude is reported.

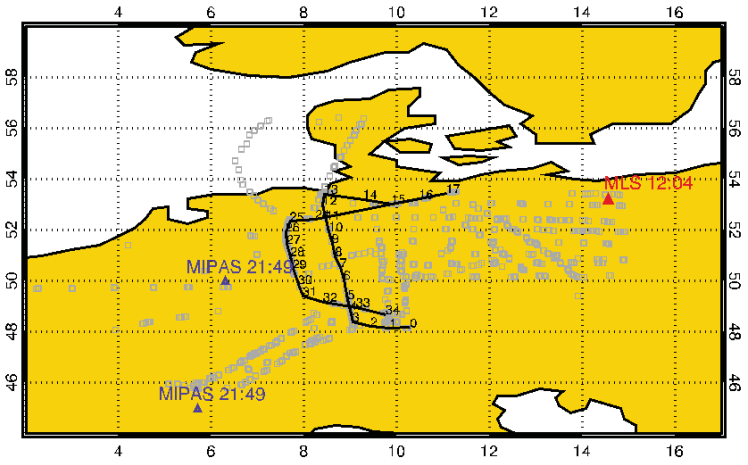

Fig. 90: MARSCHALS flight pattern, scans geolocation, MLS (red) and MIPAS (blue) data geolocations.

four instrument configurations in case of satellite or aircraft measurements. Figures 88 and 89 report the quality parameters of the retrieval (the ratio between the biased and the a priori errors in red, the Averaging Kernel integral in green and the AK FWHM in blue).

The simulated retrievals show that if the CO profile is close to its standard values it can be detected by both aircraft and satellite instruments in all the atmospheric conditions considered in the simulations. At mid-latitude we have the highest information content between 10 and 21 km for the satellite measurements, and between 10 km and flight altitude for the aircraft measurements. As expected best performances are achieved for the higher spectral resolution and the lower noise level (S4).

However the comparison of the results obtained for the S2 and S3 instrument configurations for both satellite measurements and aircraft measurements shows that a similar improvement in the CO retrieval can be obtained either improving the spectral resolution or the noise level of the measurements.

9 Validation of MARSCHALS measurements

The validation of the vertical profiles obtained during the analysis of MARSCHALS data acquired in both the Test Flight and in the Scientific Flight can be performed using different instruments onboard the Geophysica aircraft. While remote sensing instruments are the best for the validation exercise, in situ instruments can validate the retrieved profiles only close to the take off , dive and landing of the aircraft.

We have found data measured by two satellite instruments that can be used for the validation of MARSCHALS analysis: MIPAS/ENVISAT and AURA/MLS. MIPAS/ENVISAT measures Temperature, H_2O, O_3, and HNO_3 profiles from about 6 km (in absence of clouds) to 68 km. The MIPAS/ENVISAT products used for MARSCHALS validation were the ones contained in the MIPAS2D database (see Dinelli et al., 2010) retrieved over a latitude grid of 5 deg. using the GMTR approach (two-dimensional (2-D) retrievals). The 2-D approach is particularly useful to model atmospheric horizontal inhomogeneities typical for instance of the polar vortex region. MLS measures Temperature, H_2O, O_3, HNO_3, N_2O and CO and reports its data as a function of pressure. MLS data are retrieved with a 2-D approach.

9.1 Validation of the Test Flight measurements

In the case of the Test Flight the only data obtained from sensors onboard the Geophysica, that can be exploited for our validation purposes up to now, are TDC data for Temperature. Looking at available satellite data, MLS/AURA and MIPAS/ENVISAT data are in good spatial coicidence with MARSCHALS data (see figure 90) even if MIPAS coincident data are measured at 21:49 UTC more than 6 hours after the landing of the Geophysica. Considering that the flight was performed from the 12:29 to the 15:14 UTC, MLS data (measured at 12:04 UTC) are in a very good temporal and spatial coincidence with MARSCHALS scans from 6 to 12 and were selected for the Tests flight data analysis validation together with TDC data during the ascent. MLS profiles of Temperature, H_2O , O_3,

HNO_3, N_2O, CO are given on pressure levels, for this reason the comparisons are performed using pressure as vertical coordinate.

9.1.1 Temperature validation

The comparison between MARSCHALS (grey) scans 6, 9 and 12, MLS (red) and TDC (green) Temperature profiles are shown in figure 91. The retrieved Temperature values are in good agreement with both MLS and TDC data down to 300 hPa. For higher pressure values only TDC data are available for a comparison. Also in this pressure range the MARSCHALS and in situ profiles agree very well a-part from the lowest point in scan 12 retrieval.

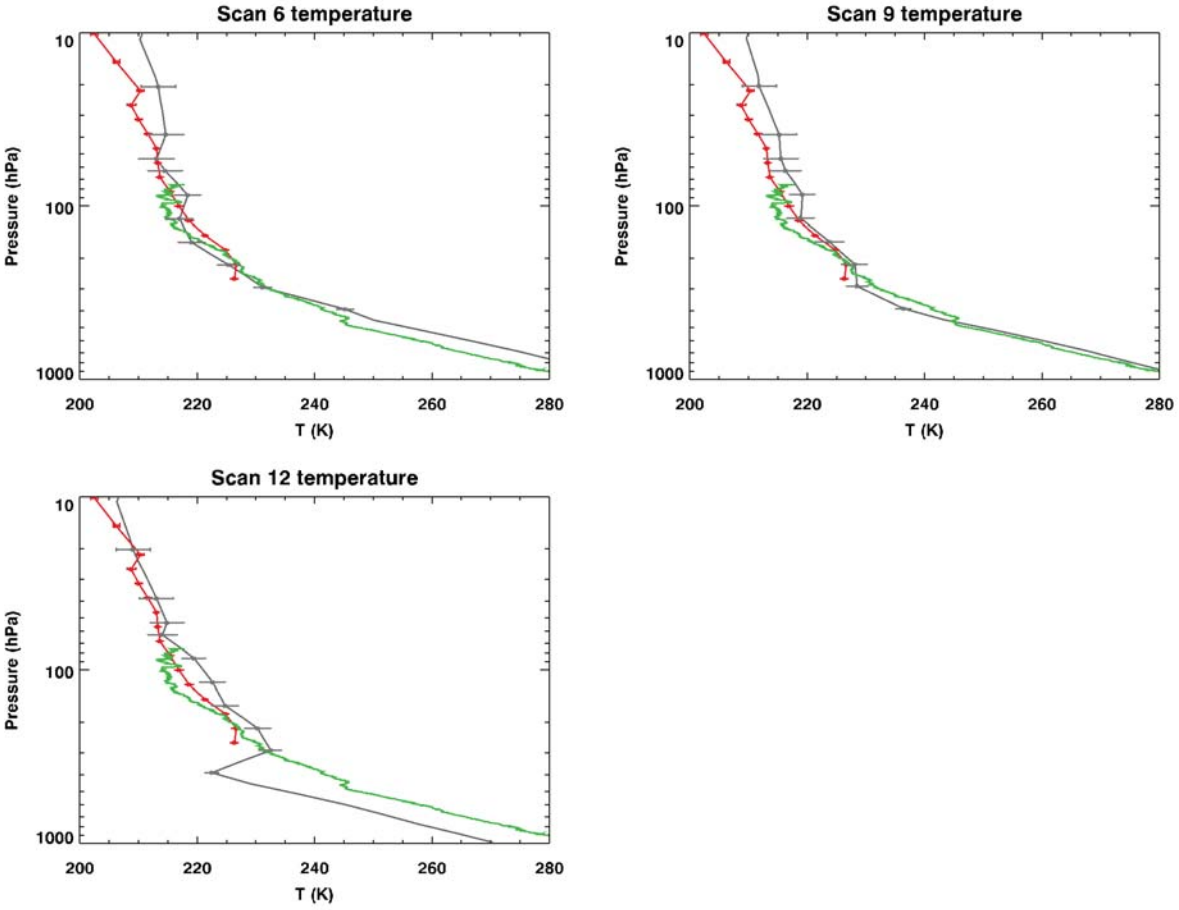

Fig. 91: Temperature retrieved from MARSCHALS (grey), MLS (red) and TDC (green).

9.1.2 H_2O validation

As for Temperature retrievals, H_2O profiles can be obtained only from band C scans. In figure 92 we compare MARSCHALS scans 6, 9 and 12 with MLS H_2O profile. Even if MARSCHALS retrieved values have large error bars in the altitude region where the comparison with MLS data can be performed, a general good agreement between the two instrument is found.

9.1.3 O_3 validation

Ozone retrievals can be performed from all the three MARSCHALS bands. The comparison between MARSCHALS scans 7,10 (band B), 6, 9, 12 (band C) and 8, 11 (band D) and MLS O_3 profiles are shown in figures from 93 to 95. Ozone profile retrieved from scan 7 in band B shows an oscillations about 60 hPa, while at higher pressure a very good agreement with MLS profile can be found. Scan 10 shows a very good agreemet in the whole altitude range with MLS data. Also O_3 profiles retrieved from band C scans agree well with MLS data even if some oscillations are present in scan 6. The same considerations can be applied to O_3 profiles retrieved from band D scans.

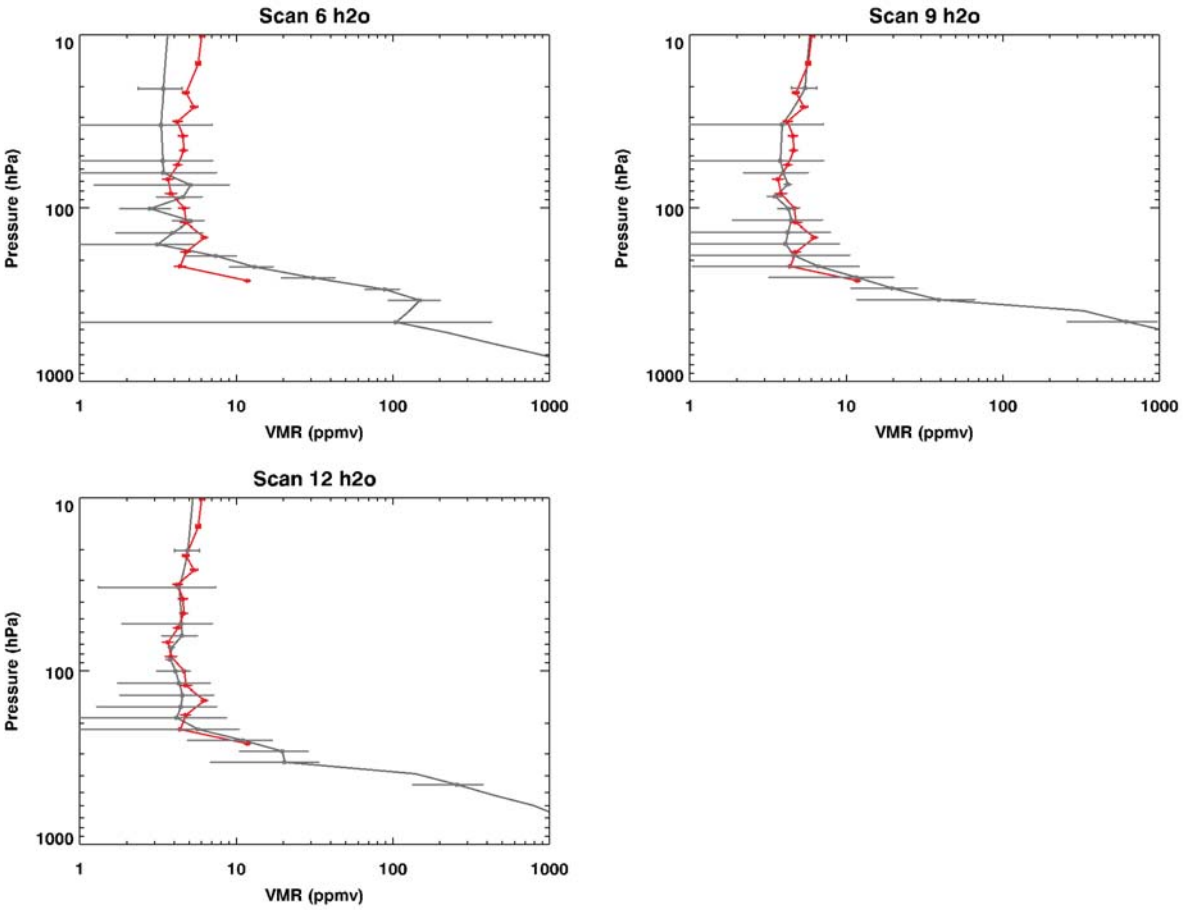

Fig. 92: H_2O retrieved from MARSCHALS (grey) and MLS (red).

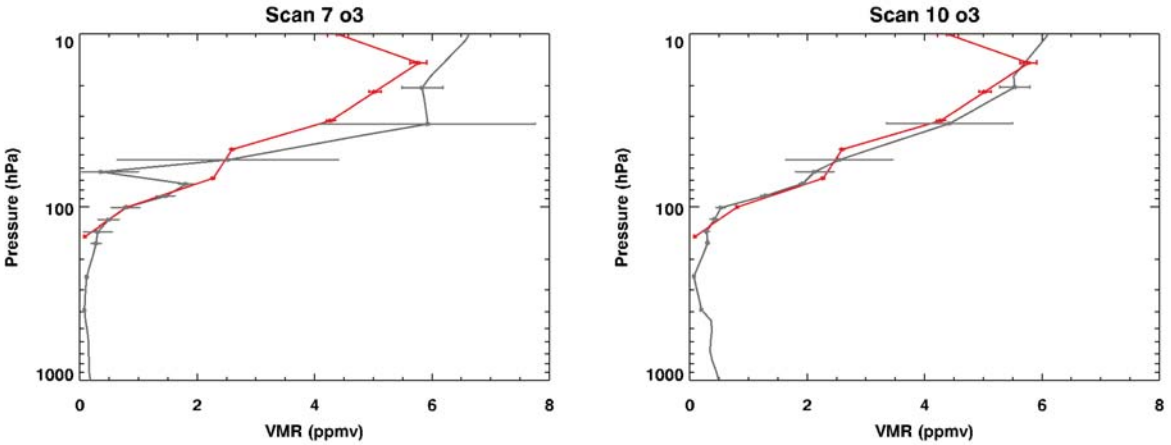

Fig. 93: O_3 retrieved from MARSCHALS band B (grey) and MLS (red).

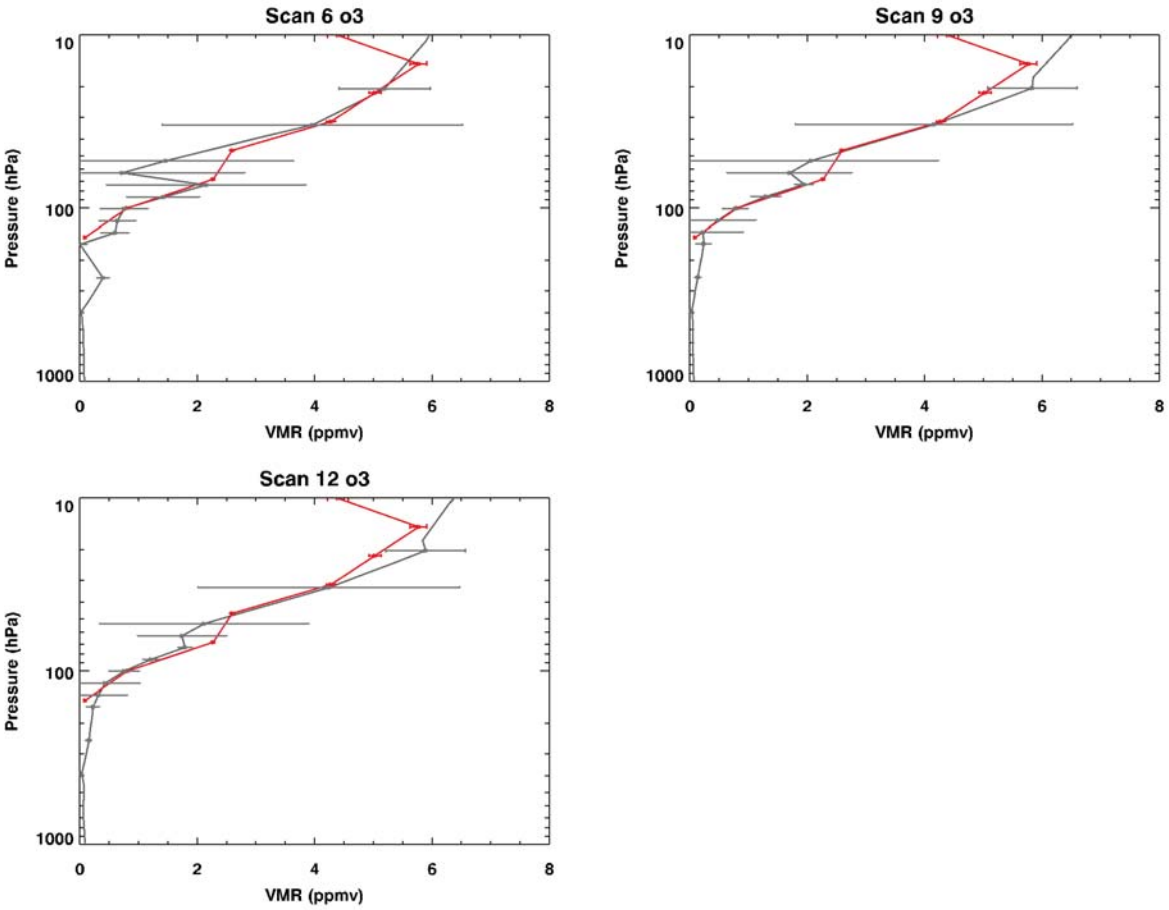

Fig. 94: O_3 retrieved from MARSCHALS band C (grey) and MLS (red).

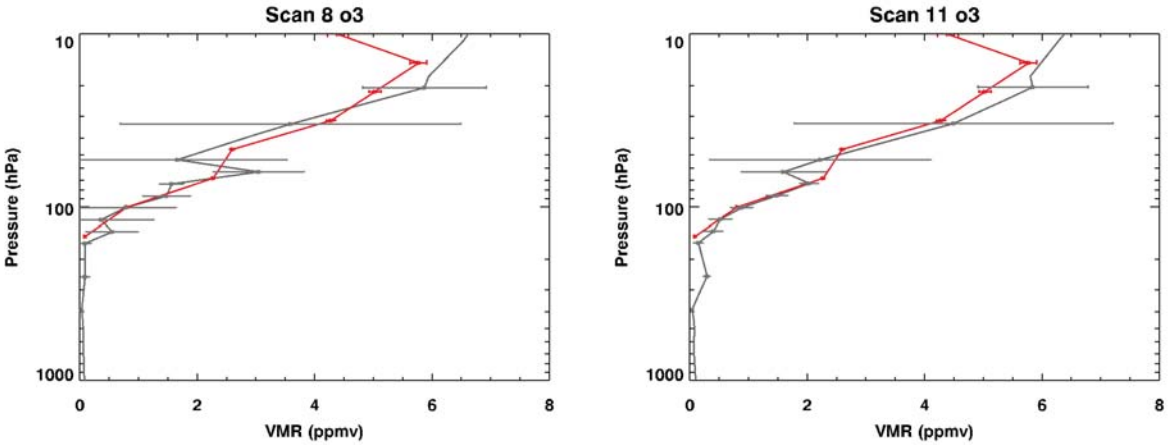

Fig. 95: O_3 retrieved from MARSCHALS band D (grey) and MLS (red).

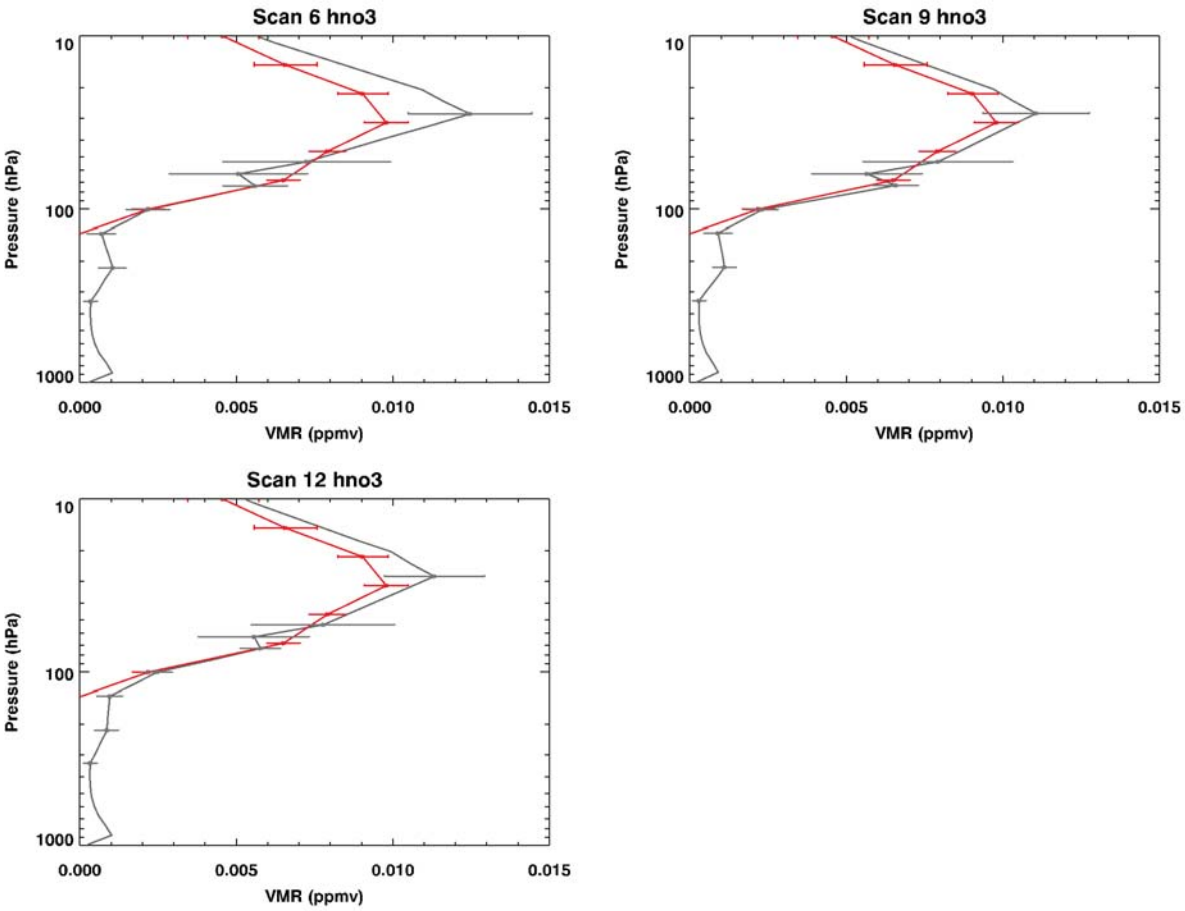

Fig. 96: HNO_3 retrieved from MARSCHALS band C (grey) and MLS (red).

9.1.4 HNO_3 validation

HNO_3 vertical profile can be retrieved for all MARSCHALS bands. However, due to the new band B definition, very low information is available in band B scans for HNO_3 retrievals. For this reason band B HNO_3 profiles were not used in the validation execise. The comparison between MARSCHALS scans 6, 9, 12 in band C and MLS data is shown in figure 96 while HNO_3 profiles from band D scans 8 and 11 and MLS data are shown in figure 97. In both cases the agreement in good, with MARSCHALS data beeing slightly higher in the higher part of the profile (at about 20 hPa).

9.1.5 N_2O validation

N_2O is retrieved using band B spectra. The comparisons between MARSCHALS scans 7 and 10 and MLS N_2O profiles are shown in Fig. 98. N_2O profile obtained from MLS in coincidence with MARSCHALS measurements has the lowermost point at 70 hPa. For this reason only the two upper points in the MARSCHALS N_2O retrieval grid can be used for a direct comparison of the two profiles. MARSCHALS profile for scan 7 has very strong oscillations in this altitude range. Scan 10 still has oscillations in the upper part of the profiles but seems to be in quite good agreement with MLS data.

9.1.6 CO validation

The comparison between MARSCHALS CO profiles obtained form band D scans 8 and 11 and MLS profile are shown in figure 99. For the altitude region with pressure values lower than 100 hPa the overall agreement is good. Below this region MLS CO profile is higher than the ones retrieved by MARSCHALS. This is also due to the fact that a positive bias (of a factor about 2) affects MLS profiles at about 200 hPa.

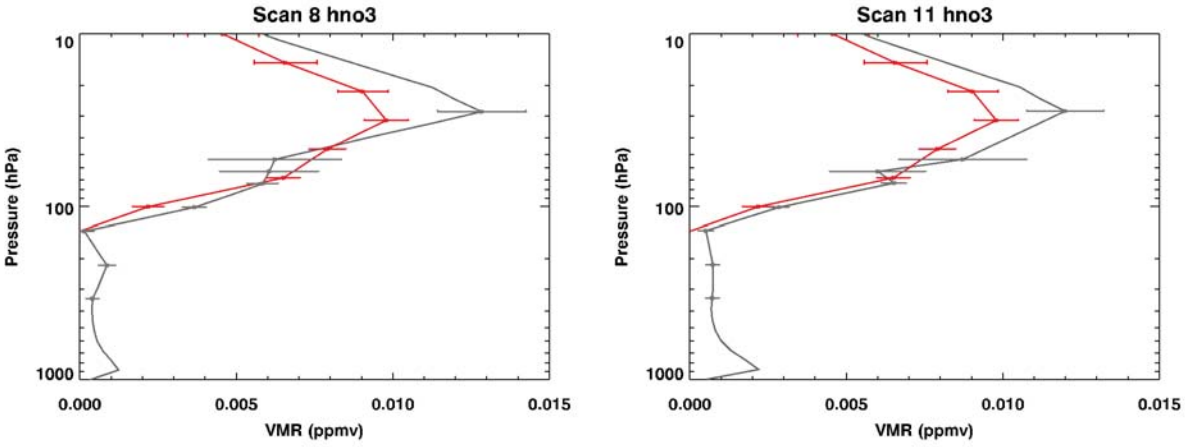

Fig. 97: HNO_3 retrieved from MARSCHALS band D (grey) and MLS (red).

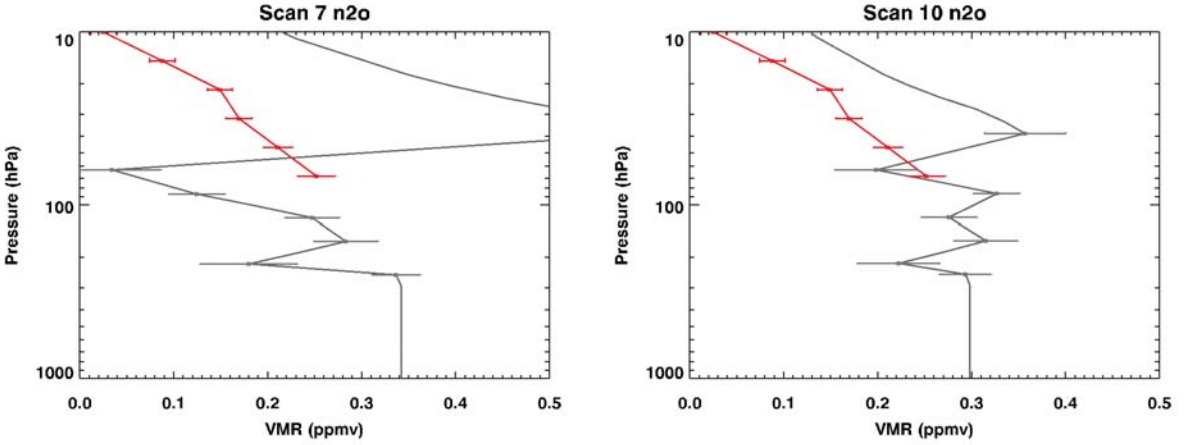

Fig. 98: N_2O retrieved from MARSCHALS band B (grey) and MLS (red).

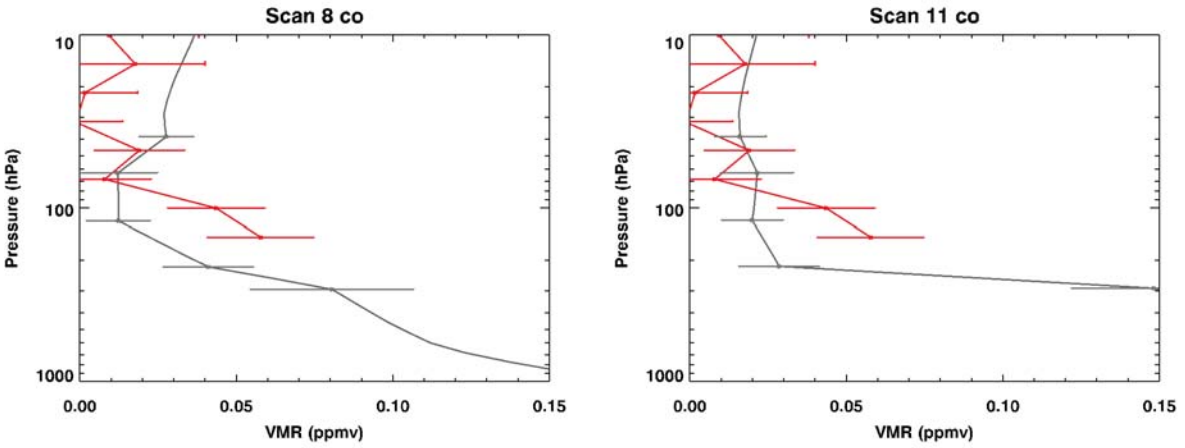

Fig. 99: CO retrieved from MARSCHALS band D (grey) and MLS (red).

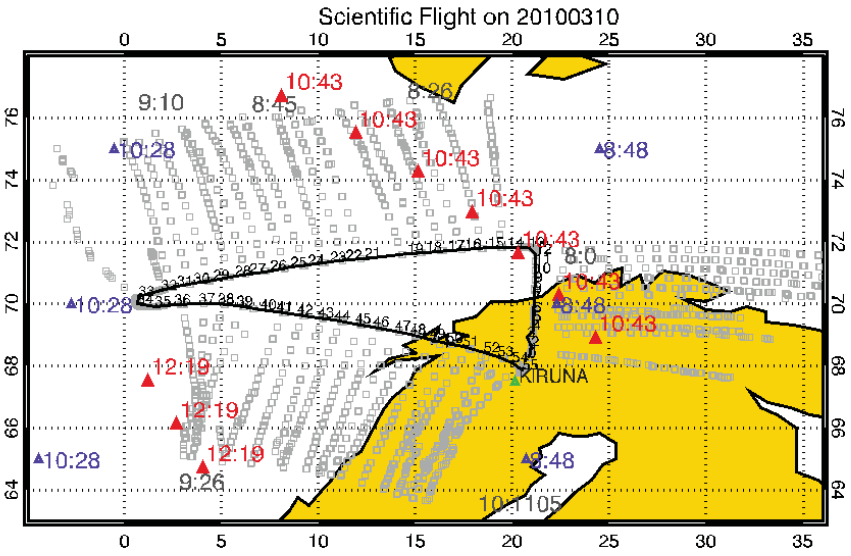

Fig. 100: MARSCHALS flight pattern, scans geolocation, and in situ (green), MLS (red) and MIPAS (blu) data geolocations.

9.1.7 Test Flight validation: Conclusions

A good agreement is generally found between the Temperature profile retrieved by MARSCHALS in the first part of the flight and MLS and TDC data. The same applies to H_2O, O_3, HNO_3 profiles retrieved by MARSCHALS and MLS data. A worse agreement can be found in case of N_2O profiles even if a reduced altitude range is available for the comparison, and for the lower part of CO retrieved profiles this, however can be due to the positive bias reported for MLS data.

9.2 Validation of the Scientific Flight measurements

The validation of the MARSCHALS data analysis for the Scientific Flight with the in situ instruments onboard the M-55 can validate the retrieved profiles only close to the take off and landing of the aircraft, since during the Scientific Flight, no dive was made. in situ sensors onboard the Geophysica that can be exploited for our validation pourposes are: TDC data for Temperature, FISH and FLASH for H_2O, FOZAN for O_3, HAGAR for N_2O. No in situ sensor measured HNO_3 concentrations. During the Scientific Flight, onboard the Geophysica there were three remote sensing instruments: CRISTA, OSKAR, and MIPAS-STR. While CRISTA did not acquire useful data during the Scientific Flight, and for OSKAR we only have a quicklook plot of the Slant Columd Density (SCD), MIPAS-STR data are in good shape and its retrieved profiles can be used for MARSCHALS validation. The MIPAS-STR HNO_3 profiles were used together with MARSCHALS HNO_3 profiles for the L1+L2 and MSS data fusion as reported in Sections 12.2. An overview of the general agreement between HNO_3 and O_3 retrieved from MIPAS-STR and MARSCHALS is given at the end of this section.

For the satellite instruments MIPAS and MLS we have found correlative measurements for both of them. On the 10^{th} of March 2010, MIPAS/ENVISAT sounded the atmosphere in its Upper Atmosphere observation mode for almost all the measuring time except for the two orbits 41959 (recorded at 8:48 UTC at around 25 deg. longitude) and 41960 (recorded at 10:28 UTC at about 0 deg. longitude). Selected scans from these orbits were used for the validation of MARSCHALS scans at the beginning of the flight (scans 6-12) and in the middle of the flight (scans 26-33).

On the 10 March 2010 MLS measurements in the region sampled by the Geophysica flight were performed at 10:43 UTC and 12:19 UTC. These data can be used for the validation of MARSCHALS scans at the beginning

of the flight, from scan 6 to 12, and from scan 14 to 26 and in the second part of the flight from scan 36 to 41. The coincidence between MLS (in red), MIPAS/ENVISAT (in blue) and MARSCHALS (grey) measurements is presented in Figure 100. The time delay between MIPAS/ENVISAT and MARSCHALS for scans number 6-12 is about 48 minutes, while for scans 26-33 is about 1 hour and 10 minutes. In the case of MLS and MARSCHALS the time displacement is about 2 hours and 43 minutes for scans 6-12 and about 3 hours for scans 36-41. Because

of the representation of MLS data in terms of atmospheric pressure, all the figures used for the validation exercise report MARSCHALS targets as a function of pressure.

As already said and as can be noticed from Figure 60 during the flight the Geophysica did not perform any dive. For this reason the possibility of retrieving informations about vertical profiles of atmospheric constituents using in situ sensors onboard the aircraft is limited to the ascending and descending part of the flight at Kiruna (in green in Figure 100). Data for in situ sensors can thus be used for comparisons with scans 6-12 and 47-51. The validation performed here is made through the comparison of the profiles as measured by MARSCHALS and by the in situ instruments.

9.2.1 Temperature validation

For the validation of Temperature we have used the data acquired during the ascent by the in situ instrument TDC for the scan 9, 12 and during the descent for scan 48 and 51. MIPAS/ENVISAT data have been used to validate scans 9, 12, 27 and 30 while MLS data have been used for scans 9, 12, 15, 18, 21, 24, 36 and 39. The comparison between MARSCHALS (grey) and the satellite and in situ data is shown in Figures 101 and 102. We can see that the data acquired during the ascent and the descent by the in situ instruments agree very well with MARSCHALS data, even if MARSCHALS fails to reproduce the oscillation present at 100 hPa. MIPAS data measure a warmer tropopause than MARSCHALS, while MLS is always in good agreement, a part from scan 36 where the retrieved Temperature values show some anomalies. In general a good agreement can be found with both satellite instrument and in situ data.

9.2.2 H_2O validation

Since H_2O can be safely retrieved only from band C scans, we have performed the validation exercise only on the band C retrieved H_2O VMRs. For the validation of Water Vapour we have used the data acquired during the ascent by the in situ instruments FISH and FLASH for the scan 9, 12 and during the descent for scan 48 and 51. MIPAS/ENVISAT data have been used to validate scans 9, 12, 27 and 30 while MLS data have been used for scans 9, 12, 15, 18, 21, 24, 36 and 39 (see Figures 103 and 104). The agreement beetween H_2O retrieved from MARSCHALS and FISH and FLASH data during the ascent and the descent can be considered good, the retrieved profiles lay within the measurements error bars. The agreement of MARSCHALS retrieved profiles with satellite data is generally good even if in some cases (e. g. scans 18, 21, 27 and 30) the error bars of MARSCHALS measurements are very large.

9.2.3 O_3 validation

O_3 can be retrieved from all MARSCHALS bands with good results. Therefore, for the validation of ozone we have used the data acquired during the ascent by the in-situ instrument FOZAN for the scans 9-12 and during the descent for scan 47-53. The validation of O_3 can be achieved using FOZAN data on ascent and descent (scans 6-12 and scans 47-53), MIPAS/ENVISAT data have been used for scans 6-12 and 27-31, while MLS data were used for scans 6-12 and 36-39.

Due to the large number (more than 30) of profiles in coincidence with MLS, MIPAS/ENVISAT and FOZAN data, we provide in Figures 105, 106, 107 only some examples of the comparison of O_3 profiles in each band.

The overall agreement for all the bands is very good except for a bias observed for MARSCHALS O_3 profile with respect to the FOZAN measurements during the ascent. However the same bias has been observed also by MIPAS/ENVISAT and MLS.

Since the O_3 profiles in band C have also been retrieved using the recursive strategy a comparison of the resulting profiles with the same correlative data used above is provided in Figures 108. As in the case of single bands retrievals, a good agreement is generally obtained for O_3 retrievals in particular with satellite data. However, no significant improvement can be noted in the validation of the results of the recursive retrievals.

9.2.4 HNO_3 validation

HNO_3 can be retrieved from all MARSCHALS bands. Band C and D give the best results, but some information is obtained also from Band B measurements. However, to date we do not have any in-situ instrument onboard the M-55 aircraft that measures HNO_3, while the comparison with MIPAS-STR measurements will be discussed in section 9.2.7. Therefore, for the validation of ozone we have used the data acquired by MIPAS/ENVISAT for scans 6-12 and 27-31, while MLS data were used for scans 6-12 and 36-39. As for ozone, due to the large number (more than 25) of profiles in coincidence with MLS, and MIPAS/ENVISAT data, we provide in Figures 109, 110, 111 only some examples of the comparison of HNO_3 profiles in each band.

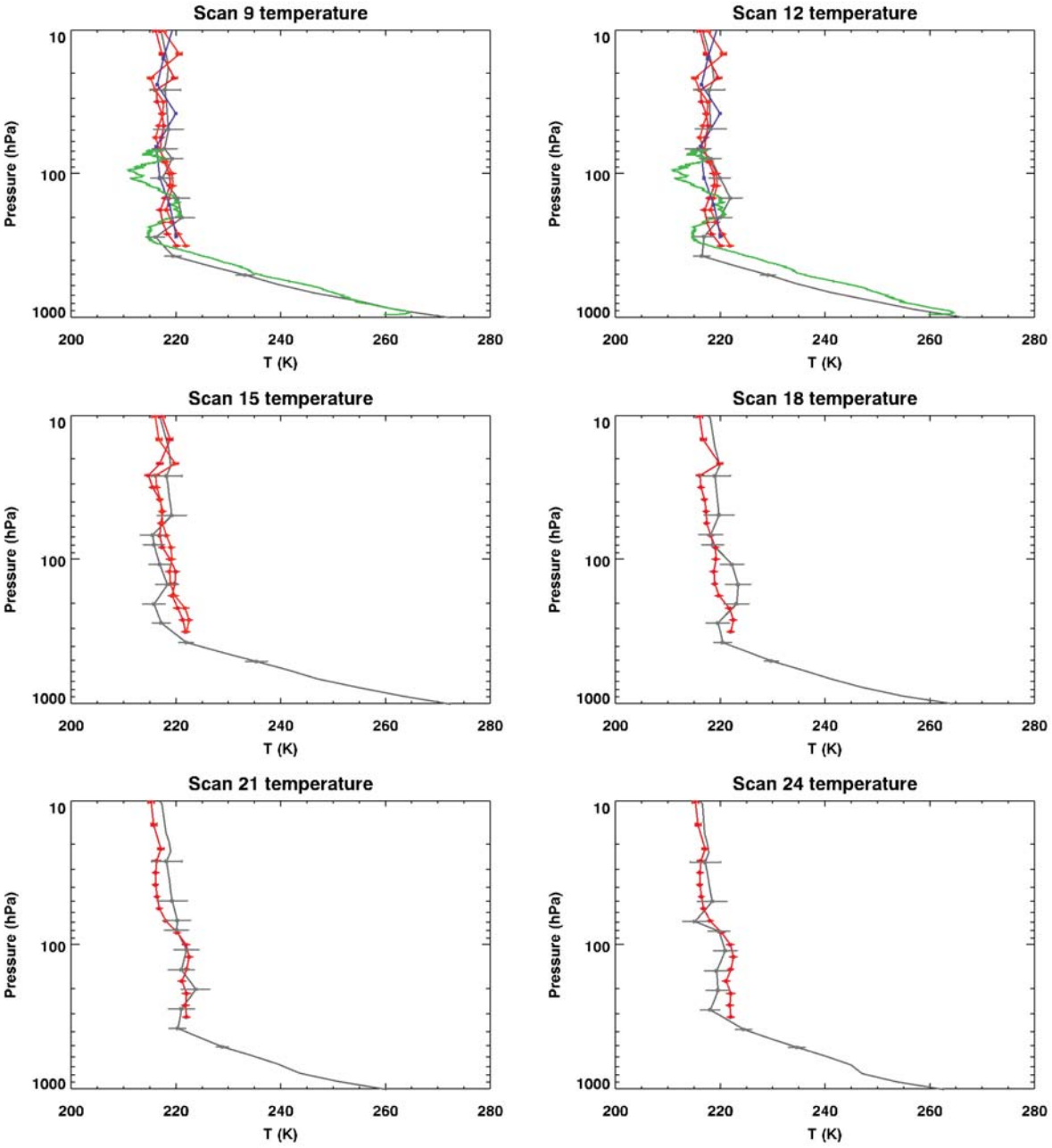

Fig. 101: Temperature retrieved from MARSCHALS (grey) and from MLS (red), or MIPAS/ENVISAT (blue) or TDC (green) (see text for details).

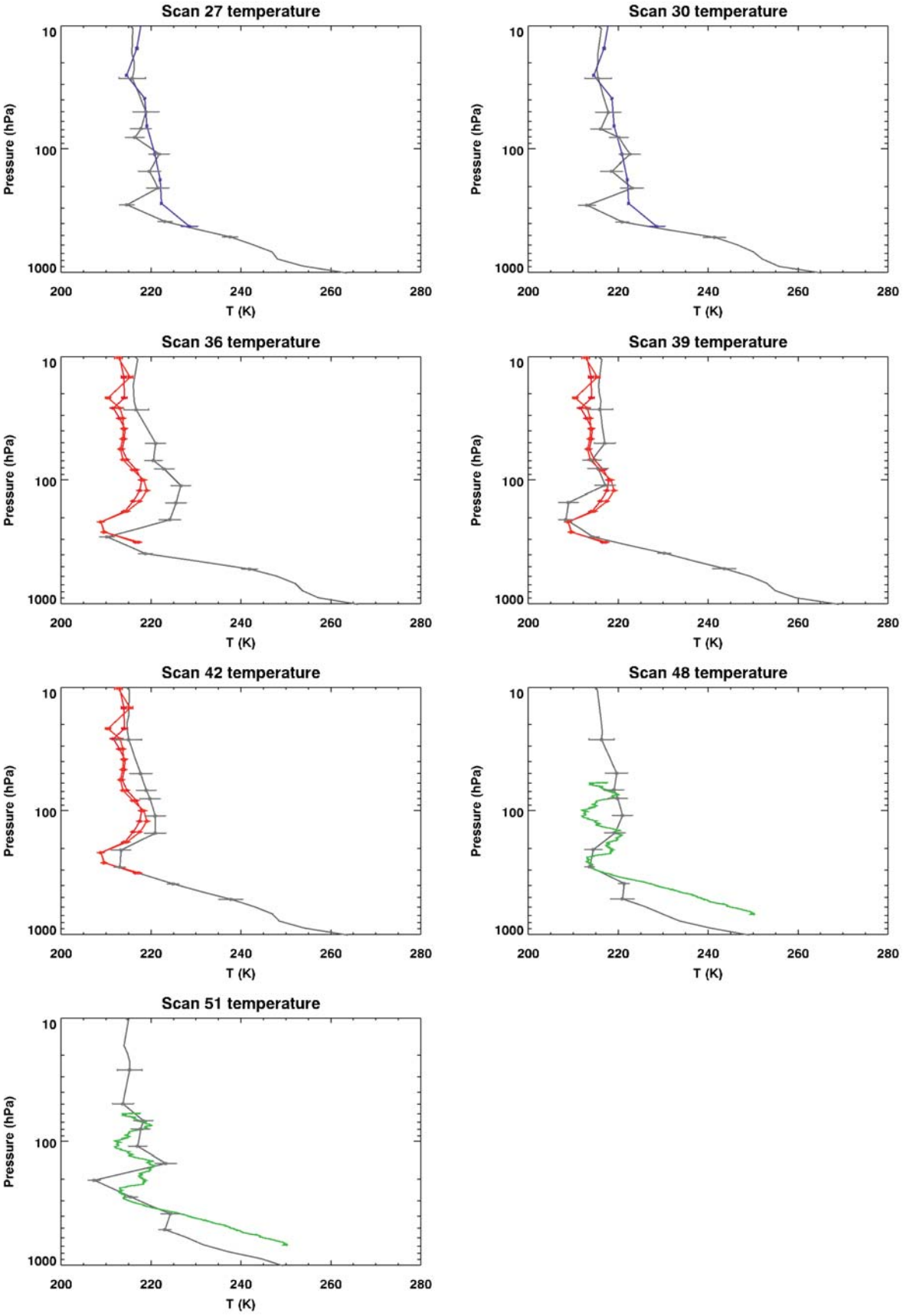

Fig. 102: Temperature retrieved from MARSCHALS (grey) and from MLS (red), or MIPAS/ENVISAT (blue) or TDC (green) (see text for details).

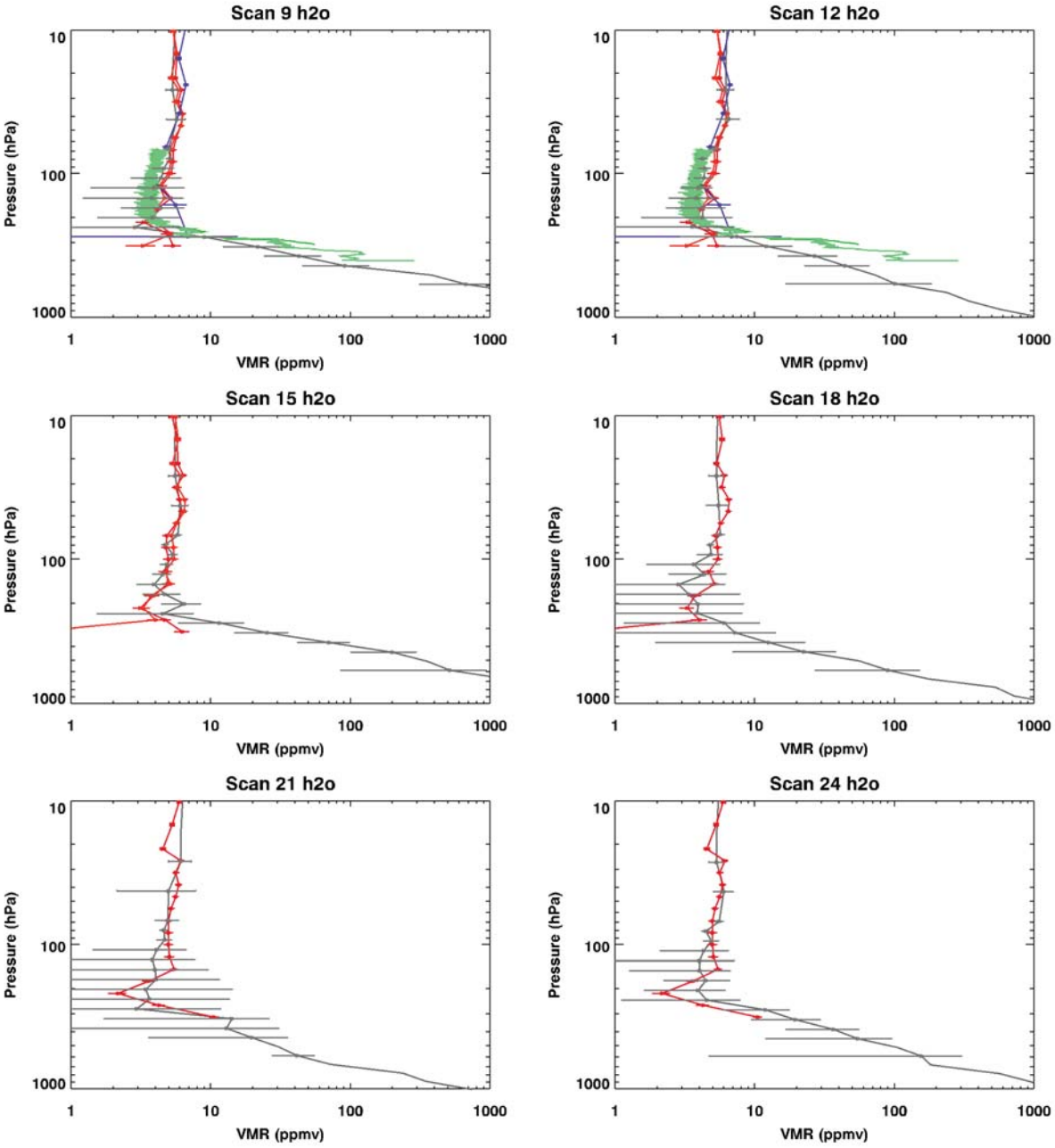

Fig. 103: H_2O retrieved from MARSCHALS (grey) and from MLS (red), or MIPAS/ENVISAT (blue) or FISH/FLASH (green) (see text for details).

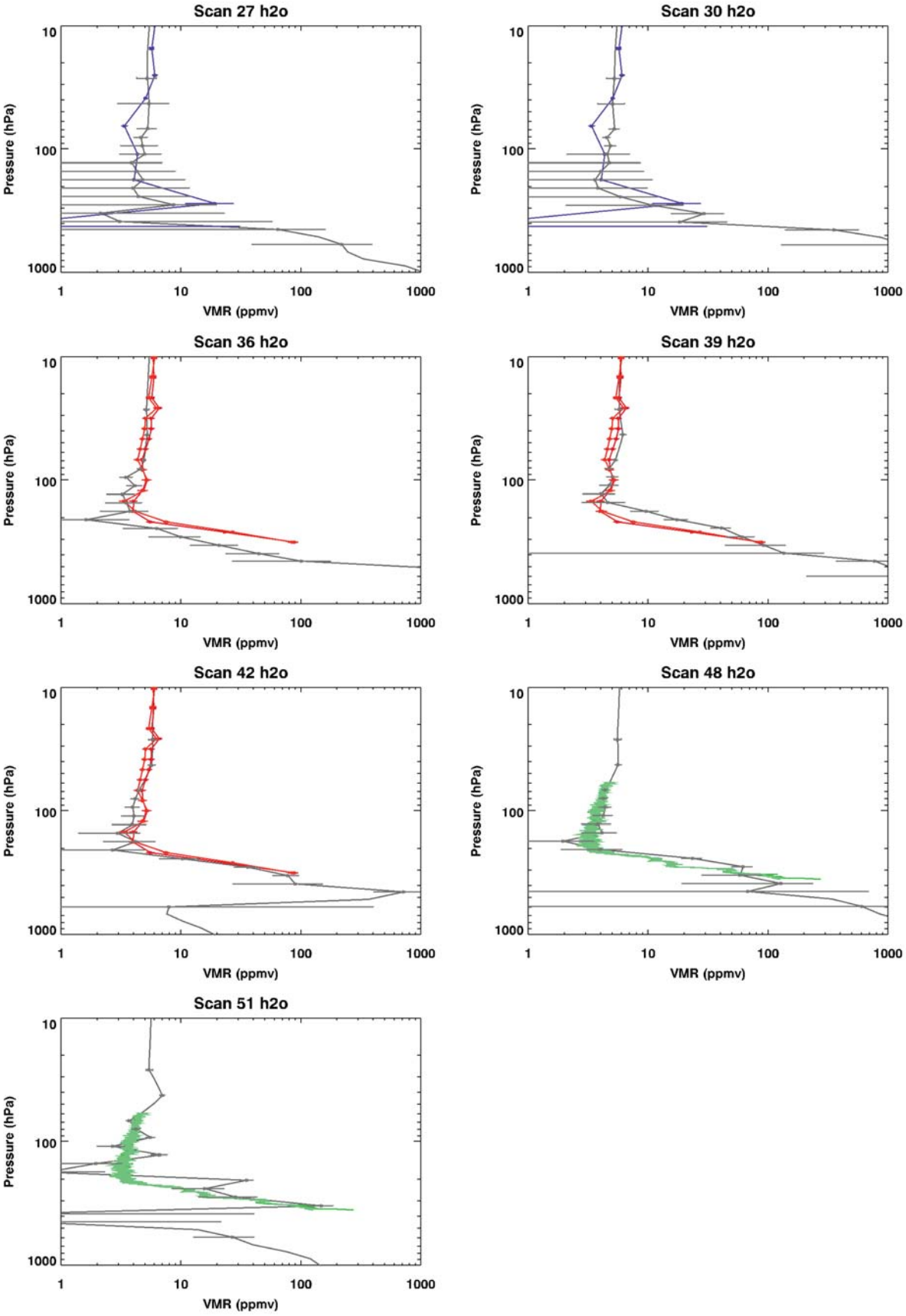

Fig. 104: H_2O retrieved from MARSCHALS (grey) and from MLS (red), or MIPAS/ENVISAT (blue) or FISH/FLASH (green) (see text for details).

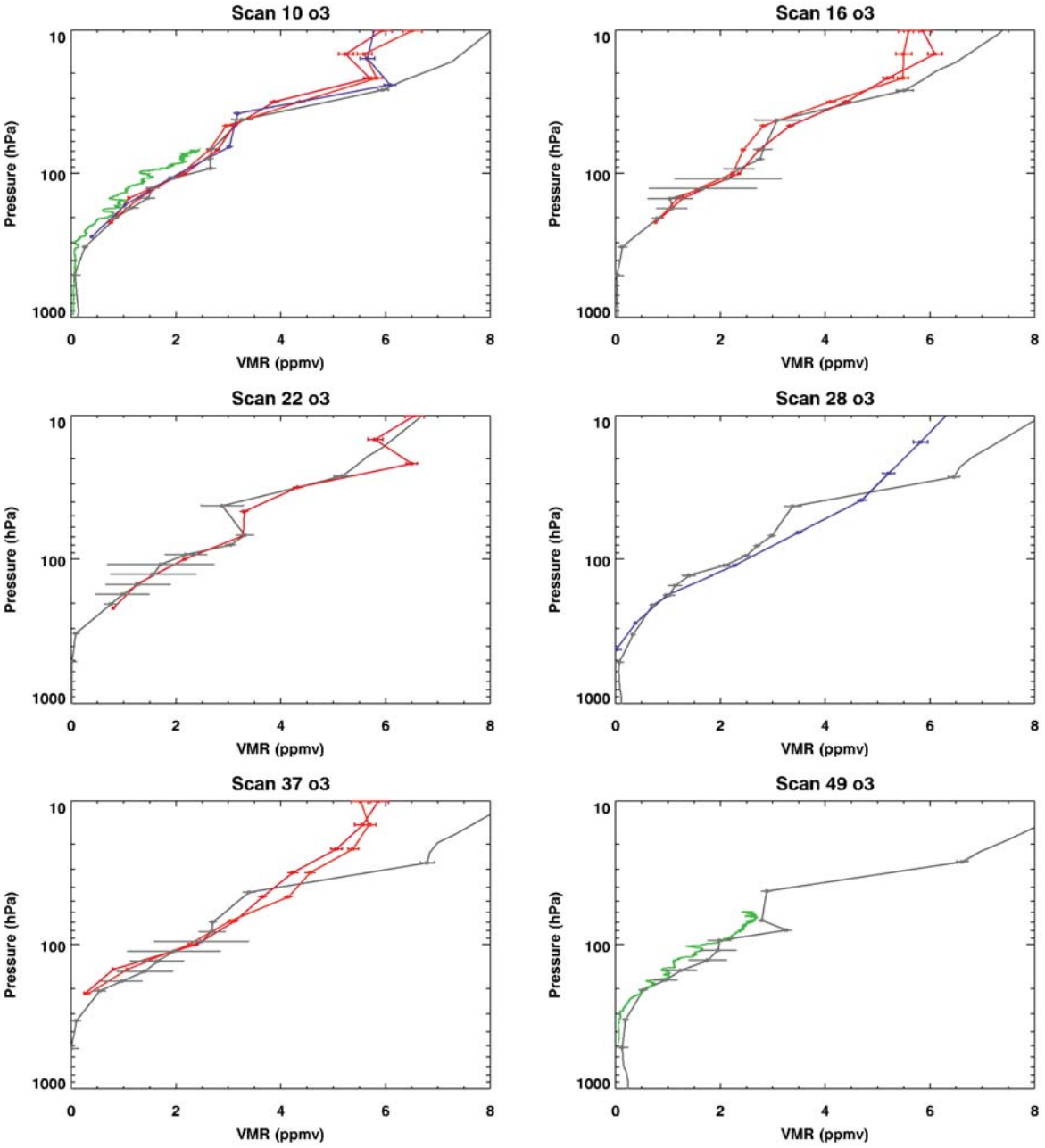

Fig. 105: O_3 retrieved from MARSCHALS (grey) and from MLS (red), or MIPAS/ENVISAT (blue) or FOZAN (green) for band B retrievals(see text for details).

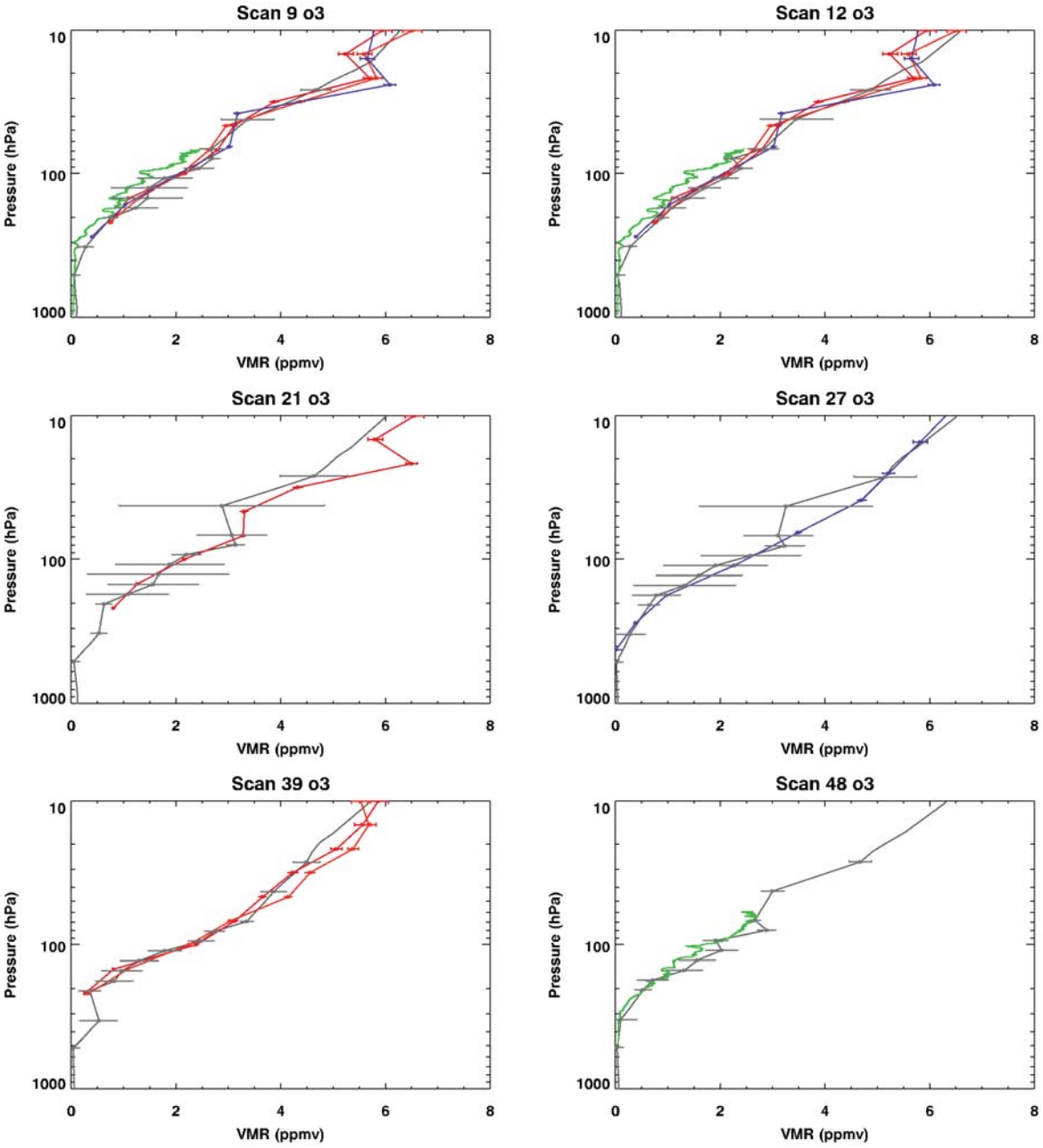

Fig. 106: O_3 retrieved from MARSCHALS (grey) and from MLS (red), or MIPAS/ENVISAT (blue) or FOZAN (green) for band C retrievals(see text for details).

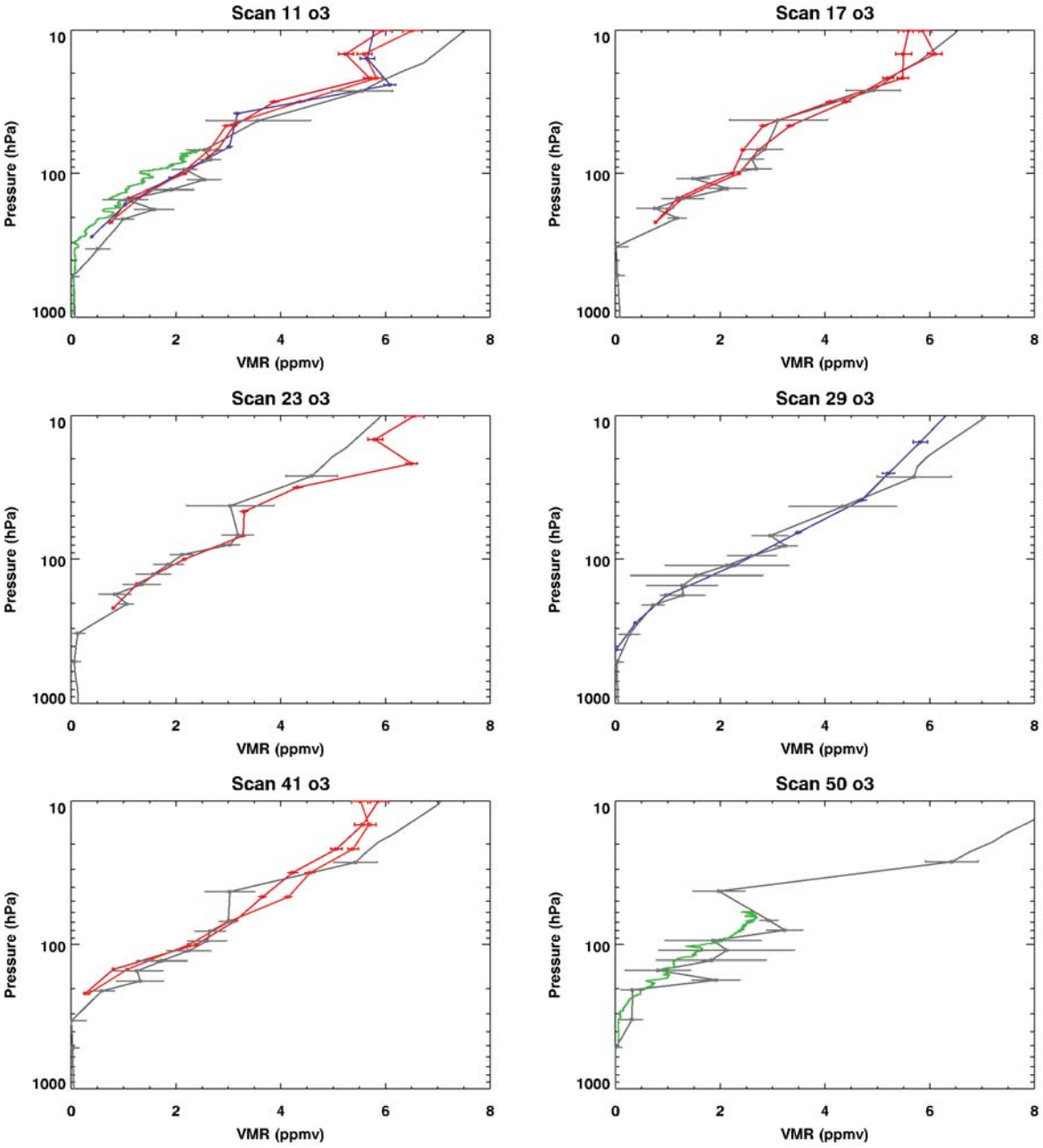

Fig. 107: O_3 retrieved from MARSCHALS (grey) and from MLS (red), or MIPAS/ENVISAT (blue) or FOZAN (green) for band D retrievals(see text for details).

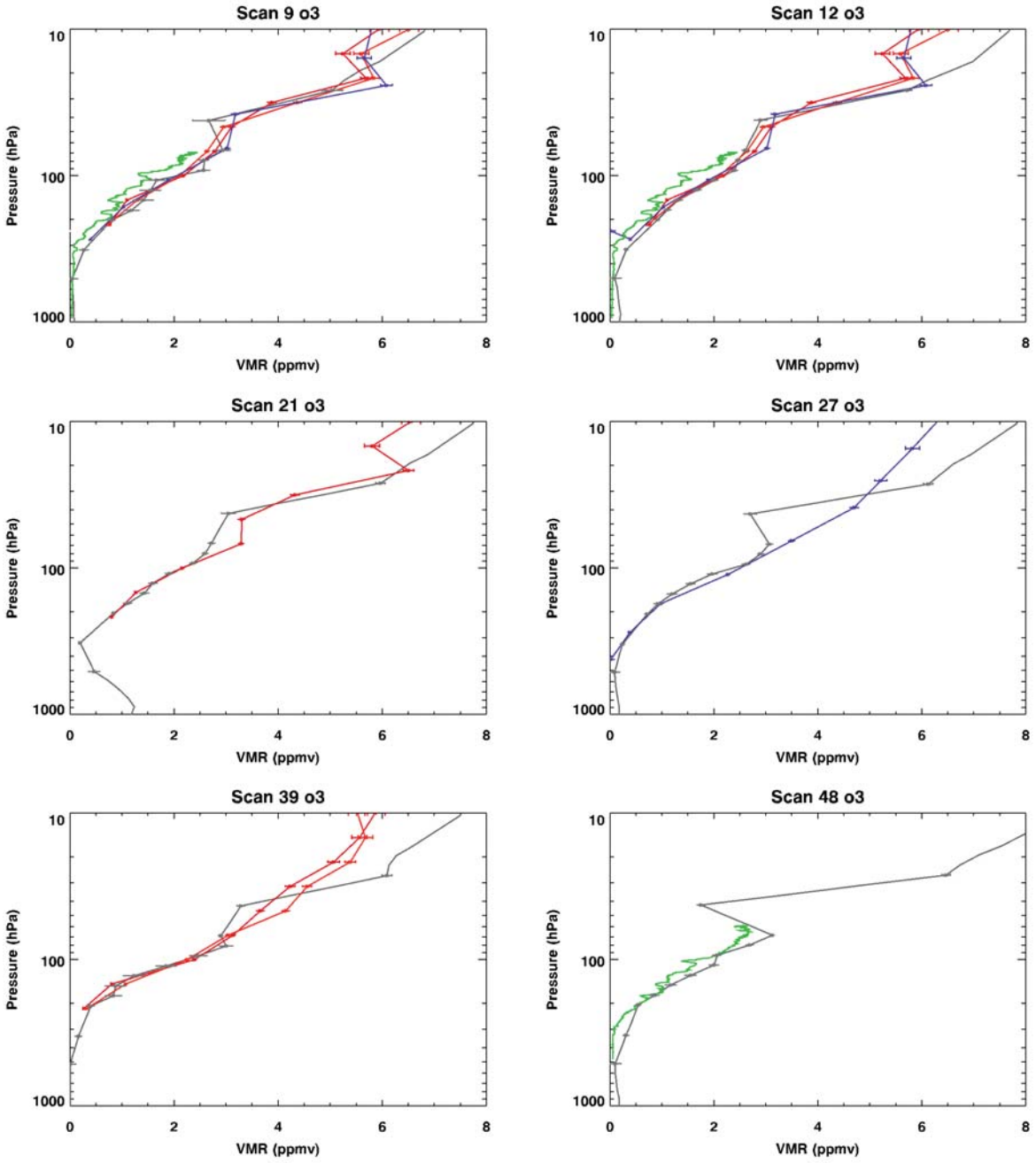

Fig. 108: O_3 retrieved from MARSCHALS (grey) and from MLS (red), or MIPAS/ENVISAT (blue) or FOZAN (green) for recursive retrievals.

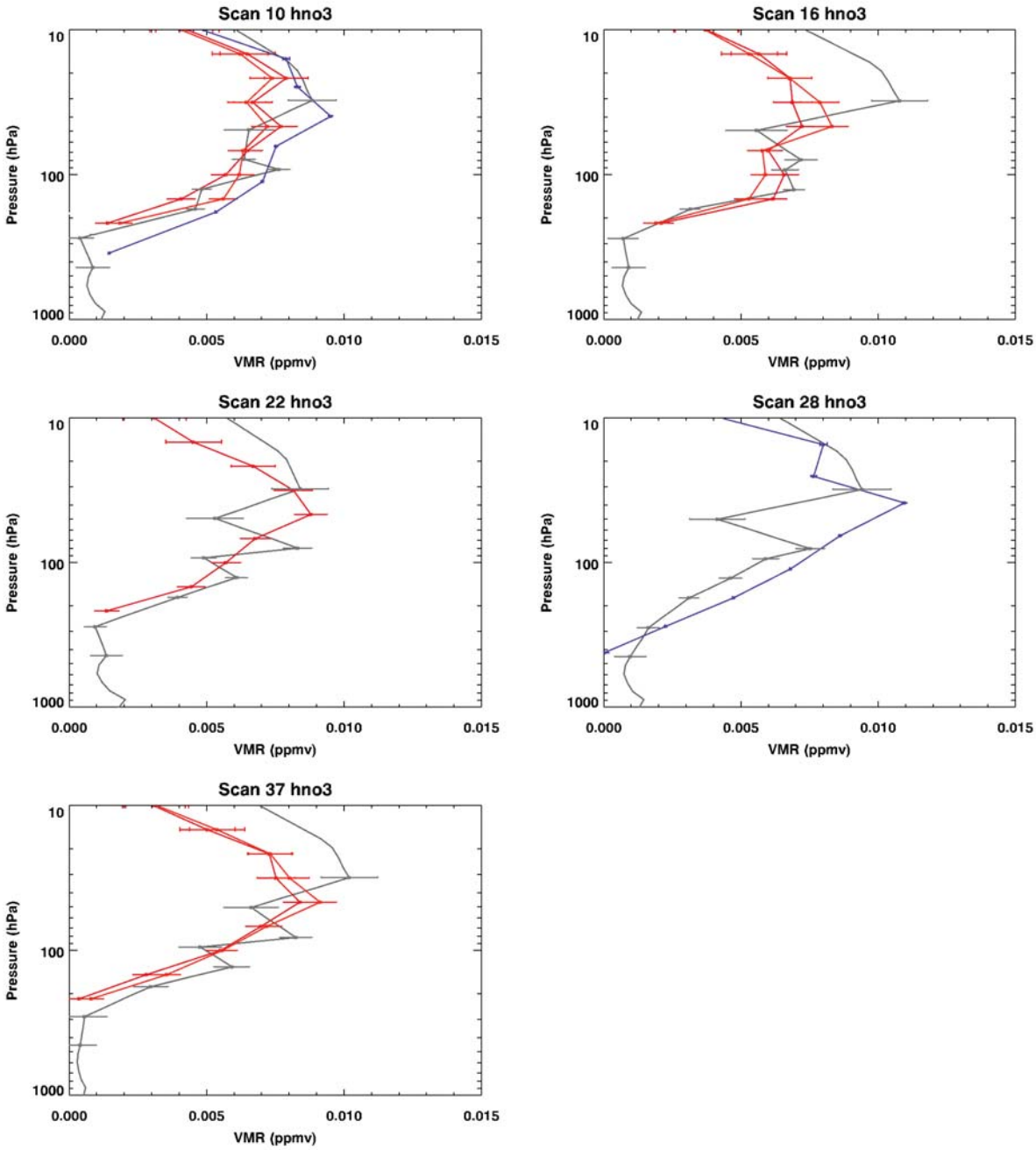

Fig. 109: HNO_3 retrieved from MARSCHALS (grey) and from MLS (red), or MIPAS/ENVISAT (blue) for recursive retrievals.

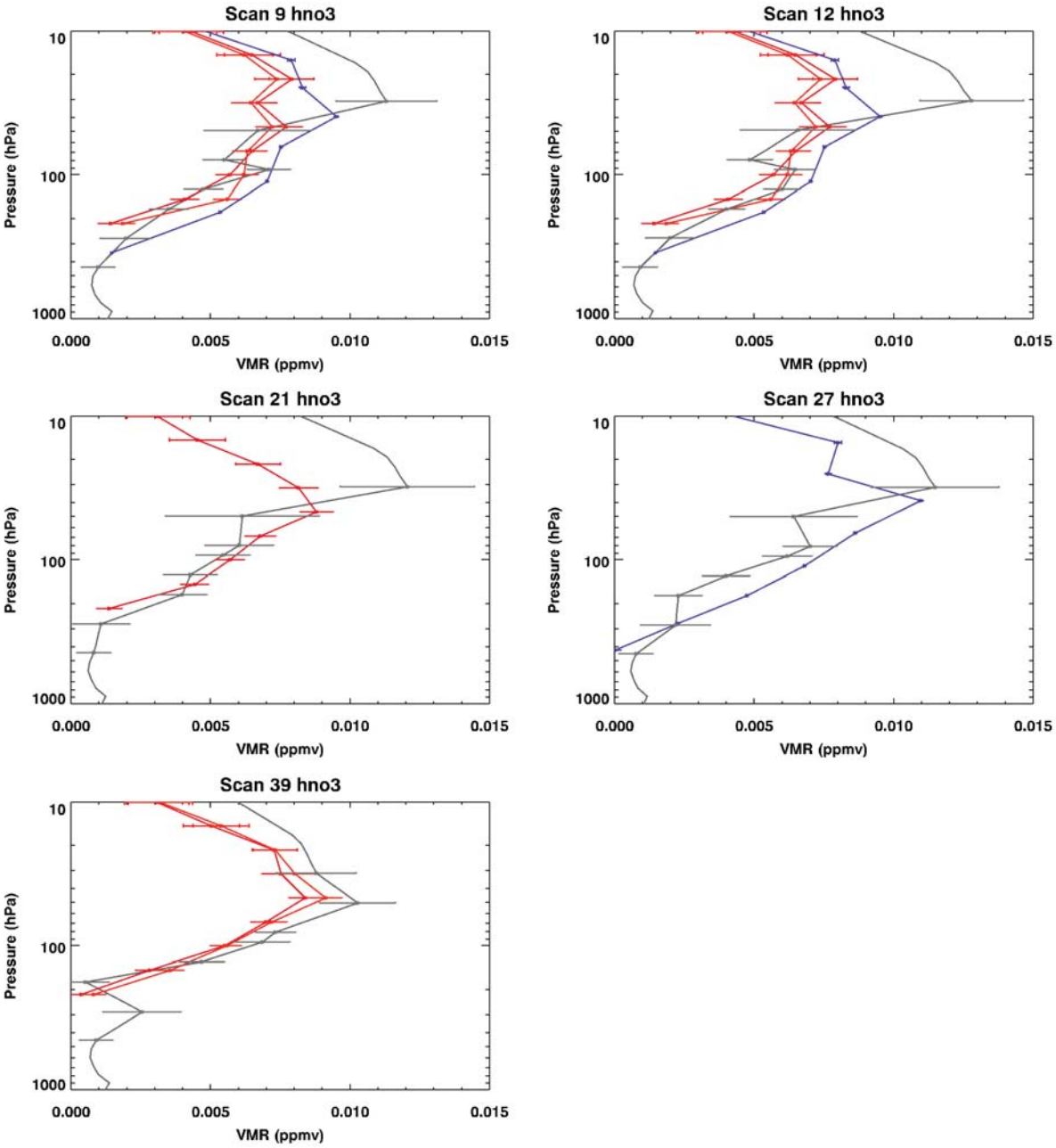

Fig. 110: HNO_3 retrieved from MARSCHALS (grey) and from MLS (red), or MIPAS/ENVISAT (blue) for band C retrievals.

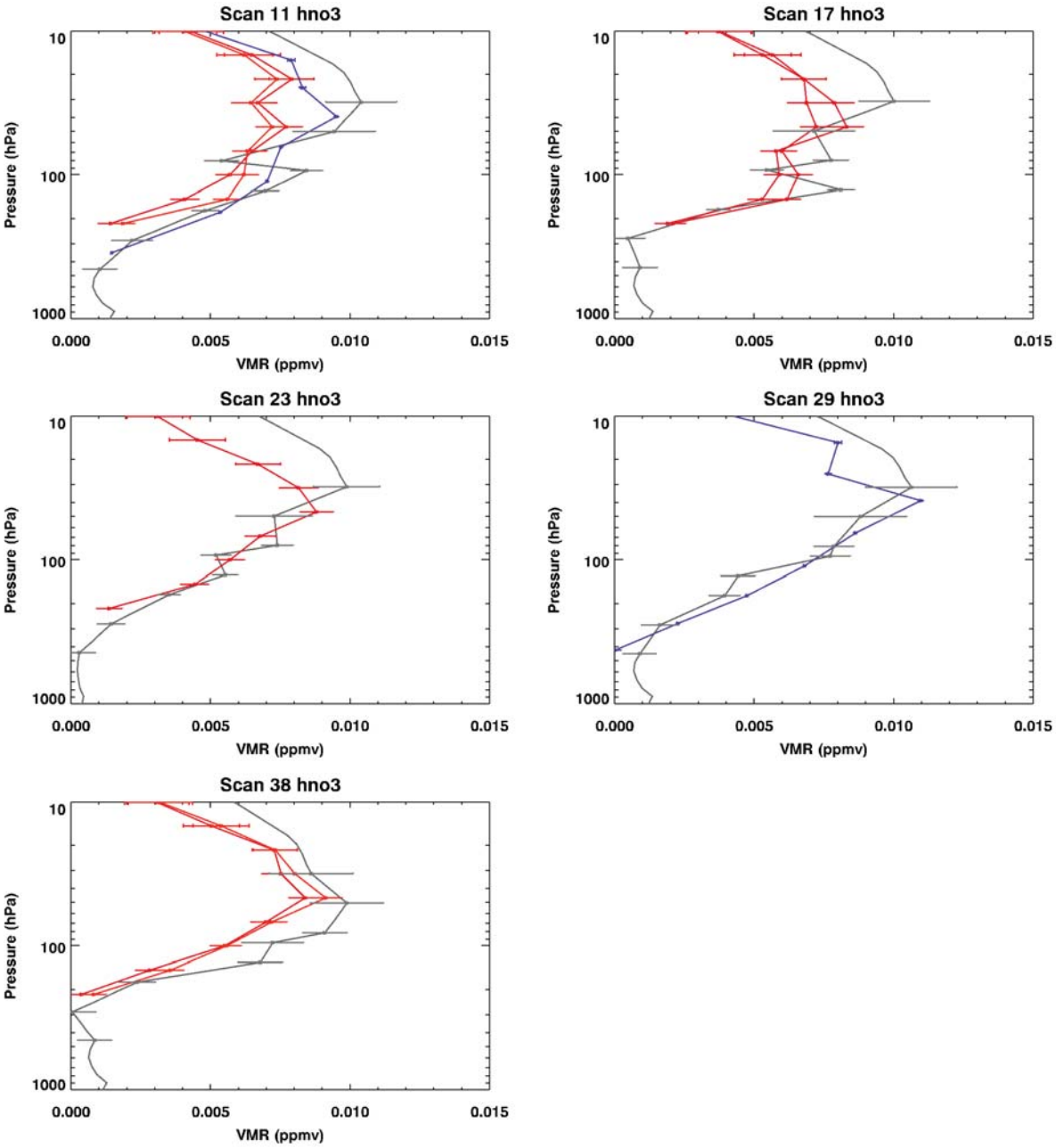

Fig. 111: HNO_3 retrieved from MARSCHALS (grey) and from MLS (red), or MIPAS/ENVISAT (blue) for band D.

The HNO_3 information content in band B is very low. Therefore the retrieved HNO_3 profiles using band B measurements show very large errors and extremely low values above the flight altitude. Since we have improved the quality of the HNO_3 retrievals using the recursive strategy we use those results for the validation of band B measurements.

In the panels of figures 109 to 111, we see that very often MARSCHALS and MLS do not agree above 50 hPa (MARSCHALS is always higher than MLS), while there is a better agreement with MIPAS/ENVISAT data. In general MIPAS/ENVISAT data appear to be higher than the MLS ones. However, in [21] it is reported that the MLS HNO_3 values are from 10 to 30 percent uniformly lower than reality throughout most of the stratosphere.

9.2.5 N_2O validation

N_2O can be retrieved only from band B measurements, and the resulting profiles are usually very unstable. Therefore, for the validation of O_3 we have used the data acquired during the ascent by the in-situ instrument HAGAR for the scans 7 and 10 and during the descent for the scans 47, 50 and 53. MIPAS/ENVISAT data have been used for scans 7, 10, 28 and 31, while MLS data have been used for scans 7, 10, 16, 19, 22, 25 and 37.

Fig. 112 and 113 report the results of these comparisons. Even if some oscillations are present in MARSCHALS profiles, the most significant ones for scans 7 and 37, a general good agreement is found with MIPAS/ENVISAT data and an satisfactory agreement with HAGAR measurements. The lowermost pressure level present in MLS data for N_2O is 100 hPa and thus only the two highest retrieval points of the MARSCHALS profiles can be compared with MLS data. Despite those two points are the most affected by systematic erros due to the assumptions made by the MARC code for the shape of the profiles above the top retrieval altitude, the comparison with MLS data is not too bad, even if MARSCHALS fails to catch the oscillatory behaviour present in both MLS and MIPAS/ENVISAT data at the beginning of the flight. In general we can say that N_2O retrievals are not completely satisfactory.

9.2.6 CO validation

The validation of CO can be performed using only MLS data, since no in-situ instrument nor MIPAS measure this molecule. MLS data have then been used to validate the retrieval of scans 8, 11, 17, 20, 23, 26, 38 and 41. As shown in Figure 114 the CO values retrieved from MARSCHALS for pressure values higher than 100 hPa are very low in comparison with MLS data. As reported in [15] and in [12] the MLS CO retrieved values at 215 hPa exhibit a significant positive bias (about a factor of 2) with respect to other instruments. At Pressure levels of 100 hPa and 147 hPa the estimated biases are of the order of $\pm$ 30 ppbv. Therefore the use of MLS data to validate MARSCHALS CO profiles cannot be considered as exaustive.

9.2.7 Comparison with MIPAS-STR measurements

A first comparison of HNO_3 and O_3 profiles retrieved from MIPAS-STR and MARSCHALS is given in figures 115 and 116. In these figures the MIPAS-STR profiles in coincidence with each MARSCHALS scan, that were then used for the L1+L2 data analysis, are plotted in the upper panel while the MARSCHALS profiles retrieved with the recursive retrieval approach are mapped in the lower panel. In case of HNO_3 retrievals, some features, like the higher HNO_3 values between 14-16 km in correspondece of scans 8-20 (possibly a filament of polar vortex air) or the high HNO_3 values at 17-19 km in correspondence of scans 26 to 41 seem to be well reproduced by both instruments even if two different retrieval grids and regularization procedure are used. In case of O_3 a general good agreement is found. Also in this case some structures like the enhanced O_3 value at 18 km in correspondence of scans 22-23 or in correspondence of scans 30-41 at 18-19 km are present in both the analysis. In the last part of the flight MARSCHALS retrieves slightly higher values at 18 km respect to MIPAS-STR even if a similar vertical structure is reported in the two cases.

9.2.8 Scientific Flight validation: Conclusions

In general a good agreement is found between MARSCHALS products and coincident satellite and in situ data. Good results are obtained for T and H_2O retrieved from band C, for O_3 in all bands and for HNO_3 in band C and D. Even if some oscillations are present in N_2O profiles the overall agreement with MIPAS/ENVISAT and HAGAR data is good (a very reduced altitude range is available for the comparison with MLS data). CO retrieved profiles shows significant deviations from MLS data that however have a well known high bias.

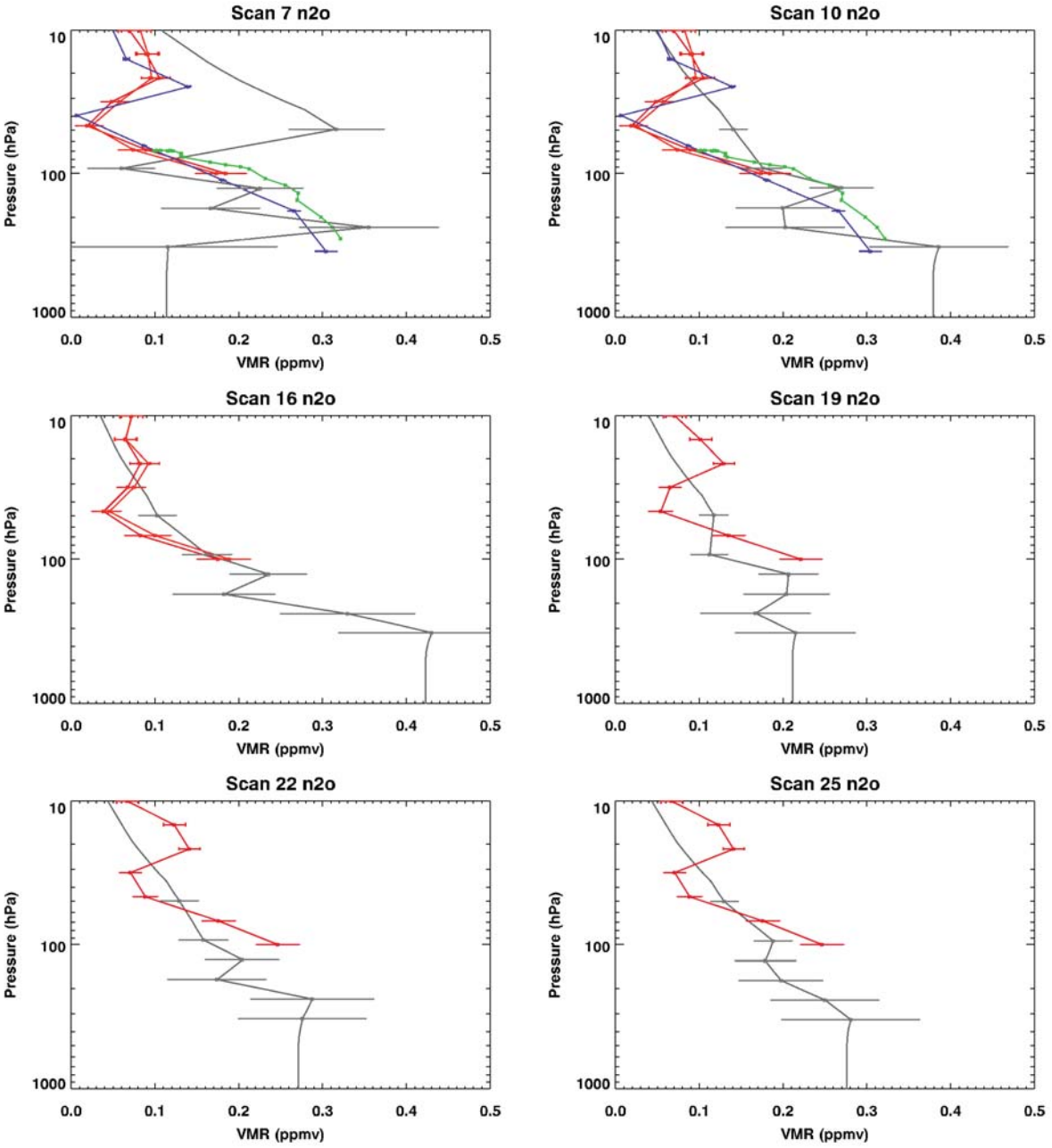

Fig. 112: N_2O VMR retrieved from MARSCHALS (grey) and from MLS, or MIPAS/ENVISAT or HAGAR (see text for details).

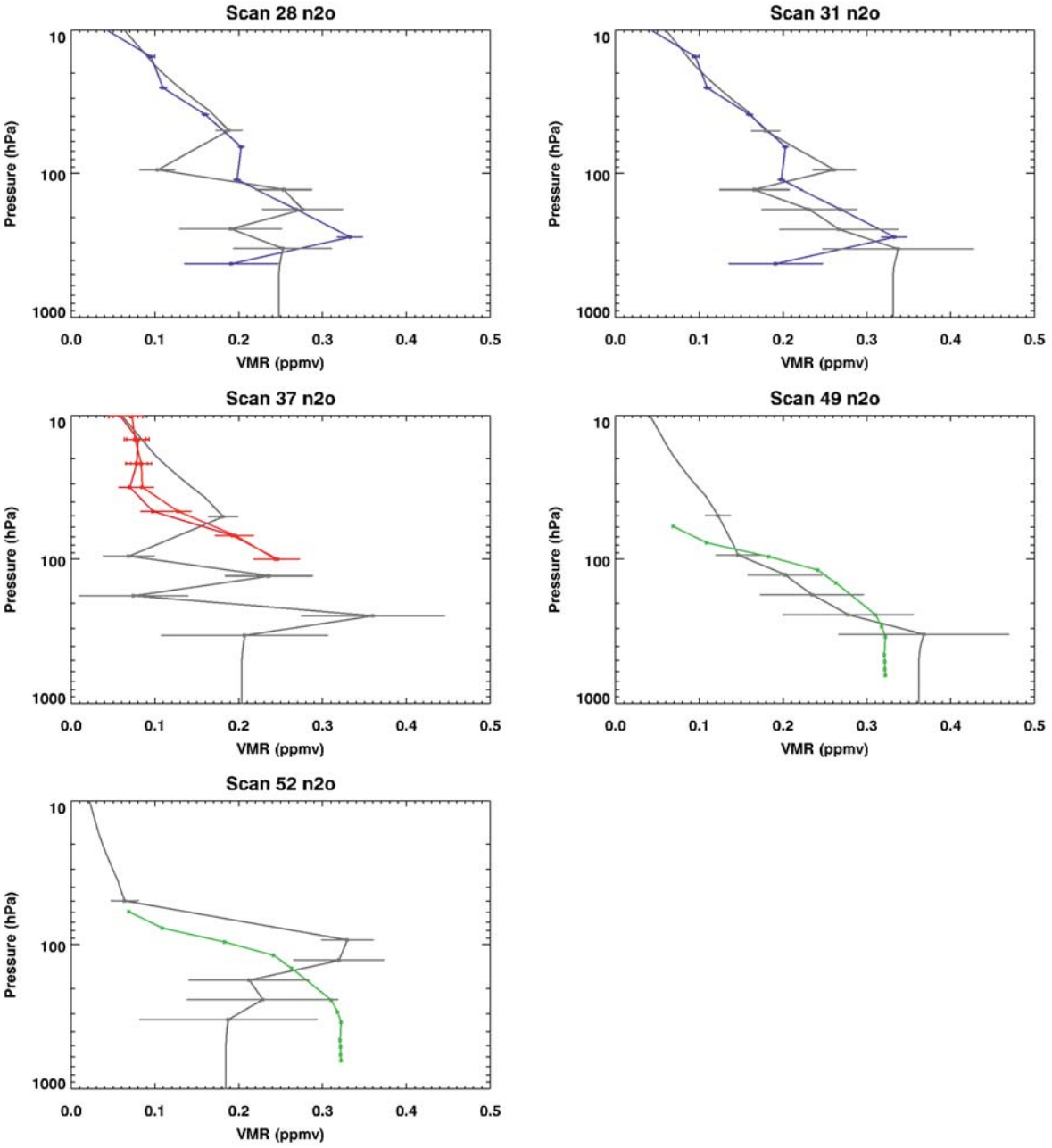

Fig. 113: N_2O VMR retrieved from MARSCHALS (grey) and from MLS, or MIPAS/ENVISAT or HAGAR (see text for details).

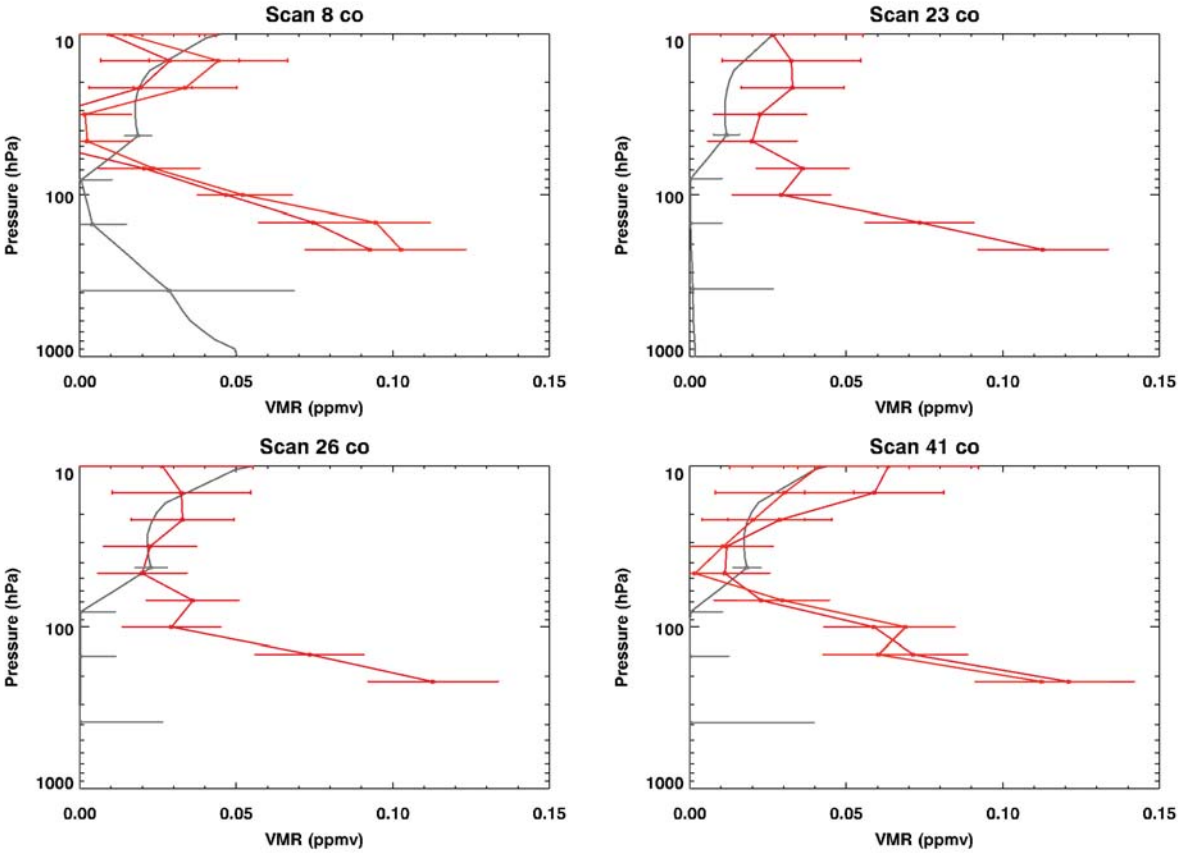

Fig. 114: CO VMR retrieved from MARSCHALS (grey) and from MLS (red).

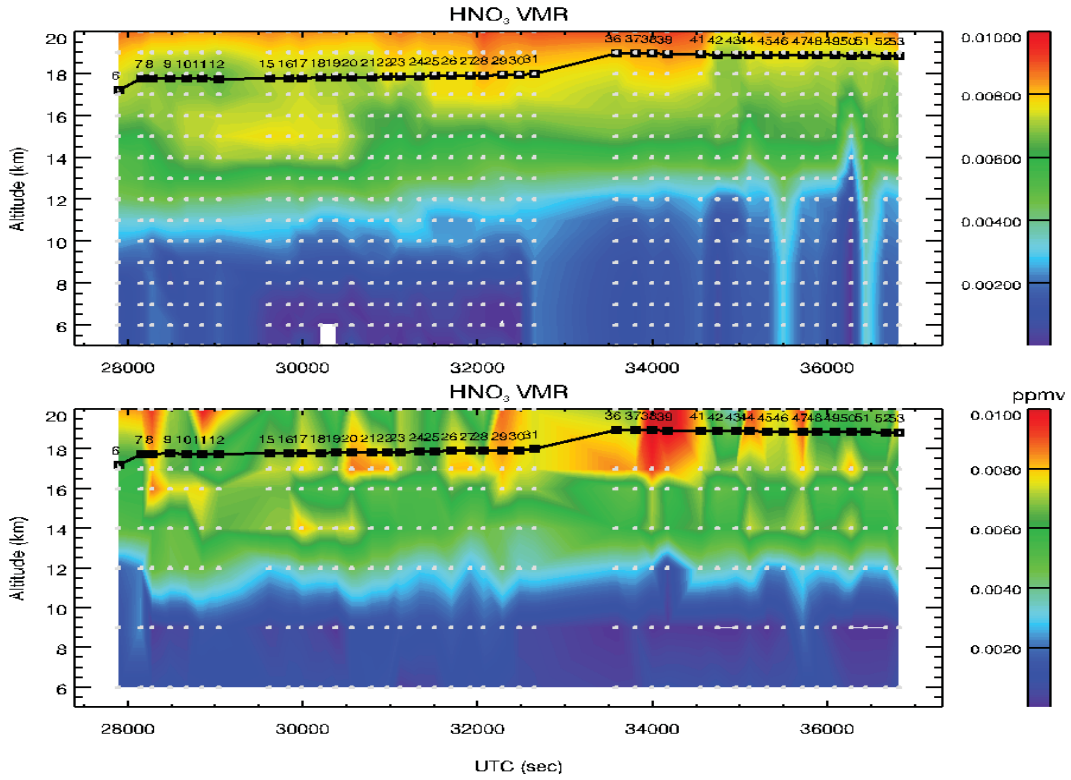

Fig. 115: HNO_3 VMR profiles retrieved from MIPAS-STR (top) and MARSCHALS (bottom).

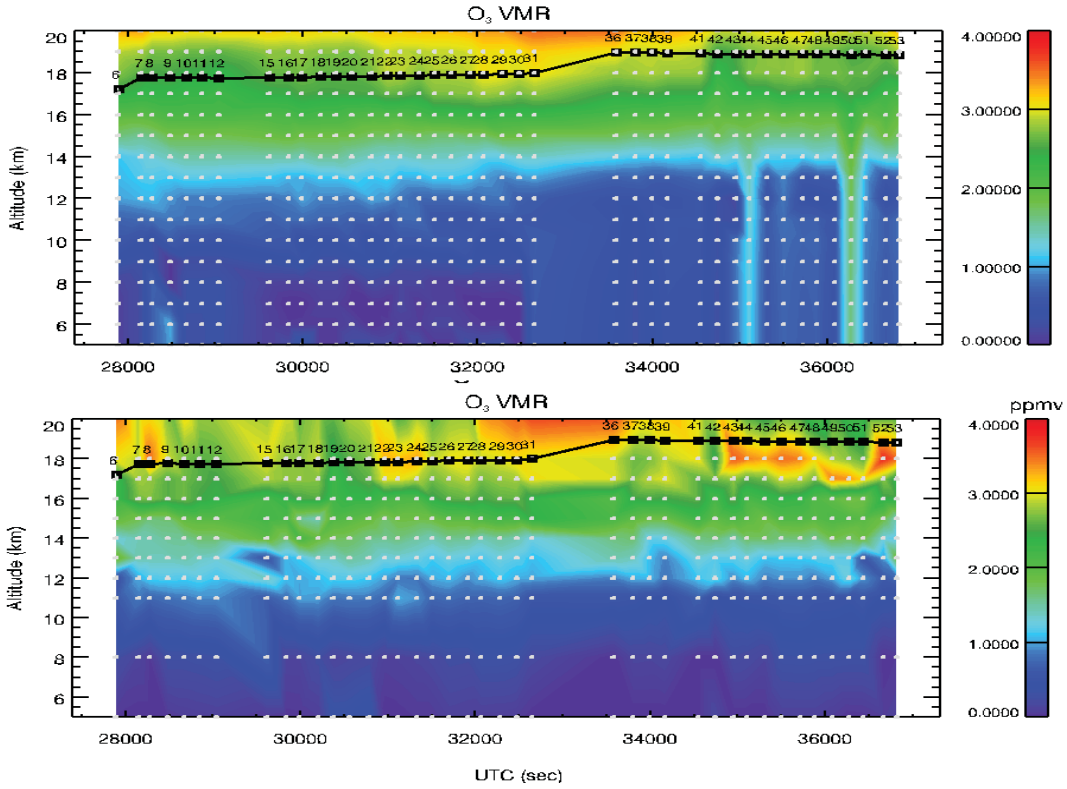

Fig. 116: O_3 VMR profiles retrieved from MIPAS-STR (top) and MARSCHALS (bottom).

10 MARSCHALS cloud products

10.1 Test Flight - Cloud detection

The retrieval of the external continuum in the analysis of the measurements of the Test Flight, reported in figure 42 and in figure 55 suggests the presence of clouds with the cloud top altitude between 10 and 8 km in the first part of the flight (clouds in the region from 10 to 14 deg. in longitude and from 50 to 54 deg. in latitude). In particular the obtained results show the possible detection of clouds in scans 6, 10 and 16. In Figure 117 we report the retrieved extinction coefficients for those scans. In the final part of the flight MARSCHALS detects some clouds at 12-13 km altitudes, whose effect can be modelled with an external continuum value lower than in the first part of the flight (see figure 118 where the external continuum profiles retrieved for scans 32, 33 and 34 are reported). Since these final scans were recorded during the flight descent, the retrieved external continuum can be affected by the variation of the plane altitude during the measurements, so that the cloud detection may not be completely trusted. Previous experience made with the SCOUT-O3 data showed that for values of the external continuum similar to the ones obtained for the Test Flight, the use of MSSF into the retrieval did not produce any improvement in the

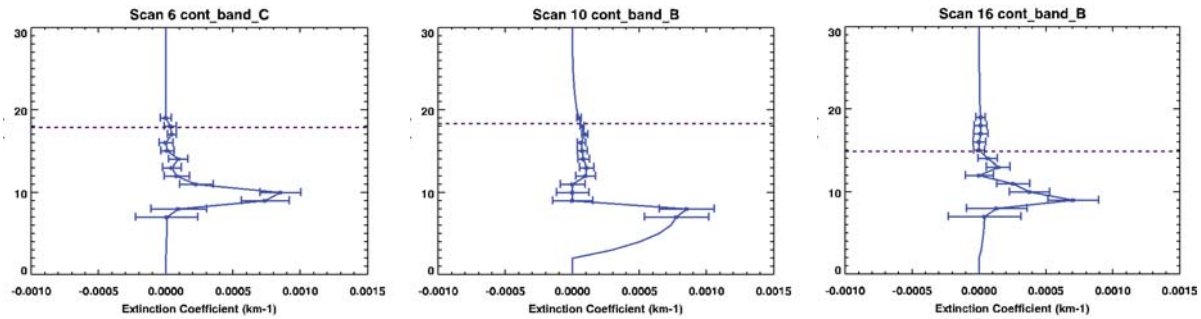

Fig. 117: Extinction coefficient profiles retrieved for scans 6, 10 and 16.

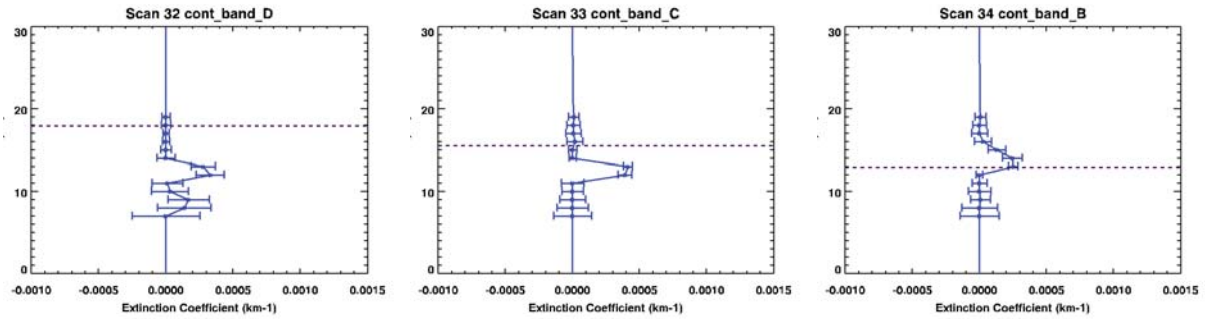

Fig. 118: Extinction coefficient profiles retrieved for scans 32, 33 and 34.

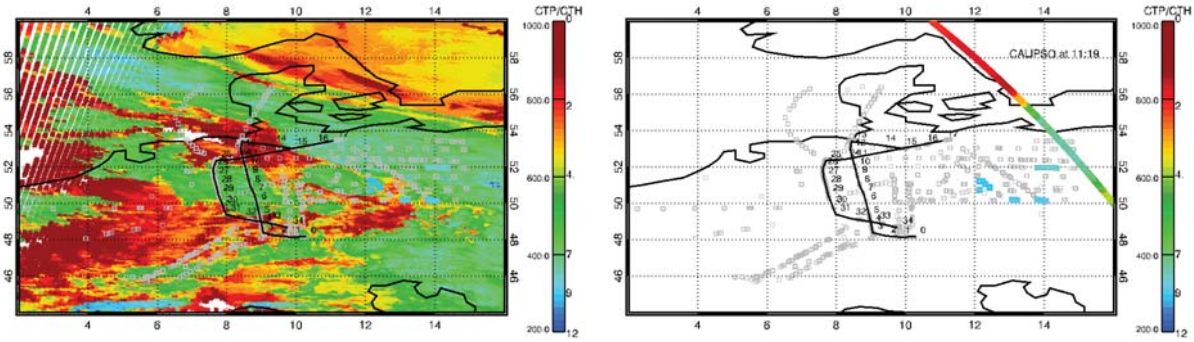

Fig. 119: MODIS cloud top pressure at 10:15 UTC (top) and CALIOP (bottom) cloud top pressure at 11:19 UTC.

retrieved products. Therefore we did not perform an additional retrieval using the MSSF module to reproduce the clouds effects in the forward model internal to the retrieval module.

10.2 Test Flight - Validation of the cloud detection

To validate the detection of clouds in MARSCHALS measurements we need external information about the cloud coverage during the flight. External cloud informations can be obtained using in-situ instruments (as CCP, CIP and FSSP) onboard the Geophysica or using the Cloud Index information obtained from MIPAS-STR spectra, that observes the same airmasses sampled by MARSCHALS. For the Test Flight the only in-situ instrument available for the intercomparison is FSSP. An overall picture of cloud coverage during the flight can also be obtained using correlative satellite data. For our validation exercise we have chosen to use the data measued by MODIS and CALIPSO.

In Figure 119 are reported the Cloud Top Pressure (CTP) values from MODIS (at 10:15) and CALIPSO (at about 11:19) together with MARSCHALS pressure values for the altitude levels at wich the retrieved external continuum exceeds a value of about 0.5 10-3 km-1 in the first part of the flight.

MODIS data (measured about 2 hours before the flight) highlight the presence of both very low clouds (CTP about 900 hPa) and higher clouds (CTP about 300 hPa) in the region explored by MARSCHALS scans 6-17. Also CALIPSO data in coincidence with MARSCHALS scans 6-10 17 show the presence of low and high altitude clouds. Comparing the geolocation of the pressure at which the retrieved extinction exceeeds the given threshold with the map of MODIS and CALIPSO CTP a general very good agreement can be found.

The FSSP instrument, as shown in Figure 120 where the effective particle radius and the number density are plotted as a function of altitude, detected a cloud layer with Cloud Top Altitude (CTA) at about 9 km during the ascent and a lower cloud layer (CTA about 3-4 km) in the final part of the flight. This is in good agreement with the CTA extimated from the external continuum retrieval for the first part of the flight that was between 10 and 8 km. Moreover, as reported in the Test Flight campaign report, also the OCM module reports cloud tops between 6 to 10 km with haze up to 16 km.

For the final part of the flight, during the descent, where MARSCHALS possibly detects some clouds at 13-12 km no data are available for CALIPSO, while no evidence of these clouds can be seen from MODIS data (that however were recorded 4 hours before the flight descent) and the FSSP reveals the presence of some clouds during

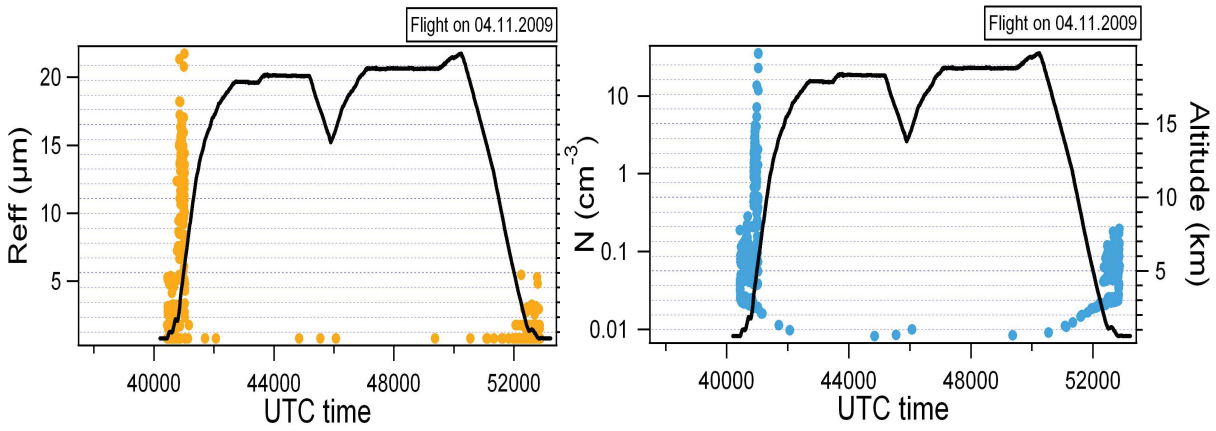

Fig. 120: Cloud particle effective radius (left) and number density (right) measured by FSSP during the flight.

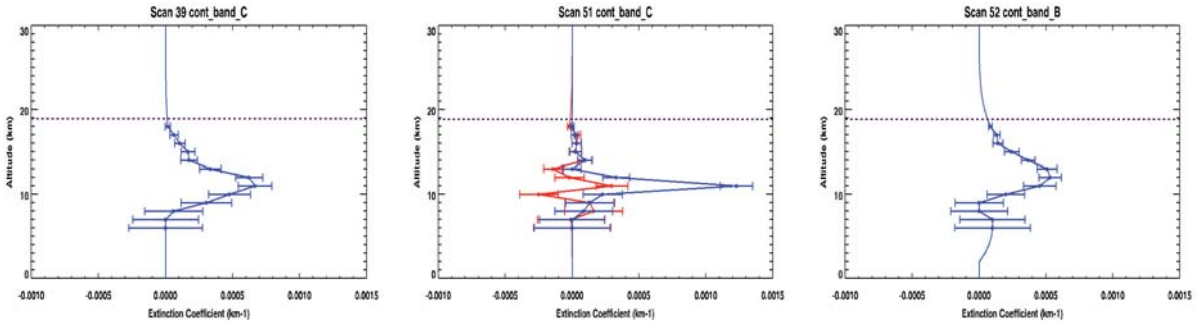

Fig. 121: Extinction coefficient profiles retrieved for scans 39, 51 and 52 (blue). For scan 51 results obtained using MSSF module are reported in red.

the descent (with also some haze at 19 km in the final part of the flight). However, as previously said, these scans were acquired during the flight descent and can be affected by the variation of the aircraft altitude during the measurement acquisition time.

10.3 Scientific Flight - Could detection and retrieval in cloudy condition

The retrieval of the external continuum over the whole Scientific Flight, reported in Figure 79, suggests that MARSCHALS possibly detected clouds in the measurements of a few scans (namely scans 39, 51 and 52).

Figure 121 shows the retrieved extinction coefficients for those scans. We can see that the value of the extinction coefficient obtained for scan number 51 (1.24 10^{-3} km^{-1}) at about 11 km is similar to the one obtained during the SCOUT-O3 campaign for a scan that was used to perform a retrieval simulating the cloud contribution to the spectra through the use of the MSSF module. For scans number 39 and 52 the value of the retrieved extinction coefficient is lower, but the shape of the retrieved external continuum is more pronunced and involves several altitudes. However, previous experience made with the SCOUT-O3 data showed that for those values of the retrieved extinction coefficient the use of MSSF into the retrieval did not produce any improvement in the retrieved products.

Therefore we decided to perform the retrieval of only scan 51 using the MSSF module to simulate the cloud effects. As reported in [5] each retrieved extinction coefficient value can be obtained using different combinations of particle radii and number densities, parameters used by the MSSF module to properly represent the cloud in the Forward Model internal to the retrieval. In order to identify the correct cloud parameters to be used during the retrieval with the MSSF cloud simulation enabled, we have used correlatives data from three in-situ instruments (CIP, CCP and FSSP), onboard the Geophysica aircraft, that measure the cloud microphysical characteristics. An example of the data provided by the FSSP sensor are reported in Figure 122 (number density on the left and effective radius on the right).

All the in-situ instruments recorded the presence of cloud particles from 10 to 12 km during the descent. In general, the in-situ instruments measured particle radii in the range from 10 to 50 μm and the nuber density from 0.01 to 0.6 cm^{-3}. Data in better spatial coincidence than the in-situ instruments can be obtained using the

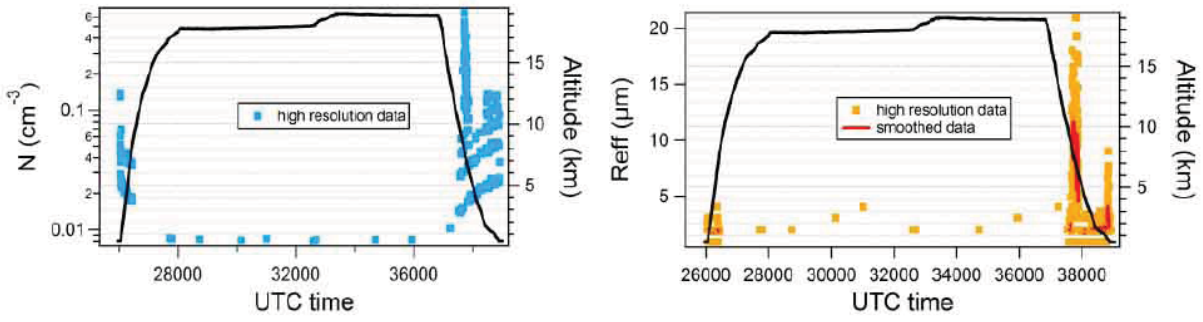

Fig. 122: Number density (left) and effective radius (right) from FSSP.

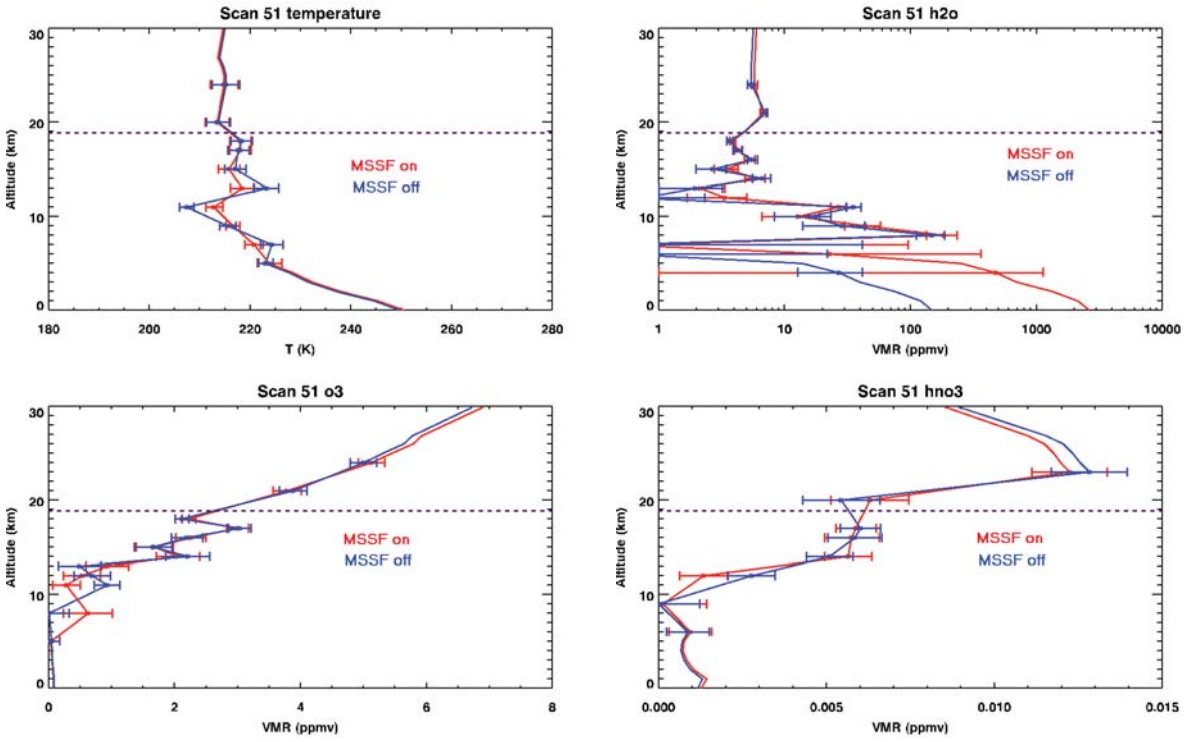

Fig. 123: Comparison between retrieval results for scan 51 with (red) and without (blue) MSSF cloud simulations.

MODIS sensor, that reports a value for the particle effective radius in the region sampled by scan 51 of 15-30 μm. Combining the correlative informations from all the external sources (radius, number density, extinction coefficients and altitude extension) we performed the retrievals injecting into MSSF the following parameters: Particle Radius = 25 μm, Number density = 0.35 cm^{-3}, altitude range = 12-10 km The simulations of the cloud using the MSSF module during the retrieval produced a value of the external retrieved continuum (and thus of the extinction coefficient) near to 0 at all altitudes (red profile in Figure 121). Retrieval results for scan 51 compared with the analysis performed without the MSSF cloud simulation are shown in Figure 123.

From the figures we can notice that while the use of MSSF mudule produces very small or negligible differences compared to the standard analysis for H_2O, for O_3, HNO_3, and Temperature we see an improvement (lower oscillations).

10.4 Scientific Flight - Validation of the cloud detection

As already said in the previous section, cloud informations can be obtained using different in-situ instruments (as CCP, CIP and FSSP) onboard the Geophysica. Furthermore MIPAS-STR Cloud Index value along the flight can provide a valuable picture of the cloud top altitude distribution at the same time and in approximately the same region explored by MARSCHALS LOS (see Figure 126 for MIPAS-STR tangent points location). An overall picture of cloud coverage during the flight can also be achieved using satellite data. In particular MODIS and

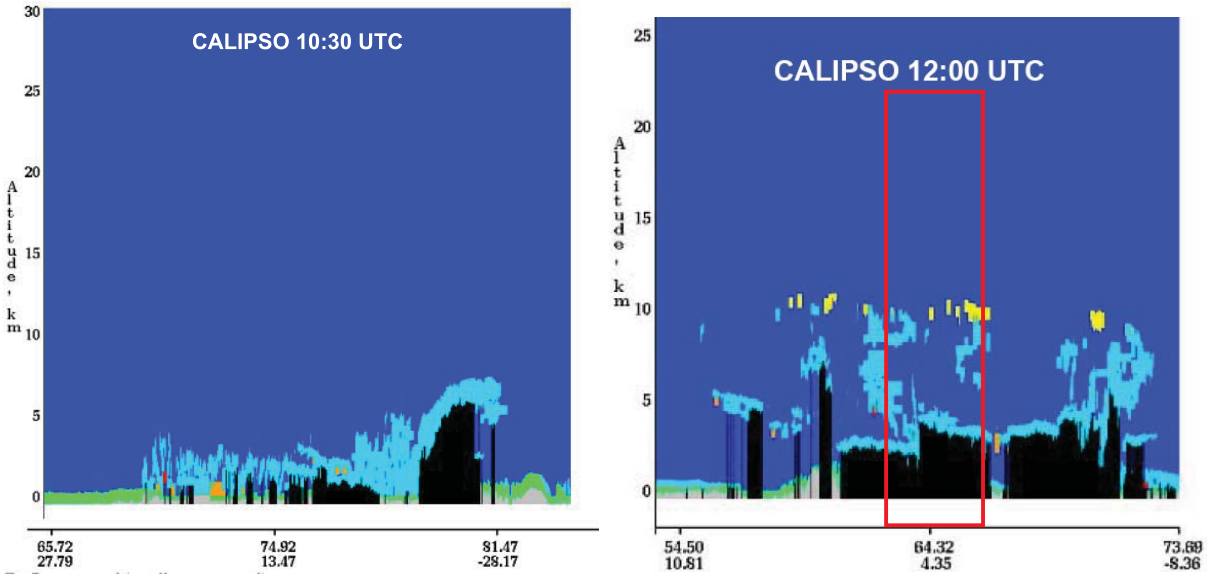

Fig. 124: CALIPSO cloud profile in the first part and last part of the flight. The red box indicates the region in coincidence with MARSCHALS scan number 39

CALIPSO products are suitable for our validation purposes.

The data acquired by the CCP, CIP and FSSP instruments suggest the presence of clouds in the final part of the flight, during the descent. In Figure 125 are reported the Cloud Top Pressure (CTP) values from MODIS (at 10:43) and CALIPSO (at about 10:30 and 12) together with MARSCHALS pressure values for the altitude levels at wich the retrieved external continuum exceeds 0.5 10^{-3} km^{-1}. MODIS data clearly indicate the presence of low clouds (CTP $\sim$ 900 hPa) in the region explored by MARSCHALS scans 10-33 and a region with high clouds (up to 300 hPa) in the region sounded by scans 36-53. Also CALIPSO data coincident with the first part of the flight show the presence of evenly distributed low altitude clouds. In the last part of the flight CALIPSO measures the presence of higher altitude clouds with a lot of variability in the CTP (Figure 124).

The MIPAS-STR Cloud Index values, shown in Figure 126, indicates the presence of clouds with a cloud top altitude (CTA) of about 6 km at the beginning of the flight and of higher clouds (about 11 km) in the last part of the flight. MARSCHALS external continuum retrieval starts at 6 km because there is a very small sensitivity to its value at altitudes below 11-10 km. Therefore the low clouds (CTA of 5-6 km) present in the first part of the flight cannot be seen (see Figure 79 lower panel). An attempt to retrieve the external continuum down to 4 km did not change this picture. In the second part of the flight, where higher clouds are reported by correlative measurements, the retrieved external continuum suggests cloud presence at about 11-12 km (see Figure 121). The in-situ instruments, as shown in Figure 122 where the effective particle radius and the number density are plotted as a function of altitude, detected a cloud layer with CTA varying from 14 to 10 km during the descent. Using satellite data, if we compare the geolocation of where the pressure at which the extinction coefficients calculated during the retrieval procedure exceeds the 0.5 10^{-3} km^{-1} with the map of MODIS and CALIPSO CTP we see a quite good agreement. The agreement is particularly good looking at the CTP found in MARSCHALS scan 39 and the high resolution CTP from CALIPSO data shown in Figures 125 and 124. The fact that the high altitude clouds are mostly not seen in MARSCHALS external continuum retrieval from scan 37 to 53 demonstrate the possibility of MARSCHALS to measure the atmospheric composition also in presence of clouds that are opaque in the infrared.

Cloud microphysical properties can not be retrieved from MARSCHALS spectra. However the code provides the cloud extinction coefficient. This coefficient can be obtained using different combinations of particle radius and number densities. Therefore external sources are needed to properly simulate the cloud effects in MARSCHALS spectra. In this study we used MODIS and FSSP measurements to find the values of the effective radius and number densities that were then used into the MSSF module. The fact that the extinction coefficient retrieved using the MSSF cloud simulations approaches zero (see red profile in Figure 121) provide a good indication of the correctness of MARSCHALS retrieved extinction coefficient.

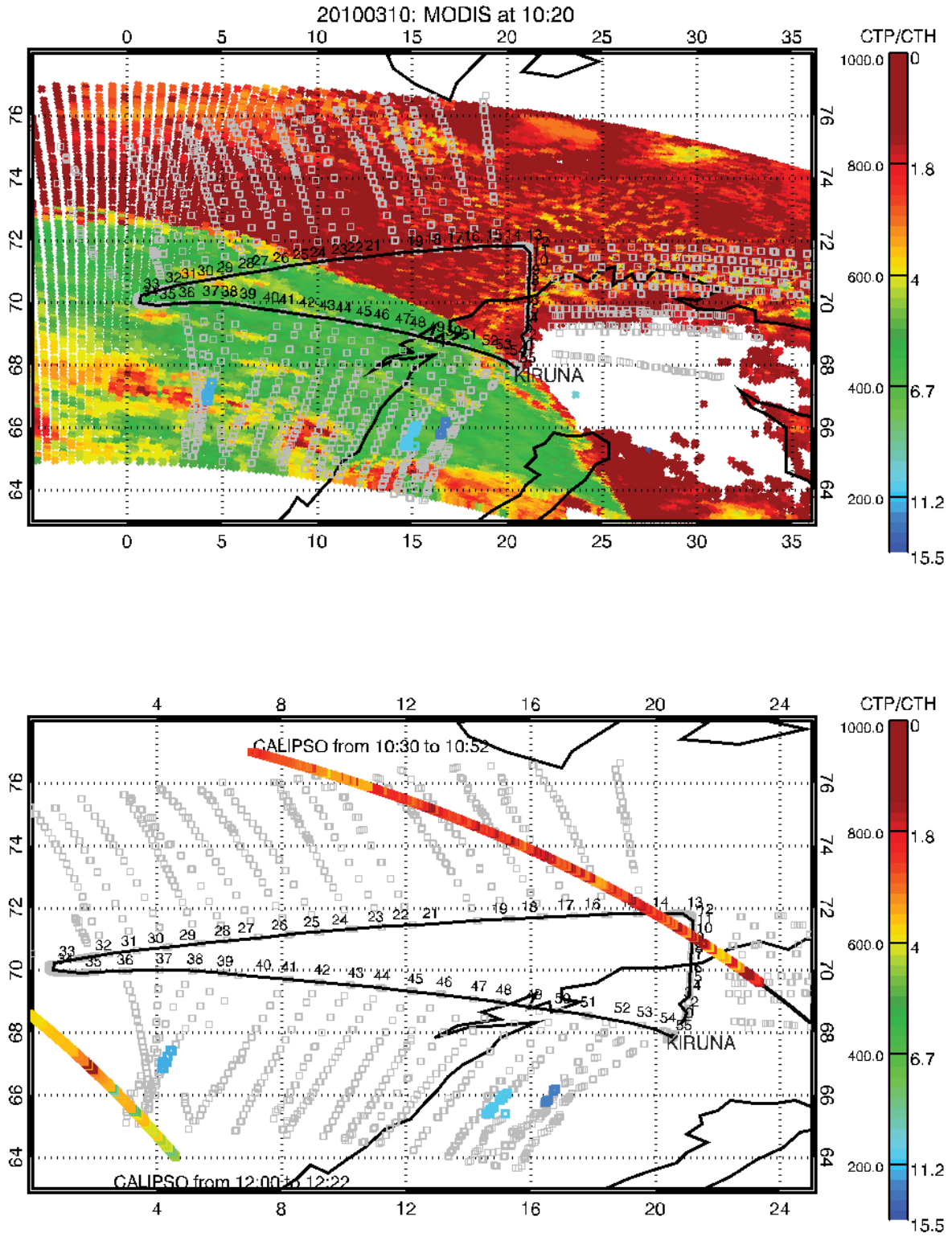

Fig. 125: MARSCHALS external continuum informations and MODIS (upper panel) and CALIPSO (lower panel) cloud top pressure

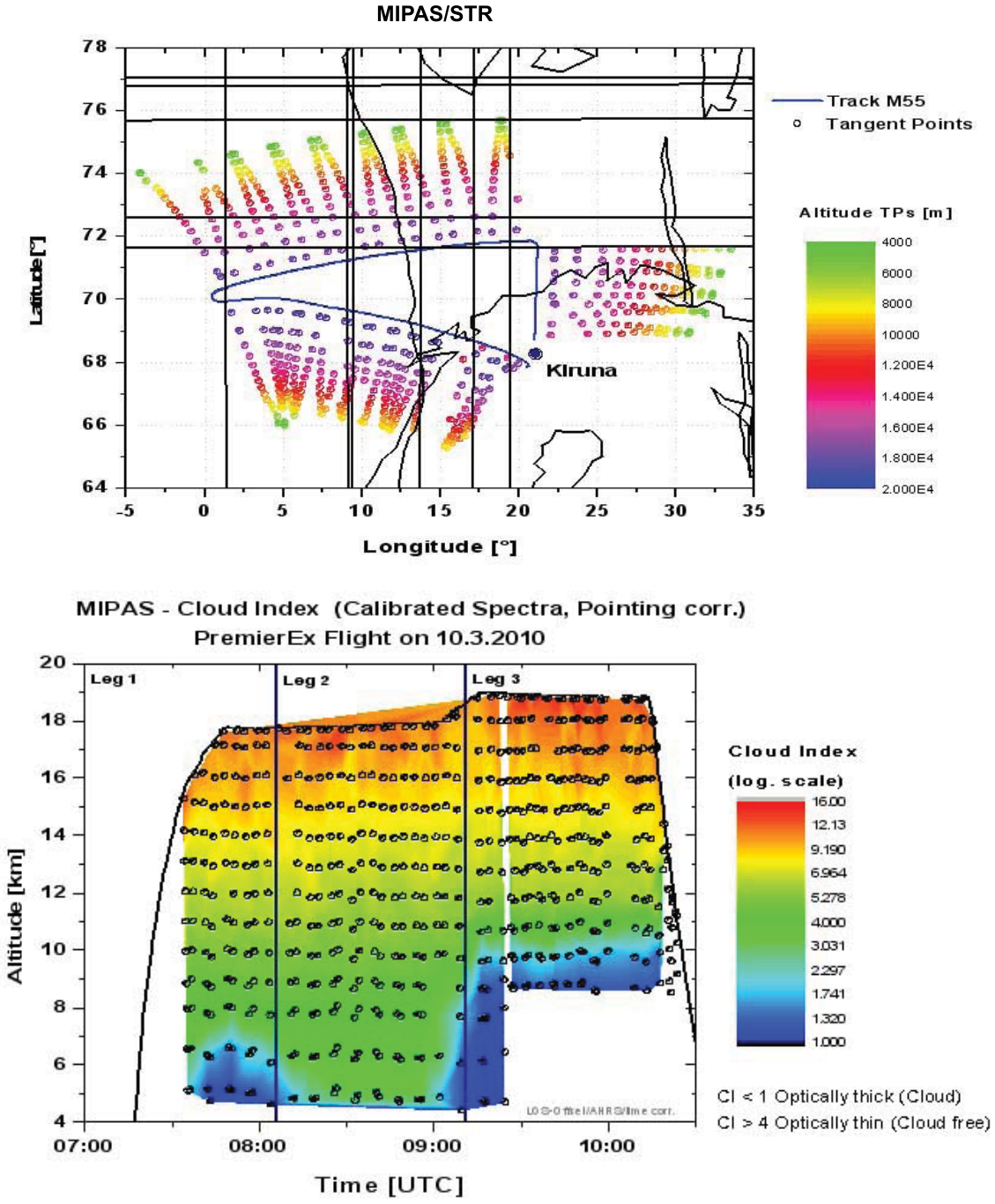

Fig. 126: Position of MIPAS-STR tangent points (left) and MIPAS Cloud Index along the flight (right)

11 Level 2 processing of MIPAS-STR data of the PremierEx Scientific Flight on 10.03.2010

11.1 Description of the Flight and Cloud Assessment

MIPAS-STR was successfully operated during the PremierEx Scientific Flight on March 10^{th} 2010 and spectra suitable for Level 2 processing were obtained for all three flight legs. The flight overview and the sampling performed by MIPAS-STR are shown in Figure 127. Takeoff was in Kiruna, Sweden (Lat. 67.8 °N, Lon. 20.4 °E) at 7:14 UTC. Three flight legs were carried out in an anti-clockwise pattern and landing was at 10:48 UTC in Kiruna. The distribution of the tangent points is indicated by the coloured dots. High tangent points are situated close to the flight path, and for low tangent points, the distance to the flight path increases steadily. In total, 767 atmospheric spectra were obtained in 52 limb sequences.

The achieved vertical sampling is shown in Figure 128 together with the cloud-index. During the third flight leg, considerable tropospheric cloud coverage was present. Hence, limb scans were only performed down to 9 km altitude during this flight section. Upward scanning was performed less frequently in order to achieve a higher horizontal sampling density.

The cloud-index is defined as the colour-ratio of the spectral microwindows between 788.2-796.25 cm^{-1} and 832.3-834.4 cm^{-1}, making use of the different sensitivity of these microwindows to background aerosol [22]. Cloud indices higher than 4 indicate cloud-free conditions, while values in the range from 1 to 4 indicate partially aerosol-affected spectra. Cloud index values close to 1 indicate dense clouds.

Partly cloud affected spectra can be caused by the following reasons:

- Presence of thin clouds/background aerosol
- The field of view of the instrument (approximately 3 km at the lowest tangent point) scratches dense clouds below the tangent altitude at the lower end of the FOV
- Signatures of trace gases affecting the cloud index (pressure-broadening of spectral lines and broad-band signatures of gases with unknown profiles)

It has to be noted, that the cloud index is primarily defined for stratospheric spectra. The threshold for cloud-affected spectra is likely to differ for tropospheric spectra. And of course, the cloud index sensitivity slightly changes for different instruments (e.g. due to effects of spectral resolution and field-of-view). Nevertheless, in this context and for other RECONCILE flights, the cloud index defined in [22] has been found to be suitable for

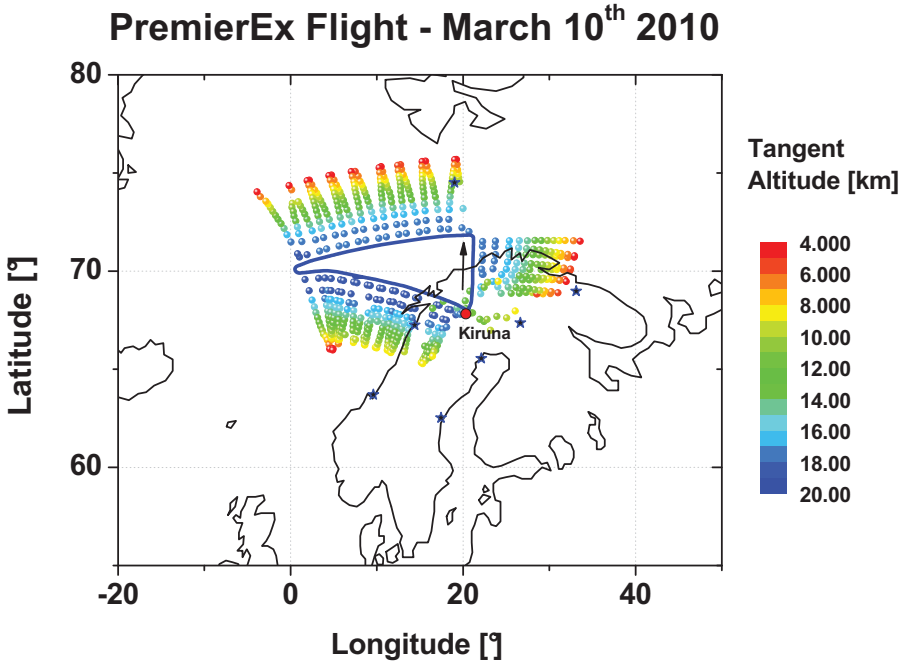

Fig. 127: Overview of the PremierEx Scientific Flight on March 10^{th} 2010. The tangent points of MIPAS-STR are shown colour-coded

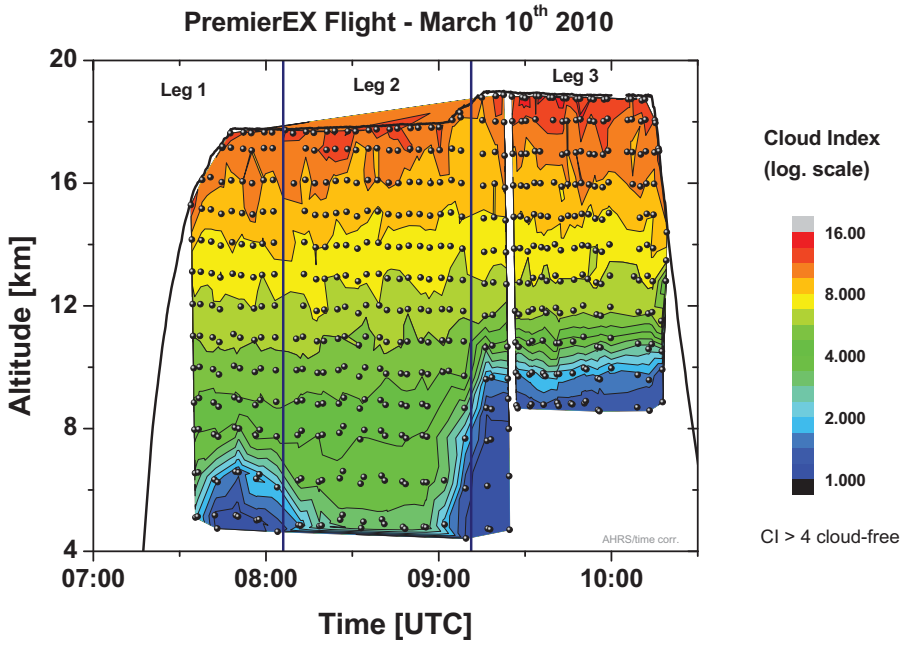

Fig. 128: Vertical sampling of MIPAS-STR (positive elevation angles not shown) and interpolated cloud index

MIPAS-STR and spectra with a cloud index higher than 4 have been found to be retrievable without any constraints. In Figure 128, dense clouds are identified in flight leg 1 mainly below 8 km (cloud indices close to 1). In contrast, flight leg 2 was cloud-free down to 5 km except at its boundaries at the lowest tangent points. The increase of the cloud top altitude is clearly visible before the turn towards flight leg 3. During this particular flight leg, dense clouds are found up to an altitude of 10 km. The threshold for cloud index 4 is represented by greenish colours. It is located at approximately 9 km for legs 1 and 2 and 11 km for leg 3, marking the lower limit for definitively cloud-free spectra.

Slightly cloud affected spectra can also be taken into account for retrievals. Examples for spectra with low cloud indices are shown in 128 together with the microwindows utilized for the derivation of the cloud index. Spectra with cloud indices lower than 4 show an asymmetric increase of the baseline (stronger increase towards lower wavenumbers). The shape of the spectra becomes more and more dominated by the grey-body contribution caused by the cloud/aerosol particles, and the spectral signatures of the trace gases are attenuated. In the case of the spectra with cloud index 1.1, the trace gas signatures are very weak and completely dominated by transmission signatures.
From Figure 129, it can be seen that for the spectra with cloud index 1.7 and higher prominent spectral emission signatures can be still identified, although the spectral baseline is obviously cloud affected. In a limited extend, effects of clouds can be compensated in the trace gas retrievals by the fitting of background continuum. Since also the effects of unknown trace gases, far line wing effects and weak background aerosol have to be compensated, background continuum has to be retrieved anyhow. But it has to be noted, that the retrieval of spectra with a cloud index lower than 4 can lead to additional systematic errors. In addition, a stronger regularization is required resulting in a loss of vertical resolution.

In order to investigate the maximum vertical retrieval range for cloud-affected spectra more in detail and to make use of the maximal vertical sampling, the retrievals are optimized for a cloud index threshold of 2 in this context.

11.2 Retrieval strategy

The trace gas retrievals are carried out using the forward model KOPRA (Karlsruhe Optimised and Precise Radiative Transfer Algortihm) [23] and the inversion model KOPRAFIT [27]. Forward calculations are performed for the observation geometries under consideration of refraction. Signatures of known interfering gases are calculated using profiles from the ESA Polar Winter Climatology, which are in some cases modified for the particular flight situation (for example, the CO_2 profile is adapted for 2010). The inversion is carried out using the Tikhonov-

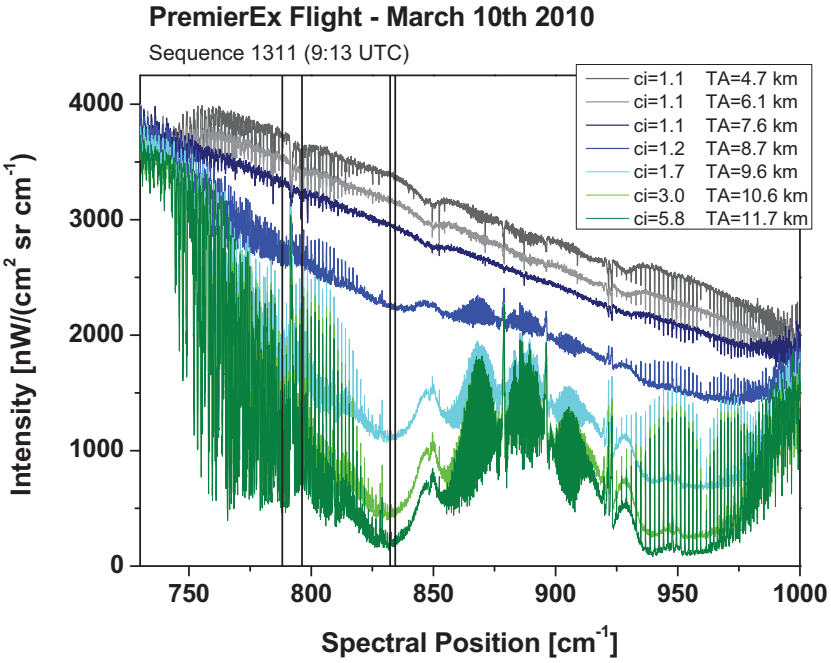

Fig. 129: MIPAS-STR spectra with low cloud indices. The spectra with cloud indices lower than 4 are clearly cloud affected. The black vertical lines indicate the microwindows used for the calculation of the cloud-index

Phillips regularisation method with constraint to the reference profile shape:

$$x_{i+1} = x_i + (K_i^T S_y^{-1} K_i + \gamma L^T L)^{-1}[K_i^T S_y^{-1}(y - f(x_i)) + \gamma L^T L(x_a - x_i)] \quad (2)$$

Here, i stands for the iteration index, x represents the vector of the unknowns, x_a the a priori vector, y corresponds to the measurement vector and f to the forward model. K represents the spectral derivatives matrix (Jacobian matrix), γ denotes the regularisation parameter, and L stands for the regularization operator and is defined as follows:

$$L = \begin{pmatrix} 1 & -1 & 0 & \cdot & \cdot & \cdot & 0 & 0 \\ 0 & 1 & -1 & \cdot & \cdot & \cdot & 0 & 0 \\ \cdot & \cdot & \cdot & \cdot & & & \cdot & \cdot \\ \cdot & \cdot & \cdot & & \cdot & & \cdot & \cdot \\ \cdot & \cdot & \cdot & & & \cdot & \cdot & \cdot \\ 0 & 0 & 0 & \cdot & \cdot & \cdot & 1 & -1 \end{pmatrix}$$

S_y represents the variance-covariance matrix of the measurements. It has to be noted, that for the retrieved profiles, the influence of the side condition (constraint to the shape of the reference profile) does not disappear completely depending on the regularization strength. Reference profiles (a priori and initial guess) are taken from the ESA Polar Winter Climatology. Regularisation is needed, since the retrieval grid is smaller than the measurement grid and the vertical field of view diameter, at least for the lower tangent altitudes. The regularisation strength is chosen as small as possible, while avoiding oscillations in the resulting vertical profiles and minimizing the influence of the reference profile on the solutions. For the retrievals, pressure and Temperature profiles are interpolated from the ECMWF T106 gridpoint analysis in space and time for the observation geometries of MIPAS-STR. Since no significant improvements are achieved using retrieved Temperatures rather than ECMWF Temperatures, for the trace gas retrievals also the ECMWF Temperature profiles are used. This approach is also consistent to the LOS retrieval, where also ECMWF Temperatures are taken into account. Spectral microwindows for the retrievals are selected with respect to a maximal sensitivity to the trace-gas of interest, and minimal spectral interference with other trace-gas signatures. In Figure 130 and in Figure 131, forward calculations are shown for the applied microwindows for HNO_3 and O_3 for a tangent altitude of 17 km. While in the case of HNO_3, practically no significant spectral interference with other trace gas signatures is apparent, in the case of O_3, signatures of mainly HNO_3 and $ClONO_2$ lead to continuum-like contributions. For O_3, the signatures of these interfering gases are fitted along with O_3 (the weak interfering CO_2 signatures and further weakly interfering signatures are modelled using the ESA Polar Winter Climatology). Since signatures of unknown trace gases are likely to be present in

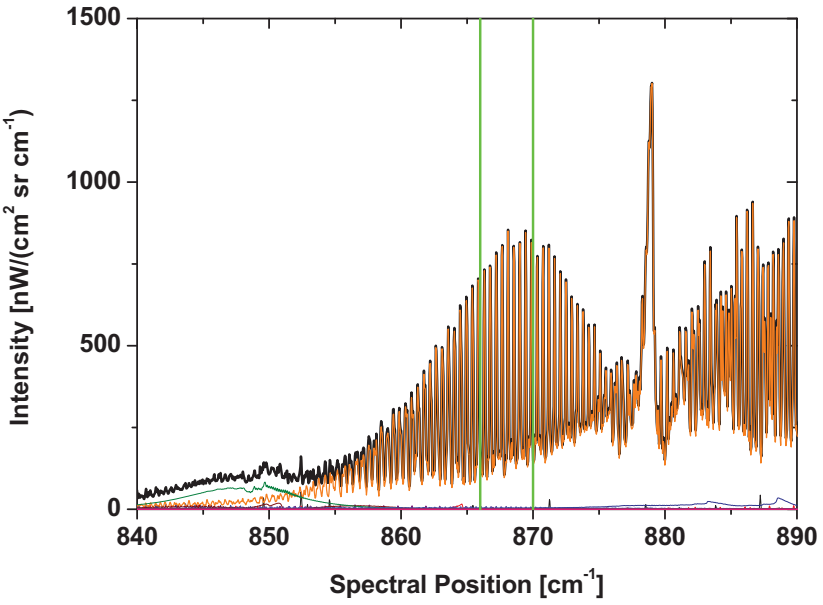

Fig. 130: Forward calculation for the microwindow used for the HNO_3 retrievals for a tangent altitude of 17 km. The black line represents the spectrum under consideration of all known interfering gases, while the spectrum of only HNO_3 is represented by the orange line. The signatures of individual interfering gases are shown in different colours (e.g. the dark green signature on the left side corresponds to CFC-11). The microwindow used for the retrievals is marked by the green bars)

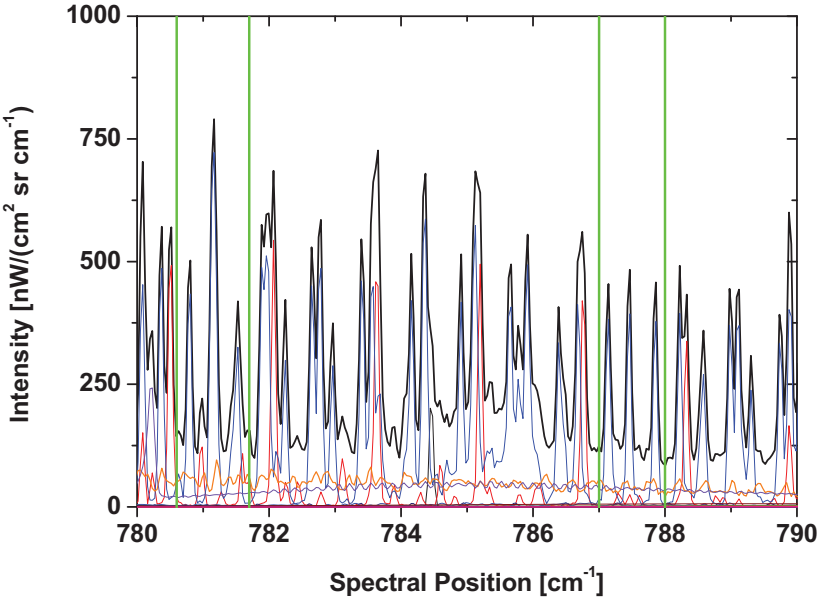

Fig. 131: The same as Figure 130, but for the two microwindows used for the O_3 retrieval. The black line shows the spectrum of all considered species. The blue line represents the spectrum of O_3 only. As significantly interfering gases, HNO_3 (orange), $ClONO_2$ (pink) and CO_2 (red) are identified)

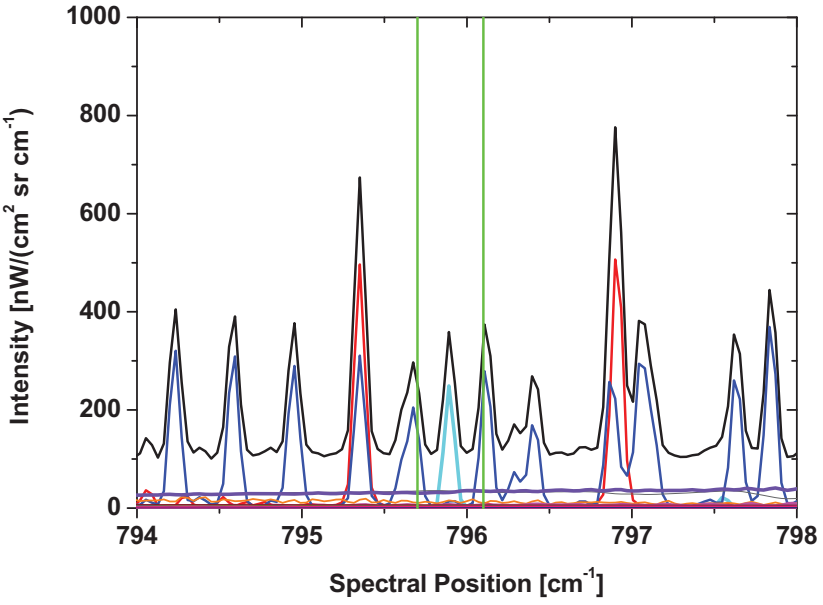

Fig. 132: The same as Figure 130, but for H_2O (cyan). Most prominent interfering species are the CCl_4 (black), $ClONO_2$ (pink) and O_3 (blue) and are considered by using climatological profiles. The signatures of CCl_4 and $ClONO_2$ appear continuum-like in the chosen microwindow and uncertainties in the climatological profile are (at least partially) compensated by the continuum-retrieval.

the spectra, and the vertical profiles of known weakly interfering trace gases are not known precisely, background continuum is retrieved along with the target species. So in summary, in the case of the HNO_3 retrieval, the volume mixing ratio of the target species is fitted along with background continuum and spectral shift, while for O_3, the interfering species HNO_3 and $ClONO_2$ are retrieved simultaneously with strong regularization. Spectral offset is not retrieved since the spectra show a suitable reliability of the base-line calibration. H_2O is retrieved using the microwindow shown in Figure 132 and is inverted logarithmically.

Different retrievals meeting the requirements for the inputs of the (L1+L2) method and the MSS method for data fusion have been carried out. In the case of the (L1+L2) input, a retrieval grid from 0-100 km was used with 1 km steps in the range between 3-20 km and increasing spacing at lower and higher altitudes. For the MSS inputs, retrievals were carried out on grids up to 30 km with 1 km-steps. Since for both inputs, retrievals on different grids were carried out, the retrievals had to be optimized separately and minor but insignificant differences between the results were found.

11.3 Retrieval Error Assessment

The quality of the retrieved profiles is determined by (i) the combined total error and (ii) the achieved vertical resolution. For the estimation of the combined total error, errors resulting from the spectral noise (noise), line-of-sight uncertainties (LOS), Temperature uncertainties resulting from ECMWF (T), spectral line data uncertainties (spec) and radiometric calibration errors (cal) are considered. All errors are treated as 1-uncertainties. For the line-of-sight error estimation, retrievals with the line-of-sight elevation angle shifted by ± 0.78 arcmin are carried out, and the corresponding changes in the trace-gas profiles are considered. The same strategy is applied for Temperature error, where retrievals with the Temperature profile shifted by ± 1 K are carried out. The corresponding deviations are calculated according to the following equation:

$$\Delta x_j = \begin{pmatrix} \Delta x_{1,j} \\ \Delta x_{2,j} \\ \vdots \\ \Delta x_{n_{max},j} \end{pmatrix} = (K^T S_y^{-1} K + \gamma L^T L)^{-1} K^T S_y^{-1} (y_{error,j} - y_{results}) \quad (3)$$

Here, Δx_j represents the deviation of the retrieval result with the shifted parameter j (LOS or T) from the initial retrieval result, n denotes the retrieval-grid-point, $y_{error,j}$ represents the calculated spectrum of the last iteration

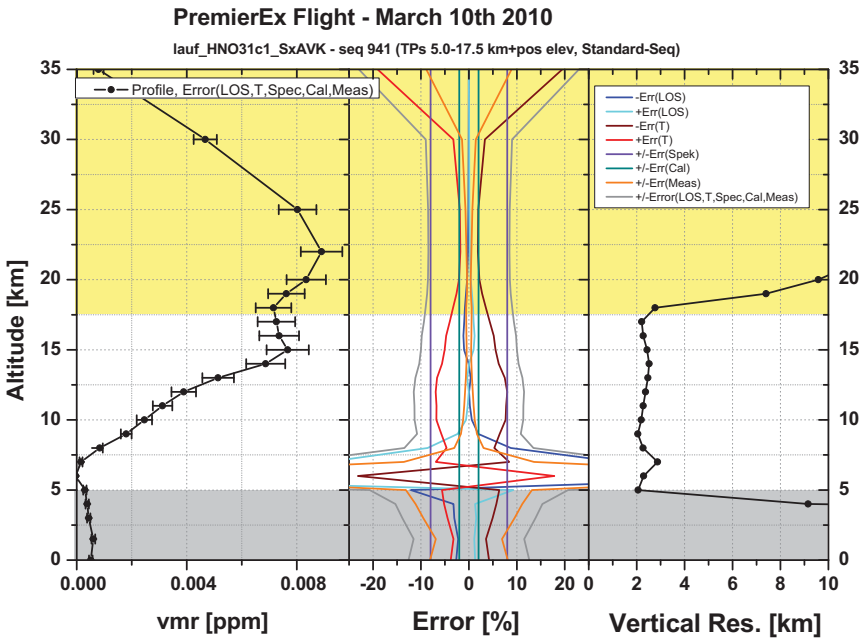

Fig. 133: Retrieved HNO_3 profile with combined total error. Middle: Contributions of noise-error (orange), LOS-error (blue and cyan), T-error (red and brown), spectroscopic line data error (pink) and errors of radiometric calibration (green) together with the total combined error (grey). Right side: Altitude resolution derived from the trace of the averaging kernel matrix. The combined error is of meaningful in the white area (limb sequence), where the altitude resolution is maximal, and slightly above thanks to the spectra recorded with upward looking angles

with the shifted parameter and $y_{results}$ the calculated spectrum of the initial retrieval result.

For spectral line data errors (mainly line intensity), a general uncertainty of 8% for HNO_3 and 7% for O_3 is taken into account, assuming a linear propagation of this error into the retrieved parameter vector. The same error characteristic is assumed for the radiometric calibration, where a general uncertainty of 2% is considered. The discussed errors are combined to calculate the estimated total error (1σ) by the root of the square sum:

$$\Delta x_{comb} = \sqrt{\Delta x^2_{noise} + \Delta x^2_{LOS} + \Delta x^2_{T} + \Delta x^2_{spec} + \Delta x^2_{cal}} \tag{4}$$

(For the input of the (L1+L2) data fusion, the noise error is initially excluded from the combination, since the combination with the other errors is carried out in a later step). It has to be noted that all errors are treated as statistic errors here, although during different flight parts, the different errors can have systematic character.

The vertical resolution of the retrieval results at certain grid points is calculated from the trace of the averaging kernel matrix using the following definition:

$$\Delta a_n = \left(\frac{A_{nn}}{\Delta h_n} \right)^{-1} \tag{5}$$

Here, Δa_n represents the local altitude resolution at the grid-point n, A the averaging kernel matrix and Δh_n the mean local (retrieval) grid-point spacing. In Figure 133 and Figure 134, the combined error and the achieved altitude resolution associated to the (L1+L2) input is shown for a typical HNO_3 and O_3 profile. In the left panels, the retrieved vertical profiles are shown together with the combined total error. The panels in the middle show the error contributions resulting from the different error sources. In the panels on the right side, the vertical resolution is indicated. The vertical resolution is mainly around 2 - 2.5 km for the HNO_3 retrieval and 2 km for the O_3 retrieval in the limb sequence altitude-range (white area) and rapidly decreases below 5 km (no data) and above 17.5 km. Due to the fact, that also upward scanning is performed, the altitude resolution decreases more slowly above the highest tangent point (17.5 km). The combined total error shown in the panel on the left side and in the middle has to be interpreted in the context of the altitude resolution. Thus, the total combined error is only of significance in the altitude range, where the tangent points are located and slightly above. At altitudes below and above, this error is practically meaningless due to the low altitude resolution. From the panels in the middle it can be seen clearly, that the combined total error is dominated by the spectroscopic line data error and the Temperature error above 9 km. At lower altitudes, the line-of-sight error and the noise error become more important. The error

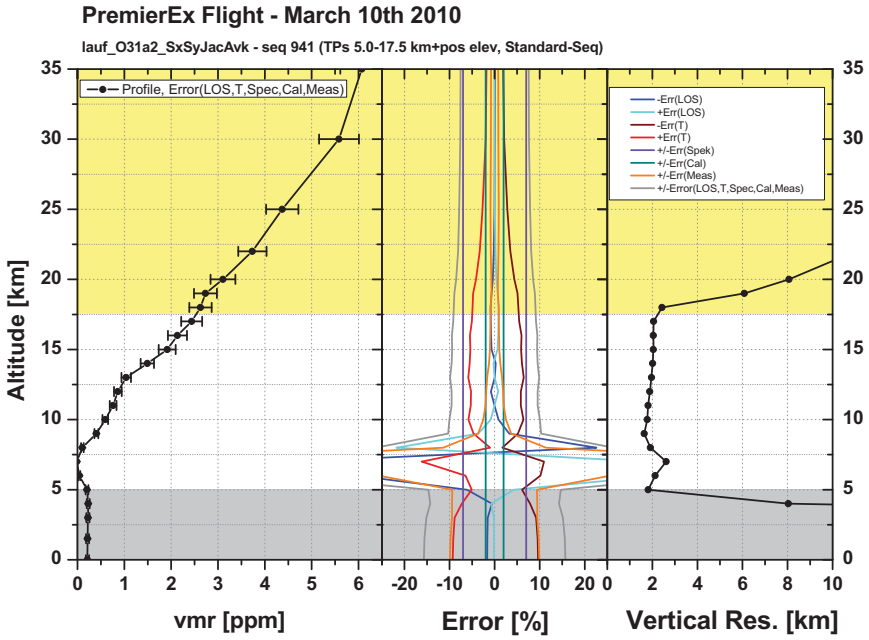

Fig. 134: The same plot as Figure 133, but for O_3

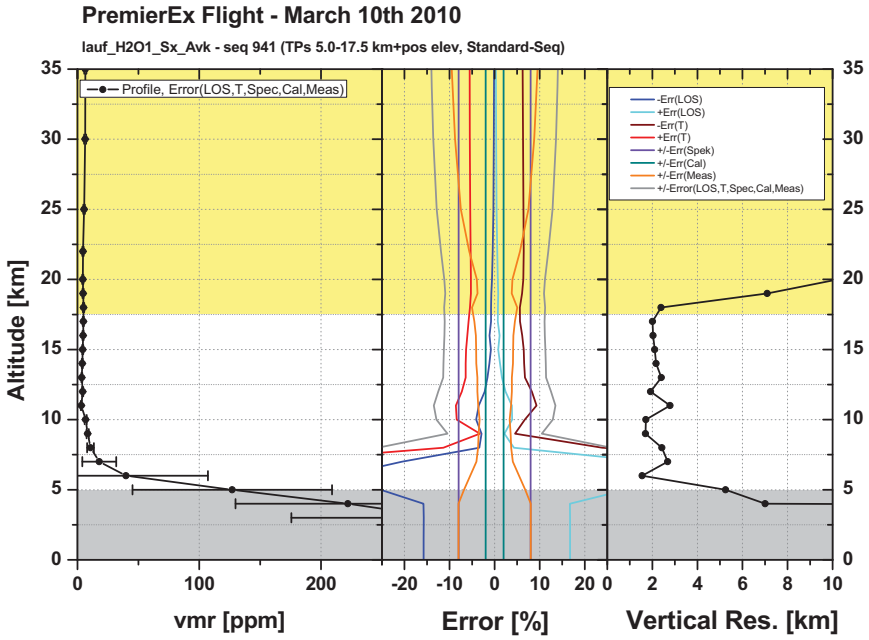

Fig. 135: The same plot as Figure 133, but for H_2O

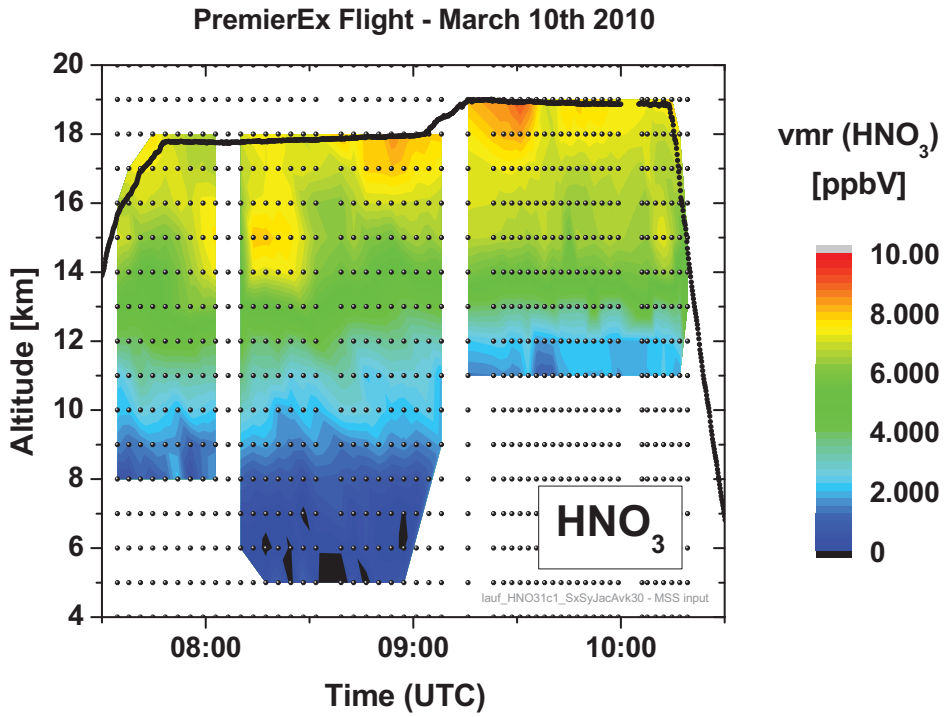

Fig. 136: Vertical cross-section of HNO_3 for the PremierEx Scientific Flight (leg 1: 7:30-8:05, leg 2: 8:05-9:10, leg 3: 9:10-10:20). The black dots indicate the retrieval grid. Linearly interpolated volume mixing ratios of HNO_3 are shown colour-coded for the grid-points with an altitude resolution of better than 5 km for VMR (HNO_3) (mainly around 2 -2.5 km between flight altitude and lowest tangent point)

due to the radiometric calibration is relatively small compared to the other error sources. The corresponding error budget for H_2O is shown in Figure 135, where an altitude resolution of mainly 2-3 km is obtained.

11.4 Discussion of the Retrieval Results

The vertical cross section for HNO_3 obtained for the PremierEx Scientific Flight is shown in Figure 136. Due to the presence of dense tropospheric clouds in the first flight leg, retrievals are carried out down to mainly 8 km (cloud index threshold of 2). For the same reason, in the last flight leg retrievals are performed down to 11 km. In contrast, during the second flight leg, virtually cloud-free conditions are found and many sequences are retrieved down to the lowest tangent point at 5 km. In the altitude range between 13 and 16 km, between 8:00 and 8:30 UTC, a structure of enhanced HNO_3 is found. Enhanced HNO_3 concentrations of approximately 1.5 ppbv indicate a renitrification remnant of the polar vortex with a vertical extend of about 2 km. A more extended structure with two HNO_3 maxima is found between 8:45 and 9:35 at altitudes above 15 km, aligned in the area around the turning point between the flight legs 2 and 3. The vertical cross section obtained from the O_3 retrieval is shown in Figure 137. At the end of the second flight leg and during the third flight leg, structures of enhanced O_3 are found at the flight altitude and slightly below. In Figure 138, the corresponding CLAMS-forecast for the vertical cross-section of N_2O is shown. In the area around the turning point C between leg 1 and leg 2, low N_2O concentrations below the flight altitude indicate a filament of the polar vortex, showing a consistent picture together with the renitrification structure found in the retrieved vertical cross-section of HNO_3 (Figure 136). In the middle of the second flight leg (C-E), a structure of increased N_2O concentrations is found in the CLAMS-forecast slightly below the flight altitude, which is correlated to low HNO_3 concentrations found around 8:40, hinting a filament of mid-latitude air. Aligned in a mirrored way, in the second half of flight leg 2 and the first half of flight leg 3, again structures with low N_2O concentrations are found in the forecast, which are correlated to the two maxima found in the retrieved cross-section of HNO_3, indicating descended vortex air. The HNO_3 maxima corresponding to the low N_2O concentrations enclose a narrow structure of high N_2O concentrations around the turning point indicating a filament of mid-latitude air. The maximum of O_3 between 8:45 and 9:35 is consistent with the high HNO_3 and the low N_2O concentrations (corresponding to descended air), while the bimodal structure as in the case of HNO_3 and N_2O is not found. The retrieved vertical cross-section of H_2O is shown in Figure 139. While at stratospheric

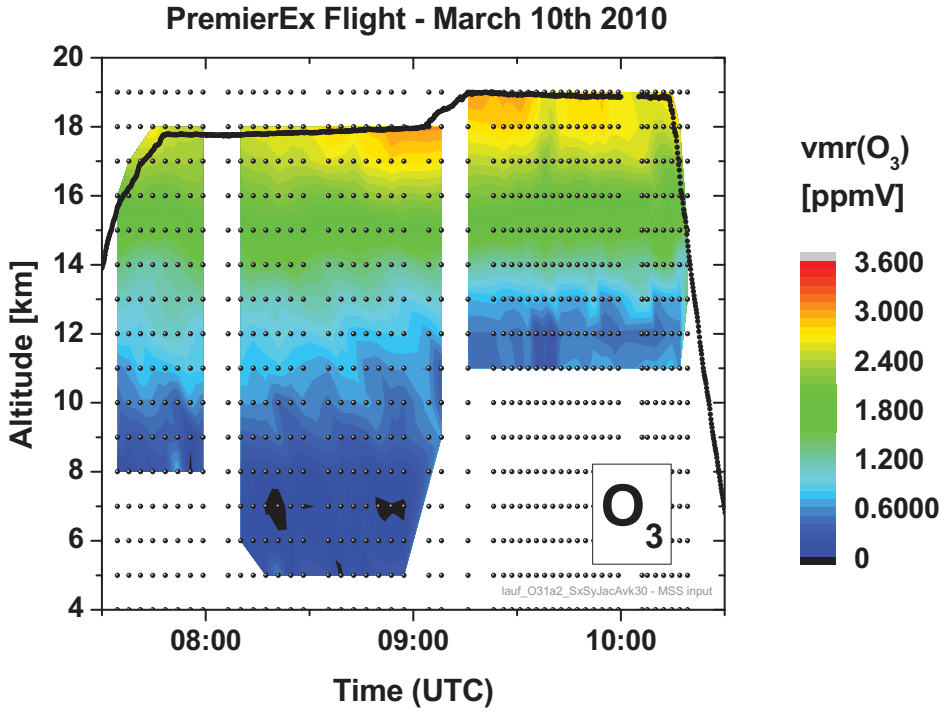

Fig. 137: The same plot as in Figure 136 but for O_3

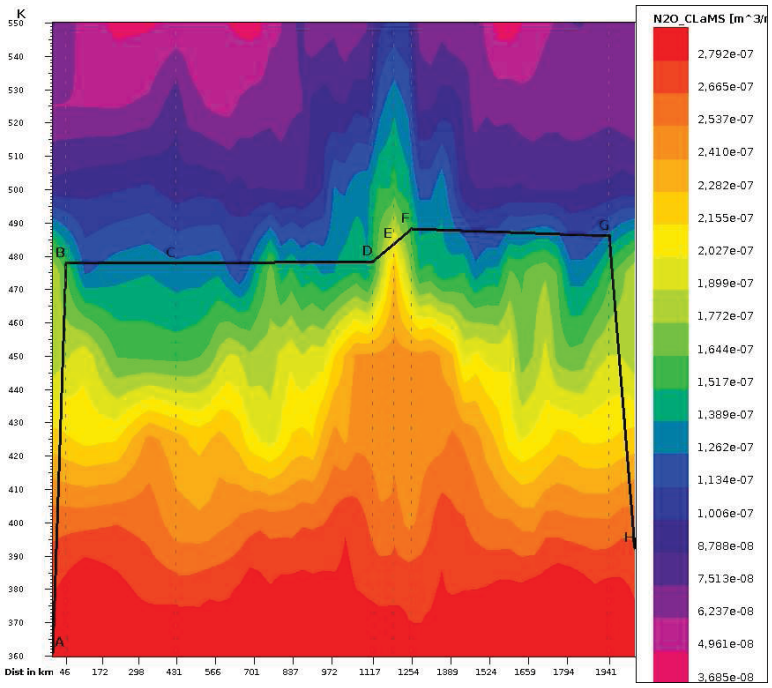

Fig. 138: CLAMS-forecast for the vertical cross-section of N_2O along the flight path. Blue and pink colours correspond to low N_2Oconentrations)

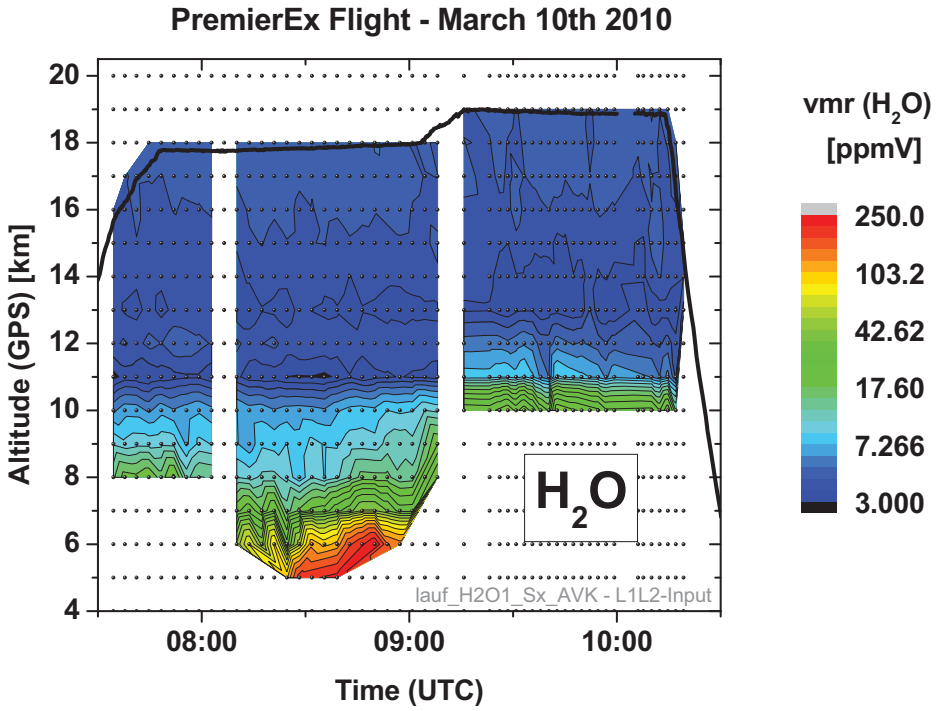

Fig. 139: The same plot as in Figure 136 but for H_2O

altitudes H_2O-concentrations of mainly 3-4 ppmv are found, the concentrations strongly increase at tropospheric altitudes. In conclusion, the applied retrieval strategy considering spectra with cloud indices higher than 2 allows for the detection of small-scale structures with a vertical extend of about 2km for the applied retrieval setup. Additional systematic errors are possible in the altitude range of the cloud-affected spectra, since the suitability of the spectra for retrievals is different from case to case. Higher vertical resolutions are possible in principle if the cloud-index threshold is set more conservatively and the retrieval grid spacing is reduced. Filaments of vortex-air and mid-latitude air can clearly be separated and the results are consistent with the CLAMS-forecast.

12 Synergy of millimetre-wave and infrared data

12.1 Overview

The exploitation of potential synergies between millimetre-wave and infrared limb sounding is one of the key issues to be considered in the frame of the PREMIER mission and it is essential to fully meet the measurement requirements of PREMIER geophysical products, as pointed out in ESA Report for Assessment 5 (ESA SP-1313/5, 2008).

The primary goal of the study of mm-wave and IR data synergy has been, therefore, to verify the advantages of combining independent and complementary measurements in these spectral regions and to achieve a quantitative assessment of the improvement in the quality of synergistic retrieval products with respect to the retrieval products obtained from the individual datasets.

The strategy adopted to carry out the task mainly relied on the availability of collocated measurements acquired by MARSCHALS and MIPAS-STR limb-sounders, in the mm-wave and infrared regions respectively, during the PremierEx scientific flight on 10.03.2010 and on the application of alternative methods, such as the so called *(L1+L2) method* and the *MSS method*, to data fusion.

A set of best matching limb sequences acquired by MARSCHALS and MIPAS-STR instruments along the flight track was selected, by choosing for each MARSCHALS sequence the MIPAS-STR sequence closest in time. In Table 7, we report the resulting pairs of collocated measurements along with the information about their temporal mismatch. The geolocation of MARSCHALS and MIPAS-STR limb sounding acquisitions is displayed in Figure 140 and in Figure 141, respectively.

The tests on data fusion were conducted on measurements of vertical VMR profiles of H_2O, O_3, and HNO_3.

Tab. 7: MARSCHALS/MIPAS Coincidences - Best matching sequences of MARSCHALS and MIPAS-STR measurements selected for the synergistic data analysis. MARSCHALS sequence number highlighted in green correspond to data acquired in optimal flight conditions and to best matching sequences actually used for data fusion.

MARS. Seq. Num.	MIPAS Seq. Num.	Time (s) mismatch	MARS. Seq. Num.	MIPAS Seq. Num.	Time (s) mismatch
00	0670	-612	01	0670	-410
02	0670	-242	03	0670	-5
04	0691	2	05	0712	-73
06	0734	-39	07	0757	-55
08	0780	-71	09	0803	-140
10	0826	-121	11	0826	62
12	0849	-19	13	0872	-81
14	0895	-81	15	0918	-40
16	0941	-107	17	0964	-105
18	0987	-169	19	0987	1
20	1010	34	21	1033	-24
22	1056	-5	23	1079	-120
24	1102	-68	25	1125	-169
26	1125	34	27	1148	75
28	1171	-48	29	1194	8
30	1217	-64	31	1240	-79
32	1240	75	33	1263	/
34	1311	/	35	1311	-64
36	1311	136	37	1359	-88
38	1381	-64	39	1396	-2
40	1411	-1	41	1426	95
42	1456	5	43	1471	37
44	1501	-54	45	1516	5
46	1546	-102	47	1561	-45
48	1576	4	49	1591	48
50	0020	-141	51	0024	-76
52	0039	-1	53	0069	-129
54	0084	-108	55	0084	88

The results for H_2O from the MIPAS-STR data represent a first test result, since logarithmical inversion is applied in contrast to the other retrievals. H_2O is not a standard gas in MIPAS-STR channel 1, showing only weak signatures in the corresponding spectral range. In contrast, for O_3 and HNO_3 prominent spectral signatures are available and the retrievals are more robust. The inverse processing of MARSCHALS L1 data was conducted by using the MARC retrieval code and the same configuration settings of the analysis presented in Section 6. The only modification introduced for the purpose of data fusion consisted in using a different vertical retrieval grid, both in the case of the (L1+L2) method, as well as in the case of the MSS method. The a priori information for the (L1+L2) method was obtained from MIPAS-STR L2 products, as provided by the IMK-KIT team. The key features of the inversion process applied to MIPAS-STR measurements and relying on Tikhonov regularization are described in more details in Section 11.

It has to be noted, that different approaches have been used for the inversion of the MARSCHALS and MIPAS-STR measurements. While in the case of MARSCHALS, optimal estimation is applied, making use of a climatological constraint (as given by the a-priori information and the corresponding VCM in addition by the choice of a retrieval-grid allowing for stable solutions), in the case of MIPAS-STR, Tikhonov-Phillips 1^{st} order regularization is used. In the case of MIPAS-STR only the shape of the resulting profile is constrained to the shape a-priori information (depending on the adjusted regularization strength together with a fixed altitude grid) and not to the values of the a-priori profile. For MIPAS-STR-related retrievals, no VCM associated to the a-priori information is considered. With regard to the regularization strength, it has to be mentioned, that the results of MIPAS-STR have been regularized conservatively, since partly cloud-affected spectra (cloud-index threshold of 2 instead of 4) have been included in the retrievals.

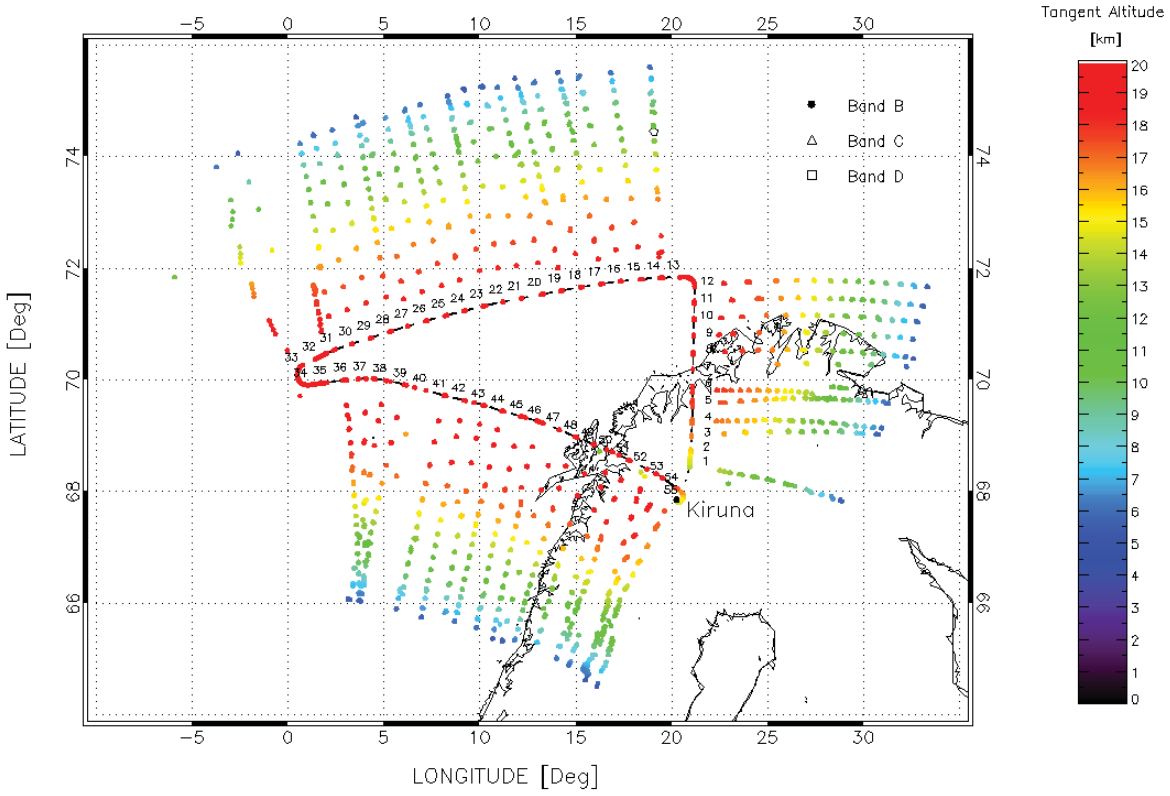

Fig. 140: Geolocation of MARSCHALS limb sounding measurements during the PremierEx flight on 10.03.2010

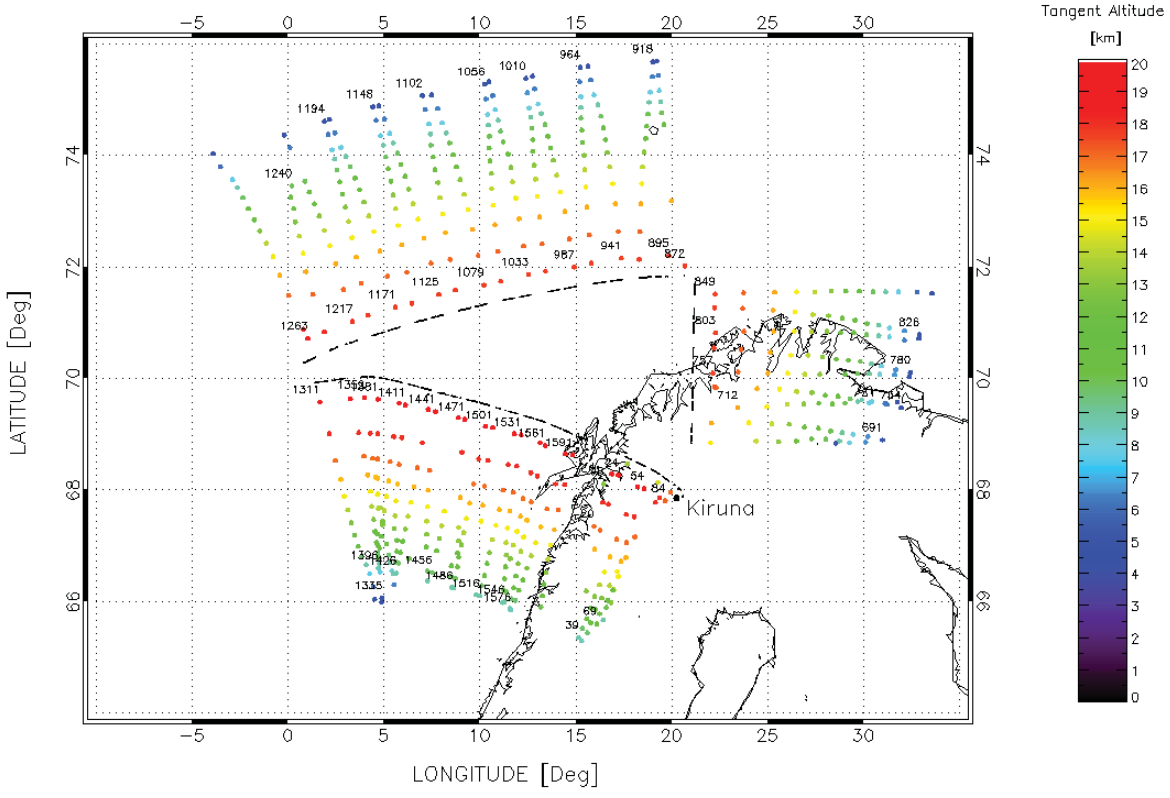

Fig. 141: Geolocation of MIPAS-STR limb sounding measurements during the PremierEx flight on 10.03.2010

12.2 MIPAS-STR and MARSCHALS data fusion using the (L1+L2) method

The (L1+L2) method for synergistic analysis of mm-wave and IR measurements consisted in the inverse processing of MARSCHALS L1 data using Optimal Estimation with MIPAS-STR L2 products adopted as a priori information. This method is used as our baseline scheme for testing the performances of MARSCHALS and MIPAS-STR data fusion.

12.2.1 Quantifiers of the performances

In this sub-section, we summarize the approach applied for comparative evaluation of the performances of MARSCHALS and MIPAS-STR retrievals and of (L1+L2) data fusion. In order to evaluate the performances of individual and synergistic retrieval from MARSCHALS and MIPAS-STR measurements, we have used the following quantifiers of the quality of the retrieval products:

- *Total Retrieval Error*
  The estimate of MARSCHALS total uncertainty on the retrieval products is described in details in [18] and includes the following systematic effects: the FM bias errors, the FM parameter errors and the instrument parameter errors.
  In order to characterize the uncertainty associated to the a priori information the full VCM of MIPAS-STR L2 products was considered, including both random and systematic components. The following sources of systematic errors have been evaluated: line-of-sight uncertainties, Temperature uncertainties resulting from ECMWF, spectral line data uncertainties and radiometric calibration errors. We assumed that no correlation exists between these error sources. Therefore, the VCM of the total error has been calculated by combining the non-diagonal VCM of the random errors (S_x) with a diagonal VCM of the systematic uncertainty. In particular, the VCM of the total error (S_{tot}) has been calculated from:

$$S_{tot}(i,j) = S_x(i,j) + \sum_k \varepsilon_k(i) \cdot \varepsilon_k(j) \cdot \delta(i,j) \tag{6}$$

  where ε_k is the systematic error vector due to the kth source of systematic error.

  As a further remark, it is important to point out that the VCM S_x takes into account both the random error and Tikhonov regularization, whose effects on the total uncertainty cannot be decoupled into two separate contributions. As a consequence, the error-contributions for the MIPAS-STR results, which are estimated from retrievals with perturbed parameters (line-of-sight and temperature), as well as the noise error, are also affected by regularization and subject to smoothing. But we emphasize, that in the case of the MIPAS-STR results, the absolute positions of profiles are completely determined from the information in the measurements, which is a characteristic of the 1^{st} order regularization, while the regularization affects only the shape of the profiles. This reflects of course on the comparative evaluation of the performances of individual and combined retrievals, but still allows us to estimate the improvement of data fusion with respect to MIPAS-STR and MARSCHALS retrieval products separately. In order to avoid the loss of information due to interpolation, we used for MARSCHALS data processing the same vertical retrieval grid adopted for MIPAS-STR analysis. The total retrieval error used as quantifier of the performances in the case of the (L1+L2) analysis is the averaged value of the total retrieval error of the selected sequences.

- *Gain of Information*
  Rodgers demonstrated that, when measuring the vertical profile of an atmospheric variable, the Gain of Information (GI) obtained from the observation with respect to the climatological profile assumed as a priori is given by:

$$GI = \frac{1}{2} log_2 \left(\frac{|S_a|}{|S|} \right) \tag{7}$$

  where S and S_a are the VCMs of the retrieved profile and of the climatological profile respectively [20].
  For the purpose of our comparison of individual and combined retrievals, we had to use a definition of GI based on a common reference, i.e. the climatological profile adopted as a priori in MARSCHALS retrieval and the associated VCM S_a.
  We calculate, therefore, the gain of information GI^{MIP}, GI^{MAR}, and GI^{Fusion}, in case of MIPAS-STR, MARSCHALS and data fusion respectively, from:

$$GI^{MIP} = \frac{1}{2} log_2 \left(\frac{|S_a|}{|S_{MIP}|} \right) \tag{8}$$

$$GI^{MAR} = \frac{1}{2} log_2 \left(\frac{|S_a|}{|S_{MAR}|} \right) \tag{9}$$

$$GI^{Fusion} = \frac{1}{2} log_2 \left(\frac{|S_a|}{|S_{Fusion}|} \right) \tag{10}$$

We must take into account that the quantity GI^{MIP} represents the gain of information of MIPAS-STR measurements constrained by Tikhonov regularization with respect to the a priori of MARSCHALS.
Once again, we highlight the fact that this procedure does not evaluate the contribution of MIPAS-STR measurements and of the regularization to the information gain separately. As already noticed, however, this is acceptable, because our primary goal is to check whether the GI^{Fusion} shows an improvement compared to GI^{MIP} and GI^{MAR}

- *Degrees Of Freedom*
  We calculate the number of Degrees Of Freedom (DOF) for the individual and combined retrieval, defined as the trace of the corresponding Averaging Kernel matrices:

$$DOF^{MIP} = Trace\left(AK^{MIP}\right) \tag{11}$$

$$DOF^{MAR} = Trace\left(AK^{MAR}\right) \tag{12}$$

$$DOF^{Fusion} = Trace\left(AK^{Fusion}\right) \tag{13}$$

  where AK^{MIP}, AK^{MAR}, and AK^{Fusion} are the corresponding AK matrices. The number of DOFs can be used to evaluate the effect of Tikhonov regularization on MIPAS-STR retrieval.

  It has to be noted, that in the case of MARSCHALS, as a consequence of the use of optimal estimation, the lower limit for the DOFs is 0, while in the case of Tikhonov-Phillips method applied for MIPAS-STR, always at least one DOF is left (independent from the regularization strength), since the absolute position of a profile is completely determined from the measured data.

12.2.2 Results

We report in this sub-section the results of (L1+L2) data fusion compared with the retrieval products from individual measurements. Data fusion was performed on H_2O, O_3, and HNO_3 profiles retrieved from the best matching sequences of MARSCHALS and MIPAS-STR, as listed in Table 7 and with all problematic measurements identified in MARSCHALS data analysis (see sub-section 6) filtered out. In the case of MIPAS-STR, all scans (also scans with incomplete vertical sampling) are included except of two scans at the turning points, which are affected by aircraft manoeuvres. As mentioned above, the results for H_2O represent a first test, since this gas is not a standard-gas in MIPAS-STR channel 1 and logarithmic inversion is applied.

The number of DOFs obtained for individual and synergistic retrieval of H_2O, O_3, and HNO_3 is plotted versus MARSCHALS sequences index in Figure 142, Figure 143, and in Figure 144 respectively. Results for the three spectral bands of MARSCHALS are reported in different panels. The number of DOFs of the (L1+L2) data fusion is inferior to that of the individual instrument data, as it represents the number of independent parameters that can be retrieved from MARSCHALS measurements in addition to the a priori knowledge given by MIPAS-STR level 2 products.

For the H_2O retrieval, the number of DOFs obtained from the (L1+L2) data fusion is about 2 in band B and D. In band C a larger number of DOFs (about 8) is obtained when MARSCHALS and MIPAS-STR data are combined. The number of DOFs calculated for the MIPAS-STR retrieval of O_3 profiles is significantly increased by the combination with MARSCHALS measurents in all spectral bands, with the average DOFs of data fusion equal to 7 in band B, 5 in band C and 4 in band D. In case of HNO_3 retrieval, data fusion with MARSCHALS band B does not increase the number of DOFs retrieved from MIPAS-STR measurement using Tikhonov regularization.

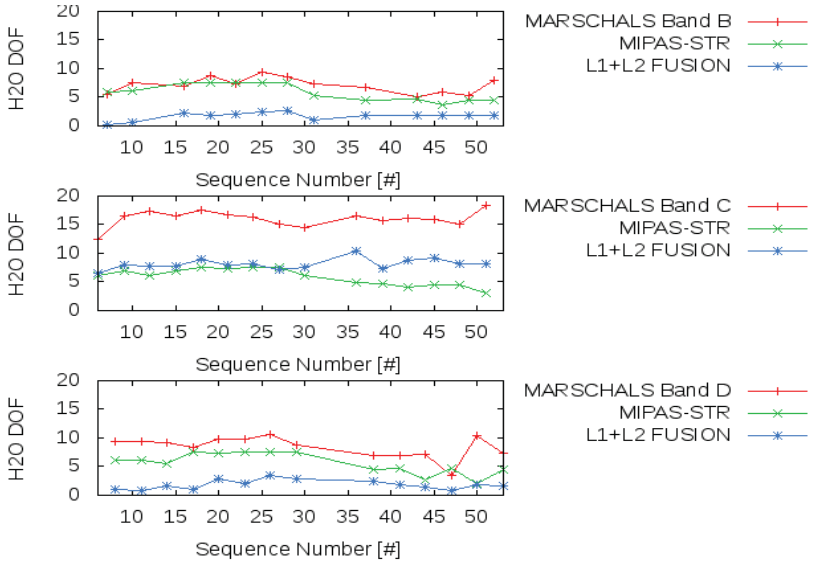

Fig. 142: Number of DOFs obtained from MARSCHALS and MIPAS-STR individual and synergistic retrieval of H_2O VMR profiles

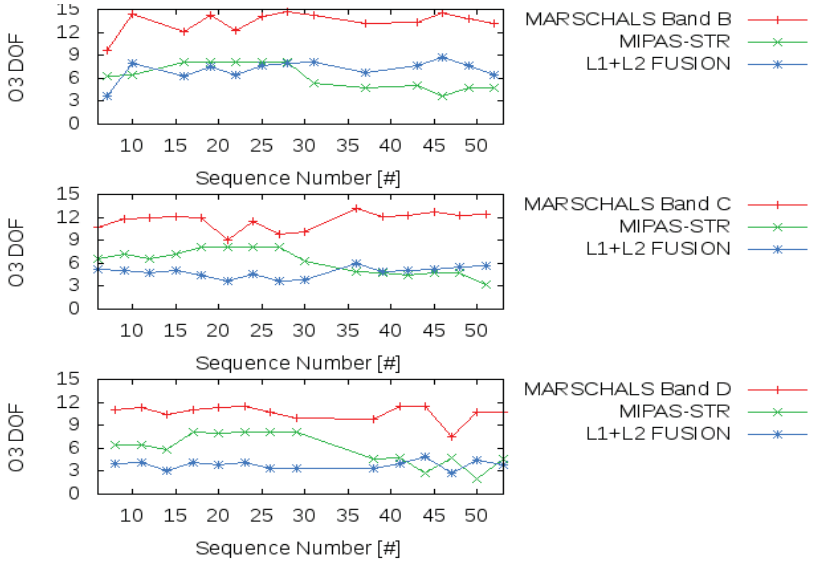

Fig. 143: As Figure 142 for O_3

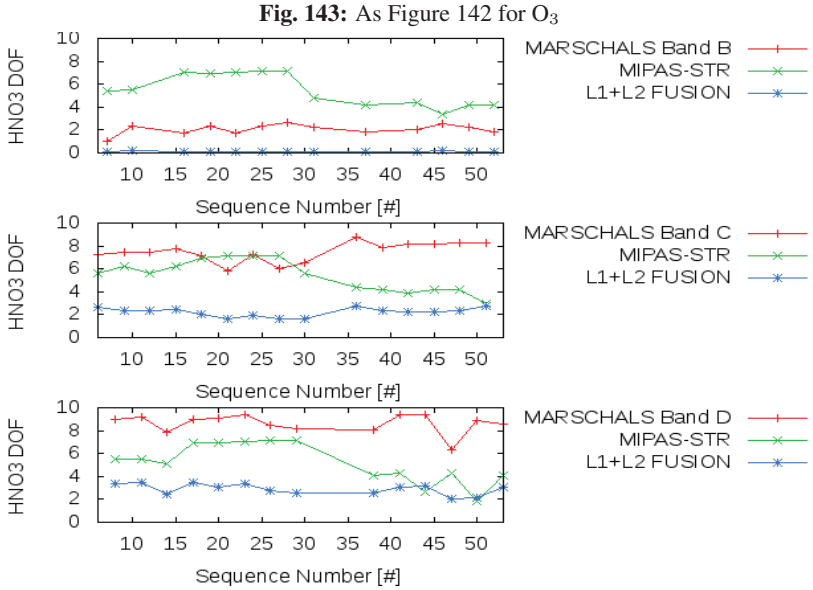

Fig. 144: As Figure 142 for HNO_3

Tab. 8: Average GI for the H_2O with respect to S_a of the climatological profile in the case of MIPAS-STR and of (L1+L2) data fusion. The table also reports the absolute and percentage improvement obtained with data fusion, defined in terms of the difference between the GI of data fusion and of MIPAS-STR (absolute value and percentage value with respect to MIPAS-STR GI)

H_2O	MIPAS-STR	L1+L2	(L1+L2) - MIPAS-STR	%
Band B	126.3	128.9	2.6	2
Band C	124.5	137.7	13.2	11
band D	123.8	126.9	3.1	3

Tab. 9: same as in Table 8 for the O_3

O_3	MIPAS-STR	L1+L2	(L1+L2) - MIPAS-STR	%
Band B	95.3	107.5	12.2	13
Band C	95.0	101.4	6.4	7
band D	91.7	96.1	4.4	5

The contribution to the number of DOF of data fusion from MARSCHALS Band C and band D, on the other hand, has an average value of 2 and 3, respectively.

The H_2O, O_3, and HNO_3 Gain of Information obtained from (L1+L2) data fusion with respect to the a priori knowledge of MARSCHALS VMR profiles is displayed in Figure 145, Figure 146, and in Figure 147 respectively, along with corresponding quantifiers calculated from MARSCHALS and MIPAS-STR individual measurements.

The average values of GI of MIPAS-STR and (L1+L2) data fusion are reported in Table 8, Table 9, and Table 10, along with the absolute and percentage improvement obtained from data fusion.

The H_2O, O_3, and HNO_3 total error profile obtained from (L1+L2) data fusion with respect to the total error profile obtained from MIPAS-STR measurements is displayed in Figure 148, Figure 149, and in Figure 150 respectively.

The (L1+L2) total error on H_2O is significantly reduced in band C between 10 and 20 km, while in band B and band D the effect of the data fusion is quite negligeble.
The total error on O_3 VMR values obtained from data fusion is significantly reduced, in the altitude range between 10 and 20 km, compared to total errors of O_3 profiles retrieved from MIPAS-STR measurements. In particular, a reduction between up to about 60% of the total uncertainty is observed, when combining MIPAS-STR data with MARSCHALS observations in band B, band C and band D.
The effect of (L1+L2) data fusion on HNO_3 total error is negligible in the case of MARSCHALS band B. A substantial improvement is only observed when MIPAS-STR data are combined with MARSCHALS measurements from band C and band D, with larger reduction of the total error obtained in the altitude range from 15 km to 20 km (percentage reduction with respect to MIPAS-STR total error up to 30 %).

12.3 Data fusion using MSS method

The Measurement Space Solution (MSS) is a new type of representation of the information on the vertical profile of an atmospheric parameter retrieved from remote-sensing observation [3]. In this new representation the profile is not given, as in classical retrievals, by a sequence of values as a function of altitude, but as the combination of

Tab. 10: same as in Table 8 for the HNO_3

HNO_3	MIPAS-STR	L1+L2	(L1+L2) - MIPAS-STR	%
Band B	24.5	24.6	0.1	0.4
Band C	25.1	27.2	2.1	8
band D	23.9	26.9	3	12

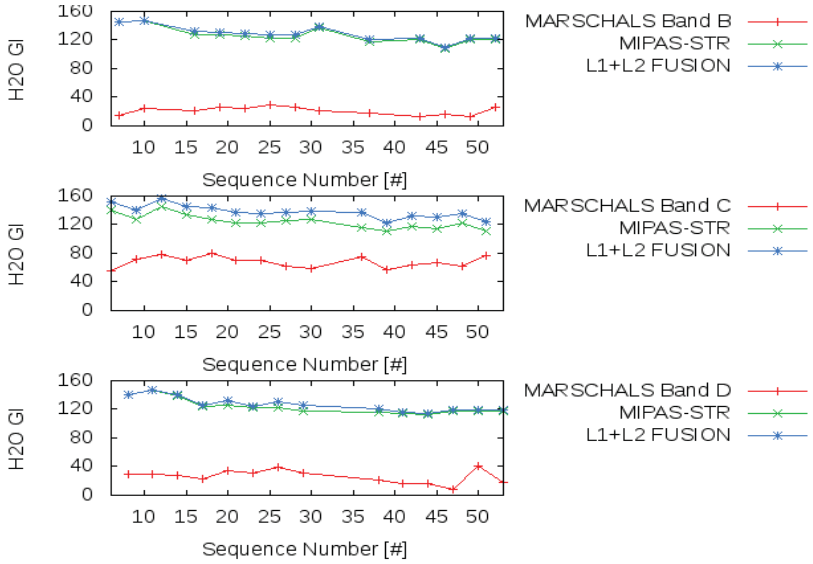

Fig. 145: GI from MARSCHALS and MIPAS-STR individual and synergistic retrieval of H_2O VMR profiles w.r.t. MARSCHALS a priori information

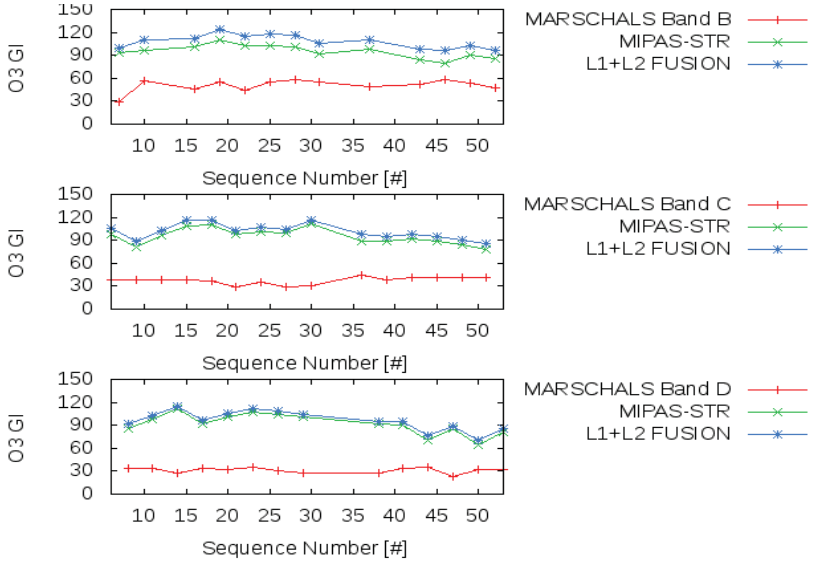

Fig. 146: As Figure 145 for O_3

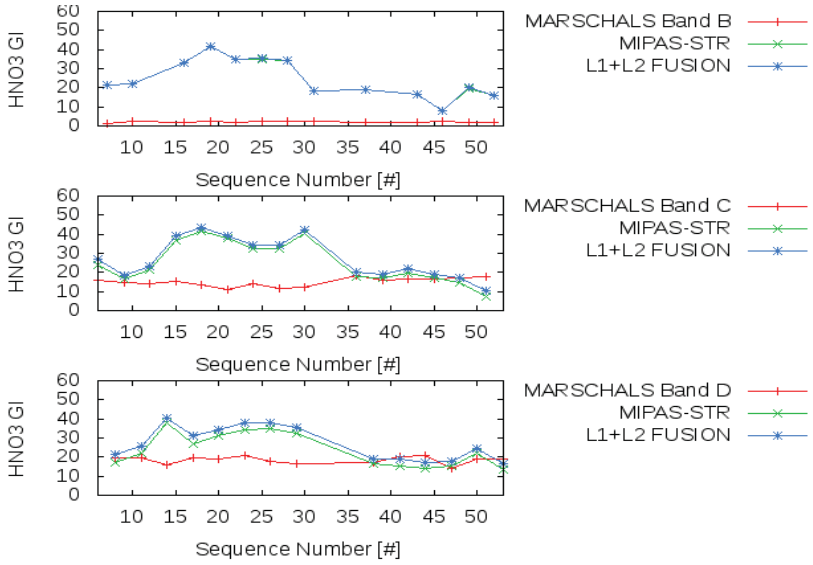

Fig. 147: As Figure 145 for HNO_3

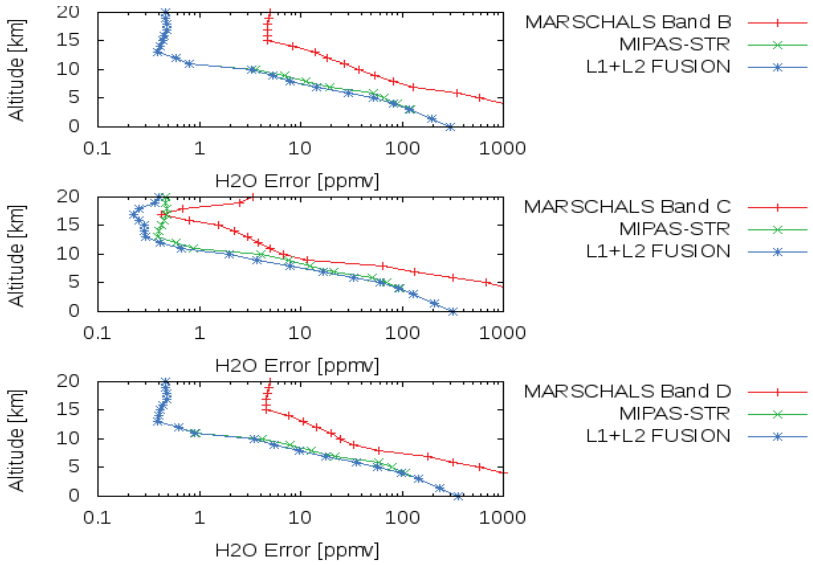

Fig. 148: Total errors from MARSCHALS and MIPAS-STR individual and synergistic retrieval of H_2O VMR profiles

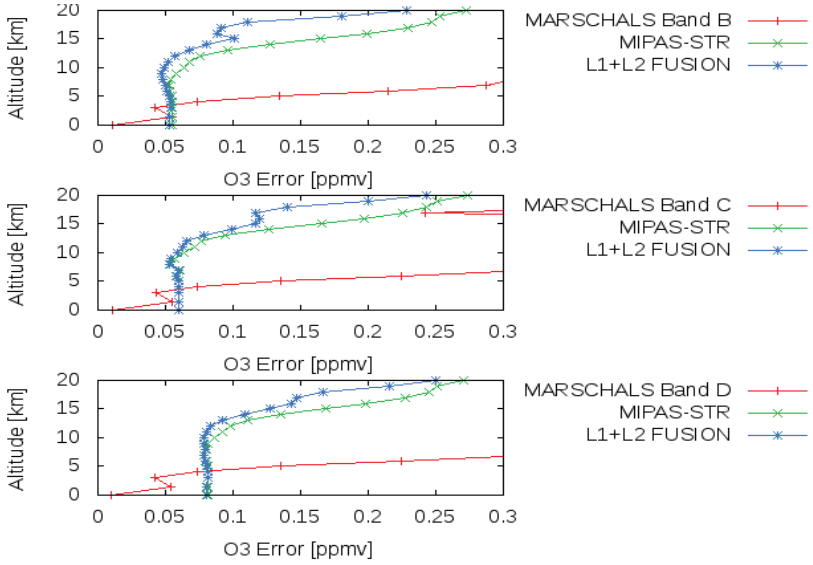

Fig. 149: As Figure 148 for O_3

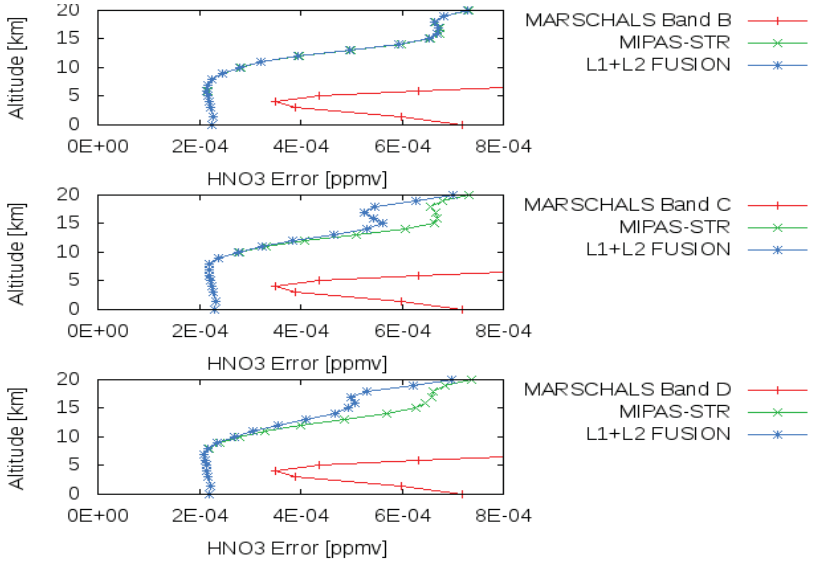

Fig. 150: As Figure 148 for HNO_3

a set of functions each weighted with a measured amplitude. The set of functions belongs to the functional space in which the measurement is performed (the so called "measurement space"). The profile obtained in this new way does not directly provide, as classical retrievals do, a useful graphical representation, but has other important advantages that make it a tool for the full extraction of the information contained in the observation about the profile to be retrieved. The MSS theory is briefly described on the IFAC web site at:

http://ga.ifac.cnr.it/products-and-facilities/mss-products.html

and full details and results of application can be found in references therein.
An alternative approach to the problem of data fusion, based on the use of the MSS, has been applied to test the performances of the combination of MIPAS-STR and MARSCHALS measurements. This alternative approach has been used for testing MIPAS-STR and MARSCHALS O_3 data fusion performances by means of the optimal exploitation of the information provided by independent and collocated, indirect measurements of atmospheric profiles.

12.3.1 Quantifiers of the performances

In order to evaluate the performances of individual and synergistic retrieval from MARSCHALS and MIPAS-STR measurements in the case of the MSS analysis, we have used the same quantifiers of the quality of the retrieval products adopted in Section 12.2.1. Here below we refer to the definitions given in Section 12.2.1 for the Total Retrieval Error, for the Gain of Information, and for the Degrees Of Freedom and we add some comments to specific differences between their meaning in the case of the (L1+L2) and MSS analyses.

- *Total Retrieval Error*
  The total retrieval error obtained by the MSS method is the total error (random + systematic) associated to the MSS combined with the error on the a priori information used to represent the retrieved profile. The same a priori information is added to the MSS of MARSCHALS measurements, to the MSS of MIPAS-STR measurements, and to fused MSS data, in order to obtain the corresponding O_3 VMR and error profiles. In the (L1+L2) method , the total retrieval error depends on the measurement error and on the error associated to the external constraint adopted by the inversion model. The total retrieval error used as quantifier of the performances in the case of the MSS analysis is the averaged value of the total retrieval error of the selected sequences.

- *Gain of Information*
  For the Gain of Information obtained from the observation with respect to the climatological profile assumed as a priori we use the same definition adopted in (L1+L2) analysis (see sub-section 12.2.1). While in the (L1+L2) analysis the quantity GI^{MIP} and GI^{Fusion} represents the gain of information of MIPAS-STR measurements constrained by Tikhonov regularization with respect to the a priori of MARSCHALS and the gain of information of (L1+L2) data fusion constrained by Tikhonov regularization with respect to the a priori of MARSCHALS respectively, the MSS procedure calculates the Measurement Space component of MIPAS-STR retrieved profile without the effects of smoothing introduced by the Tikhonov-Phillips procedure, and provide the complete profile by using the same a priori knowledge applied for MARSCHALS MSS data analysis and for MSS data fusion.

- *Degrees Of Freedom*
  In the (L1+L2) analysis, the DOFs of individual and synergistic retrievals depend either on Tikhonov regularization or on a priori information and do not refer to a common reference. In the MSS analysis, on the contrary, the Averaging Kernels matrices used to calculate the DOFs in all cases refer to common a priori information.

12.3.2 Results

We report in this sub-section the results of MSS data fusion compared with the retrieval products from individual measurements. Data fusion was performed on O_3 VMR vertical profiles retrieved from the best matching sequences of MARSCHALS and MIPAS-STR, as listed in Table 7 and with all problematic measurements identified in MARSCHALS data analysis (see sub-section 6) filtered out. In the case of MIPAS-STR, all scans (also scans with incomplete vertical sampling) are included except of two scans at the turning points, which are affected by aircraft manoeuvres.

The number of DOFs obtained for individual and synergistic retrieval of O_3 is plotted versus MARSCHALS sequences index in Figure 151. Results for the three spectral bands of MARSCHALS are reported in different

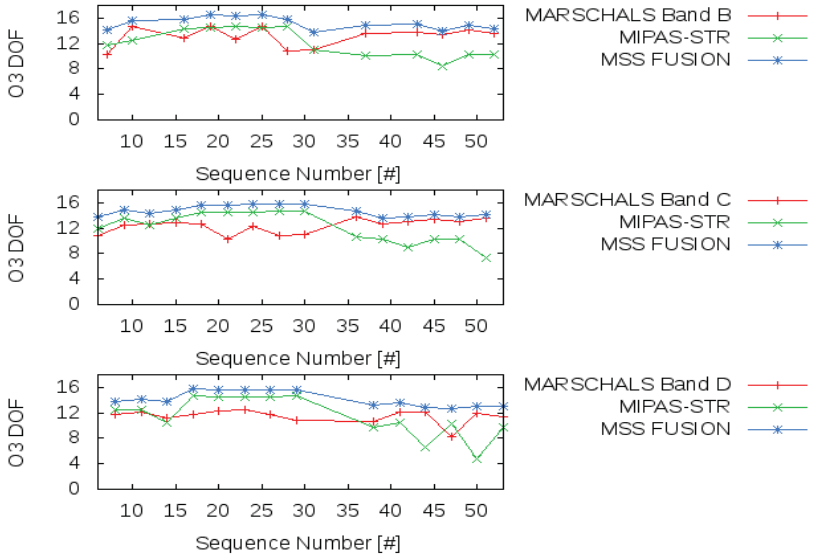

Fig. 151: As Figure 142 for O_3 using the MSS method

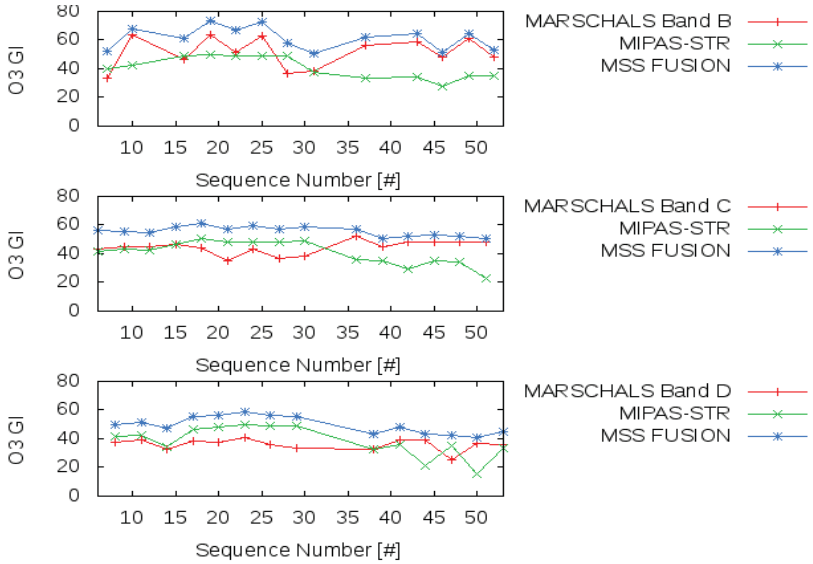

Fig. 152: As Figure 145 for O_3 using the MSS method

panels.

The impact of data synergy on the number of DOFs is evident for the entire duration of the flight and, in particular, for the second part of the flight (sequence number larger than 30), where the number of DOFs associated to MIPAS-STR observations is limited by cloud contamination.

The O_3 Gain of Information obtained from MSS data fusion with respect to MARSCHALS a priori information is displayed in Figure 152, along with corresponding values calculated from MARSCHALS and MIPAS-STR individual measurements. Once again, we stress the fact that the GI calculated from the MSS analysis is dependent on the measurements and on a common a priori information.

The O_3 total error profile obtained from MSS data fusion with respect to the total error profile obtained from MIPAS-STR and MARSCHALS measurements is displayed in Figure 153. The total error on O_3 VMR values obtained from data fusion is significantly reduced with respect to total errors obtained from the individual analyses. In the altitude range between 6 and 20 km, compared to total errors of O_3 profiles retrieved from MIPAS-STR measurements and MARSCHALS measurements, a reduction up to about 50% of the total uncertainty is observed when combining MIPAS-STR data and MARSCHALS observations in band B, band C or band D. Also in this case, we have to stress that the errors reported in Figure 153 is biased by the same a priori information.

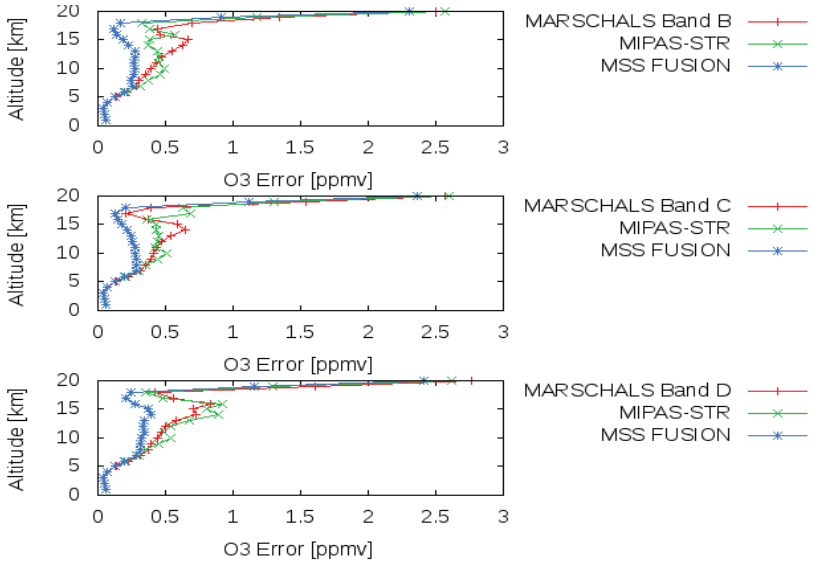

Fig. 153: As Figure 148 for O_3 using the MSS method

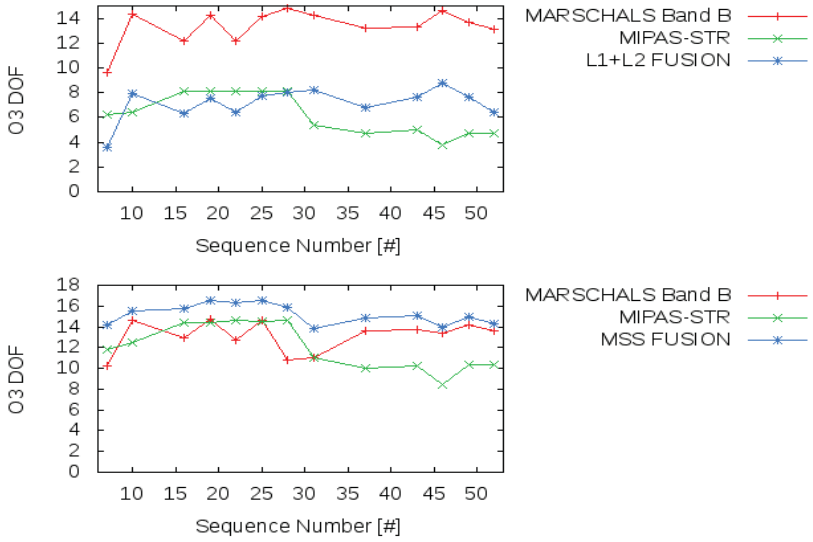

Fig. 154: Band B: Comparison of number of DOF of O_3 as reported in Figure 143 and Figure 151

The errors in context of the MSS analysis are represented using the Optimal Estimation method as common external constraint. Due to the different type of external constraint and the different influence of the a priori information, for MIPAS-STR larger errors are obtained compared to the L1+L2 method. This characteristic is tolerated here, since the focus of this study is the comparability of the individual results and the results of the data fusion rather than an optimal representation of the errors of the individual instruments.

12.4 Comparison of (L1+L2) and MSS data fusion methods

An evaluation of the performances of alternative methods of data fusion was presented, as obtained from the application of the (L1+L2) method and of the MSS method to the combination of MIPAS-STR and MARSCHALS measurements of O_3 VMR vertical profiles. Here, we briefly report a direct comparison of the results and highlight the basic differences between the (L1+L2) and the MSS approach emerging from the selected test cases.

In Figure 154, 155, and 156, the number of DOFs from individual retrievals is compared with the number of DOFs from synergistic retrieval performed using the (L1+L2) and the MSS method for data fusion of MIPAS-STR and MARSCHALS measurements in band B, band C and band D respectively.

For all bands, the improvement brought by data synergy of individual measurements is evident when using the MSS approach, that is capable to evaluate the contribution of measurement space component with no impact of dif-

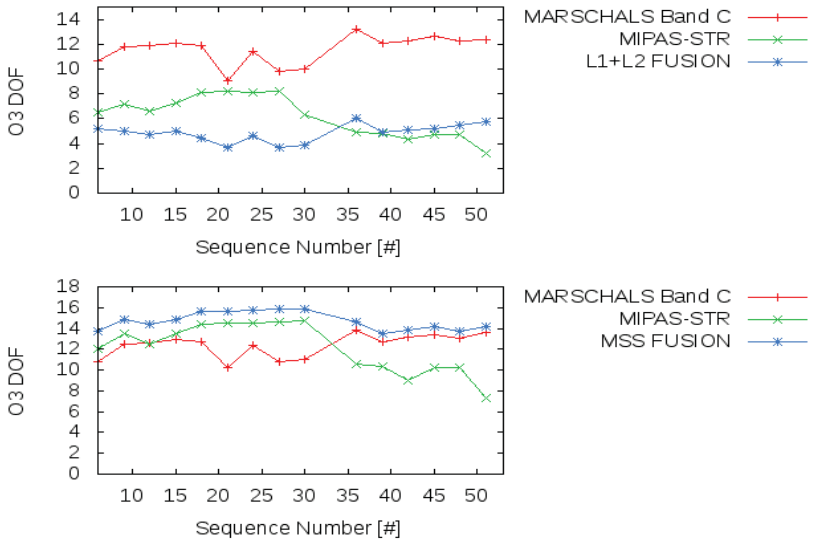

Fig. 155: As Figure 154 for Band C

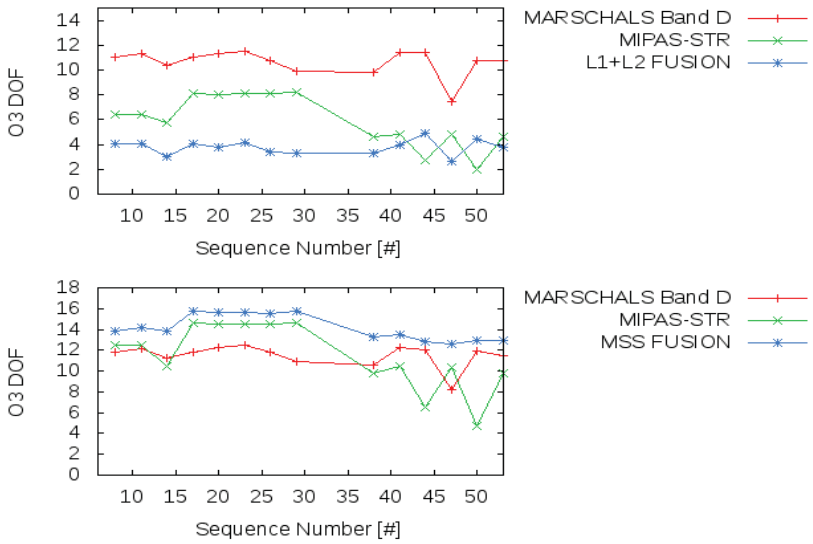

Fig. 156: As Figure 154 for Band D

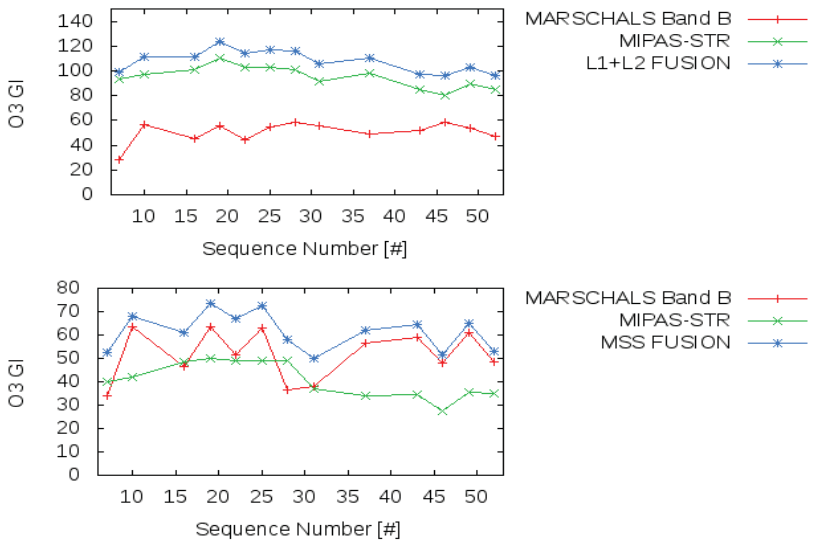

Fig. 157: Band B: Comparison of number of GI of O_3 as reported in Figure 146 and Figure 152

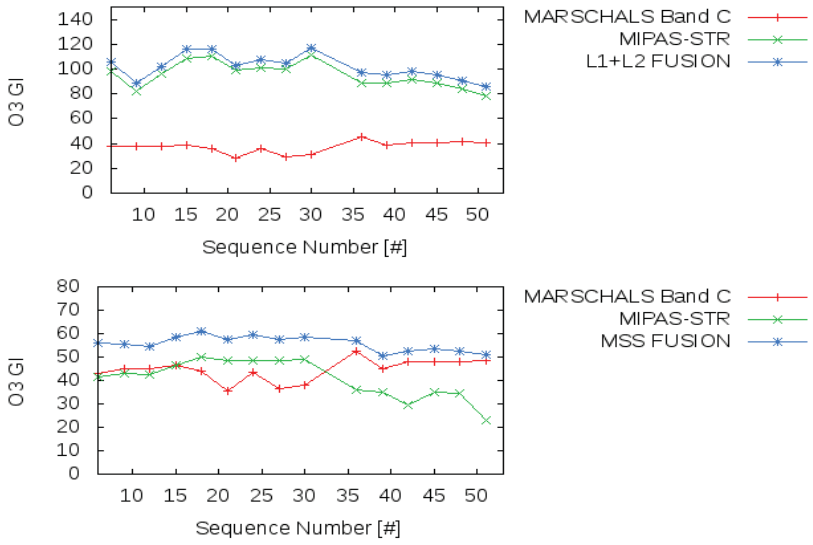

Fig. 158: As Figure 157 for Band C

ferent external constraints, such as the Tikhonov regularization which is taken into account in MIPAS-STR DOFs or the a priori information adopted in MARSCHALS retrieval processing and in data fusion using the (L1+L2) method. MSS calculations make it possible to compare the DOFs of individual retrievals from MARSCHALS and MIPAS-STR measurements in a more straightforward manner, as clearly noticeable in particular for band D in the final part of the flight (sequence number larger than 40).

In Figure 157, 158, and 159, similar plots are reported for the Gain of Information with respect to the a priori information of MARSCHALS for band B, band C and band D respectively. Also in this case the advantage of MSS individual and synergistic retrievals consists in providing an evaluation of the GI that includes the contribution of a common a priori information. This highlights the fact that the GI of MIPAS-STR measurements in the infrared is affected by the presence of clouds in the second part of the flight more than MARSCHALS measurements in the mm-wave, that make the results of data fusion insensitive to cloudiness.

Finally, in Figure 160, 161, and 162, we report the total uncertainty on the O_3 VMR profile retrieved from individual measurements and from data synergy using (L1+L2) and MSS methods of MIPAS-STR and MARSCHALS measurements in band B, band C and band D.

Here we notice that the external constraint of Tikhonov regularization adopted by MIPAS-STR inverse processing signifcantly influences the estimate of total errors from individual and (L1+L2) synergistic retrievals, while MSS calculations provide total error values associated to the measurements based on a common a priori knowledge

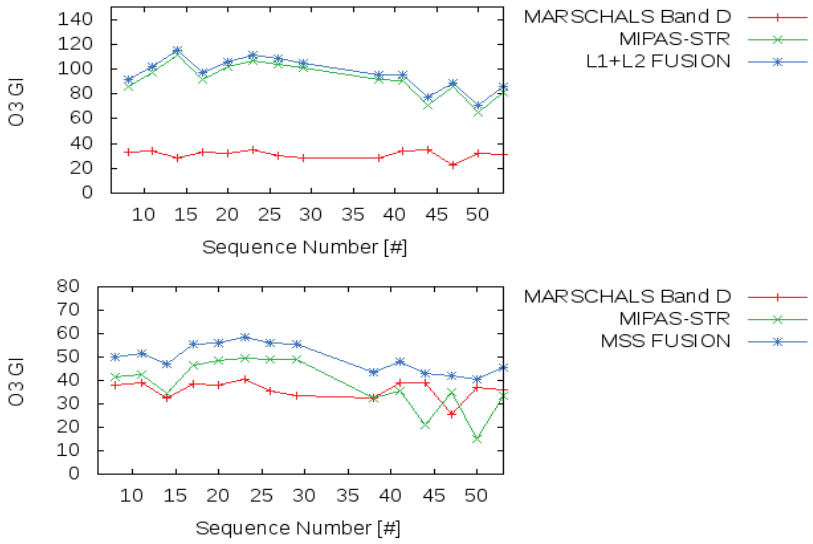

Fig. 159: As Figure 157 for Band D

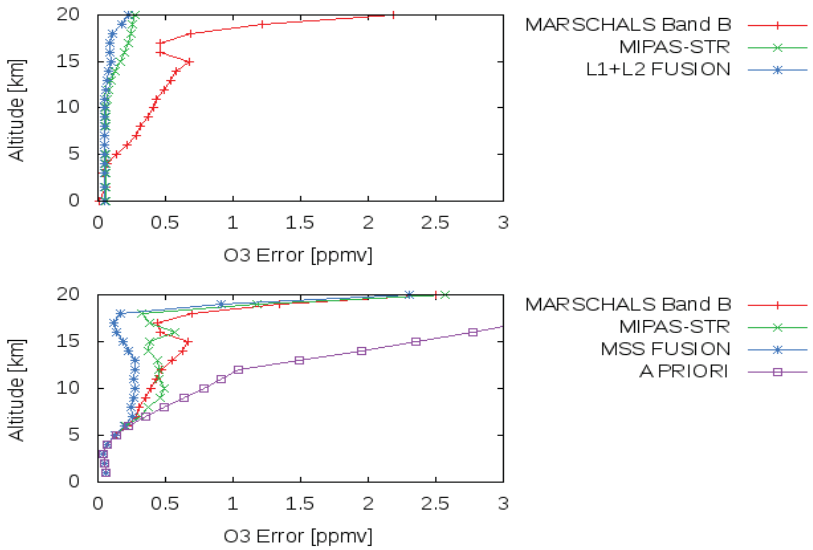

Fig. 160: Band B: Comparison of total errors of O_3 as reported in Figure 149 and Figure 153

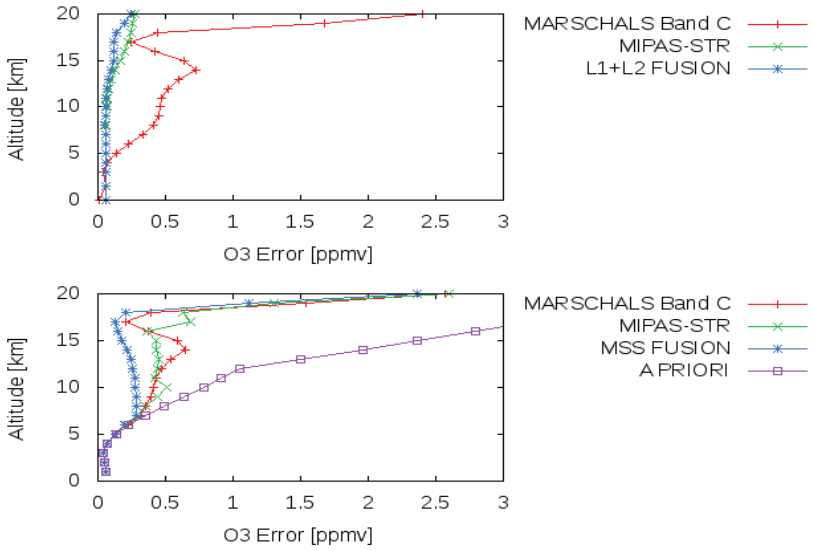

Fig. 161: As Figure 160 for Band C

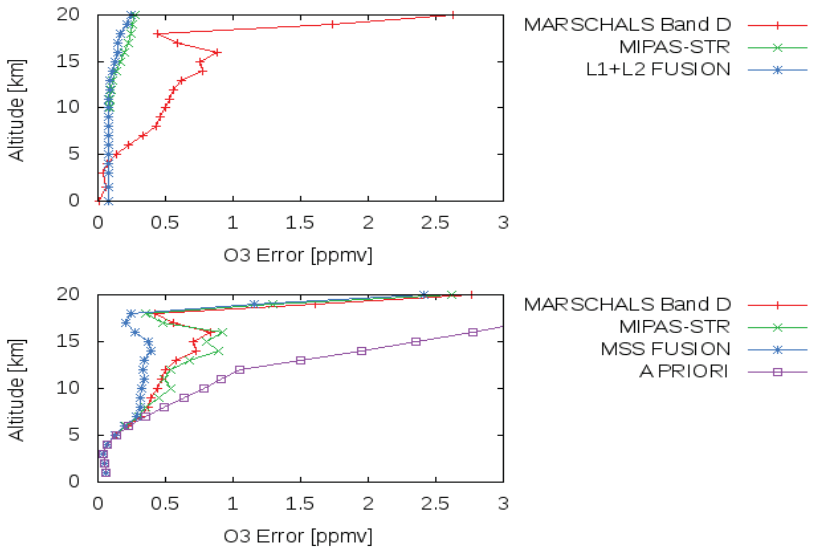

Fig. 162: As Figure 160 for Band D

Tab. 11: Characteristics of the AHRS given by the producer (SEG mbH, Riegel)

Angle	Data Rate	Resolution	Precision (3σ)
Azimuth	128 Hz	3.6”	$0.9\,^\circ$
Roll	128 Hz	3.6”	1.5’
Pitch	128 Hz	3.6”	1.5’

of the O_3 vertical profile and a common external constraint. And this facilitates the comparative evaluation of the total uncertainty associated to individual and synergistic retrieval products. We note that in the context of the MSS method, for MIPAS-STR higher total uncertainties are reported compared to the L1+L2 method. As discussed in Sect. 12.3.2, is this attributed to the different type of external constraint and different influence of the a priori knowledge on the representation of the total error profile. When plotting the total errors for the MSS analysis, we also reported the error on the a priori profile, showing that this is coincident with the retrieval errors at altitude lower than approximately 7 km.

We come to the conclusion, that the application of the (L1+L2) method using different retrieval methods for the MW- and IR- measurements qualitatively demonstrates the synergy between the different techniques. But quantitative comparisons are difficult since the characteristics of the different retrieval methods are not fully compatible (An improved quantitative comparability might be obtained by using the same retrieval method, constraint and a-priori knowledge for both techniques and optimizing the retrievals for the same key aspects). In contrast, the MSS method allows for a more clear comparison of the individual results and the results of the data synergy, since the measured components from the different techniques are treated in a similar way and the results are subject to the same external constraint.

In the frame of this study, the aim of the investigation of data synergy using the MSS method has been focused on the measurement space component and on the optimal exploitation of the information obtained from IR and mm-waves measurements. The optimal representation of the retrieved profiles and associated errors, that requires a suitable procedure also for the determination of the component in the sub-space orthogonal to the measurement space, has been given a lower priority. In fact, as a further result of this study we recommend a dedicated analysis aiming at fine-tuning this component in individual and synergistic MSS data processing for an optimal representation of the retrieved profiles and errors, particularly in those altitude range where the information is mainly provided by an external constraint.

13 Detailed pointing analysis from MIPAS-STR AHRS and M-55 GNS data

The Attitude and Heading Reference System (AHRS) of MIPAS-STR is an inertial navigation system providing accurate attitude information suited for the stabilization of the line-of-sight of the MIPAS-STR instrument. Essential components of the AHRS are two gyros, three accelerometers and a GPS, supplying the AHRS with additional geographical information for stabilization and refinement of the pointing data to be calculated. Performance characteristics of the AHRS are summarized in Table 11. The fast attitude angle information provided by the AHRS on a data-rate of 128 Hz is used for the active stabilization of the MIPAS-scan-mirror, allowing for a suitable stabilization of the line-of-sight during the recording of interferograms (recording of one single interferogram takes about 10 seconds).

The maximal effective accuracy of the line-of-sight-elevation-angle (better than 2.5 arcmin (3σ), including the errors due to the scan mirror stabilization) can be obtained after post-processing of the AHRS-pointing data including the comparison with an independent reference system providing precise attitude information (such as the GNS, the Geophysica Navigation System). Without post-processing, the accuracy of the roll-angle-information provided by the AHRS is only about 7 arcmin (3σ) due to slow drifts of the navigation system on a timescale of minutes. The AHRS is built in $91\,^\circ$ twisted with respect to the nose of the Geophysica and approximately by $0.34\,^\circ$ around the roll-axis of the plane. Since the pitch-axis of the AHRS and the roll-axis of the plane (and therefore of the GNS) nearly coincide, the pitch-axis of the AHRS will be denoted as roll-axis in the following for more clarity (consequently, the azimuth-axis of the AHRS remains unchanged and the roll-axis corresponds to the pitch-axis). Using this convention, the roll-axis of the AHRS (approximately coinciding with the axis of the scan mirror of MIPAS) is compared to the roll-axis of the GNS. Since the coordinate axes of AHRS and GNS are not absolutely congruent, the transformation of the attitude angles of the plane measured by the GNS into the roll-angle in the AHRS-coordinate system contains beside the GNS-roll-angle also small components of the GNS-azimuth-

angle and pitch-angle, mostly noticeable during ascent- and descent-phases. Due to the fact, that the MIPAS-STR instrument, including the AHRS, is connected flexible via metal-springs to the rigid frame mounted onto the Geophysica airplane, the MIPAS-STR instrument and the AHRS slightly change their positions with respect to the plane and therefore to the GNS during ascent, descent and curves. These effects can be neglected for a qualitative comparison (meaning the roll-angle of the plane measured by the GNS can by directly compared to the AHRS-roll-angle) [7] and only for quantitative comparisons, the attitude angles of the GNS are precisely transformed into a roll-angle with respect to the roll-axis of the AHRS. For the comparison of the two navigation systems in the following, two different roll-angle-differences of GNS and AHRS are considered: The direct roll-angle-difference corresponds to the direct difference between the roll-angles provided by AHRS and GNS (without coordinate transformation), while the precise roll-angle-difference references to the roll-angle-difference in the coordinate system of the AHRS, including the precise transformation of the GNS-attitude-angles into the roll-angle in the reference-system of the AHRS.

For an inertial navigation system with fixed gyros (such as the AHRS), the information on the actual alignment relative to the calculated virtual horizon is essential for the calculation of the attitude information. The estimation of horizontal- and azimuth-errors of the AHRS is realized by a real-time estimation procedure, the Kalman-Filtering [13]. Error statistics and correlations of system quantities to be estimated for this procedure are contained in a covariance matrix and estimated errors are summarized in a state vector (e.g. velocity). Since several quantities (latitude, longitude, velocities) are also known from the GPS included in the AHRS, corrections for occurring errors of all quantities provided by the AHRS (e.g. attitude angles) can be calculated. Hence, not only errors of the alignment of the virtual horizontal platform of the AHRS, but also errors for the gyros and the accelerometers can be estimated. The recording of corrections suited for the post-flight-processing of the attitude data (including a correction for the roll-angle) is performed every 20 seconds. The provided correction for the roll-angle is considered in the post-flight-pointing processing of the AHRS-data, allowing for a maximal accuracy of the roll-angle-information and therefore for the line-of-sight-elevation. The correction provided by the Kalman-filter for the roll-angle is initially non-scaled, indicating only relative variations of the roll-angle-error. By comparison with an independent roll-angle-information of suitable accuracy (such as ideally provided by the GNS), the correction for the AHRS-roll-angle can be scaled and then applied in the postflight-processing. The

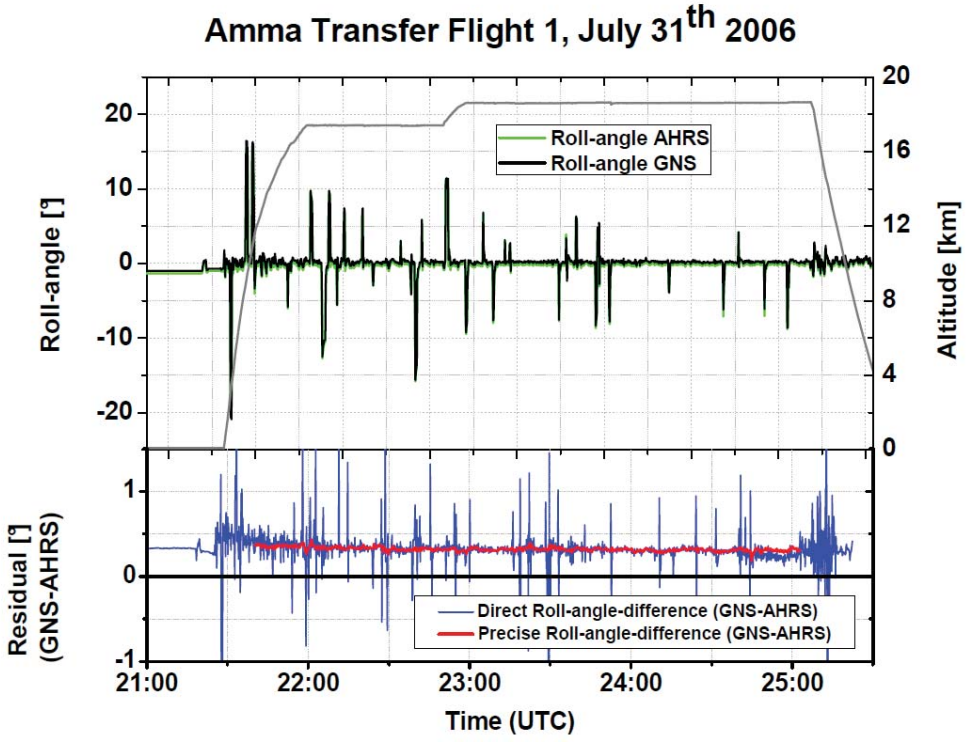

Fig. 163: Comparison of the roll-angles measured by AHRS and GNS for the Amma Transfer Flight 1. The residual shows the direct and the precise roll-angle-difference. The roll-angles provided by the two navigation-systems coincide well.

Tab. 12: Characteristics of the GNS [14]

Angle	Data Rate	Resolution	Precision (2σ)
Azimuth	5 Hz	20”	$\leq 12'$
Roll	5 Hz	20”	$\leq 6'$
Pitch	5 Hz	20”	$\leq 6'$

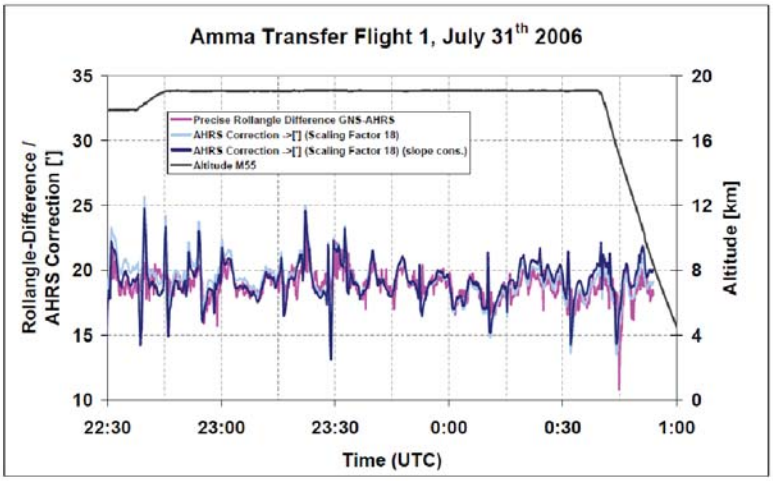

Fig. 164: Comparison of the precise roll-angle-difference between AHRS and GNS with the AHRS-correction provided by the Kalman-Filtering (optimised scaling factor of 18).

scaling-factor of the correction varies (in a certain range) from flight to flight and therefore has to be estimated for each single flight. Using this approach, a maximal accuracy of the roll-angle-information of the AHRS and therefore for the MIPAS-instruments line-of-sight can be obtained.

13.1 Standard procedure for the line-of-sight-elevation-correction of MIPAS

In the earlier campaigns with MIPAS on the Geophysica aircraft, the GNS served as an independent reference system for the postflight-correction of the AHRS roll-angle-data. The nominal characteristics of the GNS are summarized in Table 12.

In principle, the given error for the roll-angle of the GNS is higher than the corresponding error of the AHRS (after postflight-correction) and the GNS-data has a lower angular resolution, but the analysis of flights of earlier campaigns has shown, that for several flight sections, the GNS-data shows suitable data quality for a detailed comparison with the AHRS. Large errors (in the magnitude given in Table 12) in the GNS-roll-angle-data can (beside other factors) occur due the evolution of a Schuler-Oscillation [7] with a time-period of approximately 85 minutes, which can be post-flight-corrected under certain conditions. Therefore, under ideal conditions, the GNS-roll-angle-data can show much a higher precision than given in Table 12.

Figure 163 shows the comparison of the roll-angles measured by the AHRS and GNS for the Amma Transfer Flight 1 on July 31st 2006. In the residual, the direct and the precise roll-angle-differences between GNS and AHRS are shown, and the two navigation systems coincide well within a total span of about 6 arcmins for the direct difference and of about 2 arcmins for the precise roll-angle-difference during the phase after finishing the ascent and before beginning of the descent (except of corrupted data points and aircraft manoeuvres). The bias of approximately $+0.34\,^\circ$ in the residual is due to the fact, that the two navigation systems are spatially twisted against each other around the roll axis. The precise roll-angle-difference then can be compared to the AHRS-roll-angle-correction provided by the Kalman-filtering and in case of a suitable correlation of these two quantities, the scaling-factor for the AHRS-roll-angle-correction can be estimated.

Figure 164 shows the comparison of the precise roll-angle-difference between GNS and AHRS to the scaled

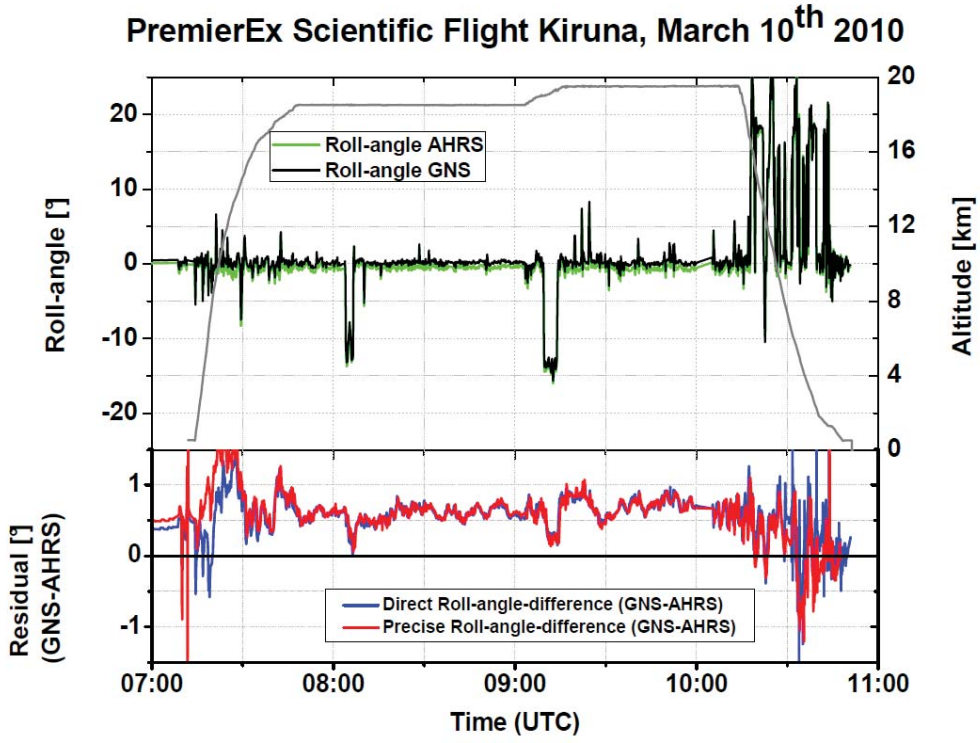

Fig. 165: Comparison of the roll-angle measured by AHRS and GNS and the direct and precise roll-angle-difference for the PremierEx Scientific Flight in Kiruna. The roll-angles provided by the two navigation-systems show large deviations from each other.

correction provided by the Kalman-Filtering of the AHRS, showing a suitable correlation for a scaling-factor of 18 for the AHRS-correction (An optimal correlation is obtained between 23:30 and 0:10). A weak slope in the roll-angle-difference due to a slow drift of at least one of the navigation systems is fitted to the AHRS-correction for means of a better correlation of the amplitudes. The scaled correction can then be applied directly to the MIPAS-line-of-sight-elevation-angle (which nearly coincides with the AHRS-roll-angle).

13.2 Error identification of the GNS for PremierEx-Flight in Kiruna on March 10^{th} 2010

In the case of the PremierEx Scientific Flight in Kiruna, the method for the correction of the MIPAS-line-of-sight could not be carried out as described above, since large deviations between the attitude angles provided by the AHRS and GNS were observed.Figure 165 shows the direct comparison of the roll-angles provided by the AHRS and GNS. Already the direct difference of the corresponding angles shows relative variations of approximately $\pm 0.5\,^{\circ}$ and the deviations in the precise roll-angle-difference are of the same magnitude. Consequently, the precise comparison between the roll-angles of AHRS and GNS does not allow for the scaling of the AHRS-correction provided by the Kalman-filtering.

Since there is no other reference available providing an accurate roll-angle-information, only from this comparison it is not clear, which navigation-system causes the observed deviations. Therefore, also the azimuth-angle corresponding to the true heading of the Geophysica airplane is also considered for both navigation systems. The benefit of this comparison is, that the true heading of the plane can also be calculated from the track-angle provided by the Geophysica-GPS and the drift-angle provided by the Geophysica-Doppler-Sensor (both quantities are included in the UCSE-dataset), as illustrated in Figure 166.

Consequently, this method allows the calculation of the true heading of the airplane independent from the two inertial navigation systems AHRS and UCSE and represents a reference for the true heading measured by each instrument. The characteristics of the Geophysica-GPS and Doppler-Sensor are summarized in Table 13.

In Figure 167, the comparison of the true heading provided by the GNS, AHRS and the combination GPS/Doppler-sensor is shown for the Amma Transfer Flight 1. The residual between GNS and the combination GPS/Doppler-

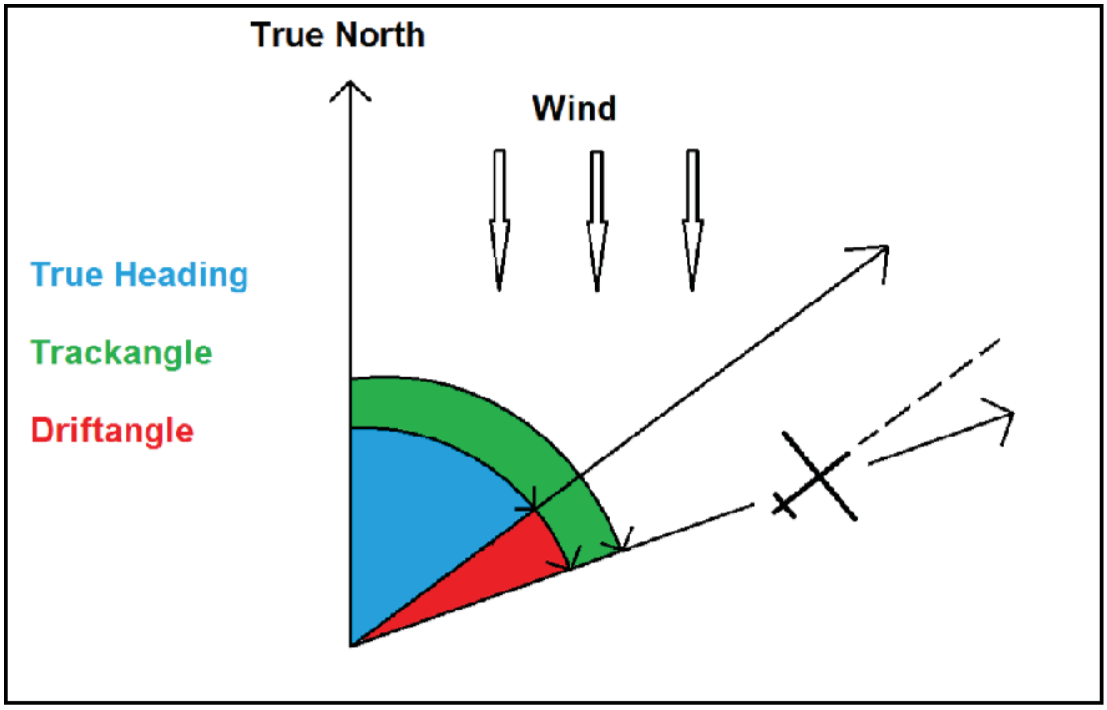

Fig. 166: The true heading of the Geophysica (corresponding to the azimuth measured by the AHRS and GNS) can be calculated independently by using the track-angle (GPS) and drift-angle (Doppler-Sensor) provided in the UCSE-data.

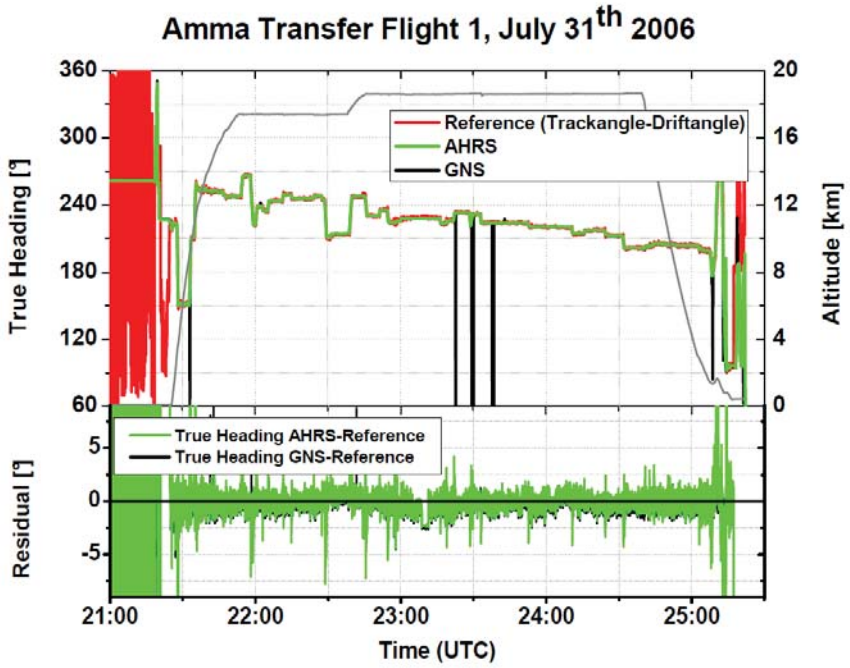

Fig. 167: The true heading provided by AHRS, GNS and the Combination GPS/Doppler-Sensor agree well for the Amma Transfer Flight 1

Tab. 13: Characteristics of the GNS [14]

	Data Rate	Measurement Error
Track Angle (GPS)	1 Hz	no information
Drift Angle (Doppler-Sensor)	2-3 Hz	$\pm 0.2 \ldots 0.3\%$

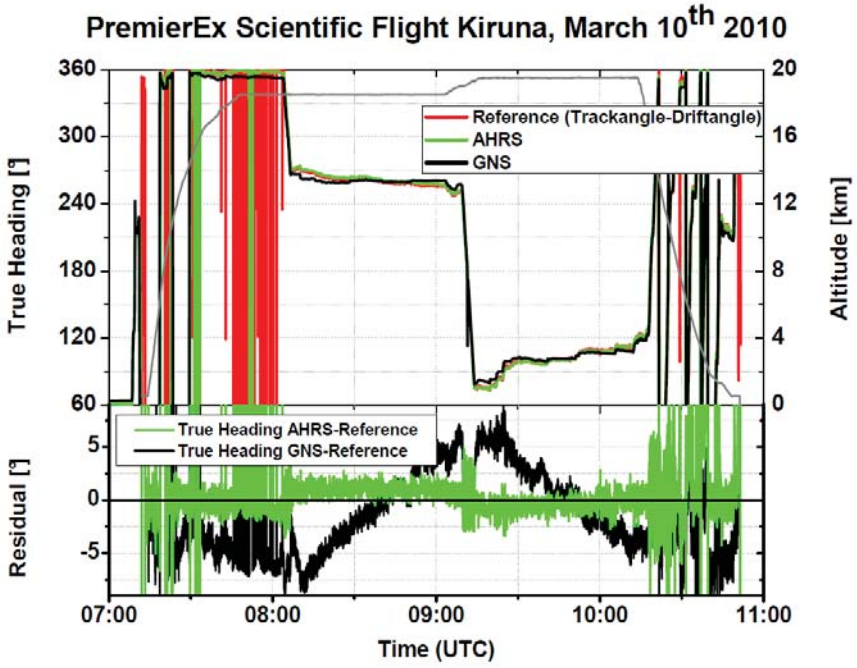

Fig. 168: The comparison of the true heading provided by the AHRS, GNS and the combination GPS/Dopplersensor shows consistency of AHRS and the combination GPS/Doppler-Sensor (within the errors of the involved systems), while the GNS shows large deviations

Sensor, as well as between AHRS and the combination GPS/Doppler-Sensor, are also shown. The curves agree well and the residua show only small variations in the order of less than 1○, lying in the uncertainty range of the involved systems. Figure 168 shows the same comparison for the PremierEx Scientific Flight in Kiruna. Again, the true heading provided by the AHRS and the combination GPS/Dopplersensor agree well, as indicated by the corresponding residuum, while the GNS-true heading shows large deviations from the other systems. The residuum between the GNS-true heading and the GPS/Dopplersensor-true heading indicates variable deviations of more than $\pm 5\,^{\circ}$.

Since the true heading of AHRS and the combination GPS/Doppler-sensor show consistency and the GNS shows large deviations from both systems, the observed discrepancies between AHRS and GNS are attributed to the GNS. Comparable discrepancies are observed for all flights during the RECONCILE-Campaign and also for the PremierEx Scientific Flight in Oberpfaffenhofen on November 4^{th} 2009. Consequently, the correction of the MIPAS-line-of-sight cannot be performed using the GNS as reference system.

13.3 Correction of the MIPAS-line-of-sight-elevation for the PremierEx Flight in Kiruna on March 10^{th} 2010

For the determination of the scaling factor of the roll-angle-correction provided by the AHRS-Kalman-filter, an independent attitude-information of suitable accuracy is desired. In principle, during the standing period of the Geophysica on the apron directly before the flight, the information on the relative attitude of the plane is known. As long as the plane makes no movements and no significant vibrations or other disturbances occur, the roll-angle of the plane is practically unchanged. During this period, the AHRS is initialized and starts providing information

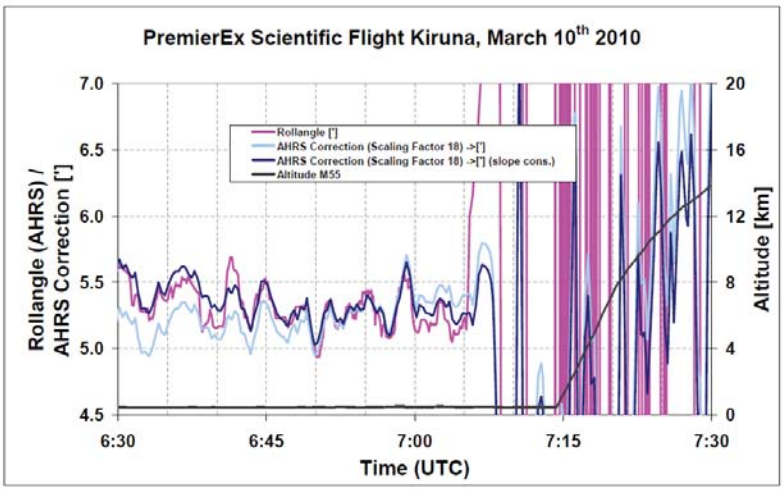

Fig. 169: Comparison of the measured AHRS-roll-angle during the preflight-standing-period due to errors and the scaled correction provided by the Kalman-Filtering. A scaling-factor of 18 results in an optimal correlation

on the roll-angle of the plane, as well as on the non-scaled correction resulting from the Kalman-filter. Due to the fact, that the real roll-angle of the plane is unchanged, all roll-angle-variations measured by the AHRS must result from errors and therefore should be found also in the non-scaled correction resulting from the Kalman-filter. In the case, that the measured roll-angles of the AHRS and the correction resulting from the Kalman-filter are correlated, the scaling factor for the correction can be estimated. Figure 169 shows the measured roll-angle and the correction provided by the Kalman-filter during the preflight-standing-period on the apron directly before the PremierEx Scientific Flight in Kiruna. Due to the fact, that at this time the AHRS just has finished its initialisation phase, the mean roll-angle still shows a weak slope, since the precise attitude-information still is converging directly after the initialisation. Therefore, this slope is also considered for the correction resulting from the Kalman-Filtering for means of correlation. In the plot, the slope-adapted correction shows a moderate correlation (mainly between 6:30 and 7:00) with the measured roll-angle, and an optimal correlation is achieved for a scaling factor of 18, which agrees with scaling factors found for flights of earlier campaigns. Due to the fact, that the AHRS has been refurbished between the Amma Campaign 2006 and the Oberpfaffenhofen Campaign 2009, the scaling factors cannot be compared directly, since the error-behaviour of the AHRS might have been changed. But the fact, that the scaling-factors estimated for flights prior to the AHRS-refurbishment are comparable (as for the Amma Transfer Flight 1) to the estimated scaling-factor for the PremierEx Scientific Flight in Kiruna, is encouraging.

Disadvantages of the described method for the determination of the scaling factor are:

- Short data acquisition time (plane standing still) of approximately 30 minutes between the initialization of the AHRS and the begin of taxiing.
- Due to the fact, that the plane is standing still, only very small changes in the roll-angle due to errors are measured, which are close to the detection limit.
- Small changes of the roll-angle of the plane occur, since the plane is touched for preflight-operations during this period, while the plane is assumed to stand still for the correlation of the measured roll-angle and the AHRS-correction band targets.

For an error-estimation, it was considered, how the postflight-corrected roll-angles differ, when scaling-factors between 13 and 23 are applied, with respect to a scaling factor of 18. For the PremierEx Scientific Flight in Kiruna (Method for correction described in this section), as well as for the Amma Transfer Flight 1 (Standard procedure including comparison with GNS) and another scientific flight in Kiruna on February 28^{th} 2003 (Standard procedure including comparison with GNS), maximal deviations of 2.25 arcmins (3σ) were found.

Therefore, this conservative estimated value is considered as the maximal expected error on the postflight-corrected roll-angle-data of the AHRS. For the line-of-sight of MIPAS, also possible errors of due to the accuracy of the scan mirror-adjustment have to be considered. The corresponding error has been estimated to 0.28 arcmin (3σ). Therefore, the estimated total error for the MIPAS-line-of-sight is estimated to 2.27 arcmin (3σ).

13.4 Conclusions of MIPAS-STR pointing analysis

For the PremierEx Scientific Flight in Kiruna on March 10^{th} 2010, the roll-angles provided by the AHRS and GNS are not consistent and show variable relative variations of $\pm 0.5\,^{\circ}$ (in contrast to flights of campaigns earlier than 2009). The comparison of the true heading (corresponding to the azimuth-angle) of both navigation systems to the true heading calculated from the track-angle and drift-angle provided by the Geophysica-GPS and Doppler-sensor shows consistency between the AHRS and the combination GPS/Doppler-sensor and deviations of $\pm 0.5\,^{\circ}$ for the GNS from the other systems (also in contrast to flights prior to 2009). Therefore, the observed deviations between the roll- and azimuth-angles between AHRS and GNS are attributed to the GNS. Comparable deviations between the AHRS and GNS are also found for the PremierEx Technical Flight on November 4^{th} 2009 in Oberpfaffenhofen. For the postflight-correction of the line-of-sight-elevation of MIPAS, a strategy independent from the comparison with the GNS-roll-angle is applied. The error for the roll-angle provided by the AHRS is estimated to 2.25 arcmin (3σ), resulting in an error of 2.27 arcmin (3σ) for the elevation of the MIPAS-line-of-sight, including the accuracy of the scan-mirror adjustment.

14 Reference Documents

RD1:
MARSCHALS Level 2 Architectural Design Document, study: The Scientific Analysis of Limb Sounding Observations of the Upper Troposphere.

RD2:
MARSCHALS Level 2 Software User and Reference Manual, study: The Scientific Analysis of Limb Sounding Observations of the Upper Troposphere.

RD3:
MARSCHALS Level 2 Report on data analysis of SCOUT O3 MARSCHALS flight campaign, study: The Scientific Analysis of Limb Sounding Observations of the Upper Troposphere.

References

[1] www.ecmwf.int/research/ifsdocs/DYNAMICS/Chap2_Discretization4.html

[2] E. Castelli, S. Del Bianco, B. M. Dinelli, A. Dudhia, M. Gai, and L, Santurri, MARSCHALS Level 2 Report on data analysis of SCOUT-O3 MARSCHALS flight campaign. Technical note of the study: The Scientific Analysis of Limb Sounding Observation of the Upper Troposphere, ESA-ESTEC contract N. 16530/02/NL/MM, 2007.

[3] Ceccherini, S., P. Raspollini and B. Carli, Optimal use of the information provided by indirect measurements of atmospheric vertical profiles, Optics Express, 17, 7, 4944-4958, (2009).

[4] Del Bianco S., B. Carli, Ceccherini S., B. Carli, U. Cortesi, S. Del Bianco, P. Raspollini, Retrieval of the vertical column of an atmospheric constituent from data fusion of remote sensing measurements, Journal of Quantitative Spectroscopy and Radiative Transfer, 111, 507-514, (2010)

[5] Del Bianco S., B. Carli, C. Cecchi Pestellini, B. M. Dinelli, M. Gai and L. Santurri, Retrieval of minor constituents in a cloudy atmosphere with remote sensing millimetre wave measurements, Quarterly Journal of the Royal Metereological Society , 133: (S2), pp. 163-170 (2007)

[6] Dinelli, B. M., Castelli, E., Carli, B., Del Bianco, S., Gai, M., Santurri, L., Moyna, B. P., Oldfield, M., Siddans, R., Gerber, D., Reburn, W. J., Kerridge, B. J., and Keim, C.: Technical Note: Measurement of the

tropical UTLS composition in presence of clouds using millimetre-wave heterodyne spectroscopy, Atmos. Chem. Phys., 9, 1191–1207, 2009.

[7] Keim, C., Entwicklung und Verifikation der Sichtlinienstabilisierung fr MIPAS auf dem hochfliegenden Forschungsflugzeug M-55 Geophysica, Dissertation, University of Karlsruhe and Research Centre Karlsruhe, Wissenschaftliche Berichte FZKA 6729, 2003.

[8] Kerridge, B.J., R Siddans, J Reburn, et al. (2001), Definition of Mission Objectives and Observational Requirements for an Atmospheric Chemistry Explorer Mission, ESTEC Contract no. 13048/98/NL/GD Final report.

[9] Kerridge, B.J., R Siddans, J Reburn, et al., Definition of Mission Objectives and Observational Requirements for an Atmospheric Chemistry Explorer Mission, ESA Contract No:13048/98/NL/GD Study Extension: Contract Change Notice No.3 Final Report. Jan. 2002.

[10] Kerridge, B.J., R Siddans, J Reburn, et al., Consideration of mission studying chemistry of the UTLS, Final Report August 2004, ESA Contract 15457/01/NL/MM.

[11] Fischera J., R. R. Gamache, A.Goldmanb, L. S. Rothmanc and A. Perrin, Total internal partition sums for molecular species in the 2000 edition of the HITRAN database, Journal of Quantitative Spectroscopy and Radiative Transfer, 82, 401-412.

[12] Livesey, N. J., et al. (2008), Validation of Aura Microwave Limb Sounder O_3 and CO observations in the upper troposphere and lower stratosphere, J. Geophys. Res., 113, D15S02, doi:10.1029/2007JD008805.

[13] Maucher, G., Das Sternreferenzsystem von MIPAS-B2: Sichtlinien-Bestimmung fr ein ballongetragenes Spektrometer zur Fernerkundung atmosphrischer Spurengase, Dissertation, University of Karlsruhe and Research Centre Karlsruhe, Wissenschaftliche Berichte FZKA 6227, 1999.

[14] MDB., MDB, High-altitude M-55 Geophysica aircraft: Investigators Handbook, 3rd Edition, Myasishchev Design Bureau, 1996.

[15] Pumphrey, H. C., et al. (2007), Validation of middle-atmosphere carbon monoxide retrievals from the MicroWave Limb Sounder on Aura, j. Geophys. res., 112, D24S38, doi:10.1029/2007JD008723.

[16] MARSCHALS Level 2 Architectural Design Document, study: The Scientific Analysis of Limb Sounding Observations of the Upper Troposphere.

[17] MARSCHALS Level 2 Software User and Reference Manual, study: The Scientific Analysis of Limb Sounding Observations of the Upper Troposphere.

[18] MARSCHALS Level 2 Report on data analysis of SCOUT O3 MARSCHALS flight campaign, study: The Scientific Analysis of Limb Sounding Observations of the Upper Troposphere.

[19] Remedios, J. J., Leigh, R. J., Waterfall, A. M., Moore, D. P., Sembhi, H., Parkes, I., Greenhough, J., Chipperfield, M.P., and Hauglustaine, D.: MIPAS reference atmospheres and comparisons to V4.61/V4.62 MIPAS level 2 geophysical data sets, Atmos. Chem. Phys. Discuss., 7, 9973–10017, 2007.

[20] Rodgers, C., (2000), Inverse Methods for Atmospheric Sounding: Theory and Practice, Vol. 2 of Series on Atmospheric, Oceanic and Planetary Physics, World Scientific., Singapore, 194.

[21] Santee, M. L., et al., (2007), Validation of the Aura Microwave Limb Sounder HNO3 measurements, j. Geophys. res., 112, D24S40, doi:10.1029/2007JD008721.

[22] Spang, R. et al., (2004), Colour indices for the detection and differentiation of cloud types in infra-red limb emission spectra, Advances in Space Research, 33, 1041-1047.

[23] Stiller, G.P. et al., (2004), The Karlsruhe Optimized and Precise Radiative transfer Algorithm (KOPRA), Wissenschaftliche Berichte FZKA 6487, Forschungszentrum Karlsruhe

[24] Dinelli, B.M. et al. Theoretical retrieval study, Report of the study: The Scientific Analysis of Limb Sounding Observations of the Upper Troposphere.

[25] Urban, J., D. Gerber, VINNOVA funded simulation study of the Swedish STEAM Science Reference group, 2010.

[26] Verdes, J.L.,et al., (2010), A sensitivity study on spectroscopic parameter accuracies for a mm/sub-mm limb sounder instrument, Journal of Molecular Spectroscopy 229 266-275.

[27] Von Clarmann, T., (2003), Zur Fernerkundung der Erdatmosphre mittels Infrarotspektrometrie: Rekonstruktionstheorie und Anwendung, Wissenschaftliche Berichte FZKA 6928, Forschungszentrum Karlsruhe.

Definitions and Acronyms

ACAP	Azimuthally Collapsed Antenna Pattern
AK	Averaging Kernel
ADD	Architectural Detailed Design
ATBD	MARSCHALS Level 2 Algorithm Theoretical Baseline Document
BTSN	Brightness Temperature Spectral Noise
CALIPSO	Cloud-Aerosol Lidar and Infrared Pathfinder Satellite Observations
DOF	Degrees Of Freedom
CKD	Clough, Kneizys and Davies (model)
CCP	Cloud Combination Probe
CIP	Cloud Imaging Probe
CRISTA-NF	Cryogenic Infrared Spectrometers and Telescopes for the Atmosphere . New Frontiers (CRISTA-NF)
CLAMS	Chemical Lagrangian Model of the Stratosphere
DOF	Degree of Freedom
ECMWF	European Center for Medium range Weather Forecasting
ENVISAT	ENVinronment SATellite
ESD	Estimated Standard Deviation
FISH	Fast In situ Stratospheric Hygrometer
FLASH	FLuorescent Advanced Stratospheric Hygrometer
FM2D	Forward Model 2D
FOV	Field Of View
FSSP	Forward Scattering Spectrometer Probe
FOZAN	Fast OZone ANalyzer
GMTR	Geofit Multi Target Retrieval
GNS	Global Navigation System
GPS	Global Positioning System
HAGAR	High Altitude Gas Atmospheric Research
HITRAN	HIgh resolution TRANsmission
IG2	Initial Guess level 2
ILS	Instrumental Line Shape
IR	InfraRed
GI	Gain of Information
FOV	Field Of View
L1, L1B, L2	Level 1,Level 1B, Level 2
LOS	Lines Of Sight
MARC	Millimetre-wave Atmospheric-Retrieval Code
MARS	Meteorological Archival and Retrieval System
MARSCHALS	Millimetre wave Airborne Receivers for Spectroscopic CHaracterization of Atmospheric Limb Sounding
MIPAS-STR	Michelson Interferometer for Passive Atmospheric Sounding - STRatospheric aircraft
MMR	Mass Mixing Ratio
MODIS	Moderate Resolution Imaging Spectroradiometer
MSS	Measurement Space Solution
MSSF	Mie Scattering Source Function
MTR	Multi Target Retrieval
PACD	Premier Analysis of Campaign Data
PREMIER	PRocess Exploration through Measurements of Infrared and millimetre-wave Emitted Radiation
OCM	Optical Cloud Monitoring
RMS	Root Mean Square
SAMM	Supervising Analyzer of MARSCHALS Measurements
SCOUT O3	Stratospheric-Climate links with emphasis On the Upper Troposphere and lower stratosphere
SOW	Statement Of Work
TC9	Test Campaign 2009

TDC	Thermo Dynamic Complex
TRS	Theoretical Retrieval Study
UCSE	Unit for Connection with Scientific Equipment
UTC	Universal Time Coordinate
VCM	Variance Covariance Matrix
VMR	Volume Mixing Ratio
VVW	Van Vleck Weisskopf

Table of Contents

1 Introduction **80**

2 New characterization data and code verification **80**
2.1 The main features of the pre-processor . . . 81
2.2 Characterization of the Level 1B data . . . 81
2.2.1 Overview of Level 1B data . . . 81
2.2.2 Sweep selection criteria . . . 81
2.3 New features of the pre-processor . . . 82
2.3.1 Spectrum contrast level . . . 82
2.3.2 Averaged Brightness Temperature of each spectrum . . . 82
2.3.3 New format for some auxiliary files . . . 82
2.3.4 Mean spectrum and standard deviation . . . 82
2.3.5 Observations dataset . . . 82
2.4 New features of the MARC code . . . 84
2.4.1 Implementation of frequency shift retrieval . . . 84
2.4.2 Frequency shift retrieval results on simulated spectra . . . 85
2.4.3 Implementation of the exportation of the MSS input products . . . 85

3 Intercomparison of MARC and RAL forward models **85**
3.1 Description of the RAL forward model . . . 85
3.2 Scope and strategy of the forward model intercomparison . . . 87
3.3 Definition of input parameters . . . 87
3.4 Monochromatic calculations . . . 88
3.5 Initial setup (full atmosphere) . . . 88
3.6 Single H_2O and O_3 lines . . . 89
3.7 Single layer homogeneous atmosphere . . . 89
3.8 Final monochromatic simulation . . . 93
3.9 Instrument line shape . . . 93
3.10 Atmospheric continuum . . . 93
3.11 Atmospheric refraction . . . 98
3.12 Field Of View convolution . . . 98
3.13 Conclusions and lessons learned . . . 98

4 Delivered Level 1B data and auxiliary information **106**

5 Analysis of MARSCHALS Test Flight measurements **109**
5.1 Geophysical Scenario . . . 109
5.1.1 Flight overview . . . 109
5.1.2 Initial Guess Atmosphere . . . 114
5.1.3 Initial Guess Atmosphere: ECMWF data . . . 114
5.1.4 Initial Guess Atmosphere: Scan dependent ECMWF profiles . . . 114
5.1.5 Initial Guess Atmosphere: a priori errors . . . 115
5.2 Retrieval results . . . 115
5.2.1 Analysed dataset . . . 115
5.2.2 Retrieval Features . . . 116
5.2.3 Preliminary analysis . . . 116
5.3 Final Analysis . . . 120
5.4 Recursive retrievals for O_3 and HNO_3 . . . 136

6 Analysis of MARSCHALS Scientific Flight measurements **136**
6.1 Geophysical Scenario . . . 136
6.1.1 Flight overview . . . 136
6.1.2 Initial Guess Atmosphere . . . 136
6.1.3 Initial Guess Atmosphere: a priori errors . . . 136
6.2 Retrieval results . . . 142
6.2.1 Analyzed dataset . . . 142
6.2.2 Preliminary analysis . . . 142

6.3 Tuning the retrieval strategy . . . 143
6.3.1 Sequential fit . . . 143
6.3.2 Impact of new band definition . . . 143
6.3.3 New noise characterization . . . 144
6.3.4 Impact of new FOV characterization . . . 144
6.3.5 Assessment of the impact of the width of the filter used for the correction of the pointing . 144
6.3.6 Tuning of the retrieval grid . . . 145
6.3.7 Frequency shift retrieval . . . 145
6.4 Final analysis . . . 146
6.5 Recursive retrievals for O_3 and HNO_3 . . . 162

7 Conclusions of MARSCHALS Test Flight and Scientific Flight data analysis 162

8 Simulated retrievals of CO from aircraft and satellite measurements 165

9 Validation of MARSCHALS measurements 170
9.1 Validation of the Test Flight measurements . . . 170
9.1.1 Temperature validation . . . 171
9.1.2 H_2O validation . . . 171
9.1.3 O_3 validation . . . 171
9.1.4 HNO_3 validation . . . 174
9.1.5 N_2O validation . . . 174
9.1.6 CO validation . . . 174
9.1.7 Test Flight validation: Conclusions . . . 176
9.2 Validation of the Scientific Flight measurements . . . 176
9.2.1 Temperature validation . . . 177
9.2.2 H_2O validation . . . 177
9.2.3 O_3 validation . . . 177
9.2.4 HNO_3 validation . . . 177
9.2.5 N_2O validation . . . 189
9.2.6 CO validation . . . 189
9.2.7 Comparison with MIPAS-STR measurements . . . 189
9.2.8 Scientific Flight validation: Conclusions . . . 189

10 MARSCHALS cloud products 193
10.1 Test Flight - Cloud detection . . . 193
10.2 Test Flight - Validation of the cloud detection . . . 194
10.3 Scientific Flight - Could detection and retrieval in cloudy condition . . . 195
10.4 Scientific Flight - Validation of the cloud detection . . . 196

11 Level 2 processing of MIPAS-STR data of the PremierEx Scientific Flight on 10.03.2010 200
11.1 Description of the Flight and Cloud Assessment . . . 200
11.2 Retrieval strategy . . . 201
11.3 Retrieval Error Assessment . . . 204
11.4 Discussion of the Retrieval Results . . . 207

12 Synergy of millimetre-wave and infrared data 209
12.1 Overview . . . 209
12.2 MIPAS-STR and MARSCHALS data fusion using the (L1+L2) method . . . 212
12.2.1 Quantifiers of the performances . . . 212
12.2.2 Results . . . 213
12.3 Data fusion using MSS method . . . 215
12.3.1 Quantifiers of the performances . . . 218
12.3.2 Results . . . 218
12.4 Comparison of (L1+L2) and MSS data fusion methods . . . 220

13 Detailed pointing analysis from MIPAS-STR AHRS and M-55 GNS data **225**
13.1 Standard procedure for the line-of-sight-elevation-correction of MIPAS 227
13.2 Error identification of the GNS for PremierEx-Flight in Kiruna on March 10^{th} 2010 228
13.3 Correction of the MIPAS-line-of-sight-elevation for the PremierEx Flight in Kiruna on March 10^{th} 2010 230
13.4 Conclusions of MIPAS-STR pointing analysis 232

14 Reference Documents **232**

References **232**

Definitions and Acronyms **235**